Nonlinear Dynamics of Stimulated Brillouin Scattering in Optical Fibres

Alan Johnstone

Submitted for the Degree of Doctor of Philosophy

Heriot-Watt University

Department of Physics

March 1992

To my parents

Contents

List of Figures iv

Acknowledgements vii

Abstract viii

1 Introduction 1

1.1 Nonlinear Dynamical Behaviour 1

1.2 Analysis of Dynamical Behaviour 3

1.3 Thesis Outline 5

2 Nonlinear Optics and Dynamical Behaviour 6

2.1 Nonlinear Optics and Optical Fibres 6

2.2 Optical Fibres 8

2.3 Stimulated Scattering Processes 11

2.3.1 Conventional Theory of SBS 12

2.3.2 SBS in optical fibres 16

2.3.3 SBS Threshold Conditions 19

2.4 Nonlinear Refractive Index Effects 20

2.5 Dynamical Behaviour of SBS 25

3 Steady-State SBS Behaviour 29

3.1 Introduction 29

3.2 SBS Generated from Spontaneous Scattering with no Feedback 30
3.2.1 Experimental Techniques 31
3.2.2 Steady-State Characteristics with no Feedback 38
3.3 SBS in a Cavity 41
3.3.1 Steady-State Characteristics in a Cavity with Natural Reflectivity 42
3.4 SBS Amplifier 43
3.4.1 Experimental Arrangement 45
3.4.2 Brillouin Gain in an SBS Amplifier 46
3.4.3 Steady-State SBS Amplifier Characteristics 47
3.5 Conclusions 51

4 Temporal Behaviour of SBS with no Feedback **52**
4.1 Introduction 52
4.2 SBS Generator 52
4.2.1 Data Acquisition and Processing 53
4.2.2 Digitisation Optimisation 56
4.3 Temporal SBS Behaviour 58
4.3.1 Comparison with Theoretical Results 65
4.4 Photosensitive Effects 67
4.5 Temporal Behaviour of SBS Amplifier 70
4.5.1 Operation below threshold 72
4.5.2 Operation above threshold 72
4.5.3 Comparison with Theoretical Results 75
4.6 Conclusions 76

5 Temporal Behaviour of SBS with Feedback **78**
5.1 Introduction 78

5.2 Natural Reflectivity 78
5.2.1 Temporal Behaviour 79
5.2.2 Comparison with Theory 94
5.3 Addition of External Feedback 96
5.4 Variation of Reflectivity 98
5.4.1 Measurement of External Reflectivity 98
5.4.2 Temporal Behaviour 100
5.4.3 Comparison with Theory 109
5.5 Conclusions 109

6 Wavefront Dislocations **111**
6.1 Introduction 111
6.2 Fibre Modes 115
6.3 Experimental Observations of Dislocations 116
6.3.1 Single-Mode Fibres 119
6.3.2 Slightly Over-Moded Fibres 120
6.3.3 Multi-Mode Fibres 133
6.4 Estimation of Intensity-Dependent Refractive Index 133
6.4.1 Introduction 136
6.4.2 Measurement of Phase Change 137
6.5 Conclusions 139

7 Conclusions **140**

A Fibre Parameters - Manufacturer's Data **147**

References **150**

List of Figures

3.1 SBS build up and pump decay in an optical fibre 32

3.2 Basic experimental setup 32

3.3 Unstable laser output 34

3.4 Effective core radius ratio against normalised frequency parameter . . 35

3.5 Steady state power characteristics for SBS without feedback 40

3.6 Theoretical and experimental SBS threshold power against fibre length. 40

3.7 SBS build up in a Cavity 42

3.8 Steady state power characteristics for SBS with and without cavity . 44

3.9 Steady state power characteristics for SBS in a cavity 44

3.10 Setup for SBS amplifier 48

3.11 Polarization dependence of Brillouin gain in ordinary single-mode fibre 48

3.12 SBS amplifier gain characteristics 49

3.13 Amplifier output power against pump power 50

4.1 Digitised sine waves 54

4.2 Fourier transforms of digitised sine waves 56

4.3 Phase portrait rotation by varying τ 57

4.4 Temporal recordings of the chopped pump, SBS and transmitted pump signals 59

4.5 Temporal behaviour and power spectra of the pump, SBS and transmitted pump signals 60

4.6 Digitised SBS behaviour 62
4.7 Digitised transmitted pump behaviour 63
4.8 SBS time series and power spectra for increasing pump power 64
4.9 Theoretical temporal evolution of SBS intensity on increasing nonlinear dispersion parameter 66
4.10 Theoretical SBS intensity and phase portraits on increasing pump power 68
4.11 Theoretical time series and power spectra for SBS and transmitted pump signals 69
4.12 Example of probe signal 71
4.13 SBS amplifier output operating below threshold 73
4.14 SBS amplifier output operating above threshold 74

5.1 Reflected signal below and close to threshold 79
5.2 Round-trip oscillations in SBS and transmitted pump 81
5.3 Variation of SBS with natural reflectivity on increasing pump power . 82
5.4 Modulations and pulsations in SBS caused by the addition of feedback 83
5.5 Phase matching conditions for four-wave mixing 86
5.6 Examples of dynamical features 88
5.7 Change in SBS signal with increasing pump power 92
5.8 Theoretical time series of Stokes signal with natural reflectivity . . . 97
5.9 SBS signal with external feedback 99
5.10 Variation of external reflectivity 100
5.11 Effect of increasing pump power on SBS in a very poor cavity 102
5.12 Effect of increasing external reflectivity on SBS 103
5.13 Change in SBS temporal behaviour with reflectivity 107
5.14 Theoretical change in dynamical behaviour on increasing cavity reflectivity 108

6.1 Single strength edge and screw dislocations 113

6.2 Examples of fibre mode patterns 117

6.3 Mach-Zehnder interferometer used to study wavefront dislocations . . 119

6.4 Fringes for single-mode fibre 121

6.5 Mode pattern and fringes for two-mode fibre 122

6.6 Close-up of first order dislocation 123

6.7 Dislocation caused by mode mixing 126

6.8 Geometry of point sources to recreate mode pattern 128

6.9 Interference pattern for two point source in antiphase 128

6.10 Interference pattern for three point source 129

6.11 Interference pattern from four point sources 131

6.12 Interference pattern from four point sources 132

6.13 Mode pattern and fringes for four-mode fibre 134

6.14 Part of the multi-mode fibre mode pattern and associated fringes . . 135

6.15 Example of chart recorder output 138

6.16 Fringe displacement against transmitted power 138

Acknowledgements

I would like to take this opportunity to thank the people who helped to make this thesis possible. I am grateful to my supervisor Professor R. G. Harrison and also to Dr. Weiping Lu, Dr. J. S. Uppal and D. S. Lim, the other members of my research group, for their support and guidance over the last three years or so.

I am also indebted to Russell Morgan, Roy McBride and the other members of the fibre optics group, here at Heriot-Watt University, for all the aid and advice they gave to someone who had never used fibres before. Also to Wladek Forysiak for the use of data acquisition and analysis programs and for showing me many of the subtleties of the Masscomp computer.

Numerous other people aided me on the rocky road but I am especially thankful to Rebbie (Wilson) for all her wisdom, I hope that she has some left for herself, and of course to Little Ed (Restall) for filling in all the gaps in my knowledge of computers, optics and Northern England; get well soon Eddie. Oh I forgot Tony, hello Tony, smile.

I also acknowledge the receipt of an SERC grant.

Abstract

This thesis presents an experimental investigation of the dynamical and steady-state behaviour of stimulated Brillouin scattering (SBS) under cw pump conditions in single-mode optical fibres. Both SBS generated from the amplification of spontaneous Brillouin scattering, an SBS generator, and from the amplification of a probe signal, an SBS amplifier, were studied.

For the generator without feedback, both the scattered wave and the transmitted pump were found to exhibit aperiodic behaviour under all operating conditions, fibres lengths between 25 m and 300 m were studied using a maximum pump power of 4 W, with the SBS showing approximately 100% modulation. The bandwidth of the chaotic SBS signal was found to be independent of the single-pass gain. The addition of feedback leads to the SBS and transmitted pump signals showing sustained or random bursts of quasi-periodic oscillations. The effects of varying the cavity reflectivity and also the pump power are shown. These were the first experimental reports of such behaviour [HAR90,JOH91] and were found to be in good agreement with the theoretical work carried out by Lu and Harrison [LU91a,LU91b]. The output of an SBS amplifier was found to dynamically follow the applied probe signal except in some cases of high pump and very low probe values.

Also investigated was the creation of phase singularities in the wavefronts of optical fibres. Only first-order screw dislocations were observed and their dependence on the number of fibre modes present was examined.

Chapter 1

Introduction

1.1 Nonlinear Dynamical Behaviour

The study of nonlinear systems has shown that, as well as showing regular and repeatable behaviour, these may also yield unstable or even chaotic solutions in time and space. Chaos is the term used to describe unpredictable and apparently random behaviour that arises from the nonlinear nature of a system rather than from stochastic driving forces. The behaviour is also termed deterministic since it is completely described by the set of equations and the initial conditions describing the system. The transition from stable to chaotic behaviour follow specific well-defined routes that are independent of the physical properties of the system they describe and may occur by varying a control parameter of the system. Unlike linear systems, nonlinear systems must be treated in their full complexity and this usually requires for numerical solutions to the nonlinear equations.

Simple nonlinear systems such as the Duffing [DUF18] and van der Pol [POL27] oscillators which were extensively investigated in the early part of this century have recently been found to exhibit chaotic behaviour when the correct control parameters are chosen [UED80,SHA81], full details of which are given by [THO86]. Lorentz demonstrated in 1963 [LOR63], while investigating turbulence in liquids in an at-

tempt to aid weather prediction, that very simple low-dimensional systems even a simple set of three coupled first order, nonlinear differential equations can display completely chaotic behaviour at certain parameter values. In general, each nonlinear system must be investigated individually to determine the nonlinear response and to verify whether chaotic solutions exist. Moreover, the behaviour of a nonlinear system may vary greatly with its parameters, and stationary or periodic solutions may prevail throughout its parameter space. Part of the approach to an investigation into a nonlinear system is to therefore discover where in the control parameter range to look for chaotic solutions.

Physical systems as diversely different as animal population dynamics and chemical reactions have been studied but many experiments are now being carried out in optical systems, both lasers and passive devices. These may provide, in some cases, almost ideal systems for quantitative investigations due to their simplicity both in construction and in the mathematics that describe them. Also the timescales involved mean that data acquisition can occur under constant environmental conditions. The major topic studied in this thesis is the optical process of stimulated Brillouin scattering using single-mode optical fibres as the nonlinear medium.

Stimulated Brillouin scattering (SBS) first observed by Chiao et al. [CHI64], is an inelastic process which involves vibrational excitation of acoustic phonons to create a frequency downshifted Stokes scattered wave. SBS can be described as a classical three-wave interaction involving the incident pump, a generated acoustic wave and the scattered Stokes wave. The pump creates a pressure wave in the medium through electrostriction where medium undergoes a density redistribution in order to minimise its free energy in the presence of the field which results in a change in the optical susceptibility. The incident light is then scattered by the acoustic wave to create the Stokes wave. As will be shown later, this process can be described by three first order, coupled differential equations and may, under the

appropriate parameter values, yield chaotic solutions. The use of optical fibres allows experiments to be conducted with modest optical powers and under the idealised conditions of a steady-state pump.

1.2 Analysis of Dynamical Behaviour

Erratic and aperiodic temporal behaviour of the variables of any system can be transformed, using a fast Fourier transform, to give a power spectrum which is broadband and continuous however other features, including noise, can lead to similar spectra. Distinguishing between deterministic, where the behaviour is determined by previous causes and is completely described by a set of equations and their initial conditions, and stochastic behaviour, which is usually related to random motion induced by thermal or quantum fluctuations, in experiments can be difficult. Power spectra alone provide insufficient information to determine if the aperiodic behaviour is due to the determinism of the nonlinear system. The analysis of the evolution of the trajectory mapped out in phase space may help distinguish between the two.

Phase space is an abstract space in which a single point completely describes the instantaneous state of a dynamical system where the dimension of the phase space depends on the number of variables needed to describe the system. As the system changes with time this point moves through phase space and the trajectory of the point traces out the systems temporal behaviour to create a phase portrait. The term attractor is used to describe the long-term behaviour of a dissipative system and is a subset of the phase space. For example a fixed point in phase space represents behaviour which has reached a steady state while periodic attractors or limit cycles, where the trajectory is repeated periodically to form a cyclical orbit, represents periodic behaviour. Phase space portraits of physical systems expose patterns of motion that may be invisible otherwise. It is not necessary to measure all of the system's variables simultaneously to construct a multi-dimensional phase portrait

as this can be done using embedding theorems involving only the measurement of a single variable [PAC80].

Chaotic behaviour is characterised by an orbit in phase space which never repeats or crosses itself, once a system returns to a state it has been in before it therafter must follow the same path. This requires the orbit to be an infinitely long line in a finite area, i.e. the phase portrait must have fractal (fractional) dimensions. Fractional dimensions are a way of measuring the degree of irregularity in an object, see for example [GLE88]. Chaotic dynamics is described by a strange attractor - an attractor with fractal dimensions. A strange attractor fills a finite volume in phase space which is in contrast to a stochastic system where high dimensional noise fills all the available phase space.

Methods of analysis of phase portraits include determination of characteristic exponents, attractor dimensions and entropy measurements [ECK85]. Lyapunov exponents are the average exponential rates of divergence or convergence of nearby orbits in phase space. They provide a measure of the topological qualities that correspond to such concepts as unpredictability providing a way of measuring the effects of stretching, contraction and folding of an attractor in phase space. An exponent greater than zero means stretching meaning that nearby points in phase space will separate as they evolve. Since nearby orbits correspond to nearly identical states, exponential orbital divergence means that systems whose initial differences which may not be resolved soon behave quite differently - predictive ability is lost. Any system containing at least one positive Lyapunov exponent is defined to be chaotic, with the magnitude of the exponent reflecting the time scale on which the system's dynamics become unpredictable.

1.3 Thesis Outline

This thesis covers research into two different topics, the first and largest being stimulated Brillouin scattering in single-mode optical fibres. Chapter 2 introduces some of the principles of nonlinear fibre optics including the basic theory of SBS and nonlinear refractive index effects. This chapter also reviews the work carried out thus far, both theoretical and experimental, concerning the dynamical behaviour of SBS including other media other than silica fibres.

Chapter 3 deals with the steady-state or time-averaged behaviour of SBS with and without feedback. Both SBS generated from the amplification of spontaneous emission and that produced by amplification of a Stokes signal produced elsewhere - an SBS amplifier - is studied.

Chapter 4 reports the experiments carried out for SBS without feedback, that is to say the open flow case, again for both SBS generated from spontaneous scattering and for the SBS amplifier. These results are compared to those reported in chapter 5 for SBS with feedback. Here the dynamics of the SBS process were investigated for fixed reflectivity and varying pump power and also for fixed pump power and varying cavity reflectivity. The experimental results in these two chapters are compared to theoretical results obtained by other members of the group, Weiping Lu and R. G. Harrison, by solving the SBS coupled wave equations which included terms to describe self- and cross-phase modulation between the pump and scattered waves.

Chapter 6 describes experiments carried out to investigate the wavefront dislocations found in the mode patterns of optical fibres. These phase dislocations in the wavefronts are analogous to those found in the lattice planes of crystals. Some of this work was carried out in collaboration with D. S. Lim.

Chapter 2

Nonlinear Optics and Dynamical Behaviour

2.1 Nonlinear Optics and Optical Fibres

A nonlinear optical process may be thought of as a light induced nonlinear response of a medium which then modifies the applied optical field as it reacts. The optical properties of a medium are characterised by the linear and nonlinear susceptibilities which depend on the detailed electronic and molecular structure of the medium. Silica, the major constituent of most glasses and also of most optical fibres, is an isotropic medium and therefore any anisotropy of the individual molecules is averaged out because of the random orientation of the molecules. Also in molecules with inversion symmetry, i.e. centrosymmetric, such as SiO_2 an applied field produces polarisation of the same magnitude but of opposite sign according to whether the electric field is positive or negative and there is no net polarisation. Consequently the second-order nonlinear susceptibility $\chi^{(2)}$ is zero for silica glass. The lowest order nonlinearities are due to the third-order susceptibility $\chi^{(3)}$. Although third-order processes are allowed in all materials, they are generally much weaker than second-order ones, since the third-order susceptiblity is much smaller than

the second-order, but they can still be easily obtained particularly if the process is enhanced by a material resonance. Third-order processes include four-wave mixing and third-harmonic generation, parametric processes involving the interaction of four optical waves to generate new frequencies, as well as both stimulated Raman and Brillouin scattering [SHE84]. Note that for efficient four-wave mixing or third-harmonic generation phase matching conditions must be met. The efficiency of a nonlinear optical process depends not only on the size of the nonlinear coefficient and the optical intensity but also on the distance over which this intensity can effectively interact with the medium.

In bulk materials the high intensities necessary to observe nonlinear effects are achieved by focusing the beam into the sample, but the depth of focus and hence the interaction length are short. The efficiency of a nonlinear interaction in a bulk material is independent of the length of the nonlinear medium and in fact depends only on the pump power and wavelength [IPP75]. In contrast, in an optical fibre the spot size is maintained over the whole length of the fibre due to the waveguiding properties of the fibre. The interaction length in fibres is limited only by the loss of the fibre α, the pump power would tend to zero if the fibre was sufficiently long, and for the low-loss fibres currently used this may be as long as 20 km.

Although the size of the nonlinearity in silica fibres is many times smaller than it is in those bulk materials commonly used for nonlinear optics, the long interaction length together with the high power density in the core of the fibre often allows experiments to be performed at lower powers than in bulk materials. This frequently allows cw lasers to be used, in many cases operating at modest powers, instead of having to use pulsed lasers, as is often the case for bulk materials. The increase in efficiency of the nonlinear interaction in fibres over that in bulk materials is given by [AGR89a]

$$\frac{\text{fibre}}{\text{bulk}} = \frac{\lambda}{\pi w_o^2 \alpha} \tag{2.1}$$

at a wavelength λ and a spot radius w_o assuming that the fibre length L is long, so that $\alpha L \gg 1$. Substituting typically values for single-mode silica fibres into equation 2.1 of $\lambda = 514.5$ nm, $w_o = 1.7$ μm and $\alpha = 4.6 \times 10^{-3}$ m^{-1} (20 dB/km) gives an enhancement of $\sim 10^7$ over bulk materials. Hence optical fibres offer the opportunity to study certain nonlinear effects under the idealised conditions of a steady state pump.

2.2 Optical Fibres

The phenomenon of total internal reflection at the interface of two dielectric materials has been known since the nineteenth century. The use of single dielectric rods to carry light was considered, but these would have been impractically small to accommodate only a single electromagnetic mode and would also have high losses at any discontinuities of the glass-air interface, for example scratches in the glass or dust settling on the uncovered core. It is the use of a cladding layer which has led to considerable improvements in optical waveguides and to the optical fibre as we know it today. Today's step-index circular waveguide consists of a core of refractive index n_{co} and radius a. This is surrounded by a cladding of refractive index n_{cl} and radius b, where b is chosen to be large enough so that the field of the confined modes is virtually zero at the outer edge of the cladding. The core, cladding or both are slightly doped so that $n_{co} > n_{cl}$ and waveguiding takes place. Dopants such as GeO_2 and P_2O_5 are commonly used to increase the refractive index of the core, while fluorine is used to decrease the refractive index of the cladding. The two are protected by a flexible plastic buffer coating which also helps to strip out radiation modes.

Two parameters which characterize the fibre [ADA81] are the relative core-

cladding refractive difference or profile height parameter Δ which is defined as

$$\Delta = \frac{n_{co}^2 - n_{cl}^2}{2n_{co}^2}, \tag{2.2}$$

which simplifies to

$$\Delta = \frac{n_{co} - n_{cl}}{n_{co}} \tag{2.3}$$

in the weak-guidance or paraxial approximation where $n_{co} \simeq n_{cl}$ and $\Delta \ll 1$, and the normalized frequency or waveguide parameter V, where

$$V = \frac{2\pi a}{\lambda}\sqrt{n_{co}^2 - n_{cl}^2} = \frac{2\pi a n_{co}}{\lambda}\sqrt{2\Delta}. \tag{2.4}$$

The numerical aperture of the fibre is also governed by the core and cladding refractive indices and

$$\mathrm{NA} = \sqrt{n_{co}^2 - n_{cl}^2}. \tag{2.5}$$

The above relationship is a useful measure of the light-collecting ability of a fibre but this was derived using geometric optics. As the core diameter of the fibre becomes comparable to the wavelength of light used, as is the case for single-mode fibres, the geometric ray model breaks down and full electromagnetic mode theory should be used.

The number of guided modes supported in fibre and their spatial distribution can be found, like any other waveguide, by solving the wave equation satisfying the appropriate boundary conditions, see for example [SNY83, chpt 11-13]. Due to the cylindrical geometry of a fibre the solutions are Bessel and modified Bessel functions and the exact expressions can become very complicated. Fortunately these can be simplified for weakly guiding fibres where the profile height parameter is small. In this limit the medium is virtually homogeneous as far as polarisation effects are concerned and the full set of modes can be approximated by linearly polarised (LP)

modes, see for example [YAR85, chpt 3]. An LP_{lm} mode has m field maxima along a radius vector and $2l$ field maxima round a circumference, where the fundamental mode is LP_{01}. The number of modes allowed is determined by the normalised frequency parameter V. For a step-index fibre to be single-mode $V < 2.405$, and generally fibres are designed so that the value of V is close to 2.405 to minimise losses due to bending. This is due to the fact that as the value of V decreases the evanescent field penetrates further into the cladding leading to greater losses [SNY83].

Typically the profile height parameter will be of the order of 3×10^{-3}, or in other words the numerical aperture will be 0.12, so that the core radius a must be 1.6 μm at a wavelength of $\lambda = 514.5$ nm and $a = 4$ μm at $\lambda = 1.25$ μm. For a single-mode fibre the diameter of the cladding is typically 125 μm and the total diameter 250 μm. The cut-off wavelength of a fibre is the shortest wavelength which will propagate in the fibre as a single-mode, this can be calculated from equation 2.4 using $V = 2.405$.

Improvements in fabrication processes have meant that the fibre loss α has been reduced to ~20 dB/km at 514.5 nm and to ~ 0.2 dB/km at 1.55 μm, thus allowing for interaction lengths of up to ~20 km. When monomode optical fibres are used in the weakly nonlinear regime, as is the case here, the only effect of the nonlinearity is to modify the propagation constant β for the guided mode. So despite the transverse intensity distribution within the fibre all parts of the wavefront in a single-mode fibre experience the same phase shift and the guided waves can be treated as plane waves. Therefore the transverse effects which are seen in bulk materials and are usually unwanted do not appear when fibres are used.

Multi-mode fibres are slightly more complicated since each mode has a different propagation constant and transit times through the fibre will be different for each modes although the difference will be small for weakly guiding fibres since $kn_{cl} < \beta \leq kn_{co}$ and $n_{co} \simeq n_{cl}$, where k is the propagation number. Perturbations

of the waveguide such as deviations in straightness, variations in core diameter and refractive index variations may change the propagation characteristics of the fibre. This leads to energy being coupled from one mode to another and therefore reduces the effects of intermodal dispersion. All the stimulated Brillouin scattering experiments carried out for this thesis used only the fundamental mode and therefore intermodal dispersion does not occur.

2.3 Stimulated Scattering Processes

The losses in silica fibres have now been reduced to near their theoretical limits determined by Rayleigh scattering and absorption. Rayleigh scattering is an elastic process so that the scattered light has the same frequency as the pump. The scattered flux density for this is proportional to λ^{-4}, therefore losses due to Rayleigh scattering are smaller at longer wavelengths. However at wavelengths longer than $\sim 1.5\ \mu$m infra-red absorption becomes significant and germania doped fibres tend to have minimum attenuation around 1.55 μm.

Elastic scattering is not the only scattering process to occur in materials and the incident light may cause some excitation of the material changing the electronic, vibrational or rotational energy levels of its atoms or molecules. Raman scattering occurs when the incoming photon is scattered by local molecular vibrations or by optical phonons, whereas Brillouin scattering involves excitation of the acoustic vibrational modes of the material. The fraction of light that undergoes any of these spontaneous scattering processes is however very small, about 1 in 10^6. The scattering is inelastic and the frequency of the scattered photons is shifted below or above the incident photon frequency. Photons which are frequency downshifted, those that give up some energy to the material, are known as Stokes photons and those which are frequency upshifted as anti-Stokes photons. Anti-Stokes photons are even rarer than the Stokes photons since for photons to gain energy the incoming

pump photons must interact with a molecule in its excited state.

The Stokes wave exists in the material initially as spontaneous scattering. This wave may combine with the incident wave to nonlinearly drive the material wave. The material wave will then cause more photons to be inelastically scattered and so on - this is stimulated scattering and the Stokes wave may now experience gain.

In particular stimulated Brillouin scattering (SBS) results from the parametric interaction of light and acoustic waves. The light waves generate an acoustic wave through electrostriction which in turn causes a periodic modulation of the refractive index of the medium. The pump induced index grating scatters the pump through Bragg diffraction and the scattered light is frequency downshifted because of the Doppler shift associated with a grating moving at the acoustic velocity v_A.

SBS was first observed by Chiao et al. [CHI64] in quartz and sapphire using a Q-switched ruby laser. It has also been studied extensively in a variety of liquids, solids and gases [KAI72] and the first observations in optical fibres were by Ippen and Stolen [IPP72] in 1972 using a pulsed Xenon laser. The use of very long low-loss optical fibres has enabled SBS to be observed at launched power levels of only a few milliwatts using a cw pump source [COT82]. Using a high finesse all-fibre ring resonator, a resonator with low round-trip fractional intensity loss which leads to a significant circulating pump power enhancement, observations of SBS have been made with input powers of only 65 μW [KAD88].

2.3.1 Conventional Theory of SBS

The basis theory of SBS deals with the interaction of two lightwaves and a generated acoustic wave. These are usually written in the form of three coupled wave equations, see for example [SHE84, chapter 11] or [KRO65,KAI72,TAN66].

$$\left[\nabla \times (\nabla \times) + \frac{n_P^2}{c^2}\frac{\partial^2}{\partial t^2}\right] \mathbf{E}_P = \omega_P^2 \mu_o \mathbf{P}^{NL}(\omega_P) \tag{2.6}$$

$$\left[\nabla \times (\nabla \times) + \frac{n_S^2}{c^2}\frac{\partial^2}{\partial t^2}\right] \mathbf{E}_S = \omega_S^2 \mu_o \mathbf{P}^{NL}(\omega_S) \tag{2.7}$$

$$\left[\frac{\partial^2}{\partial t^2} - 2\Gamma_B \frac{\partial}{\partial t} - v_A^2 \nabla^2\right] \Delta\rho = -\nabla \cdot \mathbf{f} \tag{2.8}$$

where n is the refractive index, c the speed of light in vacuum, $\mathbf{E}$ the electric field, ω the frequency, μ_o the permeability of free space, $\mathbf{P}^{NL}$ the nonlinear polarisation and the subscripts P, S and A refer to the pump, Stokes and acoustic waves respectively. The acoustic wave is represented by the density variation $\Delta\rho$ and has a velocity v_A, which is related to the Young's modulus E_o and the density of the material ρ_o by the relationship

$$v_A = \sqrt{\frac{E_o}{\rho_o}}. \tag{2.9}$$

Γ_B^{-1} is the acoustic phonon lifetime resulting in a spontaneous Brillouin scattering linewidth of $\Delta\nu_B = \Gamma_B/\pi$ (FWHM), in bulk silica $\Delta\nu_B = 145$ MHz [PEL75] at a wavelength of $\lambda = 514.5$ nm and is found to vary as λ^{-2} [HEI79]. The driving force $\mathbf{f}$ is generated by the two light wave through electrostriction, a field induced density change which leads to a change in the optical susceptibility, where

$$\mathbf{f} = \nabla\left(\frac{1}{2\pi}\epsilon_o \gamma \mathbf{E}_P \cdot \mathbf{E}_S^*\right), \tag{2.10}$$

the electrostrictive coefficient γ being related to the change in permittivity ϵ with density ρ by the relationship

$$\gamma = \rho_o \frac{\partial \epsilon}{\partial \rho} \tag{2.11}$$

and ϵ_o is the permittivity of free space. The other two coupling terms are given by

$$\mathbf{P}^{NL}(\omega_P) = \frac{1}{4\pi}\frac{\partial \epsilon}{\partial \rho}\mathbf{E}_S \Delta\rho \tag{2.12}$$

$$\mathbf{P}^{NL}(\omega_S) = \frac{1}{4\pi}\frac{\partial \epsilon}{\partial \rho}\mathbf{E}_P \Delta\rho^* \tag{2.13}$$

To solve these equations in steady state conditions, (the time dependant case will be examined later), the slowly varying amplitude approximation is assumed, so that

$$\left|\frac{\partial^2 \mathcal{E}(z)}{\partial z^2}\right| \ll \left|k\frac{\partial \mathcal{E}(z)}{\partial z}\right| \tag{2.14}$$

where $\mathcal{E}(z)$ is the amplitude of the electric field. The frequencies of the three waves are related by the conservation of energy law, so that $\omega_A = \omega_P - \omega_S$, and maximum power transfer occurs when the phase matching condition $\mathbf{k}_A = \mathbf{k}_P + \mathbf{k}_S$ is met between the fields wave vectors. The frequency shift between the pump and Stokes waves is equal to

$$\omega_A = |k_A| v_A = 2v_A |k_P| \sin(\theta/2) \tag{2.15}$$

where θ is the angle between the pump and Stokes waves. This assumes the approximation $|k_P| \simeq |k_S|$ which is true because the acoustic frequency is several orders of magnitude lower than the optical frequencies. Therefore only the backward SBS process need be considered since forward SBS does not occur as the frequency shift is equal to zero when the pump and Stokes waves are propagating in the same direction. Let $\mathbf{E}_P = \hat{e}_P \mathcal{E}_P \exp(ik_P z - i\omega_P t)$, $\mathbf{E}_S = \hat{e}_S \mathcal{E}_S \exp(-ik_S z - i\omega_S t)$ and $\Delta\rho = \mathcal{A} \exp(ik_A z - i\omega_A t)$, then following the slowly varying amplitude approximation equations 2.6 to 2.8 can be simplified to three first order differential equations thus

$$\left(\frac{\partial}{\partial z} + \frac{\alpha}{2}\right)\mathcal{E}_P = \frac{i\omega_P^2}{2k_P c^2}\frac{\partial \varepsilon}{\partial \rho}(\hat{e}_P\dagger \cdot \hat{e}_S)\mathcal{E}_S \mathcal{A} \exp(-i\Delta k z) \tag{2.16}$$

$$\left(\frac{\partial}{\partial z} - \frac{\alpha}{2}\right)\mathcal{E}_S^* = \frac{i\omega_S^2}{2k_S c^2}\frac{\partial \varepsilon}{\partial \rho}(\hat{e}_P\dagger \cdot \hat{e}_S)\mathcal{E}_P^* \mathcal{A} \exp(-i\Delta k z) \tag{2.17}$$

$$\left(\frac{\partial}{\partial z} + \frac{\Gamma_B}{v_A}\right)\mathcal{A} = \frac{ik_A}{4\pi v_A^2}\rho_o \frac{\partial \varepsilon}{\partial \rho}(\hat{e}_P\dagger \cdot \hat{e}_S)^* \mathcal{E}_P \mathcal{E}_S^* \exp(i\Delta k z) \tag{2.18}$$

where $\Delta k = k_P + k_S - k_A$ is the phase mismatch, $\mathcal{E}_P$, $\mathcal{E}_S$ and $\mathcal{A}$ are the slowly varying amplitudes of the pump, Stokes and material fields respectively and $\hat{e}$ represents the

field polarisation.

These equations are further simplified by considering the material attenuation coefficient Γ_B/v_A which is usually much larger than the gain coefficient of the stimulated scattering, hence the acoustic wave excitation can be considered to be highly damped. In silica fibres $\Gamma_B/v_A = 2.4 \times 10^4$ m^{-1}, which is much larger than the Brillouin gain (this is calculated later), and this allows $\mathcal{A}$ to be eliminated using the approximation $\delta\mathcal{A}/\delta z \simeq i\Delta k\mathcal{A}$ resulting in the following solutions

$$\left(\frac{\partial}{\partial z} + \frac{\alpha}{2}\right)\mathcal{E}_P = \frac{i2\pi\omega_P^2}{k_P c^2}\chi_B^{(3)}|\mathcal{E}_S|^2\mathcal{E}_P \tag{2.19}$$

$$\left(\frac{\partial}{\partial z} - \frac{\alpha}{2}\right)\mathcal{E}_P^* = \frac{i2\pi\omega_S^2}{k_S c^2}\chi_B^{(3)}|\mathcal{E}_P|^2\mathcal{E}_S^* \tag{2.20}$$

where

$$\chi_B^{(3)} = \left[\frac{(\hat{e}_P\dagger \cdot \hat{e}_S)}{4\pi v_A}\left(\frac{\partial\varepsilon}{\partial\rho}\right)\right]^2 \frac{k_A\rho_o}{\Delta k - i\Gamma_B/v_A}. \tag{2.21}$$

For the backwards travelling Stokes wave to grow the gain it experiences must of course be greater than the loss, which means that the threshold conditions are given by

$$\left(\frac{2\pi\omega_S^2}{k_S c^2}\right) Im\chi_B^{(3)}|\mathcal{E}_P|^2 > \frac{\alpha}{2}. \tag{2.22}$$

where $Im\chi_B^{(3)}$ is the imaginary part of $\chi_B^{(3)}$. Solving equation 2.20 in the case of negligible pump depletion, the small signal regime, gives

$$|\mathcal{E}_S(z)|^2 = |\mathcal{E}_S(l)|^2 e^{(G_B-\alpha)(l-z)} \tag{2.23}$$

where $\mathcal{E}_S(l)$ is the Stokes field amplitude at $z = l$ and the Brillouin gain G_B is given by

$$G_B = \frac{4\pi\omega_S^2}{|k_S|c^2} Im\chi_B^{(3)}|\mathcal{E}_P|^2. \tag{2.24}$$

This shows that the Stokes SBS signal experiences exponential gain as it travels

counter-directionally to the pump. The full solutions to the steady-state equations accounting for pump depletion due to both fibre loss and conversion to Stokes wave are given in chapter 3.

2.3.2 SBS in optical fibres

The geometry of optical fibres helps to simplify the solution of the above equations. The waveguiding nature of optical fibres means that only two directions of propagation are allowed, so that a forward travelling pump wave produces a backwards travelling Stokes wave where the frequency difference between the two is equal to the frequency of the acoustic wave and is calculated from equation 2.15 by setting $\theta = 180°$, so that the frequency shift is

$$\nu_B = \frac{\omega_A}{2\pi} = \frac{2v_A n}{\lambda}. \tag{2.25}$$

Using typical values for silica fibres of refractive index $n = 1.46$ and acoustic velocity $v_A = 5960$ ms^{-1}, the frequency shift is calculated to be 34 GHz at a wavelength of $\lambda = 514.5$ nm. The frequency shift is small in comparison to the pump frequency, here only $\sim 5.8 \times 10^{-3}$%, so the assumption that $|k_P| = |k_S|$ holds.

The expression given in equation 2.24 for the Brillouin gain can be transformed into the more useful form of [COT87]

$$G_B = g_B \left(\frac{P}{\pi w_o^2}\right) = \frac{2\pi n^7 p_{12}^2 K}{c\lambda_P^2 \rho_o v_A \Delta\nu_B} \left(\frac{P}{\pi w_o^2}\right), \tag{2.26}$$

where P is the pump power and πw_o^2 is the effective mode area, using the following substitutions and by assuming that phase matching conditions are met, so that $\Delta k = 0$ and therefore $k_A = k_P + k_S \simeq 2|k_P|$. Silica, like any isotropic solid, has only two independent Pockels elasto-optic coefficients, p_{12} and p_{44} which are related to

the change in the dielectric constant according to the relationship [HEI79]

$$\gamma = \varepsilon^2(p_{12} + \tfrac{2}{3}p_{44}). \tag{2.27}$$

The pressure wave, which propagates in the positive z-direction, is longitudinal and is a normal mode of the fibre [THO79]. Therefore only the longitudinal coefficient p_{12} need be considered and the electrostrictive coefficient reduces to $\gamma = n^4 p_{12}$. The factor K account for any polarisation scrambling which may occur in the fibre and is the integrated average of $(\hat{e}_P^{\dagger} \cdot \hat{e}_S)^2$. This has the value of unity for polarisation maintaining fibre and $\frac{1}{2}$ for non-polarisation maintaining fibre. The value of $\Delta\nu_B$ has been shown to be the same for silica fibres as for bulk silica [ROW79] where $\Delta\nu_B = 145$ MHz at $\lambda = 514.5$ nm.

Substituting typical values for these parameter in silica fibres [COT83,PEL75], $n = 1.46, p_{12} = 0.256, K = \frac{1}{2}, \rho_o = 2.21 \times 10^3$ kgm^{-3} and $v_A = 5.96 \times 10^3$ ms^{-1}, gives a value for the Brillouin gain coefficient of $g_B = 2.39 \times 10^{-11}$ W^{-1}m at a wavelength of 514.5 nm.

In the derivation of the above equation it was assumed that the acoustic attenuation constant Γ_B/v_a was much larger than the gain. The value calculated for Γ_B/v_a was 2.4×10^4 m^{-1} compared to a Brillouin gain of ~ 1.66 m^{-1}, for an effective mode area of 1.44×10^{-11} m^2 and a pump power of 1 W, so this assumption was fair. The Brillouin gain of silica is much smaller than that of materials used to conduct bulk SBS experiments, for example the gain of carbon bisulphide (CS_2) is 1.3×10^{-5} W^{-1}m [SHE84], but the long interaction length make experiments with fibres possible.

Thus far the pump has been assumed to be of single frequency and infinitesimally small linewidth. The effect of the pump linewidth must be considered since all lasers have a finite linewidth. The SBS gain is affected by the phase relation between the pump and the Stokes wave, by the pump linewidth and also by the ratio of

the pump coherence length to the characteristic gain length of the SBS process [VAL86,LIC87a,LIC87b,AOK88].

In the case of SBS building up from amplification of spontaneous scattering the Stokes wave is fully correlated with the pump wave and the gain is unaffected. The other case is that of an SBS amplifier where the Stokes signal is produced externally and may not be fully correlated. The gain depends on the correlation between the pump and the Stokes wave and is reduced if the two become uncorrelated.

If the pump bandwidth is small compared to the Brillouin gain bandwidth (spontaneous Brillouin scattering bandwidth) then the gain is unchanged. However if the pump bandwidth exceed that of the Brillouin gain then this is known as broad-band SBS and the gain is changed. To explain the effect of a broad-band source it is perhaps useful to begin with the case of a pump containing only two longitudinal modes separated by a frequency Ω. When the mode spacing Ω is larger than the the Brillouin gain bandwidth $\Delta\nu_B$ then each Stokes mode experiences gain from only its own pump frequency. There are no cross interactions and each frequency builds up independently of the other mode. If the two modes are of equal intensity this means that the combined SBS gain will be half of that for a single-mode pump with the same total intensity. The second case is when the frequency spacing is less than the Brillouin bandwidth, $\Omega < \Delta\nu_B$, there are now cross interactions between the two pump modes since the Brillouin gain bandwidths overlap. The strength of the cross interactions depends on frequency separation, see equation 2.21, and these become stronger as the frequency separation decreases.

The complete solution for a broad-band pump shows that the gain is reduced to

$$g'_B = \left(\frac{\Delta\nu_B}{\Delta\nu_P + \Delta\nu_B}\right) g_B \tag{2.28}$$

for a pump of bandwidth $\Delta\nu_P$. So for a pump of bandwidth $\Delta\nu_P = \Delta\nu_B$ the gain will be reduced to half of that of a narrow-band pump.

2.3.3 SBS Threshold Conditions

For the SBS process to occur requires a signal at the correct frequency to be counterpropagating to the pump. In an SBS amplifier this signal is produced separately and introduced into the fibre so as to be counterdirectional to the pump. However SBS is normally generated by the amplification of spontaneous Brillouin scattering.

In the case of a piece of optical fibre, length L, where the pump is injected at $z = 0$, the power of the backscattered Stokes signal at $z = 0$ is given by rewriting equation 2.23 as

$$P_S(0) = P_S(L)\exp(G_B L_{eff} - \alpha L). \tag{2.29}$$

The term L_{eff} is introduced to account for pump depletion due to the fibre loss α and is calculated by averaging the power over the entire length of the fibre, so that

$$L_{eff} = \int_0^L \exp(-\alpha z)dz = \frac{(1-\exp(-\alpha L))}{\alpha}. \tag{2.30}$$

For long fibre lengths, such that $\alpha L \gg 1$, equation 2.30 reduces to $L_{eff} = \frac{1}{\alpha}$. To calculate the power of the Stokes signal leaving the fibre the value of the initial Stokes signal $P_S(L)$ must be known. In the case of spontaneous scattering this is done by summing all the contributions from the spontaneous emission along the length of the fibre and multiplying by the gain. This is equivalent to injecting a single Stokes photon per black-body radiation mode falling within the Brillouin bandwidth at the point where the gain equals the loss of the fibre [SMI72]. The threshold power P_{th} is defined theoretically as the pump power for which the Stokes power equals the pump power at $z = 0$, neglecting pump depletion. This is given by

$$P_{th} = 21\left(\frac{\pi w_o^2}{g_B L_{eff}}\right). \tag{2.31}$$

Using typical values for silica fibres for a 100 m length of fibre with a loss of

6.2×10^{-3} m^{-1} (27dB/km) at $\lambda = 514.5$ nm the a threshold power is calculated to be 169 mW. However for a very long piece, 13 km, of low loss fibre, 0.4 dB/km, operating at 1.32 μm the threshold power may be as low as 5 mW [COT82]. In both cases the pump linewidth is much less than the Brillouin gain bandwidth.

2.4 Nonlinear Refractive Index Effects

Although the size of the nonlinearity in silica fibres is small, effects due to the intensity-dependent refractive index still occur. Thermal changes in the refractive index lead to phase changes in the carried light waves. These changes may be caused by heating of the fibre due to absorption, but also occur if the external temperature changes, this principle has been used to construct temperature sensors made from fibre optic interferometers [LAG81]. Self-focusing, which is observed in bulk materials, should also occur in optical fibres but the effects of this are very small since the spot size is only a few microns and any additional confinement due to self-focusing is negligible. SiO_2 is a symmetric molecule and hence $\chi^{(2)} = 0$ and the lowest order nonlinear effects are caused by $\chi^{(3)}$. These are third-harmonic generation, four-wave mixing and nonlinear refraction and must have phase matching for efficient generation of new frequencies.

Effects due to the intensity-dependent refractive index include self-phase modulation (SPM) and cross-phase modulation (XPM) [AGR89a,WIN86]. These effects are particularly important when using pulsed laser sources with the associated high peak powers and can lead to the production of optical solitons [MOL80] and also to pulse compression [NAK81] when acting with group velocity dispersion (GVD). This section includes a brief description of some of this behaviour since, as will be shown later, SPM and XPM may lead to a dramatic change in the predicted behaviour of SBS even when a cw pump is used.

The intensity dependence of the refractive index n on the optical field E, is given

by

$$n = n_o + n_2|E|^2 \tag{2.32}$$

where n_o is the linear refractive index and n_2 is the nonlinear refractive index coefficient and in an isotropic medium is related to $\chi^{(3)}$ by the relationship

$$n_2 = \frac{3}{\varepsilon_o n}\chi^{(3)}. \tag{2.33}$$

A number of physical mechanisms can contribute to the optical field induced refractive index, see for example [SHE84], these include electronic, arising from the distortion of electron distribution and electrostrictive, arising from the increase in density of the medium. In silica $n_2 = 2.3 \times 10^{-22}$ m^2V^{-2} or alternatively 3.2×10^{-16} cm^2W^{-1} which is small in comparison with most other nonlinear media, for example in CS_2 $n_2 = 2.0 \times 10^{-20}$ m^2V^{-2} [YAR85].

The phase shift $\Delta\phi$ introduced to a wave of constant intensity travelling through a nonlinear medium of length L and loss α is given by

$$\Delta\phi = \frac{2\pi n_2|E|^2}{\lambda}\left(\frac{1-\exp(-\alpha L)}{\alpha}\right), \tag{2.34}$$

For a pulsed or modulated signal the intensity varies with time and hence the intensity modulation will cause different parts of the signal to have different phase shifts. This conversion of an amplitude modulation to a phase modulation through the nonlinear refractive index is known as self-phase modulation (SPM) [STO78].

If the phase is varying with time then this implies that the instantaneous optical frequency differs across the pulse from its central value ω_o, the difference is given by

$$\delta\omega(T) = -\frac{\partial\Delta\phi}{\partial T}. \tag{2.35}$$

The variable frequency shift $\delta\omega$ can be viewed as a SPM induced frequency chirp

which increases with propagation distance. For a Gaussian shaped pulse in silica optical frequencies in the leading half of the pulse are lowered, whereas those in the trailing half are raised but the pulse shows no temporal broadening. The chirp is greatest where the intensity is changing most rapidly and so this will be larger for pulses with steep edges. The dispersion in the refractive index leads to GVD so that the different frequency components will usually travel at different speeds leading to pulse broadening.

The mode propagation constant β can be written in the form

$$\beta(\omega) = n(\omega)\frac{\omega}{c} = \beta_o + \beta_1(\omega - \omega_o) + \tfrac{1}{2}\beta_2(\omega - \omega_o)^2 + \cdots \qquad (2.36)$$

where

$$\beta_m = \left[\frac{d^m\beta}{d\omega^m}\right] (m = 0, 1, 2\ldots)$$

The pulse envelope moves at the group velocity $v_g = 1/\beta_1$, while β_2 is responsible for pulse broadening and is given by

$$\beta_2 = \frac{1}{c}\left[2\frac{dn}{d\omega} + \omega\frac{d^2n}{d\omega^2}\right] \simeq \frac{\omega}{c}\frac{d^2n}{dw^2} \simeq \frac{\lambda^2}{2\pi c^2}\frac{d^2n}{d\lambda^2}. \qquad (2.37)$$

In fused silica below a wavelength of $\lambda = 1.27$ μm the GVD parameter β_2 is positive, giving normal dispersion, and so the higher frequency components travel more slowly than the lower frequency ones leading to a linear frequency chirp. Above this wavelength β_2 is negative, giving anomalous dispersion, and the converse is true. However waveguide dispersion, which depends on the structure, dimensions and refractive-index profile of the fibre, shifts the zero-dispersion wavelength λ_D so that $\lambda_D = 1.31$ μm for typical fibres [AGR89a]. Manipulation of the waveguide design makes it possible to position λ_D anywhere in the range of approximately 1.25 μm to 1.60 μm [NEL85]. Acting alone GVD always leads to the broadening

of a transform-limited input pulse, regardless of its sign. For fibres which are long enough for propagation effects to be important the interplay between GVD and SPM must be considered. When acting together these two effects can produce different behaviour from SPM or GVD alone, so that a pulse propagating in a fibre can undergo broadening, compression, deformation or even splitting into multiple pulses.

Without dispersion SPM causes a frequency chirp and therefore increases the spectral width of a pulse but the temporal shape and width do not change, while in the absence of nonlinearity dispersion causes a Gaussian pulse to spread temporally while keeping its shape. Acting together SPM and normal GVD cause dramatic pulse shaping - SPM lowers the frequencies at the front of the pulse while increasing those at the rear, so that with positive GVD the front of the pulse travels faster than the rear and so stretches out the pulse. If however the GVD is negative the high frequency components at the rear of the pulse travel faster than the low frequency ones at the front, the rear of the pulse catches up with the front and pulse compression can take place. If the pulse has the correct amplitude and shape the narrowing action may exactly balance the broadening and the pulse propagates without changing shape, i.e. a fundamental soliton. Higher order solitons may be used to obtain pulse compression but the resulting pulses are accompanied by a broad pedestal which contains a substantial fraction of the pulse energy.

Pulse compression is however usually obtained using a fibre to obtain a chirped and spectrally broadened pulse which at the appropriate intensity and fibre length can be deformed into a nearly square pulse with more than 90% of the pulse assuming a linear frequency modulation. Then by propagating this pulse along a delay line with a negative GVD the pulse can be greatly compressed with more than 90% of the energy contained in the narrow peak [NIK83]. The most widely used delay line is a pair of suitably aligned diffraction gratings, see for example [TRE69], where

the different frequency components diffract at slightly different angles and therefore experience different time delays during transit. Optical pulses as short as 6 fs at a wavelength of 620 nm have been achieved using this method [FOR87]. It is however possible to use optical fibres for both the pulse broadening and compression stages, [BLO85], by suitably adjusting the waveguide dispersion.

Modulation instability, the process in which the amplitude and phase modulations of a wave grow as a results of the interplay between the nonlinearity and anomalous dispersion, have also been observed optical fibres [TAI86]. Modulation instability manifests itself as the break-up of a continuous-wave or quasi-continuous-wave into a train of ultrashort pulses. Through modulation instability any amplitude or phase modulation may be amplified with energy being transferred from the pump frequency to a set of side bands causing pump to become distorted. Modulation instability has been used to generate 5 THz repetition rate optical pulses [SUD89].

The refractive index can also be changed by other fields which may be present in the fibre, then the waves can interact through the nonlinearity to change each others phase, this is cross-phase modulation XPM. The total nonlinear phase shift for a field $E_1 = \mathcal{E}_1 \exp[i(k_1 z - \omega_1 t)]$ interacting with a second field $E_2 = \mathcal{E}_2 \exp[i(k_2 z - \omega_2 t)]$ is

$$\phi_1 = \frac{\omega_1 L}{c} \Delta n_1 = \omega_1 L n_2 [|\mathcal{E}_1|^2 + 2|\mathcal{E}_2|^2] \tag{2.38}$$

where the first term on the right-hand side of equation 2.38 is due to SPM and the second due to XPM. For XPM to occur the waves may differ in wavelength, polarisation or direction of propagation. Counter-propagating beams interacting through XPM have shown optical bistability when operating a ring cavity [SHE88] and have also shown modulation instability. Modulation instability due to XPM has been found even when both the counter-propagating beams are in the normal-GVD regime [AGR89b]. Even though XPM only affects the phase of cw beams it can lead to dramatic changes in the stability of the cw beams in the presence of GVD.

The above examples show that even though the nonlinearity in silica fibres is small it is sufficient to cause dynamical behaviour. The conventional treatment of the coupled wave equations for SBS ignores the effects of SPM or XPM as these were traditional though to be small enough to be neglected, since n_2 is very small and the powers used are relatively low. Computational work carried out in parallel to the experimental work presented here [LU91a] shows that these terms should be included and the solutions to these equations leads to new dynamical features, in agreement with the experimental work in this thesis, which are not predicted otherwise.

2.5 Dynamical Behaviour of SBS

The first experimental observations of SBS in optical fibres by Ippen and Stolen [IPP72] showed that oscillations with a small modulation depth were present in both the transmitted pump and stimulated scattered signals. These oscillations, with a period equal to twice the transit time of the fibre, were explained as being due to the finite length of the fibre - the build-up of the backward Brillouin wave results in a depletion of the pump wave near the input end of the fibre causing the gain to be reduced until the depletion region has passed out of the fibre. Although no external reflectivity was added, a weak cavity was present due to the Fresnel reflectivity of the fibre end faces. Finite-cell relaxation oscillations were predicted by Johnson and Marburger [JOH71] and can occur whenever a forward-travelling pump beam causes a stimulated scattered beam in the backward direction in a finite medium. Again the period of the oscillations is equal to twice the transit time of the medium T_r, where $2T_r = \frac{2nL}{c}$ for a fibre of length L. Whether the oscillations observed by Ippen and Stolen were relaxation or sustained oscillations is difficult to determine since the pump was pulsed and the pulse length was only at best eight times the oscillation period. Another pulsed experiment [AND76], conducted using

ethanol as the nonlinear medium, reported that the depth of modulation decreased over the pulse suggesting relaxation oscillations.

The theoretically predicted relaxation oscillations require no feedback, however steady oscillations have been seen [BAR85] with the addition of external feedback. By solving the conventional SBS equations with the additional boundary conditions required to account for the cavity they found that relaxation oscillations exist when no cavity was present, but with the addition of reflectivity the relaxation oscillations turned into steady oscillations. However if the reflectivity was increased above a certain level then these again became relaxation oscillations, the period of the oscillations was again found to be $2T_r$. Similar results were also obtained experimentally and in both cases the total reflectivity of the cavity was small, so the interaction of the reflected SBS and pump with the forward pump and backwards generated SBS could be neglected.

If the backwards travelling wave, either the generated SBS or the reflected pump, is sufficiently intense then this may itself produce a counterdirectional frequency shifted beam. This has been studied theoretically by Randall and Albritton [RAN84] where the reflectivity is sufficiently large to produce counterpropagating pump beams of the the same frequency each producing its own scattered wave. They found that the scattered light behaves chaotically in time and that it is frequency shifted by both multiple and fractional harmonics of the acoustic wave frequency. Another theoretical study predicting chaotic behaviour was carried out by Montes and Coste [MON87]. Again a second pump was used but this time the second pump was frequency shifted from the first pump by twice the frequency of the acoustic wave and no cavity was used. They found that the SBS passes a Hopf bifurcation, a point at which on increasing a certain control parameter, in this case interaction length, the systems changes from stable to to oscillatory behaviour. This becomes more and more anharmonic and finally chaotic for a large interaction length. Both

these examples are more complicated than the basic process of just one pump and its Stokes shifted beam - there are multiple interactions between the two pump waves and their generated Stokes waves which may produce many more frequency components. Chaotic behaviour is predicted for the basic process [BLA88] but only in the limit of a semi-infinite lossless medium.

The time dependent versions of equations 2.16 to 2.18 including terms to account for SPM and XPM of the pump and Stokes waves are [JOH91]

$$\left(\frac{\partial}{\partial z}+\frac{n}{c}\frac{\partial}{\partial t}-\frac{in_2\omega_P}{c}(|\mathcal{E}_P|^2+2|\mathcal{E}_S|^2)+\frac{\alpha}{2}\right)\mathcal{E}_P = \frac{i\omega_P^2}{2k_Pc^2}\frac{\partial\varepsilon}{\partial\rho}(\hat{e}_P\dagger\cdot\hat{e}_S)\mathcal{E}_S\mathcal{A}e^{-i\Delta kz} \tag{2.39}$$

$$\left(-\frac{\partial}{\partial z}+\frac{n}{c}\frac{\partial}{\partial t}-\frac{in_2\omega_S}{c}(|\mathcal{E}_S|^2+2|\mathcal{E}_P|^2)+\frac{\alpha}{2}\right)\mathcal{E}_S = \frac{i\omega_S^2}{2k_Sc^2}\frac{\partial\varepsilon}{\partial\rho}(\hat{e}_P\dagger\cdot\hat{e}_S)\mathcal{E}_P\mathcal{A}^*e^{-i\Delta kz} \tag{2.40}$$

$$\left(\frac{\partial}{\partial z}+\frac{1}{v_A}\frac{\partial}{\partial t}+\frac{\Gamma_B}{v_A}\right)\mathcal{A} = \frac{ik_A\varepsilon_o}{v_A^2}\gamma(\hat{e}_P\dagger\cdot\hat{e}_S)^*\mathcal{E}_P\mathcal{E}_S^*e^{i\Delta kz}. \tag{2.41}$$

The third term in equations 2.39 and 2.40 describes the phase changes in the pump and Stokes fields in both space and time. The response time of n_2 is considered fast such that it adiabatically follows the electric field amplitude in time and space. Again the material attenuation coefficient, Γ_B/v_A, is assumed to be much larger than the Brillouin gain allowing the $\frac{\partial A}{\partial z}$ term to be omitted. The equations can then normalised to allow computation work to be carried out more easily. Using the normalised field amplitudes of

$$P=\frac{\mathcal{E}_P}{\mathcal{E}_o},\ S=\frac{\mathcal{E}_S}{\mathcal{E}_o}\text{ and }B=\frac{i\mathcal{A}\Gamma_B}{\mathcal{E}_o^2V_3}$$

the above equations become

$$\frac{\partial P}{\partial \tau} + \frac{\partial P}{\partial \zeta} - iu(|P|^2 + 2|S|^2) + \frac{\beta P}{2} = -gSB \tag{2.42}$$

$$\frac{\partial S}{\partial \tau} - \frac{\partial S}{\partial \zeta} - iu(|S|^2 + 2|P|^2) + \frac{\beta S}{2} = gPS^* \tag{2.43}$$

$$\frac{1}{\beta_A}\frac{\partial B}{\partial \tau} + B = PS^* \tag{2.44}$$

where the parameters used are

$$\tau = \frac{ct}{nL},\ \zeta = \frac{z}{L},\ u = \frac{n_2 \omega L}{c}|\mathcal{E}_o|^2,\ \beta = \frac{\alpha n L}{c},\ \beta_A = \frac{\Gamma_B n L}{c} \text{ and } g = \frac{V_1 V_3 n L}{\Gamma_B c}|\mathcal{E}_o|^2.$$

The solutions obtained to these equations by other members of the group, both without and with feedback, are given in chapters 4 and 5 and compared to the experimental ones obtained. The theory does not take into account the noise structure of the initial spontaneous scattering which is included in other recent work [DIA89,BOY90,GAE91], although these authors still omit the nonlinear refraction terms. The results obtained by these workers are also discussed and compared to the experimental results.

Chapter 3

Steady-State SBS Behaviour

3.1 Introduction

SBS can grow either from the amplification of spontaneous scattering or from an injected signal at the correct frequency shift to the pump - an SBS generator or amplifier. In both cases the steady-state behaviour of the pump and Stokes signals is given by the solutions of equations 2.19 and 2.20. These can be rewritten in the simpler form of

$$\frac{\partial I_P}{\partial z} + \alpha I_P = -g_B I_P I_S \tag{3.1}$$

$$\frac{\partial I_S}{\partial z} - \alpha I_S = -g_B I_P I_S \tag{3.2}$$

$$\text{where } g_B = \frac{2\pi n^7 p_{12}^2 K}{c\lambda_P^2 \rho_o v_A \Delta\nu_B}$$

and I_P, I_S are the forwards travelling pump and backwards travelling Stokes intensities. In the case of an SBS amplifier $I_S(L)$ is generated externally and so its magnitude is known, but for the generator this arises from spontaneous scattering and is therefore generated internally and so its size is not known. However it is possible to estimate the size of the spontaneous scattering from the threshold conditions

for SBS discussed in section 2.3.3.

The full solutions to equations 3.1 and 3.2, i.e. including the effects of pump depletion, in the case of a lossless medium, i.e. $\alpha = 0$, are given by Tang [TAN66]. In the case of $\alpha \neq 0$ then the solutions are [ENN69,AGR89a], again assuming pump depletion,

$$I_S(z) = \frac{b_o(1-b_o)}{G(z)-b_o} I_P(0)\exp(-\alpha z) \tag{3.3}$$

$$I_P(z) = \frac{(1-b_o)G(z)}{G(z)-b_o} I_P(0)\exp(-\alpha z) \tag{3.4}$$

where $G(z) = \exp\left(\frac{(1-b_o)g_o}{\alpha}\right)(1-\exp(-\alpha z))$, $b_o = \frac{I_S(0)}{I_P(0)}$ and $g_o = g_B I_P(0)$.

Figure 3.1 shows how the SBS signal builds up as it propagates backwards along the fibre and how the pump decays in a forward direction, these curves were obtained by solving the above equations using the values $\alpha L = 0.57$, $g_o/L = 83.3$ and $b_o = 0.42 \times 10^{-9}$. In this case the pump signal is depleted rapidly in the first fifth of the fibre since the SBS signal has by this stage become large enough to cause pump depletion. In the rest of the fibre the SBS signal is small and pump depletion is due mainly to the linear loss of the fibre.

3.2 SBS Generated from Spontaneous Scattering with no Feedback

The first case to be considered is SBS generated from the amplification of spontaneous scattering in a fibre where there is no feedback - all reflecting boundaries having been removed - and both pump and SBS signal experience only a single pass through the fibre. The basic experimental setup is shown in figure 3.2. Light from the laser was directed through an optical isolator and coupled into the optical fibre

using a microscope objective and the input pump and generated Stokes signals are monitored via a beam splitter. The steady-state or time-averaged behaviour was obtained using a power meter which averages out any fast oscillations which may be contained in the SBS and the transmitted pump.

3.2.1 Experimental Techniques

The laser used was a cw argon ion (Coherent Innova 100-10) operating at 514.5 nm. The output power of the laser is actively stabilised to about ±2% rms when operating in light regulation mode and a maximum power of around 4 W was available. An intracavity temperature stabilised Fabry-Perot etalon was used to ensure operation on only one longitudinal mode, without the etalon the laser operates on several modes and has a linewidth of 10 GHz. The bandwidth of the laser when operating on a single longitudinal mode depends on the temperature stability of the etalon - here the long-term temperature stability is approximately 0.01° C giving an effective laser bandwidth of 50 MHz. The instantaneous laser linewidth is much less than this and on a millisecond timescale is only a few 10's of kHz or less. As discussed in section 2.3.2 the SBS gain is found to depend on the laser bandwidth by the relationship

$$g_B' = \left(\frac{\Delta\nu_B}{\Delta\nu_P + \Delta\nu_B}\right) g_B. \tag{3.5}$$

The Brillouin bandwidth is 145 MHz at 514.5 nm [ROW79] compared to the instantaneous laser linewidth of a few 10's of kHz and so the Brillouin gain is unaffected.

The laser was optically isolated from the experiment by a Faraday isolator (FI), (Burleigh Model No. IO-5-VIR), providing an isolation of ~ 25 dB between the two, although this reduces the available power since the FI transmits only about 70% of the incident power. In carrying out SBS experiments in optical fibres other types of isolation have been used - commonly a quarter wave plate and polarising

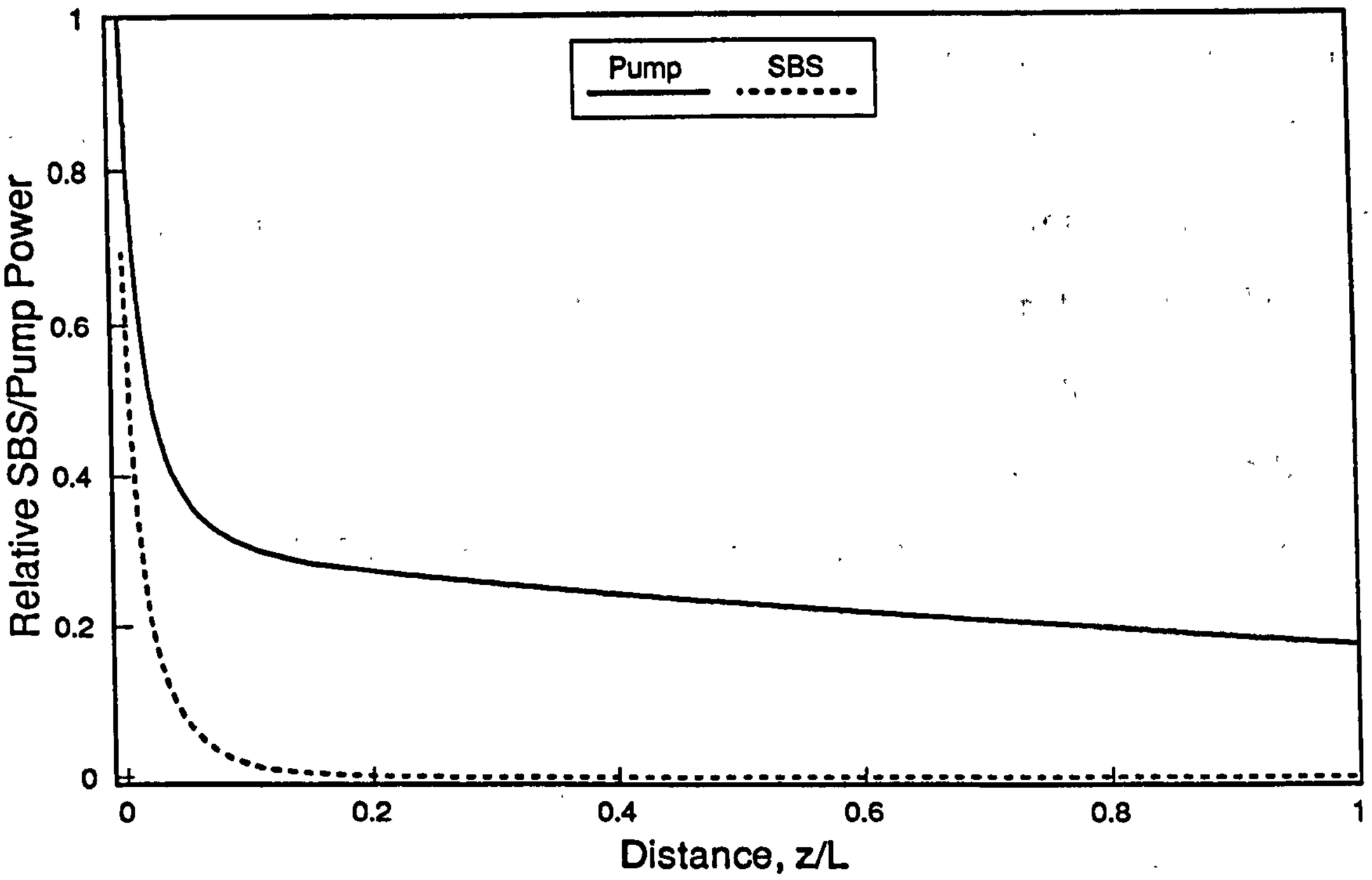

Figure 3.1: SBS build up and pump decay in an optical fibre

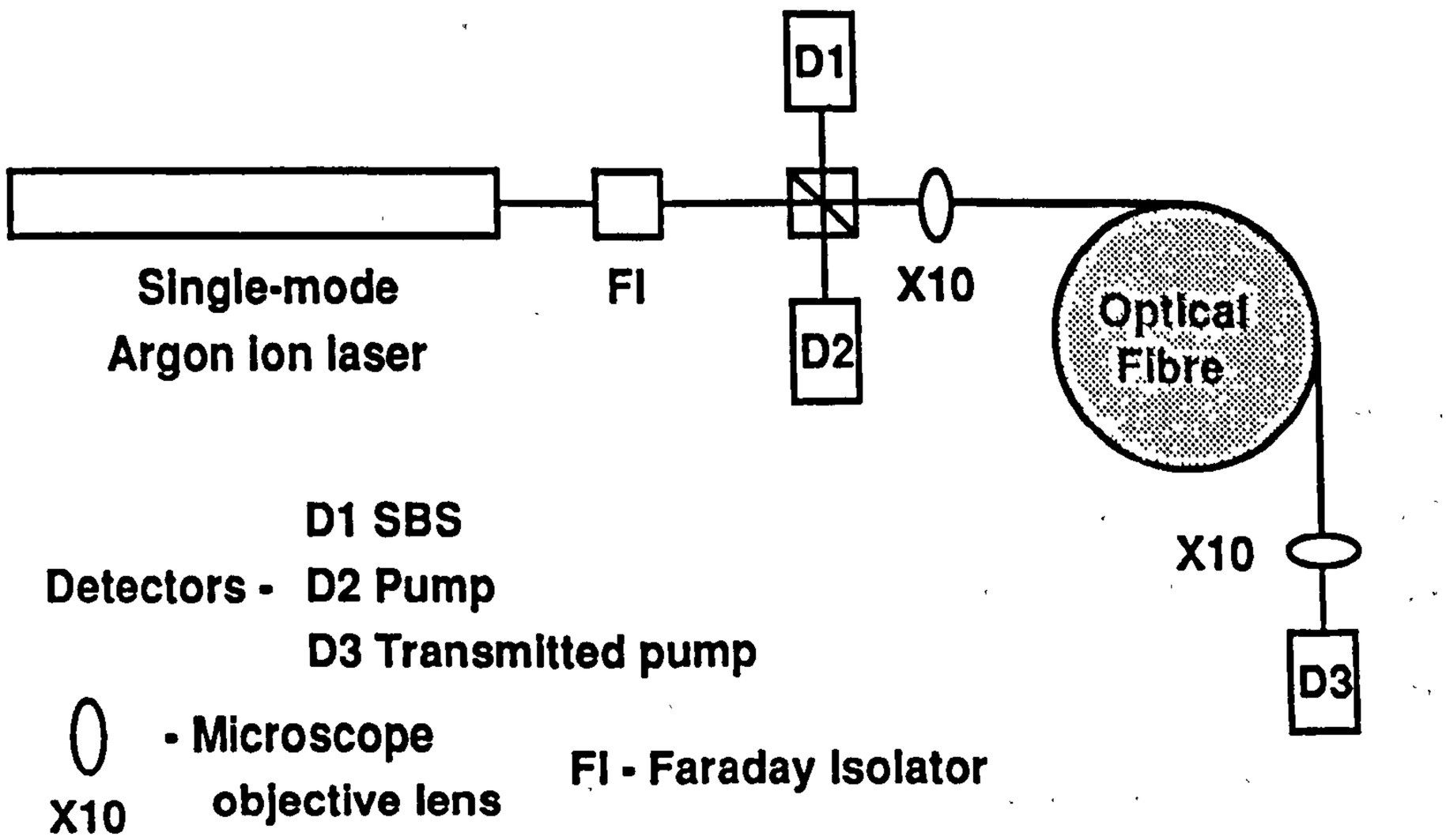

Figure 3.2: Basic experimental setup

beam splitter combination. The isolation is required for two reason, firstly the generated SBS signal produced is counter-propagating to the pump and so travels back towards the laser. The Stokes signal is frequency shifted from the pump by 34 GHz and therefore should be out of the laser's gain bandwidth and should not affect the lasing action. However the Stokes signal is reflected from the laser's output coupler and may then be relaunched into the fibre. If this occurs there would a strong frequency shifted signal travelling codirectional to the pump which can lead to the generation of multiple orders of Stokes and anti-Stokes frequencies [HIL76a,LAB80] through parametric four-wave mixing. It has been shown [AOK88] that a quarter wave plate and polariser combination may not provide sufficient isolation due to the polarisation scrambling which can take place in the fibre, so a non-reciprocal isolator such as a Faraday isolator must be used. The second reason for the isolator is that part of the pump may be reflected from the fibre end faces back into the laser causing the laser to become unstable leading to large fluctuations in the output power. This can be simulated by simply placing a mirror in front of the laser and reflecting the output back into the cavity. This was done using a beam splitter to sample the laser output and the results are shown in figure 3.3 which clearly shows the large oscillations caused by external feedback.

Light is coupled into and out of the fibre using microscope objective lenses. When launching light into a fibre the optimum conditions are achieved by matching the numerical aperture (NA) of the lens used to that of the fibre giving the optimum beam spot size. The NA of the fibres used was typically 0.11 or 0.12 and that of a $\times 10$ objective is 0.25 when fully filled. However the laser beam diameter was only $\sim$ 3 mm and so the lens was not completely filled and so has a lower NA so that the numerical apertures are well matched. When the input beam was carefully set up to be central to the lens launch efficiencies of up to 80% were possible. The launch efficiency and the fibre loss were measured using the traditional 'cutback' method.

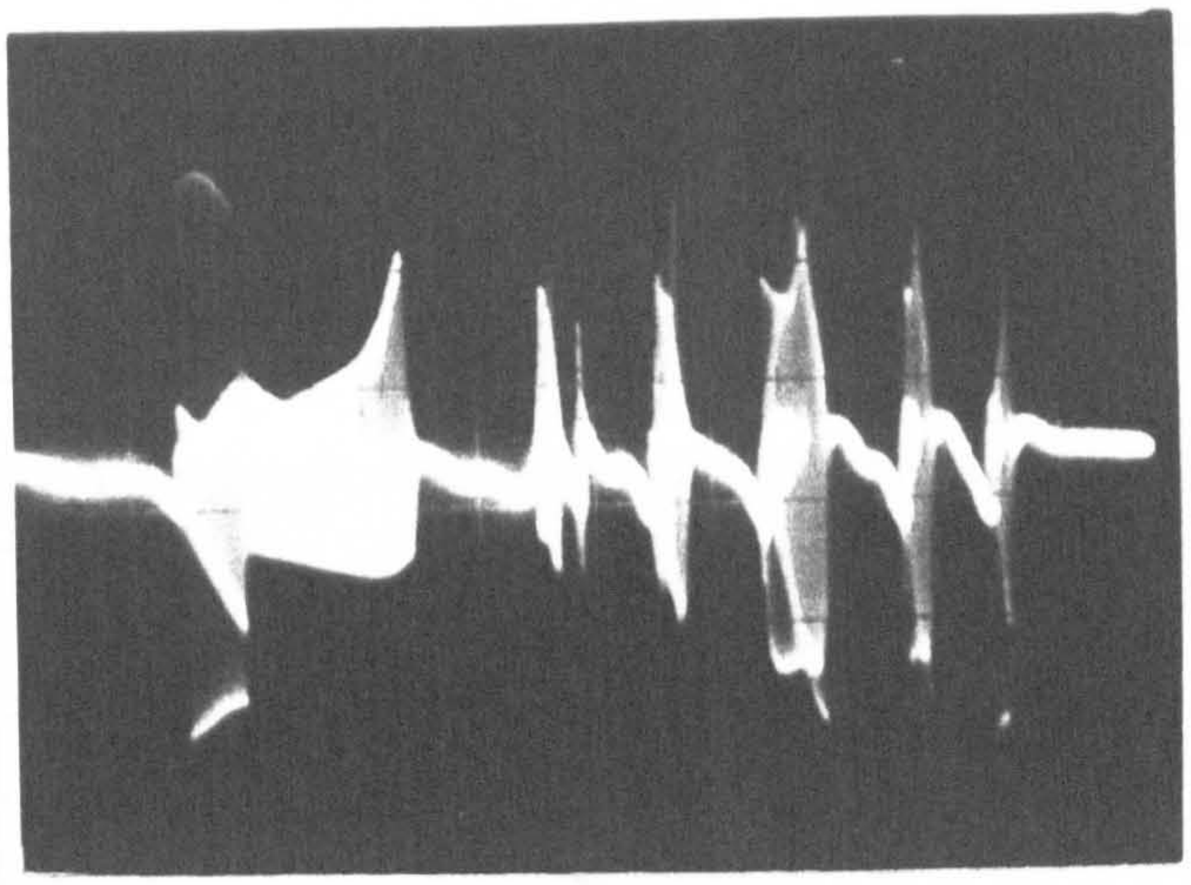

Figure 3.3: Unstable laser output caused by external feedback (time scale is 1 ms/div)

The power through a known length of fibre is measured, then without altering the launch the length is cutback to a few tens of centimeters and the power is again measured. The power transmitted through this short piece divided by the input power gives the launch efficiency and the difference between the first and second measurements allows the fibre loss to be calculated if the length is known.

Another factor which must be obtained is the effective mode cross-sectional area, A_{eff}. For a step-index fibre the mode can be approximated by a Gaussian and the area is simply πw_o^2, where w_o is the $1/e$ field radius. An empirical formula has been derived [MAR78] which allows w_o to be calculated from the core radius a and the normalised frequency parameter V. For a step-index fibre this is

$$\frac{w_o}{a} = 0.632 + \frac{1.478}{V^{\frac{3}{2}}} + \frac{4.76}{V^6} \tag{3.6}$$

and the relationship holds for $1.5 < V < \infty$. Figure 3.4 shows how the ratio w_o/a varies with V, depending on the wavelength of the light used w_o may be greater or less than a, showing that more of the power contained in the mode is transmitted through the cladding at small values of V. To use this relationship a and the NA of the fibre must be known, however it is possible to measure A_{eff} experimentally

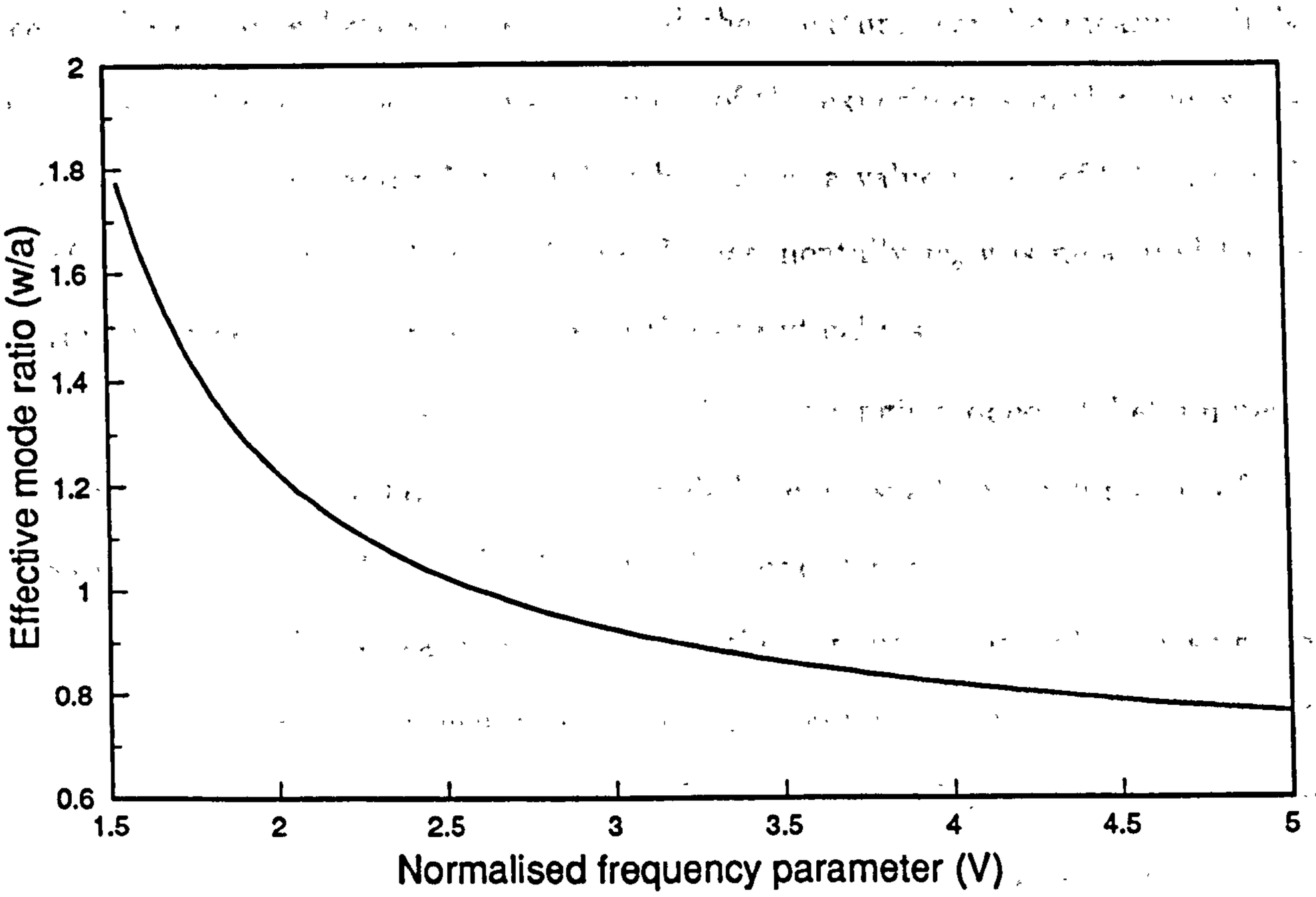

Figure 3.4: Effective core radius ratio against normalised frequency parameter

without knowing either of these. This can done by placing an aperture of a suitable size in the diverging beam exiting the fibre at a known distance z and measuring the power with and without the aperture giving its transmittance. For a Gaussian beam the transmittance through an aperture of radius r is

$$T = 1 - \exp\left(\frac{-2r^2}{w^2}\right) \tag{3.7}$$

where w is the beam radius at a distance z from the fibre and is connected to w_o by the relationship

$$w^2 = w_o^2\left(1 + \frac{z^2}{z_o^2}\right) \text{ and } z_o = \pi w_o^2/\lambda.$$

Normally $z/z_o \gg 1$ so that w is given by

$$w = \frac{z\lambda}{\pi w_o}. \tag{3.8}$$

Since z, the distance between the fibre and the aperture, can be measured it is simple to solve for w_o. The fibre used in most of the experiments in this thesis has a core radius of 2.4 μm and a NA of 0.11 which gives a value for w_o of 2.14 μm and A_{eff} of 1.44×10^{-11} m^2 at $\lambda = 514.5$ nm. Experimentally w_o was measured to be 2.16 μm giving very good agreement with the analytical result.

This fibre (LTI) is actually manufactured to be single-moded at helium-neon laser wavelengths and so the transmitted mode here is usually a combination of the two lowest order modes, LP_{01} and LP_{11}. The higher order mode is easily removed by putting a few tight bends near the input end of the fibre or by carefully choosing the launch conditions and the transmitted mode shows only the near Gaussian profile of the fundamental mode. This fibre was used for cost reasons but similar results were achieved when the experiments were repeated using both true single-mode (SM 450) and single-mode polarisation-maintaining argon-ion fibre (HB 450). Full details of all the fibres used in the SBS experiments are given in appendix A.

This section is concerned with SBS when there is no feedback so the small amount of reflectivity caused by the fibre end faces must be removed. Basically this can be done in two ways - index matching or polishing the fibre ends to an angle. The first method is the one which was used here simply because it was found to be quick and successful, although sometimes a little messy. A small reservoir was made to hold the index matching liquid, both glycerol and liquid paraffin were used, fronted by a microscope cover-slip at a small angle. A relatively large amount of fluid was required to stop any burning occurring due to the large intensities used. The end of the fibre was placed a few millimetres from the cover-slip which further reduces the reflectivity. The refractive index of glycerol is 1.4735 at 20°C for sodium light [CRC85] which will not be very different at 514.5 nm so the reflectivity is reduced to $\sim 3 \times 10^{-3}$% and the fibre was index matched at both ends to remove completely any cavity effects. Index matching gel is often used in fibre experiments and usually

has a refractive index closer to that of the core. This was not used since it was not found to scatter the incident light when used in the quantities required to stop any burning.

Polishing the end of the fibre to a small angle from the normal is also a successful way to eliminate reflections. This works because the light is reflected at an angle such that it is not guided back down the fibre. If the fibre axis is at an angle of θ radians to a front surface mirror of reflectivity R then the fraction ρ of the incident power that is successfully coupled back into the fibre can be approximated by [MAR86]

$$\rho = R\exp(-k_{cl}^2 w_o^2 \theta^2) \tag{3.9}$$

where k_{cl} is the propagation constant in the cladding. For an angle of only 3° $\rho = 0.018R$ for the fibre used, therefore an angle of only a few degrees is needed and this does not significantly affect the launch efficiency which is also true of the first method.

The spectral content of the signals was examined using a Fabry-Perot interferometer, either using a scanning Fabry-Perot and a detector to produce the usual oscilloscope traces or using a non-scanning interferometer with a divergent source to produce ring patterns on a screen. Parameters such as the free spectral range and the finesse of the Fabry-Perot were not measured and therefore the frequency shift of the scattered light was not calculated. Perhaps this was an experimental oversight but such measurements have been carried out by numerous other people, with no reported irregularities, and the experiments carried out here showed that the backwards scattered signal was frequency shifted from the pump and there was no reason to doubt that this was the Stokes component at the appropriate frequency shift. The real purpose of these experiments was not to measure the frequency separation of the pump and Stokes components but only to show how many frequency components were present.

3.2.2 Steady-State Characteristics with no Feedback

The threshold conditions for an SBS generator is as given in equation 2.31,

$$P_{TH} = \frac{21 A_{eff}}{g_B L_{eff}} \tag{3.10}$$

where the interaction length is $L_{eff} = \frac{1}{\alpha}(1 - \exp(-\alpha L))$.

This is the power required to give a small-signal Stokes gain which in the absence of pump depletion would amplify the weak spontaneous Brillouin Stokes to a level that implies total conversion of the pump wave. This is a purely theoretical definition and cannot in practice occur as pump depletion must occur to amplify the Stokes wave to such a level. For practical purposes the threshold power is the maximum laser power that can be launched into the fibre before the effects of SBS become detectable. Fortunately although these are two entirely different definitions the difference between the theoretical threshold based on small-signal theory and the experimental threshold based on detectability is small enough to be neglected. The amplification of a fictional Stokes intensity at the far end of the fibre, $z = L$, $I_S(L)$ by an input pump intensity $I_P(0)$ in the small-signal, where no pump deletion is considered, to output Stokes intensity $I_S(0)$ is given by

$$I_S(0) = I_S(L) \exp(I_P(0) g_B L_{eff} - \alpha L). \tag{3.11}$$

Substituting equation 3.10 into 3.11 gives

$$P_S(L) = P_{TH} \exp(\alpha L - 21) = \left(\frac{21 A_{eff}}{g_B L_{eff}}\right) \exp(\alpha L - 21). \tag{3.12}$$

Using the value for g_B calculated in section 2.3.2 of 2.4×10^{-11} $W^{-1}m$ the size of the spontaneous Brillouin signal is about 2.21×10^{-10} W for a fibre length of

100 m, an effective core area of 1.44×10^{-11} m^2 and a fibre loss $\alpha = 5.7 \times 10^{-3}$ m^{-1} (25 dB/km), these parameters corresponding to fibre LTI. The threshold power is calculated by summing all the contributions from the spontaneous scattering along the length of the fibre and so the size of this fictitious spontaneous 'input' signal obviously depends on the fibre length and effective core area. Using this as the probe signal it is now possible to show how the SBS and transmitted pump powers change with input pump power by solving for $I_S(0)$ and $I_P(L)$ in equations 3.3 and 3.4. These results together with the experimental ones using fibre LTI for the same fibre length are shown in figure 3.5 giving the saturation and gain depletion characteristics of the process.

At low pump power the SBS signal shows no real gain and is very small, too small to be seen experimentally and the transmitted pump experiences only linear loss due to the loss of the fibre. At about 0.1 W the reflected signal becomes large enough to be detected experimentally but this is due mostly to spurious reflections from optical components and so the experimental curve is a little higher than it should be. A little above this power threshold is reached, the SBS signal grows exponentially and the pump signal starts to show depletion due to its conversion to SBS. The pump depletion causes the gain of the process, $g_B I_P$, to decrease and so the rate of increase of the Stokes signal decreases as the pump power is further increased. At high powers it can be seen that the transmitted pump power saturates and shows no significant increase with increasing pump power and the SBS continues to grow but at a decreasing rate. Therefore the maximum power that can be transmitted by an optical fibre is limited by the process of SBS.

Figure 3.6 shows how the SBS threshold power decreases with increasing fibre length for the same fibre used above. The close agreement of the experimental points to the theoretical curve plotted using equation 3.10 and the agreement shown in figure 3.5 shows the suitability of the values chosen to calculate g_B. The effective

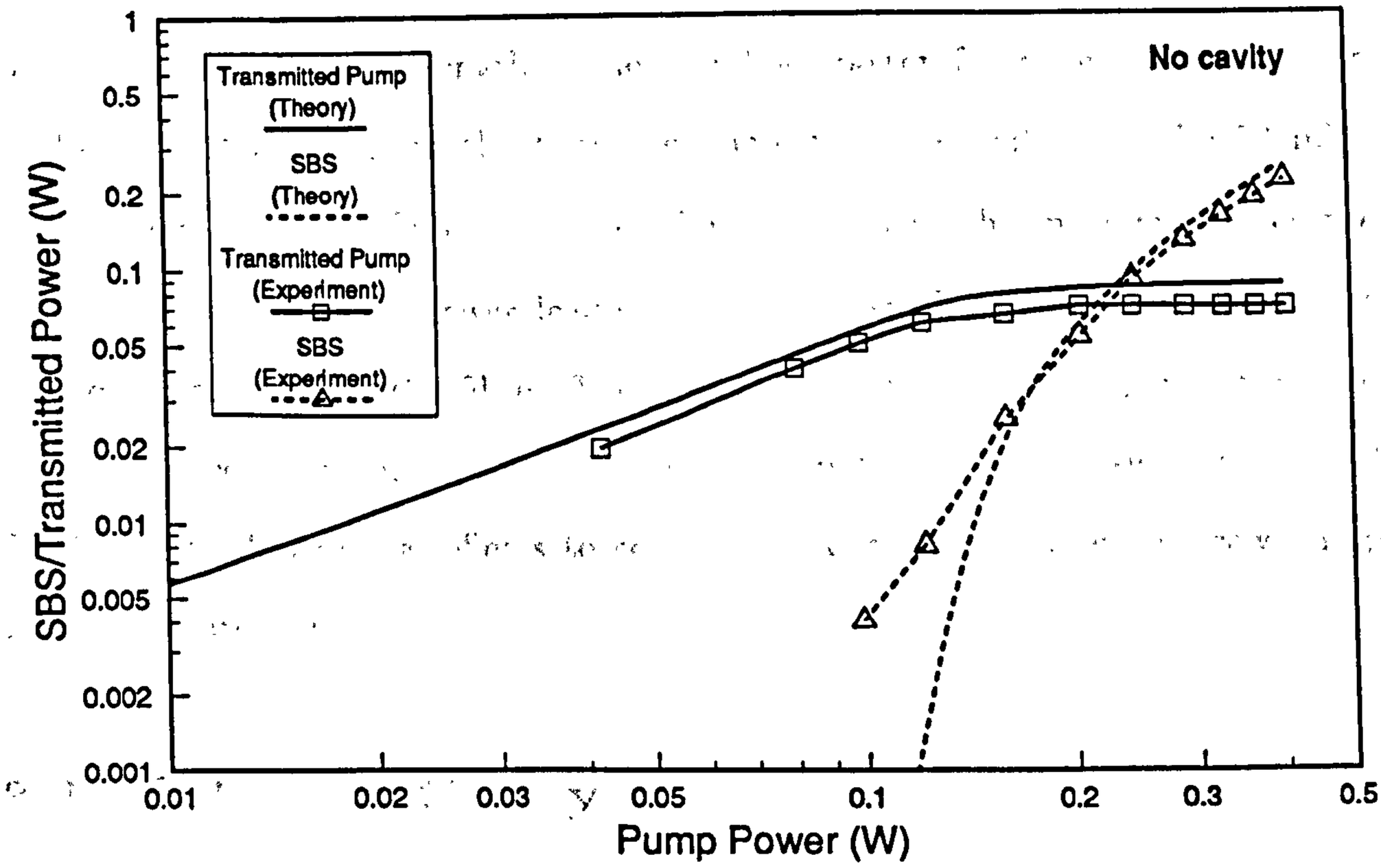

Figure 3.5: Steady state power characteristics for transmitted pump and SBS grown from spontaneous scattering.

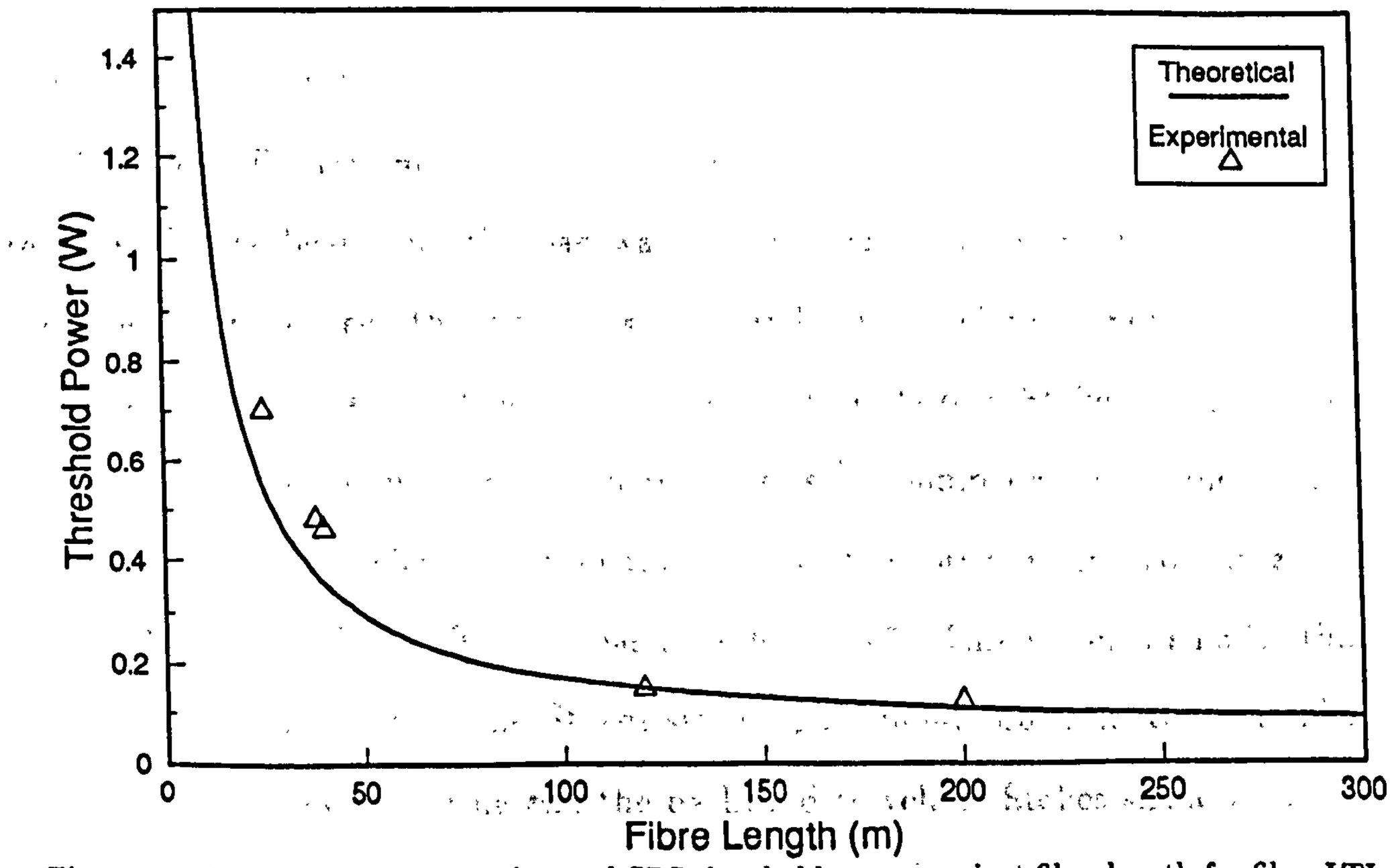

Figure 3.6: Theoretical and experimental SBS threshold power against fibre length for fibre LTI.

interaction length of the process, L_{eff}, reduces to $1/\alpha$ for long fibre lengths such that $\alpha L \gg 1$ and so the threshold power for long fibres is determined by the fibre loss α and not the fibre length. The threshold power for a long fibre is given by $P_{TH} = 21 A_{eff}\alpha/g_B$, for the fibre used here this is calculated to be 72 mW. However for a low-loss fibre the interaction length is much longer and hence the threshold power is much lower leading to a much smaller maximum power that can be transmitted by the fibre. The maximum single frequency power that can be transmitted by a long optical fibre may be limited to only a few mW by SBS [UES81] with detrimental effects to communications systems where narrow pump bandwidths are used.

3.3 SBS in a Cavity

The previous section studies SBS in an open-flow situation, the addition of feedback, whether by using external mirrors, by coating the fibre ends or merely from the natural Fresnel reflections of the air/glass interfaces changes the steady-state behaviour of the process.

If R_1 and R_2 are small then the interaction between the forward travelling reflected Stokes beam and the backwards travelling pump is much smaller than the interaction between the incident signals and can therefore be neglected. Also the reflected pump is not strong enough to produce its own Stokes signal. Again studying the small signal regime where there is no pump depletion due to conversion to SBS, the reflected pump travelling in the forward direction at $z = 0$ is $I_P(0)R_1R_2\exp(-2\alpha L)$ after one pass, see figure 3.7. This is much smaller than the incident pump $I_P(0)$. The Stokes signal again builds up from the amplification of spontaneous scattering and the backward travelling Stokes signal at $z = L$ is $I_S(L)R_1R_2\exp(g_oL_{eff} - 2\alpha L)$ after one pass. This however may be larger than

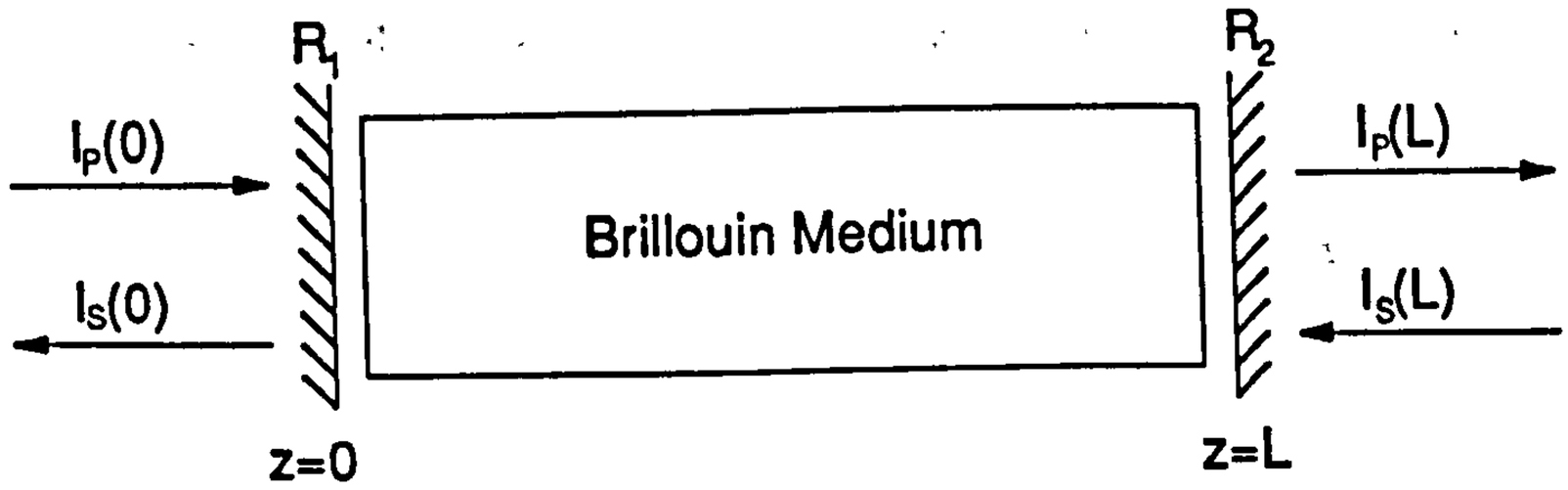

Figure 3.7: SBS build up in a Cavity

$I_S(L)$ and the Stokes signal may build up by amplifying this signal rather than the spontaneous noise signal. After n-passes through the fibre (or any Brillouin medium) the Stokes signal at $z = 0$ can be derived as

$$I_S(0) = I_S(L)\exp(g_o L_{eff} - \alpha L)\left(\frac{1-(R_1R_2\exp(g_oL_{eff}-2\alpha L)^n}{1-R_1R_2\exp(g_oL_{eff}-2\alpha L)}\right). \qquad (3.13)$$

So the threshold for gain is given by $R_1R_2\exp(g_oL_{eff} - 2\alpha L) = 1$, similar to that for a laser resonator.

3.3.1 Steady-State Characteristics in a Cavity with Natural Reflectivity

Using the experimental setup shown in figure 3.2 the index matching was removed and a cavity formed using only the natural reflectivity of the cleaved fibre ends. The reflectivity at either end is approximately 3.5% but its exact value depends on

how normal and uniformly the cleave is made. If the cleave is not exactly normal then some of the reflected light will not be guided back along the fibre and any non-uniformity will cause light to be scattered at the interface. Careful cleaving using one of the modern cleaving tools available will result in the a reflectivity close to the Fresnel limit.

The effect of adding reflectivity was to reduce the SBS threshold, increase the SBS conversion efficiency and reduce the saturation level for the transmitted pump. Figure 3.8 shows experimental curves for the transmitted pump and SBS comparing the cases with and without cavity, again for a 100 m piece of LTI fibre with an effective core area of 1.44×10^{-11} m^2. The two sets of curves show similar behaviour with the cavity set shifted to the left (lower power) due to the lower threshold power caused by adding reflectivity.

The effect of adding a cavity seems to produce the same effects as increasing the Brillouin gain therefore using the threshold value for the cavity experiment in equation 3.10 a value for the effective Brillouin gain can be calculated. For a 100 m piece of fibre where $\alpha = 5.7 \times 10^{-3}$ m^{-1} and effective cross-sectional area 1.44×10^{-11} m^2 the threshold power is about 100 mW when the cavity is formed by natural reflectivity compared to 165 mW when there is no cavity. The Brillouin gain is therefore enhanced by a factor of around 1.65 to give an effective gain of 3.97×10^{-11} W^{-1}m. Using this value to produce theoretical SBS and transmitted pump characteristics shows good agreement with the experimental results presented earlier, see figure 3.9.

3.4 SBS Amplifier

Perhaps the best way to study the theory of SBS is to use an oscillator-amplifier arrangement. An SBS amplifier produces gain by amplifying a probe signal at

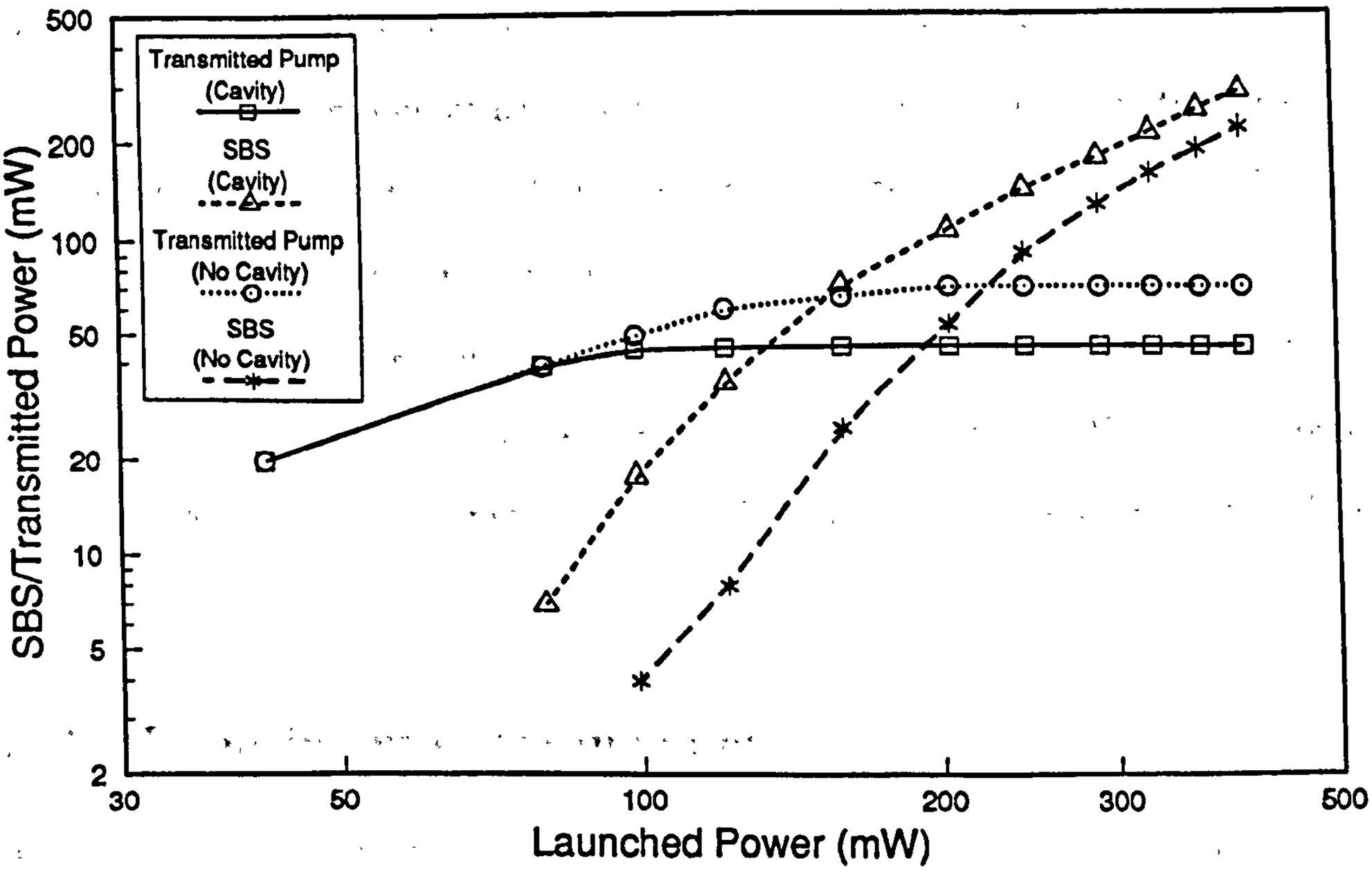

Figure 3.8: Steady state power characteristics for SBS with and without cavity

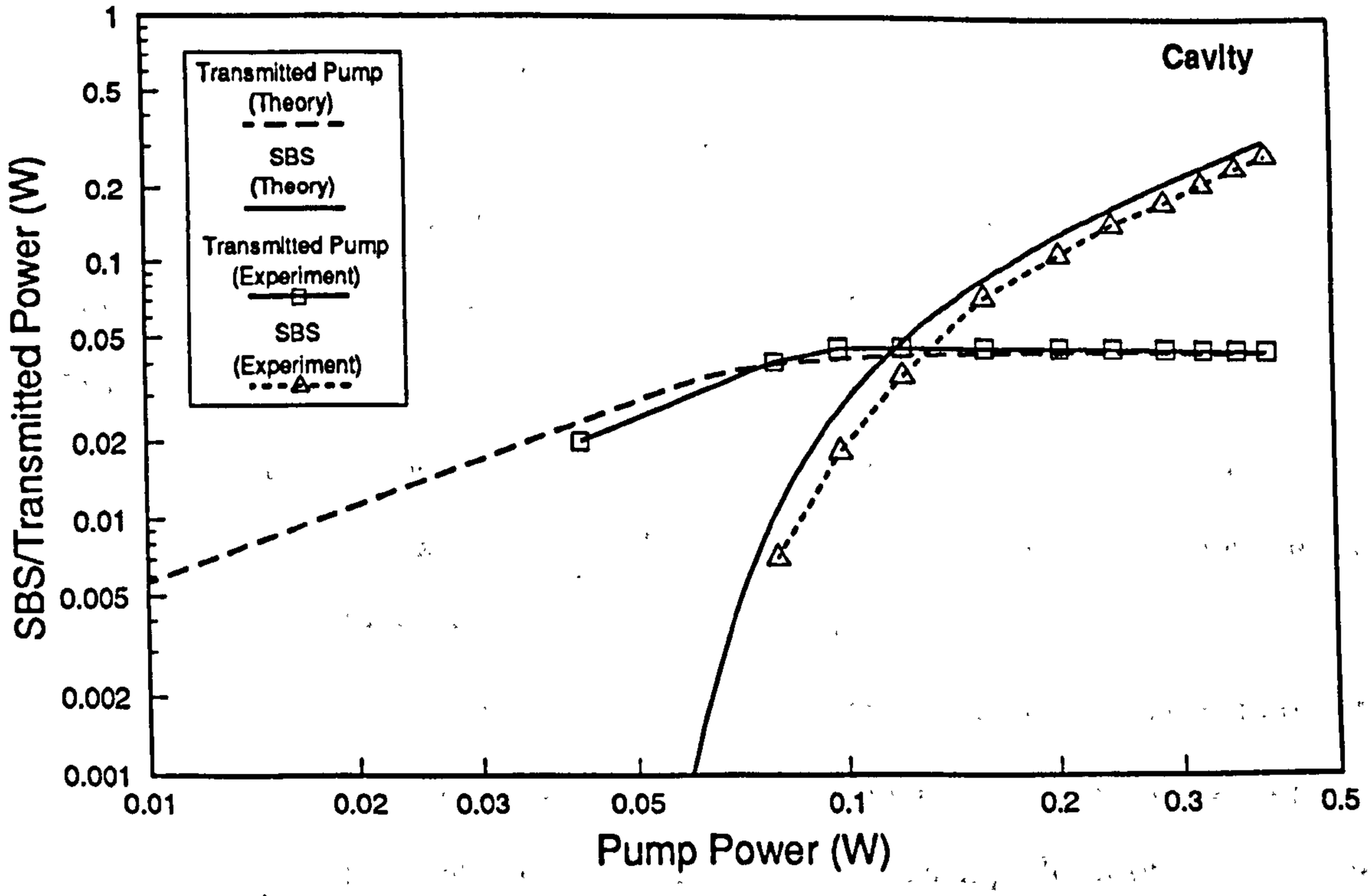

Figure 3.9: Steady state power characteristics for transmitted pump and SBS in a cavity.

the Stokes frequency shift from the pump which is generated externally and then introduced into the amplifier so as to be counter-propagating to the pump. In this case the signal was produced using an SBS generator with reflecting boundaries which under the correct operating conditions will produce a stable dc Stokes signal, the details of the operating conditions required and the full temporal behaviour of this probe signal are given later in chapter 5.

Identical fibre was used in the generator and the amplifier to ensure that the probe signal had exactly the correct frequency shift. Using another fibre would have meant a frequency mismatch due the Brillouin shift depending on the fibre parameters.

3.4.1 Experimental Arrangement

The experimental setup used is shown in figure 3.10. The pump signal was divided between the amplifier and generator either using a 70/30 beam splitter or a holographic grating. The grating divides the input power between the zeroth order and one of the first order with very little power going into any of the other orders. The ratio in which the beam is divided depends on the angle of grating to the incident beam so that at the appropriate angle almost all of the power can be directed into one of these orders thus allowing the beam to be divided in any ratio required. These devices are used in the production of holographic attenuators since the power in the zeroth order can be attenuated by $\sim$ 18dB with very little beam deviation since the grating needs only to be rotated a few degrees [RED88].

All possible feedback routes between the amplifier, generator and laser must be removed. It was therefore necessary to use a second isolator to stop the pump passing through the amplifier entering the generator and causing the probe to become unstable. This time a home-made Faraday isolator was used, the magnetic field being provided by an electro-magnet which allows the isolator to be used for more than

one wavelength. Unfortunately the Faraday rod used was anti-reflection coated for 1.06 μm and therefore has quite a large reflectivity at 514.5 nm, this did not cause any feedback problems, since the rod can be place at an angle, but it did reduce the maximum probe signal available.

Using a long fibre in the generator, the longest available was 134 m, means that a stable probe signal can be produced using as little of the pump power as possible, again fibre LTI was used. This leaves most of the pump power for characterising the amplifier. The amplifier fibre was index matched at both ends to remove all cavity effects.

3.4.2 Brillouin Gain in an SBS Amplifier

The Brillouin gain depends upon the relative polarisation states of the pump and Stokes fields. This polarisation dependence is accounted for by the factor K in equation 2.23 which means that in the case of SBS generated from the amplification of spontaneous scattering the gain halved and threshold power is therefore twice as large in fibres where the polarization state is completely scrambled than when it is maintained. However ordinary single-mode fibres neither completely scramble nor maintain the polarization, typically about 70% of the transmitted light will have the same polarisation as the input. Therefore when considering a Brillouin amplifier the gain will depend on the angle between the polarization of the pump and probe fields even if ordinary single mode fibre is used. Horiguchi et al. [HOR89] show that the gain for polarisation maintaining fibre when the pump is launched along one of the birefringent axes of the fibre is maximum when the pump and probe have the same polarisation and is almost zero when the angle between the two is 90°. Between these points the gain is found to follow a $\cos(2\theta)$ dependency, where θ is the angle between the pump and probe polarisations. When the pump is launched at an angle of 45° to axis the gain is about half of the maximum gain and varies little

as the angle between the pump and the probe polarisation is changed. However for ordinary single-mode fibre the gain was found to follow the relationship

$$g_B = G(1 + A\cos(2\theta)) \tag{3.14}$$

where G is the average gain and A is the amplitude of the gain variation normalised by the average gain G. Figure 3.11 shows how the SBS power varies as the pump polarisation is rotated using a half-wave plate. The half-wave plate changes the polarisation of the light it transmits by twice the angle it is rotated through. So rotating the wave plate through 45° rotates the probe polarisation through 90° and the gain characteristics repeat every 90°. Also plotted in this figure is the curve $P = 3.85(1 + 0.35\cos(2\theta))$, this does not exactly follow the experimental curve probably due to the gain saturation being larger when the gain is largest, i.e. when the pump and probe are of the same polarisation or perhaps due the beam-splitter showing some degree of polarisation dependent reflectivity. This leads to a smaller value of G being calculated and so the curves to not match completely.

3.4.3 Steady-State SBS Amplifier Characteristics

The gain characteristics for an SBS amplifier are found by solving equations 3.3 and 3.4. Figure 3.12 shows how the SBS power varies with probe power for different pump powers, (a) showing the experimental curves and (b) the theoretical ones for a amplifier fibre length of 100m. These curves show similar trends but not a one to one correspondence. Experimentally the probe power was difficult to keep constant due to variations in the output power of the Brillouin generator used. Also the value of g_B used to evaluate the theoretical curves may not be correct due to the angle between the pump and probe polarisations being arbitrary, this was however kept constant throughout the experiment. The experiment was conducted at pump

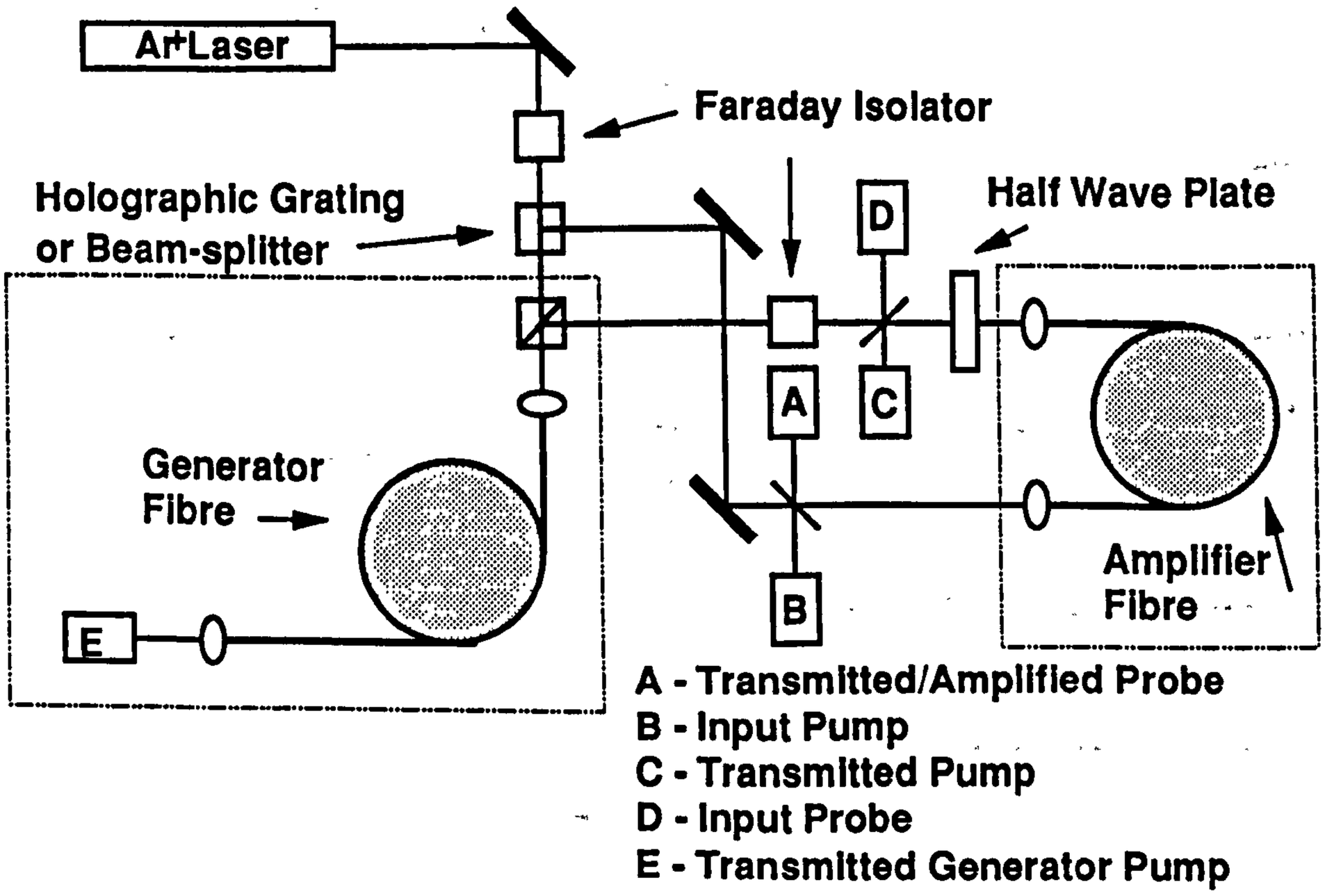

Figure 3.10: Setup for SBS amplifier

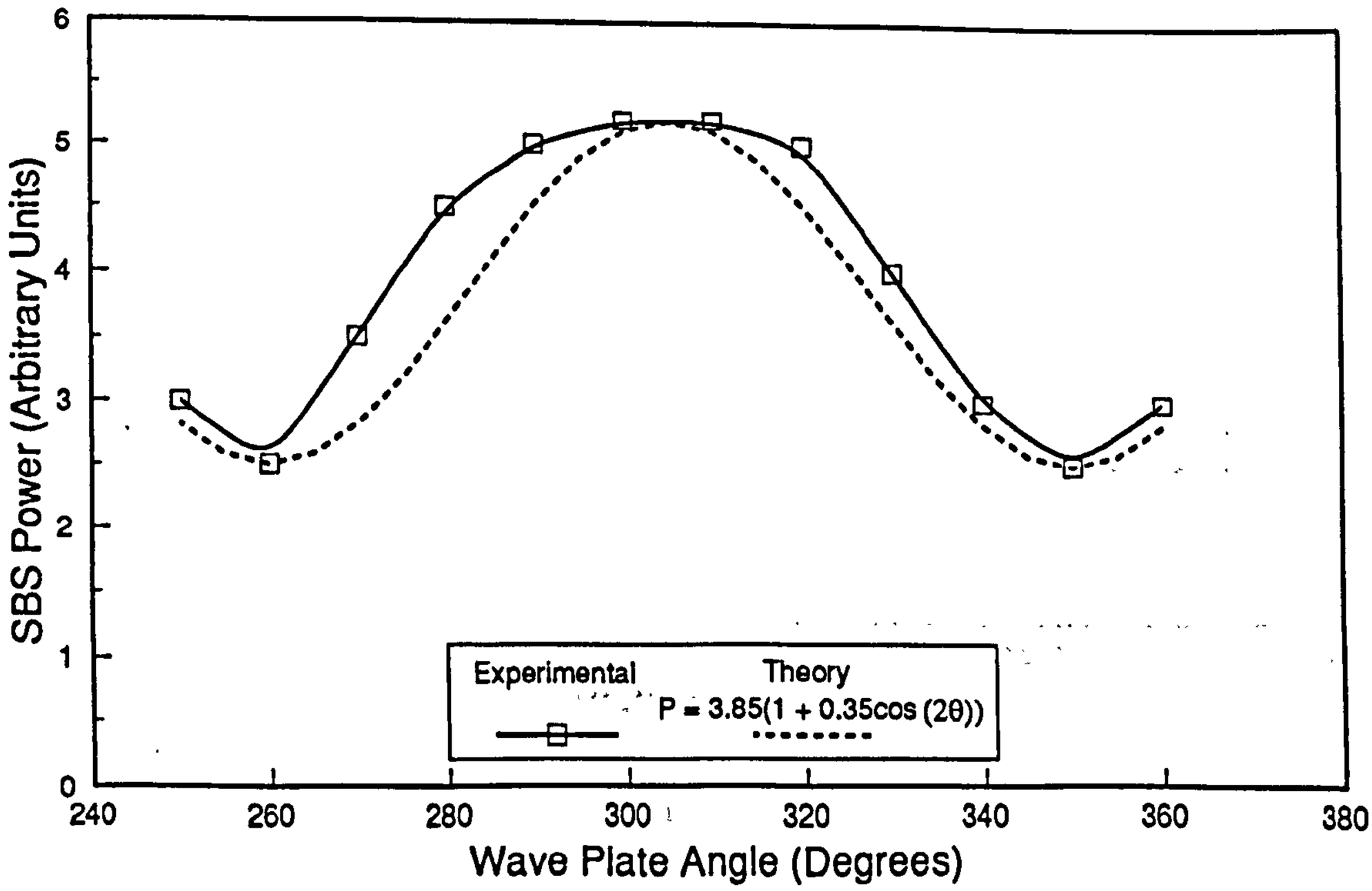

Figure 3.11: Polarization dependence of Brillouin gain in ordinary single-mode fibre

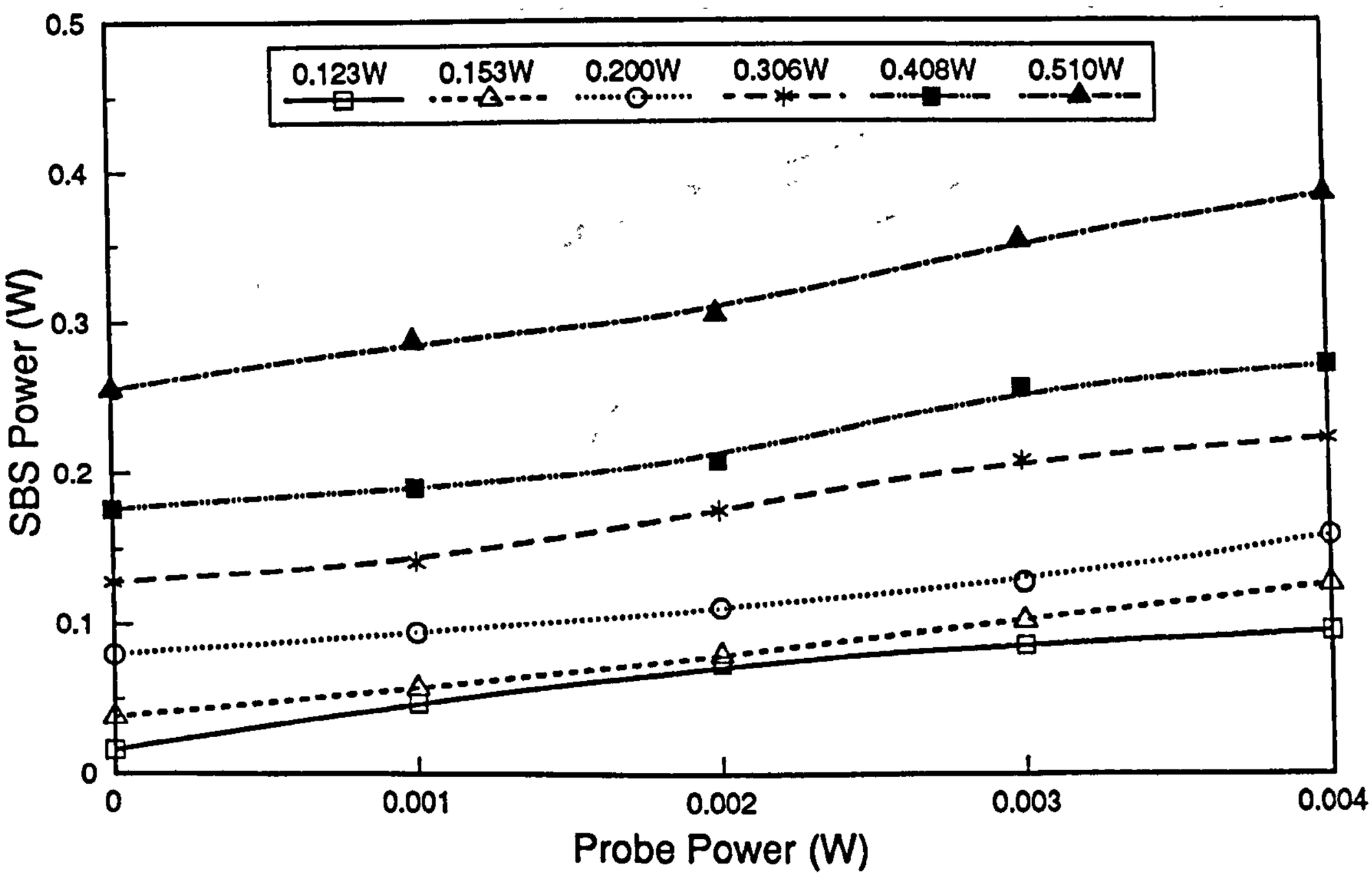

(a)

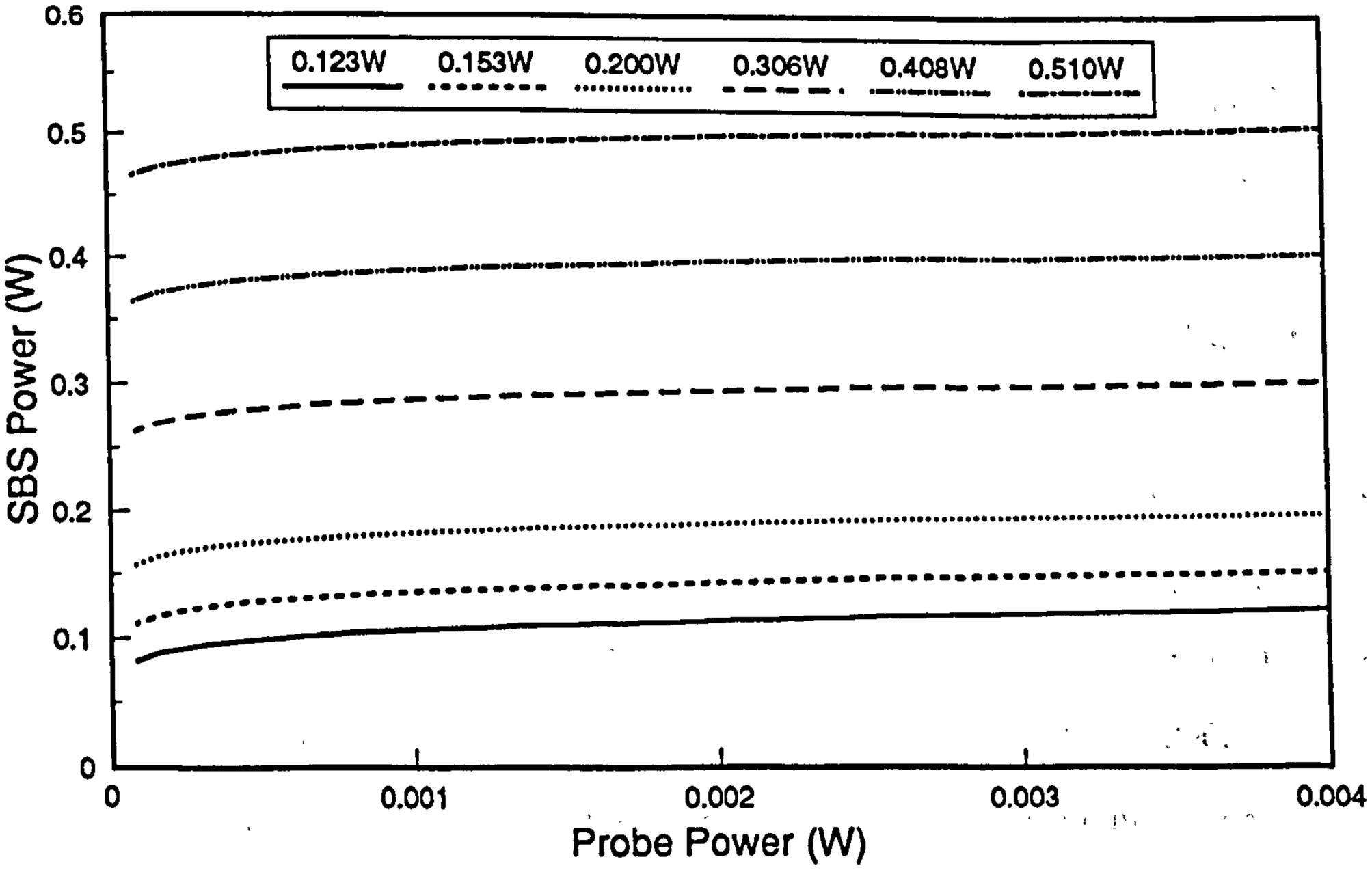

(b)

Figure 3.12: Gain characteristics for a SBS amplifier : (a) experimental and (b) theoretical. Showing the variation of SBS power with probe power for different pump powers.

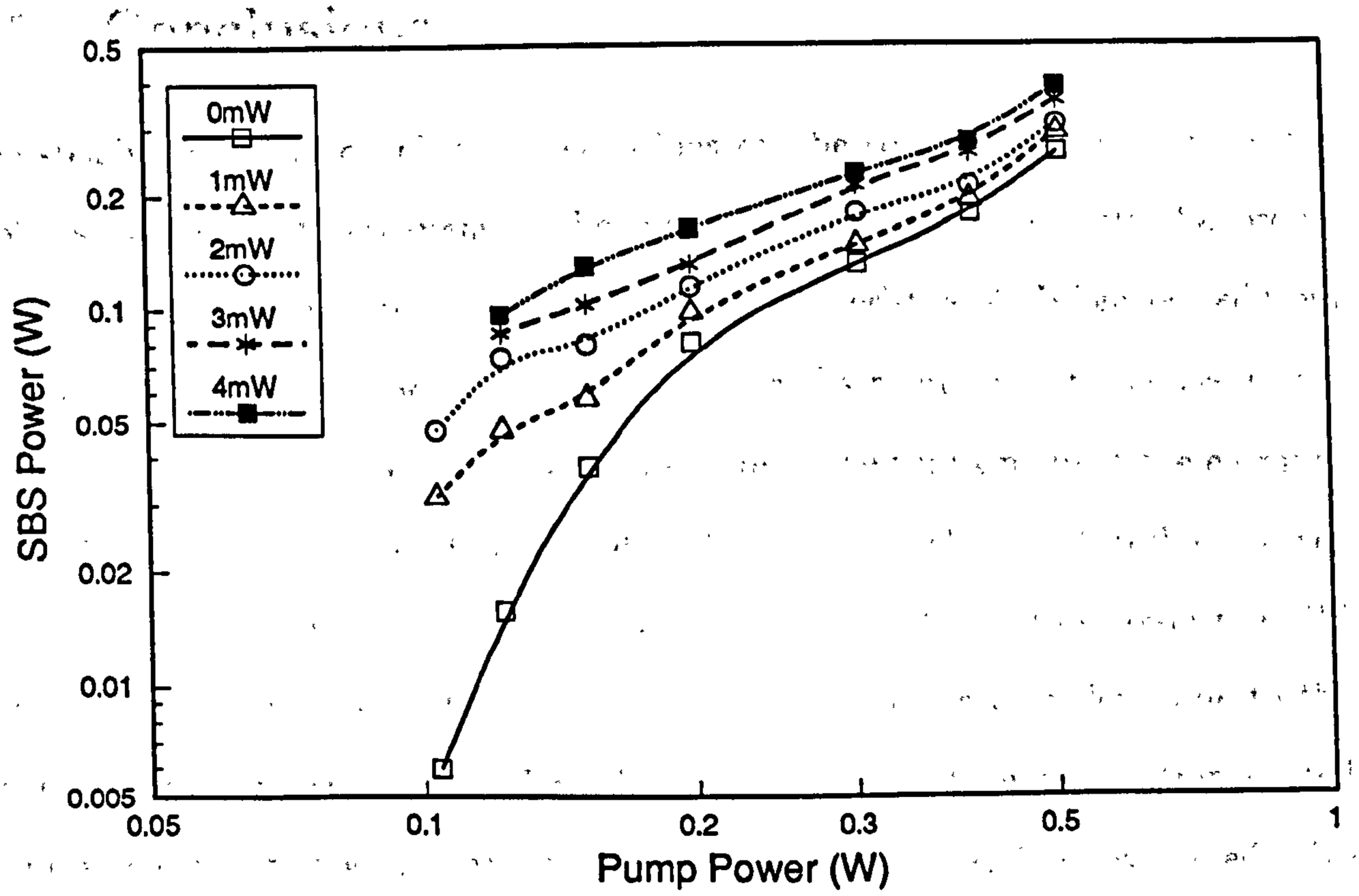

Figure 3.13: Amplifier output power against pump power for various probe powers

powers which are above threshold for this fibre length - this was done to obtain SBS signals which were large enough to measure. Even so the injected pump signals are much larger than the probe due to spontaneous scattering so this should not affect the results.

To compare the amplifier characteristics to those for SBS building up from spontaneous scattering figure 3.13 shows the SBS output power against pump power for various probe signals. The curves show that the amplifier is operating in the saturated regime where the pump is heavily depleted and the output power (SBS power) varies almost linearly with both pump and probe power. Operating in this area means that the gains obtained are modest, typically only 100 to 200, but the conversion of pump to SBS is large with 75% of a 0.5 W pump being converted to SBS using a 4 mW probe signal.

3.5 Conclusions

The steady-state SBS coupled rate equations can be solved to show how the the Stokes signal grows at the expense of the pump. Calculating the intensity of a 'probe' signal from the threshold conditions allows the characteristics of SBS generated from spontaneous scattering to be produced. The spatial distribution of the powers within the fibre shows that the both SBS and pump are at their maximum at the entrance of the fibre, z=0, and then decay rapidly. The SBS signal has a threshold power determined by the Brillouin gain and interaction length. Above this power the SBS signal grows exponentially at first, but then the rate of increase slows due to the decrease in gain caused by pump depletion. SBS severely attenuates the transmitted pump signal and at high powers limits this to a power determined by the effective interaction length and gain of the fibre. Adding a cavity, even a poor one, around the system increases the effective Brillouin gain and therefore increases the SBS conversion efficiency and decreases the threshold power. Apart from the increased gain the steady-state SBS behaviour with and without a cavity are identical.

In an amplifier the gain depends on the angle between the pump and probe polarisations, even in ordinary non-high birefringent fibres. This is found to follow a $\cos(2\theta)$ relationship, where θ is the angle between the pump and the probe polarisations. Operating in the saturated regime, where the pump is heavily depleted due to the high SBS conversion efficiency, the amplifier output was found to vary almost linearly with both pump and probe power.

Chapter 4

Temporal Behaviour of SBS with no Feedback

4.1 Introduction

The previous chapter dealt with the steady-state behaviour of the SBS process, now the temporal behaviour is investigated in the absence of external feedback for both the SBS generator and amplifier. The use of optical fibres allows this to be done in the ideal conditions of a cw pump. Details of the data acquisition procedures are given and the results obtained are compared to the theoretical ones which were obtained by solving equations 2.39 to 2.41 [LU91a].

4.2 SBS Generator

The experimental arrangement used here is the same as that detailed in section 3.2 except photodiodes were used instead of a power meter. Again the fibre was index matched at both ends to remove all cavity effects.

The detectors used (D_1, D_2 and D_3) were simple biased photodiodes, type BPX-65, with typical rise times of 0.5 ns, giving a bandwidth of 700 MHz (using the

relationship rise time × bandwidth = 0.35), and a cut-off frequency of 500 MHz. These together with an oscilloscope (Tektronix 7104) allow the temporal behaviour of the signals to be studied. The available information may often be clearer when viewed in a frequency domain rather than in time, a spectrum analyser (HP8590A) was available for spectral analysis. To achieve the required resolution the sweep time of the spectrum analyser used was relatively long, 1.2 s for a resolution bandwidth of 30 kHz, so if the signal is changing over this time, as was often the case, then the spectrum will contain elements of all the different temporal behaviours. Phase portrait reconstruction can also be achieved directly by using the oscilloscope in x-y mode and plotting the SBS against the transmitted pump signal. The oscilloscope has an intrinsic delay between the two channels of 50 ns which can be altered, if required, by adding a delay line made from coaxial cable of the required length in the appropriate position. These facilities allowed the temporal, frequency and phase space behaviour to be examined directly in the laboratory.

4.2.1 Data Acquisition and Processing

In parallel to the above facilities a transient digitiser (LeCroy 8828C) was also used to capture and transfer data to a Masscomp computer for subsequent processing and analysis. The LeCroy 8828C is an 8-bit single channel digitiser and has a range of data sampling rates available between 5 ns and 320 ns with normally 16K points being recorded. A suite of computer programs allowed time series, frequency spectra and phase portraits to be constructed from the digitised points.

Power spectra are formed by taking the fast Fourier transform of the time series, hence the frequency span is determined by the sampling rate Δt, span $= 1/2\Delta t$ and the resolution by the number of data points n used, resolution $= 1/n\Delta t$. Using a sampling rate of 5 ns and 16K points a span of 100 MHz and a resolution of 12.2 kHz are achieved. When recording data it is important that the sampling rate is fast

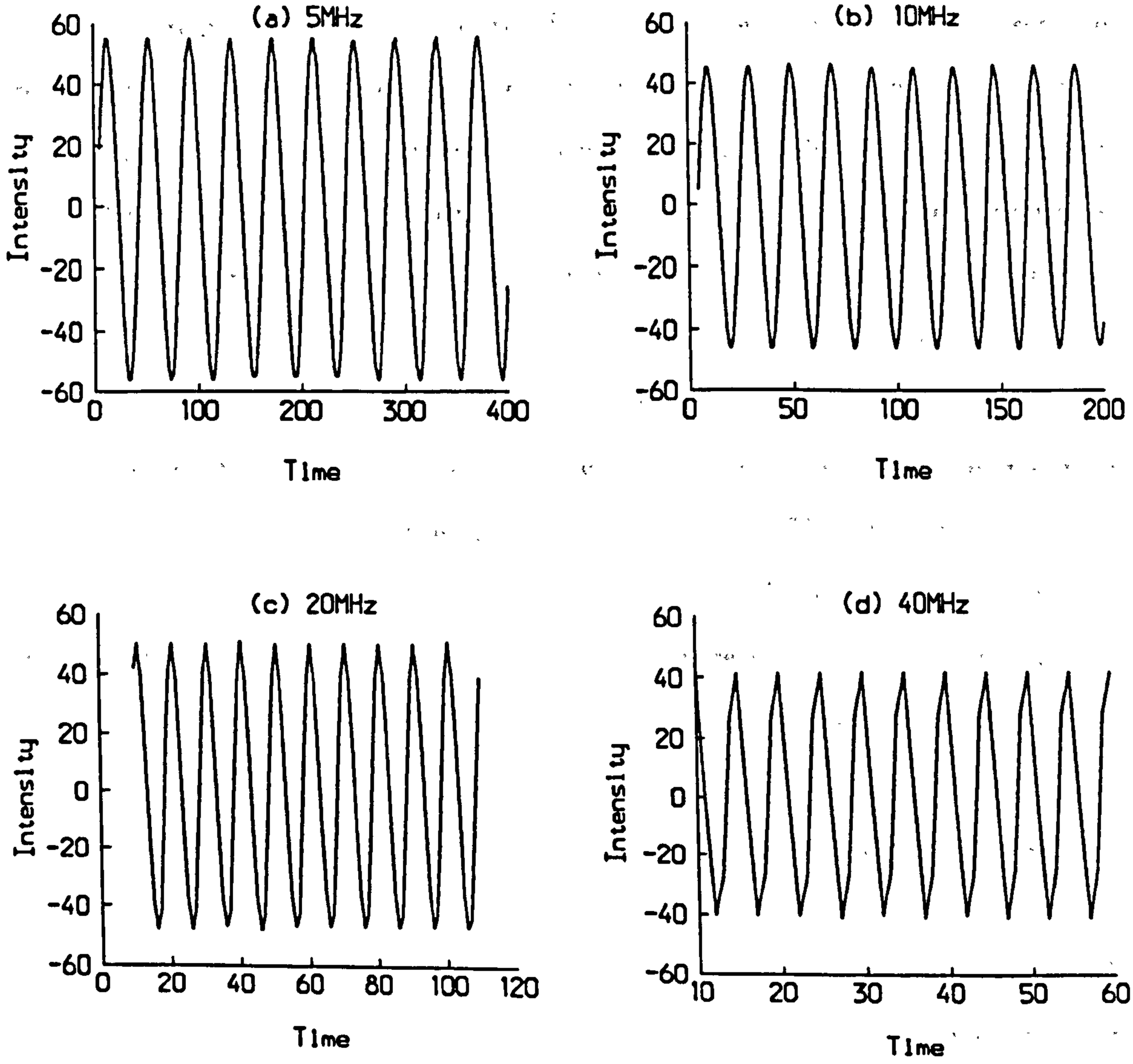

Figure 4.1: Digitised sine waves

enough compared to the period of the observed waveform or information may be lost and the recorded waveform may be distorted. The fastest sampling rate available is 5 ns and the shortest period observed is about 30 ns giving only about 6 points per period. The effect of reducing the number of digitisation points per period was studied using a signal generator to produce a sine wave which was recorded and the time series then reconstructed to show if distortion had occurred. The results are shown in figure 4.1 using sine waves of frequencies (a) 5 MHz, (b) 10 MHz, (c) 20 MHz and (d) 40 MHz.

As the frequency was increased and fewer points per period were digitised the reconstructed sine waves become more distorted and the recorded waveforms begin to look 'sharp'. A frequency of 40 MHz corresponds to 5 points per period, similar to the fastest frequency experimentally observed, and the reconstructed sine waves are clearly deformed. The power spectra generated from this set of data are shown in figure 4.2. The Fourier transform of a perfect sine wave should show only a single frequency, but the signal generator unfortunately does not provide a perfect sine wave and hence the power spectra, even those examined using the spectrum analyser, show harmonics of the fundamental frequency. The harmonics are much smaller than the fundamental frequency, typically ~ 30 dB less. Although the time series may become distorted as the frequency is increased the power spectra seem to remain unaffected. In fact a Fourier transform may be conducted under certain circumstances with as few as 2 points per period.

Since some of the data to be recorded contains waveforms with periods of ~ 30 ns the time series will be slightly distorted and some of the very high frequency components may be lost but the power spectra should be unaffected. Data processing such as the spline fitting of points may help to smooth the data but the only satisfactory way to correct the digitised data is to increase the sampling rate which, with the digitiser used, is not possible. However comparison of the digitised data and that directly from the oscilloscope shows that the distortion is not too great.

It is possible to construct a multi-dimensional phase portrait from measurement of a single variable $V(t)$ [PAC80], sampled at intervals t_k by plotting $V(t_k)$ against $V(t_k + \tau)$ for $k = 1 \ldots n$ where τ is the delay time. The value of τ can in principle be chosen almost arbitrarily for an infinite amount of noise free data. However, for a finite amount of data of finite resolution there is an optimum choice of τ which is found by trial and error. As can clearly be seen in figure 4.3, changing the value of τ rotates the phase portrait in phase space. This shows a limit cycle type behaviour

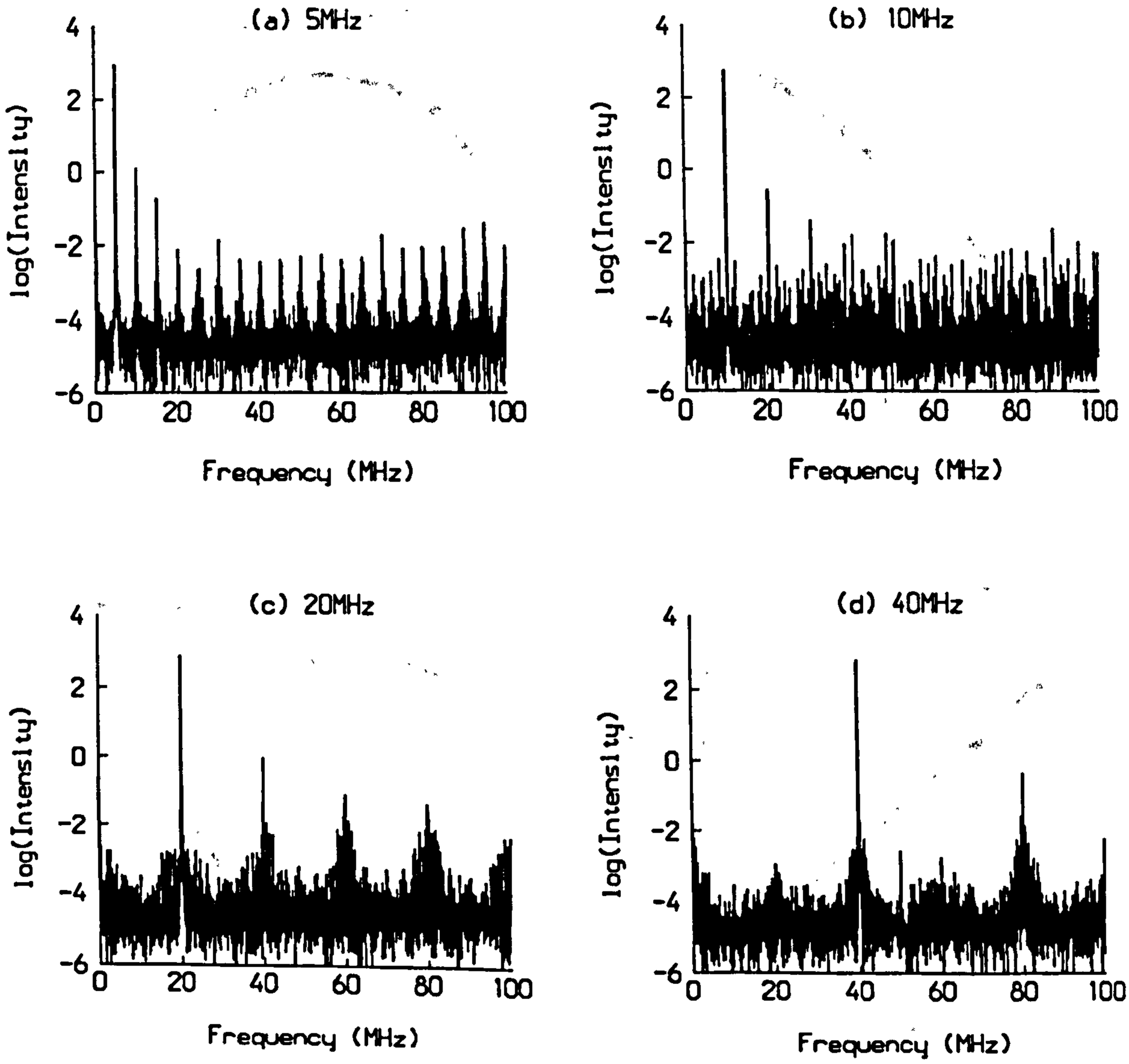

Figure 4.2: Fourier transforms of digitised sine waves

constructed from a digitised 5 MHz sine wave using 3000 points, varying τ by 10, in this case, rotates the phase portrait through 90°. This is similar to Lissajous figures where the phase difference is varied. The phase portraits may also suffer distortions due to the fact that they are created from time series.

4.2.2 Digitisation Optimisation

When sampling a bipolar signal the digitiser requires an input of between -255 mV and +255 mV. To get this voltage from the photodiodes unfortunately meant that

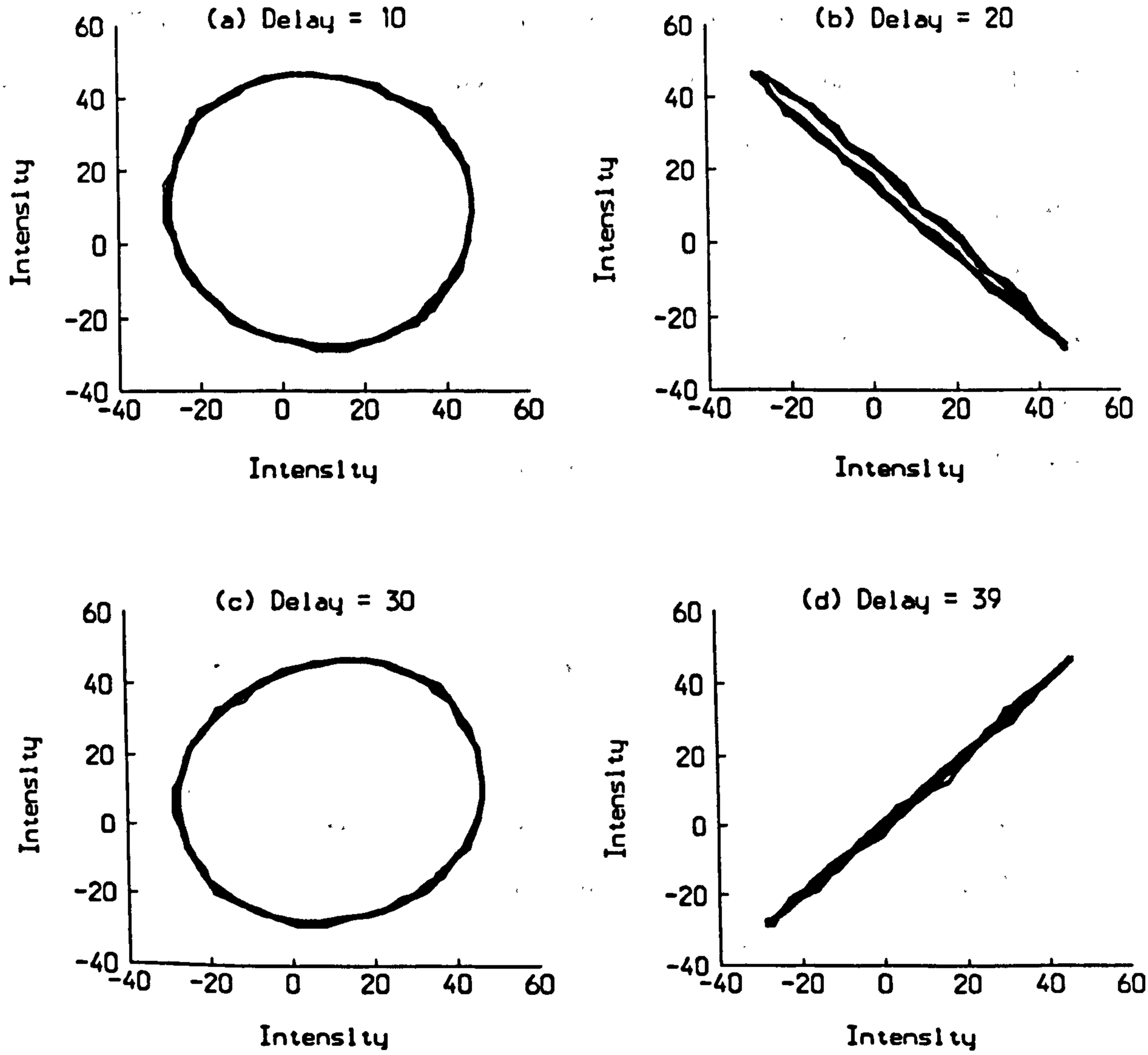

Figure 4.3: Phase portrait rotation by varying τ

amplifiers had to be used. These have a bandwidth of ~300 MHz and therefore amplify the signal satisfactorily but they introduce some extra noise to the signal. The amplifiers also add a dc off-set to the signal which can be removed using a capacitor to block the dc component leaving only the ac part for digitisation.

The digitiser has an 8-bit resolution meaning that the digitised points can have integer values between -127 and 128. To gain the best resolution clearly this digitisation window should be entirely filled by making the input voltage as large as possible between -255 mV and +255 mV without saturating either the detectors or

amplifiers. The signal was not always bipolar and in some cases was almost totally positive meaning that only half of the digitisation window could be used. The size of the signal to the detectors also changes as the laser power, and hence the SBS and transmitted power, was increased and so the digitisation window was not always optimised. The amplifiers cause a background digitisation noise of 5 units which varies slowly compared to the frequencies of the signals recorded. Typical signals were about 100 units giving a signal to noise ratio of 20 to 1. Since the digitiser has only one channel simultaneous recording of the SBS and the transmitted pump signals was not possible.

4.3 Temporal SBS Behaviour

The laser produces a stable dc steady-state input signal which was monitored at D_2. Figure 4.4 (a) shows the clean square waveform of the chopped input signal. In contrast to this the SBS signal was found to show sustained aperiodic oscillations with modulation depths of almost 100% under all operating conditions including those close to threshold. This was also found to be the case for all the various fibres and lengths investigated, between 25 m and 300 m, with only the threshold powers changing. Figure 4.4 also shows representative recordings of the chopped signal for (b) the SBS signal for a pump power close to threshold, (c) at a higher power together with (d) the transmitted pump at the higher power all for a 200 m piece of fibre LTI.

Figure 4.4 (b) shows the chopped SBS signal for a launched power of 0.12 W, close to the threshold power of ~ 105 mW. The signal consists of a large modulated portion and a small unmodulated part. The unmodulated part of the signal is due to spurious reflection from uncoated optical elements, probably the microscope objective and cover-slip. As the pump power is increased the SBS signal grows

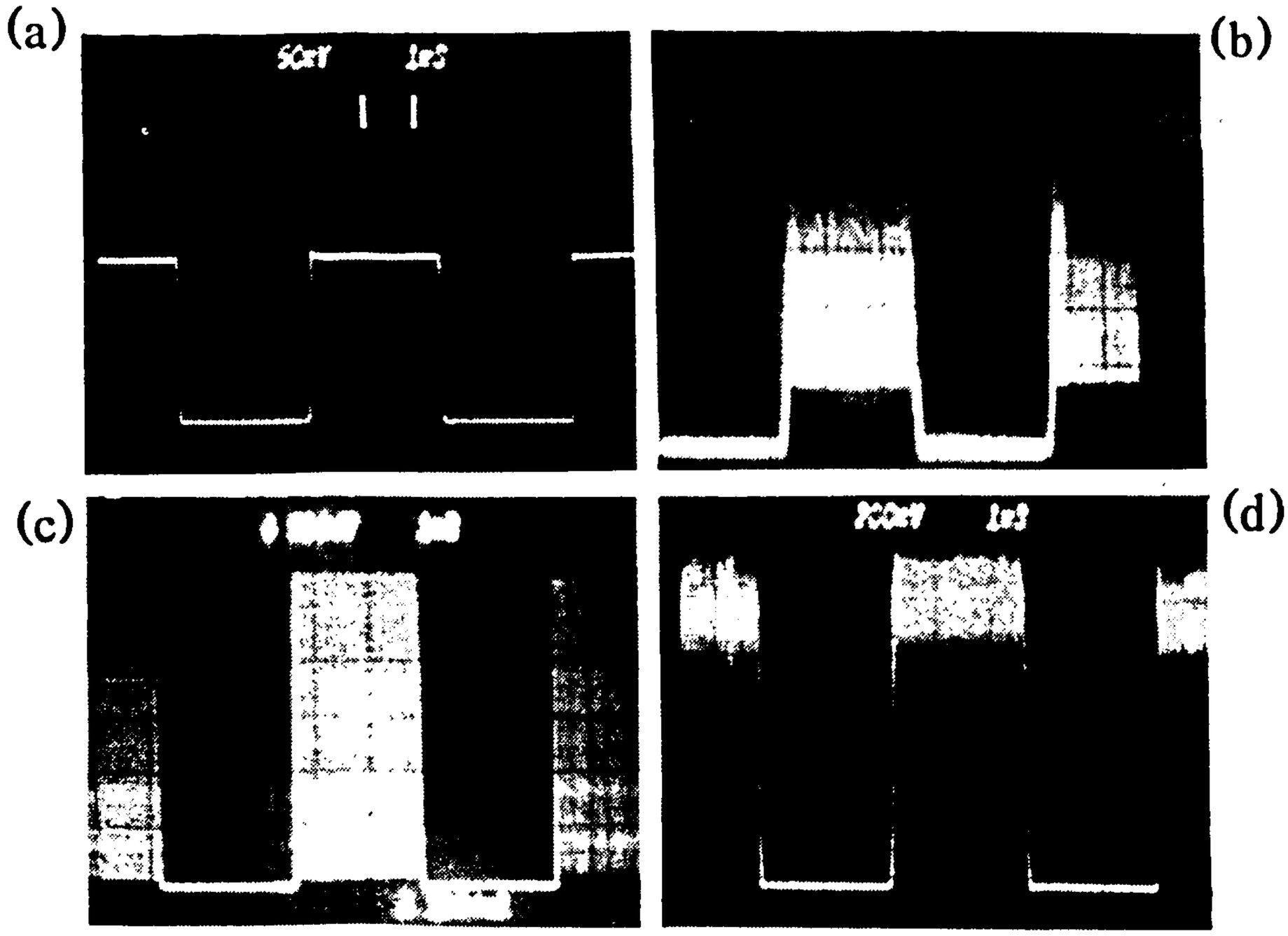

Figure 4.4: Temporal recording of (a) the chopped pump, (b) and (c) the SBS and (d) the transmitted pump signals, (time scale is 1 ms/div throughout).

exponentially while the reflection increases only linearly. Hence the SBS signal for the higher launched power of 0.33 W, figure 4.4 (c), is now much larger than this reflection and the signal shows almost 100% modulation. Figure 4.4 (d) shows the transmitted pump signal for the same power. The ratio of the stable portion of the waveform to the modulated part gives a measure of the SBS conversion efficiency, in this case $\sim 35\%$. The expanded time scale used in figure 4.5 (a) shows clearly the stable nature of the pump signal contrasting with the aperiodic behaviour of both (c) the SBS and (e) the transmitted pump signals corresponding to the chopped signals shown in figure 4.4 (c) and (d). The power spectra of the SBS and the transmitted pump traces (d) and (f) both show pure broadband features with no discrete frequencies, the SBS having a bandwidth of ~45 MHz FWHM. The tem-

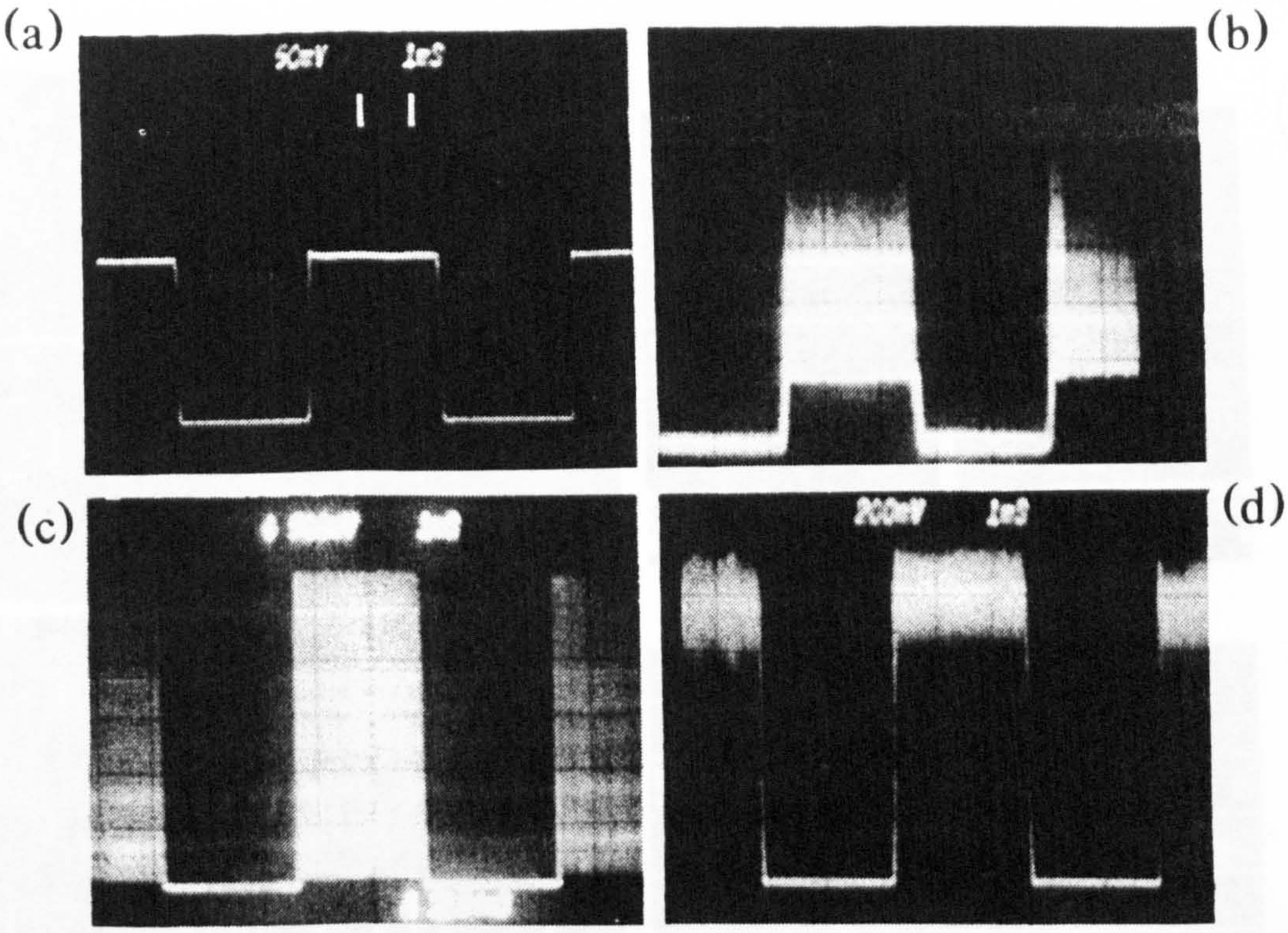

Figure 4.4: Temporal recording of (a) the chopped pump, (b) and (c) the SBS and (d) the transmitted pump signals, (time scale is 1 ms/div throughout).

exponentially while the reflection increases only linearly. Hence the SBS signal for the higher launched power of 0.33 W, figure 4.4 (c), is now much larger than this reflection and the signal shows almost 100% modulation. Figure 4.4 (d) shows the transmitted pump signal for the same power. The ratio of the stable portion of the waveform to the modulated part gives a measure of the SBS conversion efficiency, in this case $\sim 35\%$. The expanded time scale used in figure 4.5 (a) shows clearly the stable nature of the pump signal contrasting with the aperiodic behaviour of both (c) the SBS and (e) the transmitted pump signals corresponding to the chopped signals shown in figure 4.4 (c) and (d). The power spectra of the SBS and the transmitted pump traces (d) and (f) both show pure broadband features with no discrete frequencies, the SBS having a bandwidth of ~45 MHz FWHM. The tem-

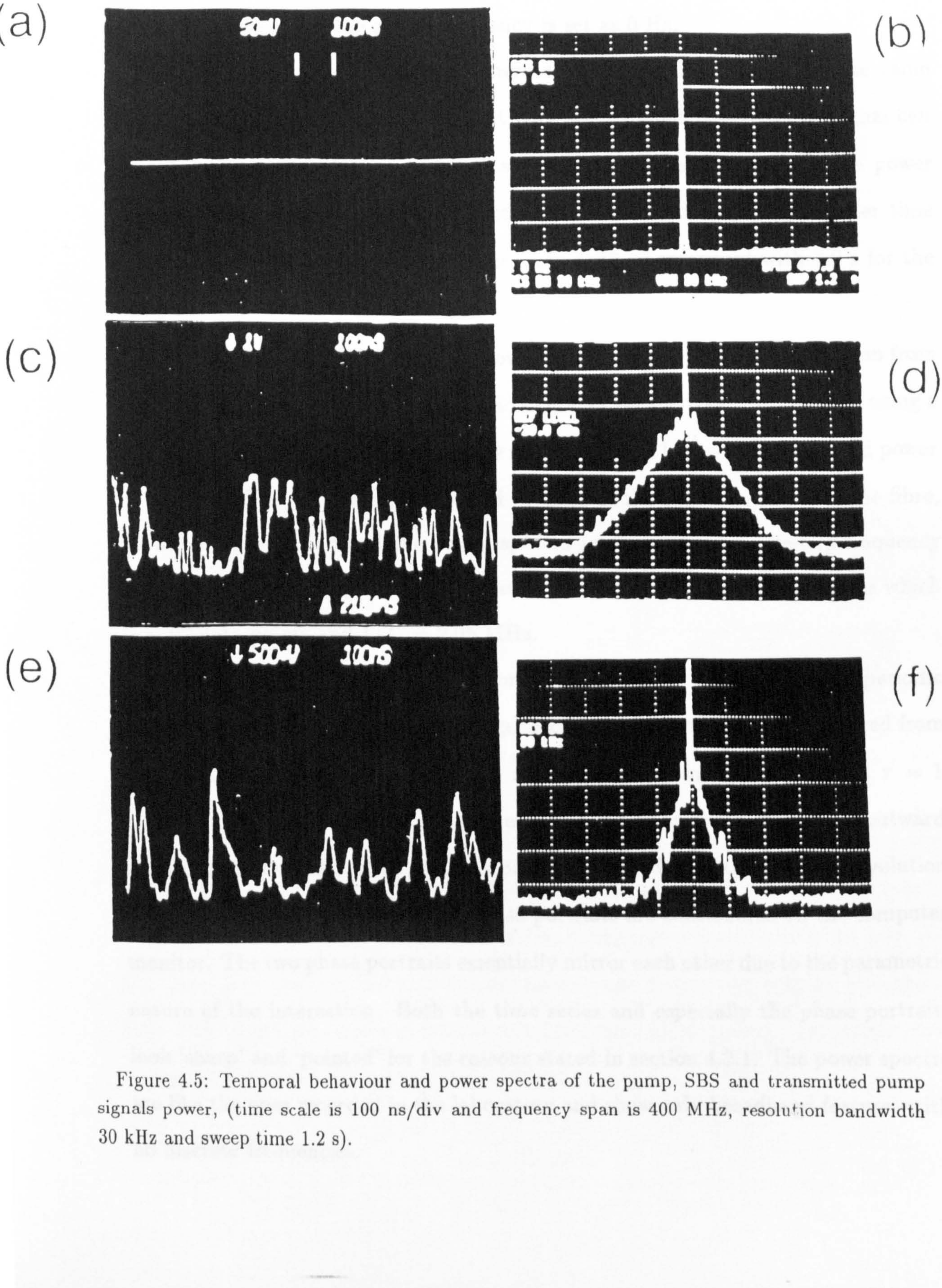

Figure 4.5: Temporal behaviour and power spectra of the pump, SBS and transmitted pump signals power, (time scale is 100 ns/div and frequency span is 400 MHz, resolution bandwidth 30 kHz and sweep time 1.2 s).

poral recordings in figure 4.5 have a time scale of 100 ns/division and the power spectra have a span of 400 MHz, a resolution bandwidth of 30 kHz, a vertical scale of 10 dB/division and the centre frequency is set as 0 Hz.

Time series and power spectra generated from digitised data show the same features. It should be remembered that only the modulated part of the signal can recorded because of the dc blocking capacitor. Also when comparing the power spectra those formed from the digitised data are taken over a much shorter time than those using the spectrum analyser, only $\sim 82\ \mu$s compared with 1.2 s for the analyser.

Figure 4.6 shows the times series, power spectrum and phase portrait taken from digitised recordings of the SBS signal and figure 4.7 for the transmitted pump using a sampling rate of 5 ns. These results are for 100 m of LTI fibre and a launched power of 570 mW. The time series are scaled in units of the single-trip time of the fibre, T_r where $T_r = n_{co}L/c$ and the power spectra in units of the single-trip frequency $1/T_r$. For this fibre length and a core refractive index $n_{co} = 1.46$, $T_r = 487$ ns which is ~ 97 data points and $1/T_r = 2.05$ MHz.

Traces (a), which are constructed from 400 data points, clearly show the aperiodic behaviour, while traces (b) show a longer section of the time series constructed from 4000 points. The phase portraits are reconstructed from 2000 points and $\tau = 1$ and 3 for figures 4.6 (c) and 4.7 (c) respectively. These both exhibit an outward spiraling and folding motion which is particularly evident if the temporal evolution of the trajectory is followed as the phase portraits are constructed on the computer monitor. The two phase portraits essentially mirror each other due to the parametric nature of the interaction. Both the time series and especially the phase portraits look 'sharp' and 'pointed' for the reasons stated in section 4.2.1. The power spectra are like the ones recorded in the laboratory and show only broadband features with no discrete frequencies.

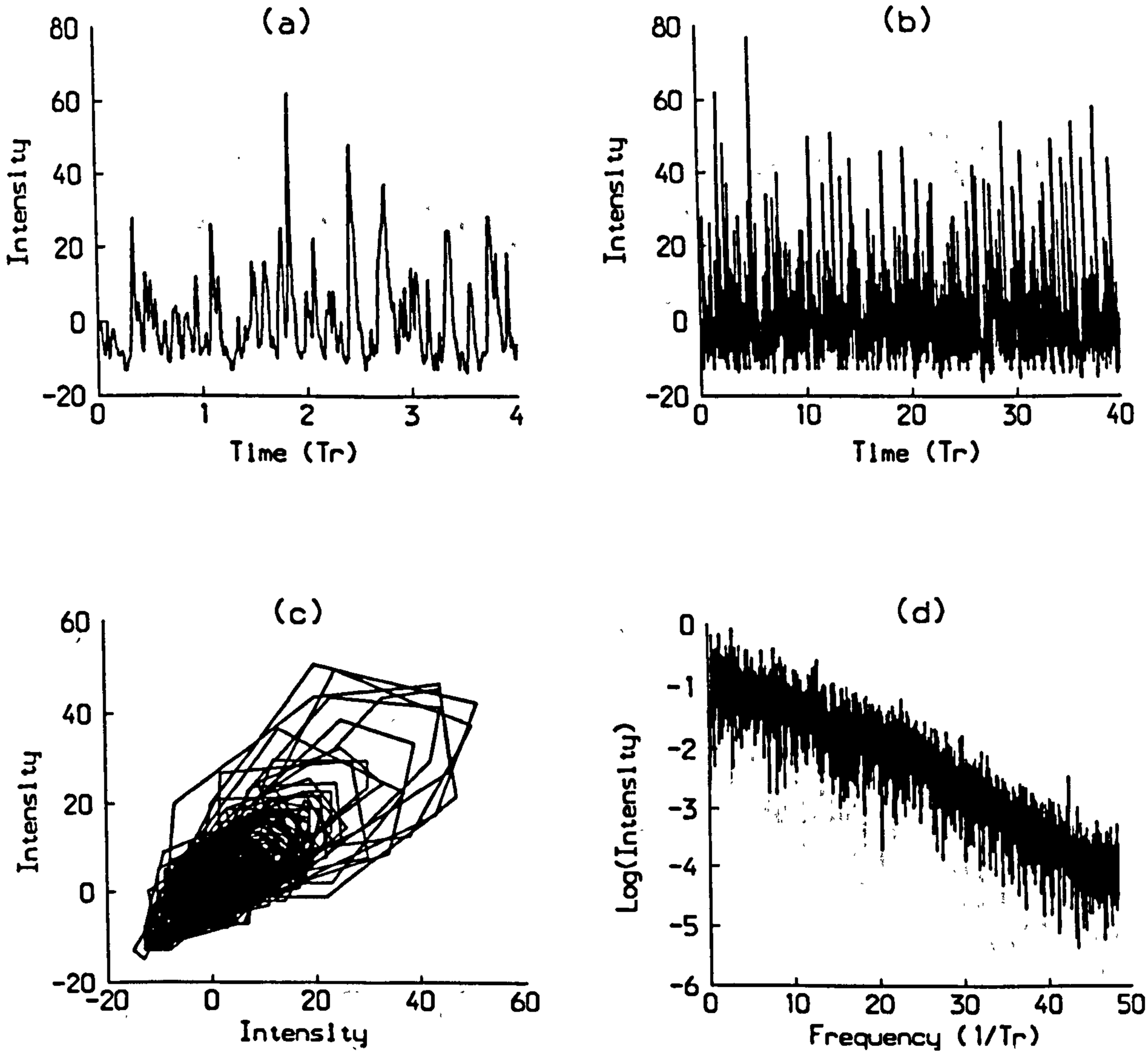

Figure 4.6: Digitised data showing (a) times series for 400 points, (b) time series for 4000 points, (c) Phase portrait and (d) power spectrum for the SBS signal from a 100 m fibre and a pump power of 570 mW.

These features were found to be independent of the pump power with only the signal amplitude changing. Figure 4.8 shows the time series and corresponding power spectra for the SBS signal on increasing the pump power from 0.18 W to 1.08 W. The period of the oscillations show no change and the power spectra also show little difference with the bandwidth staying the same at all powers. The single-pass intensity gain of the Stokes field G is defined as

$$G = \frac{g_B P L_{eff}}{A_{eff}}, \tag{4.1}$$

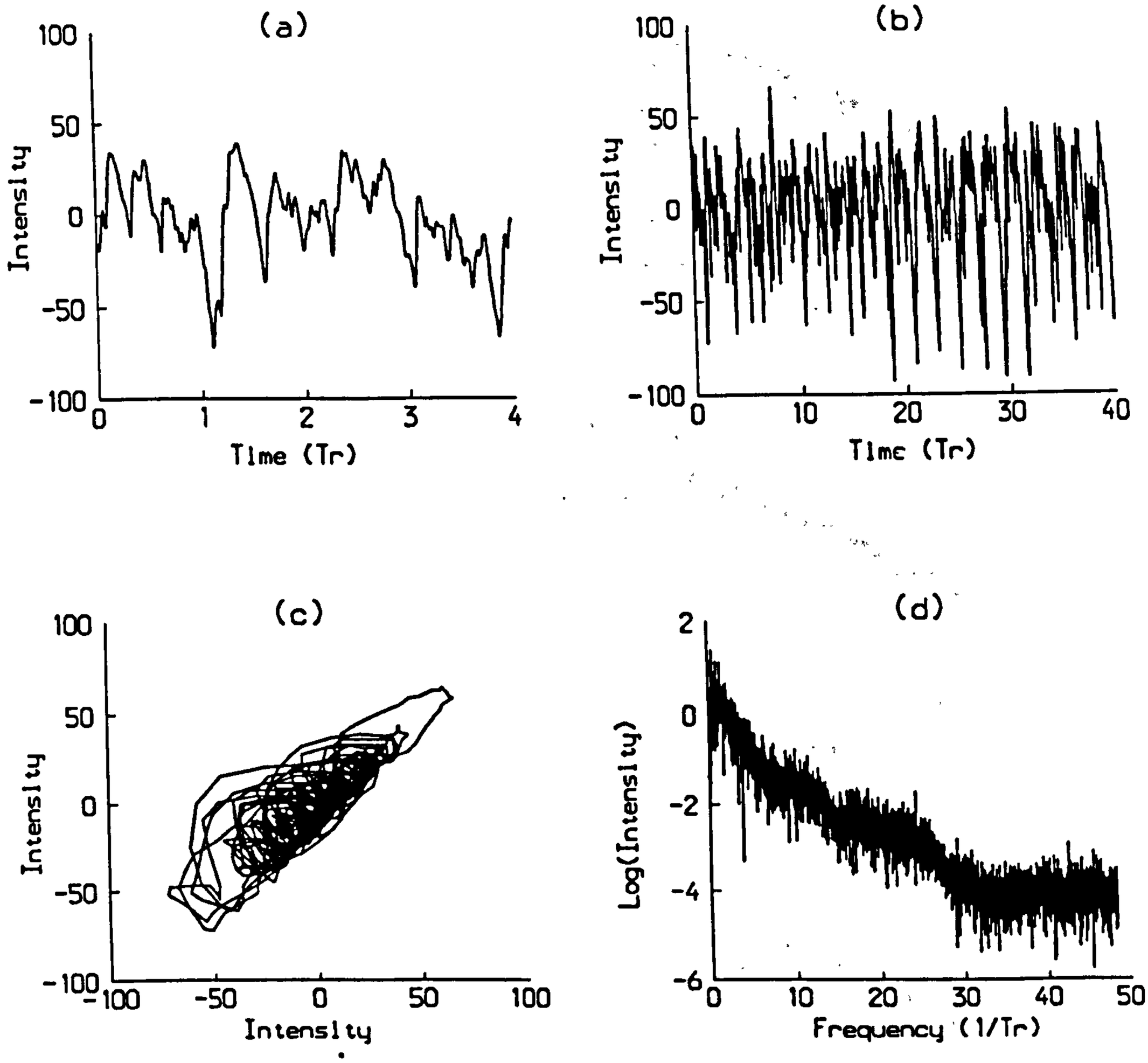

Figure 4.7: Digitised data showing (a) times series for 400 points, (b) time series for 4000 points, (c) Phase portrait and (d) power spectrum for the transmitted pump signal from a 100 m fibre and a pump power of 570 mW.

where the terms in equation 4.1 have their usual meanings and the value G must equal 21 for the SBS to reach threshold. Assuming that a pump power of 0.18 W is close to threshold this means that the bandwidth of the SBS was found to be constant for $21 < G <\sim 125$. According to equation 4.1 the single-pass gain can be changed by altering the fibre length, although not shown here this was found not to change the temporal behaviour of the SBS. The bandwidth was also found to be independent of the value of the single-pass intensity gain.

Broadband noise may also show the same broadband power spectra and although

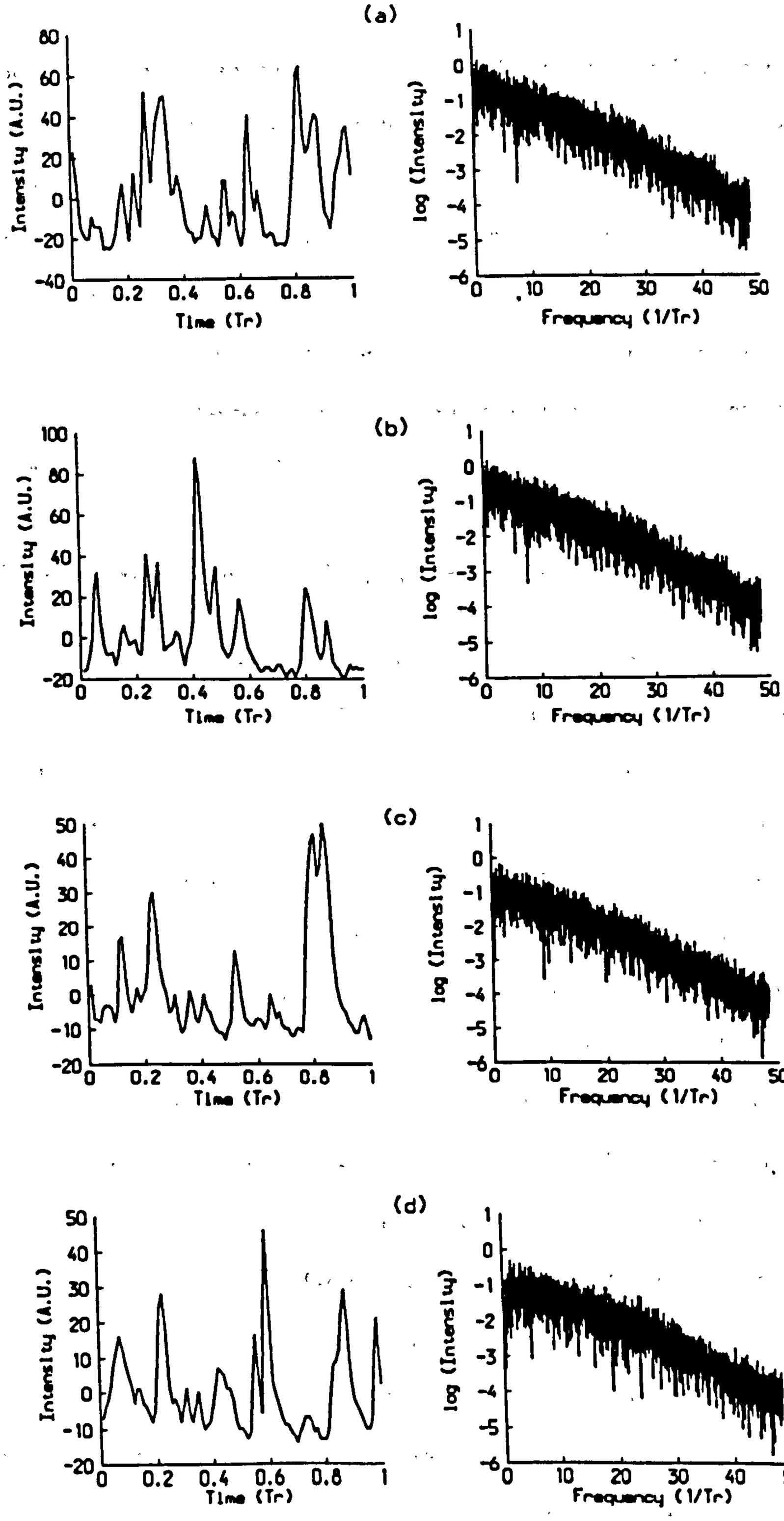

Figure 4.8: SBS time series and power spectra for increasing pump power. (a) 0.18 W, (b) 0.38 W, (c) 0.85 W and (d) 1.08 W.

the phase portraits are not suggestive of a stochastic process full interpretation of these results should include some analysis of the phase portraits, for example measurement of the attractor dimensions, entropy or Liapunov exponents [ECK85]. Only then can the process be confirmed to be stochastic or deterministic. An attempt to calculate entropy measurements of the attractor was undertaken by another member of the group but has not yet been completed. The slow sampling rate and hence the poor quality of the reconstructed phase portraits may cause attempts to measure the attractor entropy to be unsuccessful.

4.3.1 Comparison with Theoretical Results

The theoretical results presented here were obtained by other members of the group by solving equations 2.39 to 2.41, [LU91b]. The SBS is assumed to grow from a single frequency at the correct Stokes shift from the pump injected at $\zeta = 1$, ($z = L$). Parameter values were chosen to agree with those for the single-mode fibres used here. The value selected for the nonlinear refractive index, n_2, is particularly important since the XPM and SPM terms which promote the dynamical behaviour are dependant on n_2. Figure 4.9 shows the effect of increasing the nonlinear refractive coefficient, u, while keeping the other parameters unchanged. The SBS intensities shown in figure 4.9 are normalised to the pump intensity by the relationships given in section 2.5. When u is small the SBS is stable and is approached through a transient relaxation oscillation of period $2T_r$, figure 4.9 (a), agreeing with the early work of Johnson and Marburger [JOH71]. On increasing u the waveform undergoes a series of bifurcations with the evolution of new frequencies corresponding to successive harmonics of the round-trip frequency, figure 4.9 (b) to (d). On increasing u these periodic and quasi-periodic signals show a gradual spectral broadening which finally develops into fully chaotic behaviour, figure 4.9 (e). In experiments the value of u cannot be changed without affecting the Brillouin gain because n_2 is fixed by the

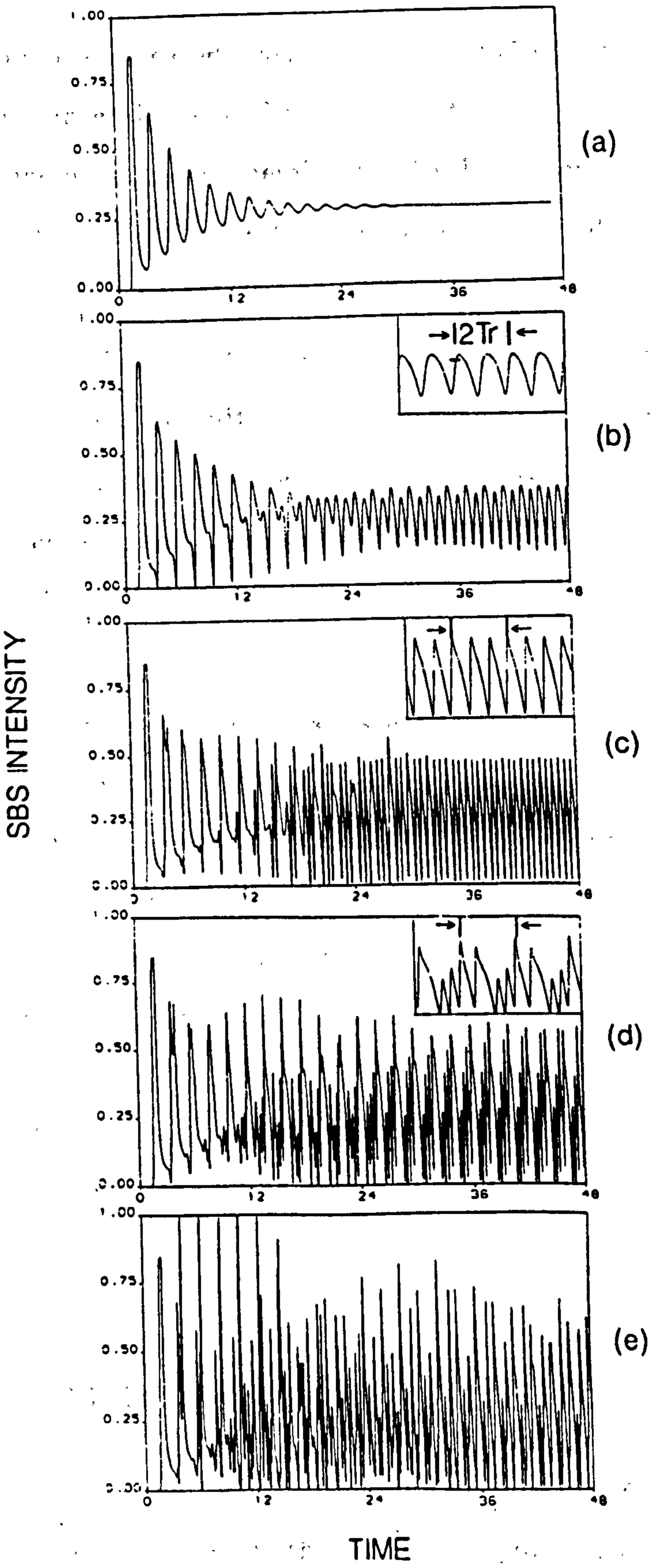

Figure 4.9: Theoretical temporal evolution of SBS intensity on increasing the nonlinear dispersion parameter. (a) $u = 0.0$, (b) $u = 6.4$, (c) $u = 10.5$, (d) $u = 12.0$ and (e) $u = 16.5$. The other parameters are fixed at $\beta_A = 250$, $\beta = 0.175$ and $g = 22.5$. SBS intensity is in normalised units.

material and only one wavelength could be used and changing the fibre length or the pump power changes the value of g. Experimentally the only control parameters are fibre length and pump power, therefore to allow better comparison of the theory and experiment the intensity rather than the value of u should be varied. This was done and the solutions are shown in figure 4.10.

Close to threshold, figure 4.10 (a) and (b), the SBS was found to exhibit regular periodic emission. Steady dc SBS emission was only found in a small operating region very close to threshold which was found to decrease as the effect of nonlinear dispersion was increased. Increasing the pump power again sees the SBS developing into fully chaotic behaviour, figure 4.10 (e) and (f).

Figure 4.11 shows the time series and the power spectra for the SBS and the transmitted pump corresponding to values used in figure 4.10 (e) after the transients have been allowed to decay. Comparing these results to the experimental ones, figure 4.6 and 4.7 shows some agreement but also some differences. Theory predicts periodic oscillations very close to threshold which were not found experimentally. Also the power spectra of the SBS and transmitted pump both show discrete frequencies on a large broadband shoulder whereas the experiment shows no discrete frequencies. The phase portraits do however show the same outward spiraling and folding trajectory with the pump signal phase portrait being an inverted form of the SBS and chaotic dynamics dominate with modulation depths of $\sim 100\%$.

4.4 Photosensitive Effects

In the blue-green region of the spectrum optical fibres frequently exhibit peculiar transmission characteristics where the transmitted power changes nonlinearly with input power and is sometimes seen to change with time. This induced loss and

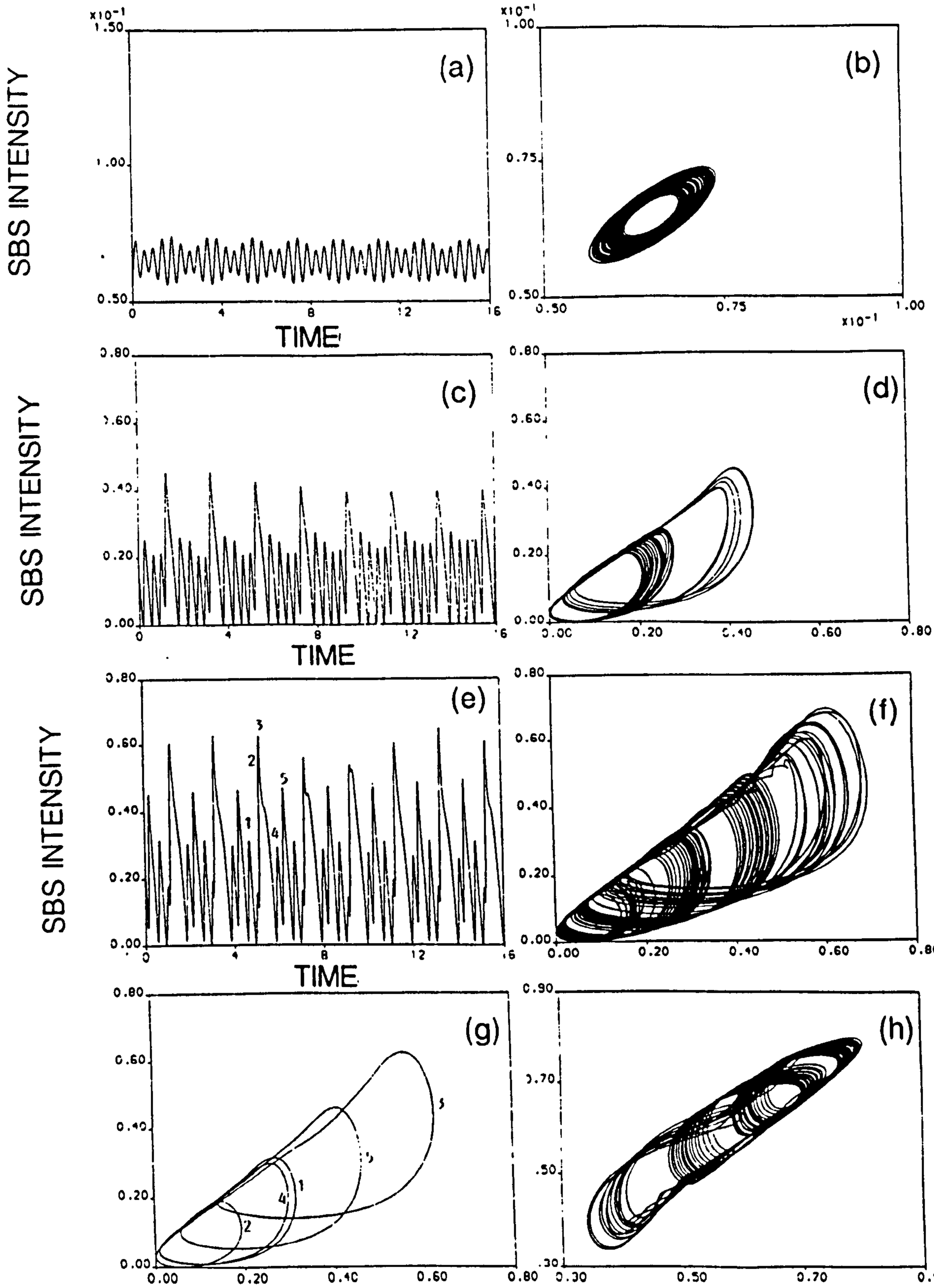

Figure 4.10: Theoretical SBS intensity and corresponding phase portraits on increasing pump power. (a) $|\mathcal{E}_o|^2 = 1.86 \times 10^{14}$, (c) $|\mathcal{E}_o|^2 = 2.08 \times 10^{14}$ and (e) $|\mathcal{E}_o|^2 = 2.31 \times 10^{14}$. The other parameters are $\beta = 0.175$, $\beta_A = 250$, $u = 7 \times 10^{-14}|\mathcal{E}_o|^2$ and $g = 9.4 \times 10^{-14}|\mathcal{E}_o|^2$ and the SBS intensity is in normalised units.

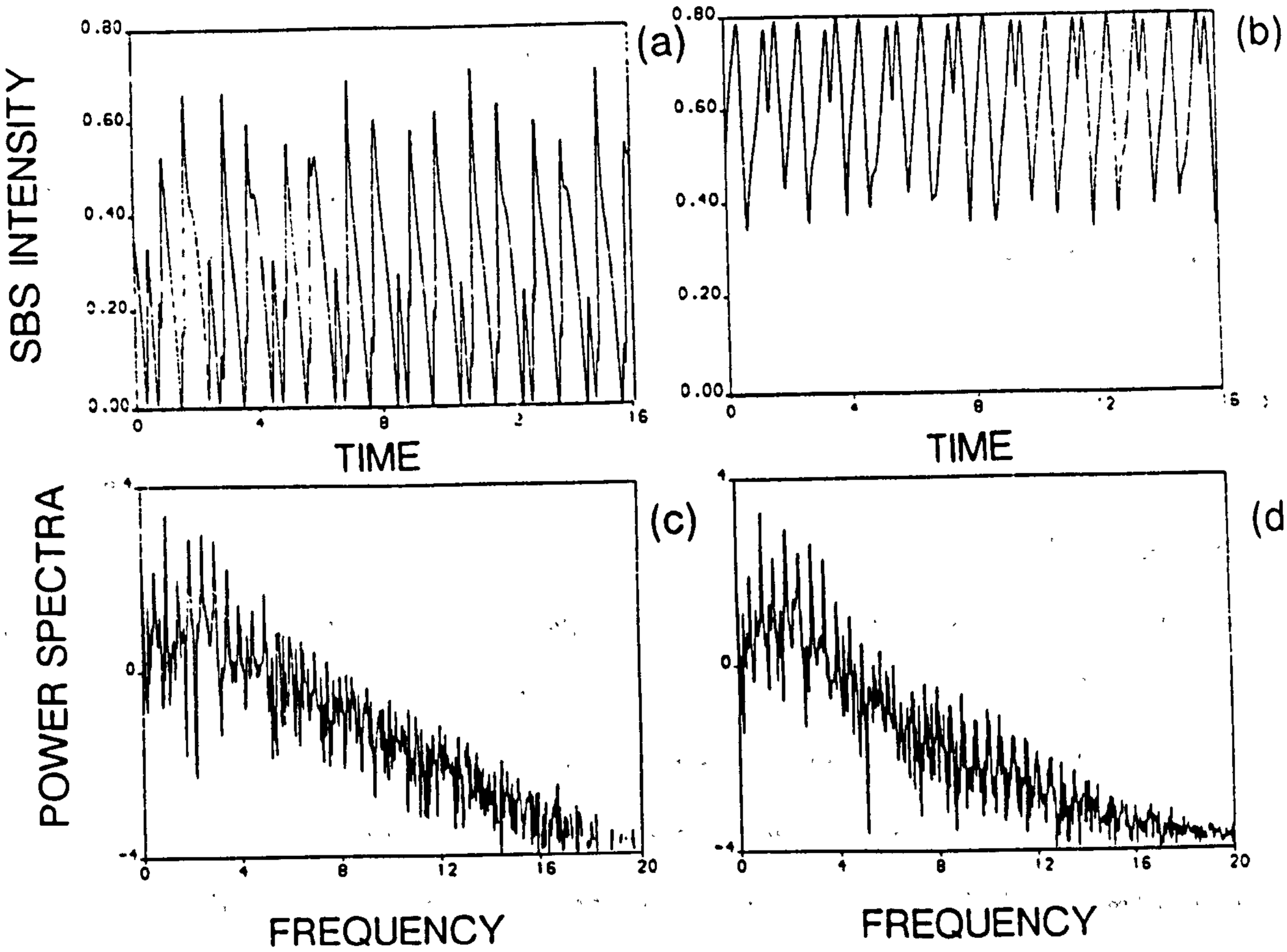

Figure 4.11: Theoretical time series and power spectra for SBS and transmitted pump signals. The parameters are as for figure 4.9 (e). SBS intensity is in normalised units.

nonlinear transmission has been associated with the formation of color centres, defects in the crystalline structure of the fibre, through two-photon absorption and is linked to the germania dopant in the fibre core [POY88,MIZ91]. Such effects have been observed in single-mode fibres at 514.5 nm using cw powers of a few hundred milliwatts - conditions identical to those used here.

Counter-propagating beams from a single longitudinal mode argon laser have been found to induce a periodic index change in the core of germania doped silica fibres [HIL78b]. In these experiments light was launched into a short piece of fibre, 1 m, with the Fresnel reflection at the air/glass interface providing the counterpropagating beam. Using a pump power of 1 W the reflected signal was seen to rise from 4% to 44% over a period of 9 minutes. Such an experiment was carried out, with a

set-up similar to that shown in figure 3.2, using a 1 m piece of LTI fibre and a pump power of 1 W but no increase in reflected power was observed over a 30 minute period. Even though fibre LTI has a germania doped core the dopant concentration is less than that in the fibres usually used to carry out such experiment, 5% compared to typically 20%.

Although the formation of gratings was not observed it would be thought that color centre formation should still occur leading to the fibre loss increasing with time and that this should also have happened to all the fibres used in the SBS experiments. These processes are slow, they occur over timescales of many minutes, and it is therefore thought that they will not interfer with the dynamical behaviour of the SBS which occurs in the timescale of nanoseconds. The major effect that is expected is an increase in SBS threshold as the fibre loss increases but for a 40 m piece of LTI fibre, most of the experiments were conducted with similar lengths, even if the loss doubles from 25 dB/km to 50 dB/km this only reduces the interaction length and hence the threshold power by 10%. So although these processes many cause significant changes to experiments carried out with long fibres their effects here are only small.

4.5 Temporal Behaviour of SBS Amplifier

Using the experimental setup shown in figure 3.10 the temporal behaviour of SBS generated by an amplifier was also studied. The SBS oscillator part of the amplifier can produce, under suitable pumping conditions, an almost stable dc output using a piece of fibre without index matching - full details of this are given in chapter 5. Figure 4.12 shows an example of such a probe signal, a stable dc signal which contains only infrequent spikes of modulation. This was obtained using a launched power of $\sim$ 360 mW and a 130 m piece of LTI fibre. The spikes are typically less than 0.1 ms long at intervals of typically 10 ms, although the probe signal may

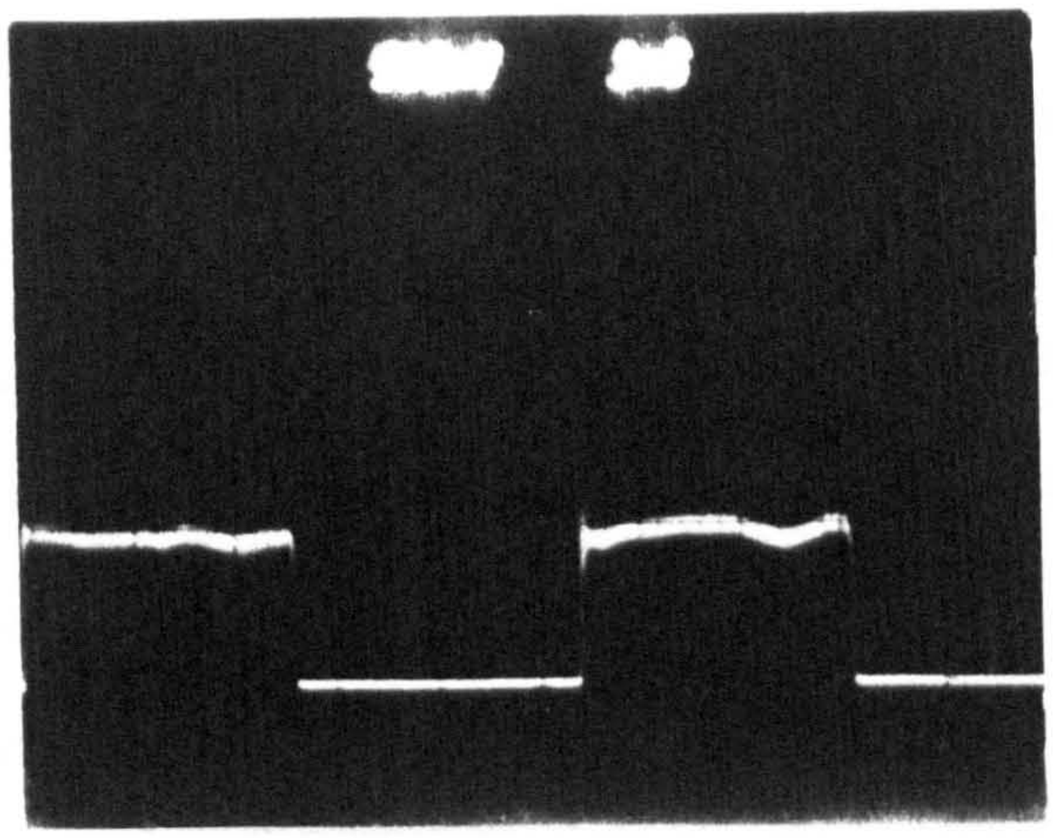

Figure 4.12: Example of probe signal, (time scale is 1 ms/div).

become less stable than this and contains longer bursts of periodic behaviour due to drifting of the launch conditions of the oscillator. This too can be useful to show whether the amplifier output dynamically follows the input but can be avoided or at least reduced by careful choice of the pump power to the oscillator.

The size of the probe signal introduced into the amplifier fibre was varied simply by changing the launch conditions with the maximum probe power available being a few mW's. Amplification of the probe signal could still be seen even when the probe signal itself was too small to be detected with the detectors used. To study the SBS process in the absence of feedback the fibre in the amplifier was again index matched at both ends to prevent any cavity effects.

The amplifier can be operated in two distinct two areas - either the pump power is below the threshold power for SBS to be generated from spontaneous scattering so that in the absence of a probe signal there is no SBS signal or when the pump power exceeds threshold and there is an SBS signal even without a probe. The threshold power, as shown previously, depends on the fibre length and Brillouin gain.

4.5.1 Operation below threshold

The simplest of these two cases should be when the pump power is less than threshold and there is no SBS signal when the probe signal is zero. The threshold power for a 100 m piece of LTI fibre is approximately 145 mW when both ends of the fibre have been index matched. The input beam from the laser was divided such that sufficient power was available to the oscillator while the amplifier pump was still below threshold, in this case the amplifier pump power used was ~ 130 mW. Figure 4.13 (a) shows the signal detected at A, see figure 3.10, in the absence of a probe and the very small signal is due only to spurious scatter of the pump while figures 4.13 (b) to (f) show the SBS signal as the probe is increased. The SBS shows only the slow modulations and spikes which are present in the incident probe and no additional dynamics where seen. This was shown clearly by viewing the probe and SBS signals simultaneously on the oscilloscope. This was found to be the case for all the probe powers used, from the maximum available of ~ 4 mW to probe powers so small that the SBS signal was barely detectable, and for all pump powers up to threshold.

4.5.2 Operation above threshold

Operating the amplifier with a pump power greater than threshold means that even when the probe power is zero there is an SBS signal. At small probe values the SBS output is a combination of the signal due to amplification of the probe signal and also of the spontaneous scattering. As the probe is increased the SBS power due to the probe will increase while that due to spontaneous scattering will remain the same. The proportion of the SBS signal due to spontaneous scattering will therefore decrease as the probe is increased. The experimental results support this argument and the SBS outputs for increasing probe power operating above threshold are shown in figure 4.14.

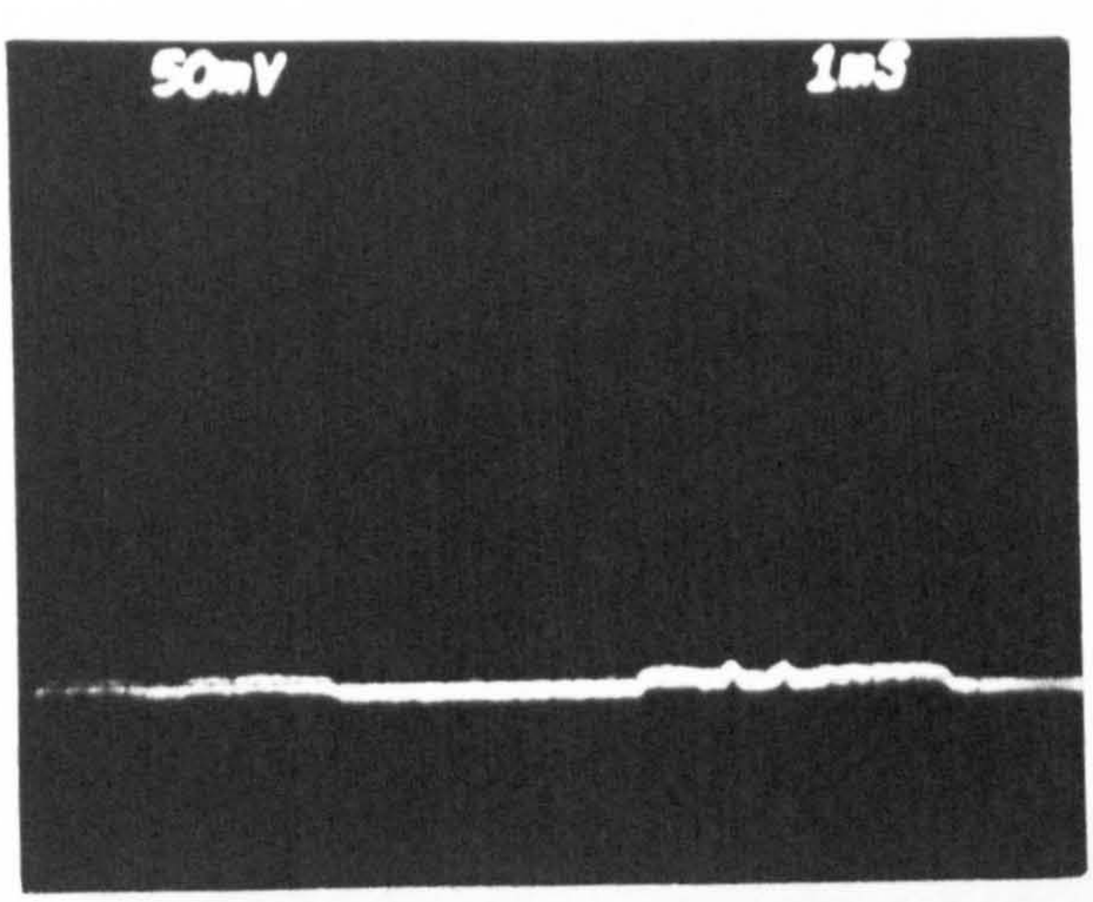

(a)

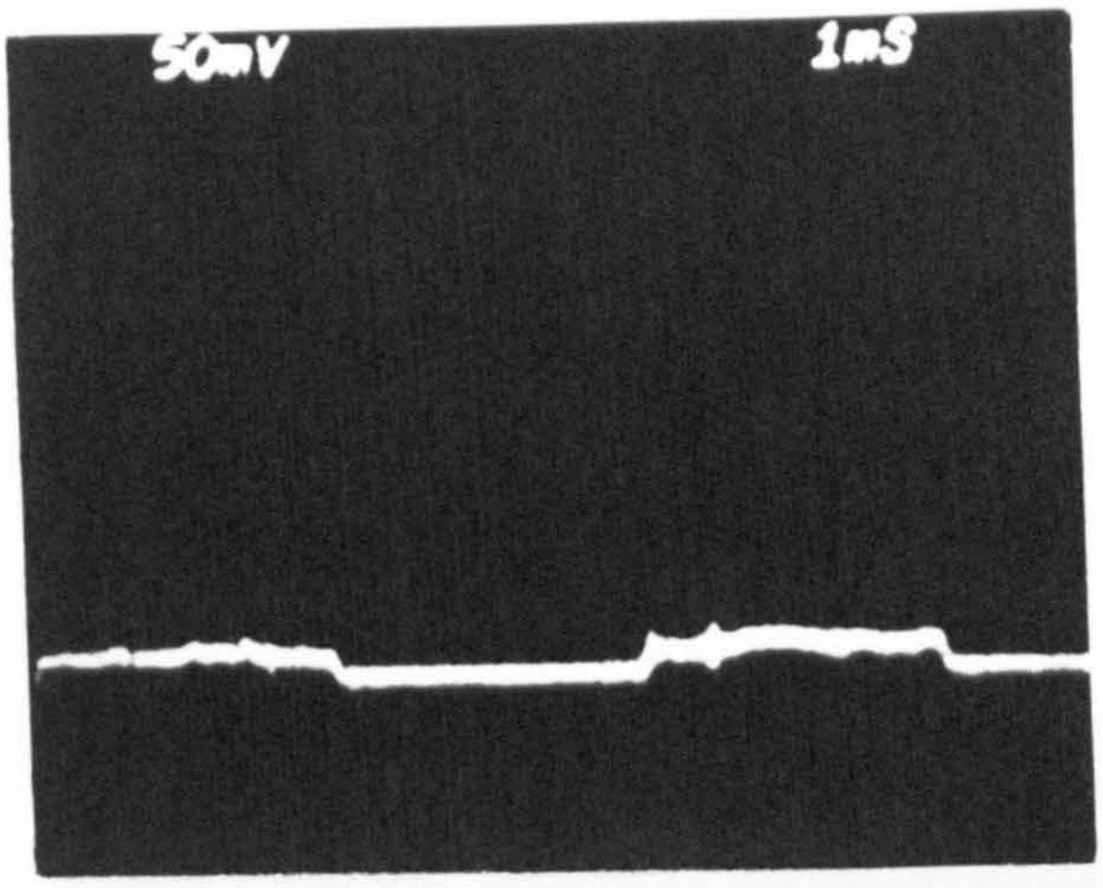

(b)

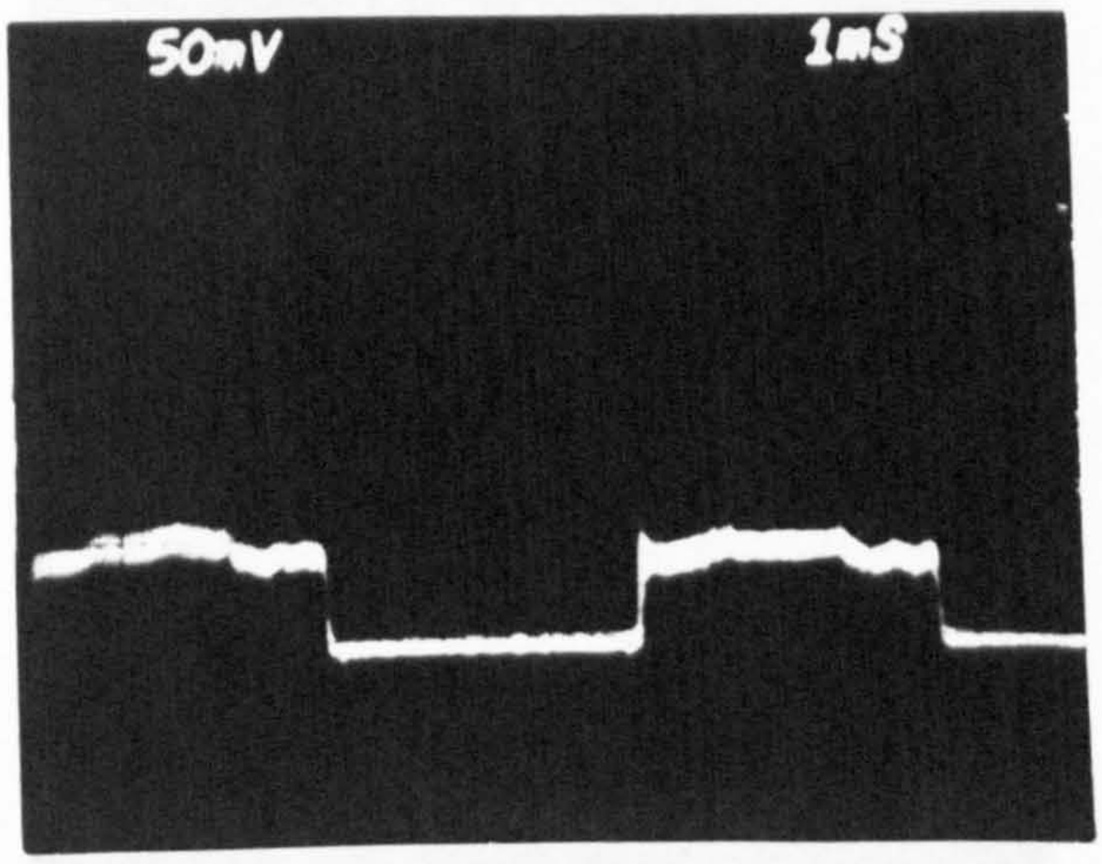

(c)

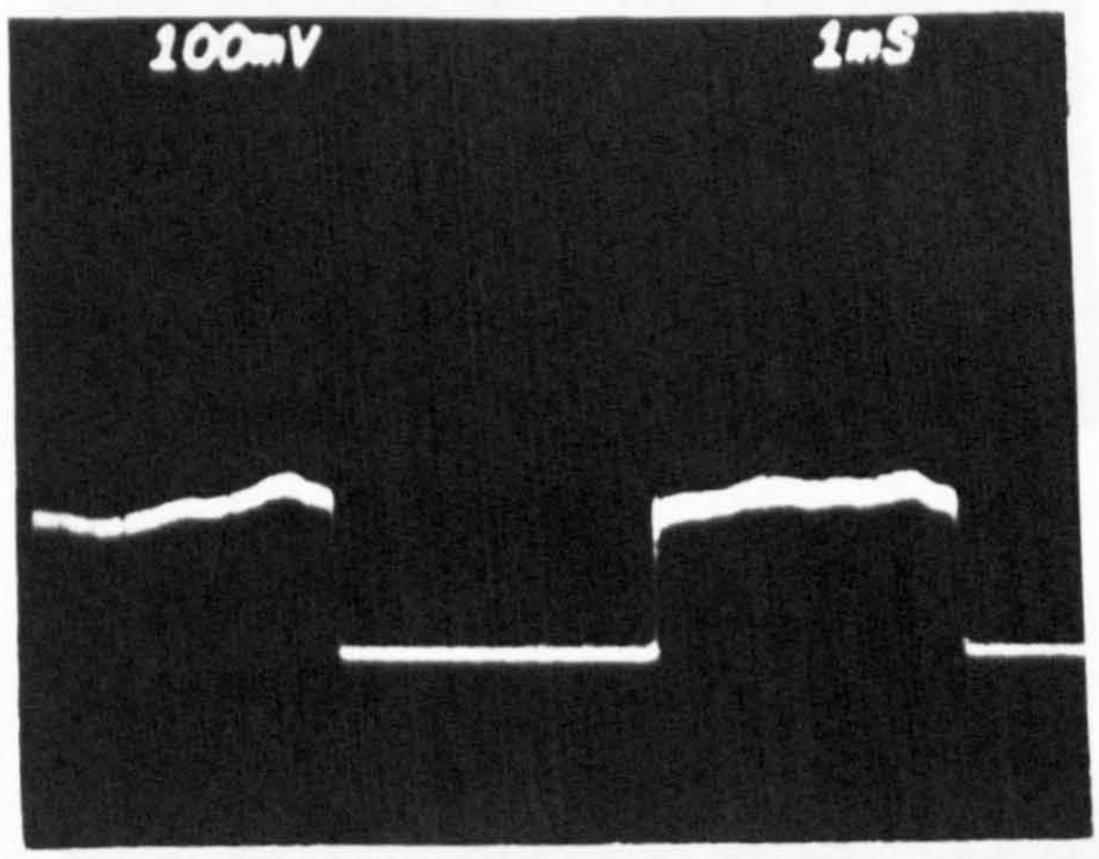

(d)

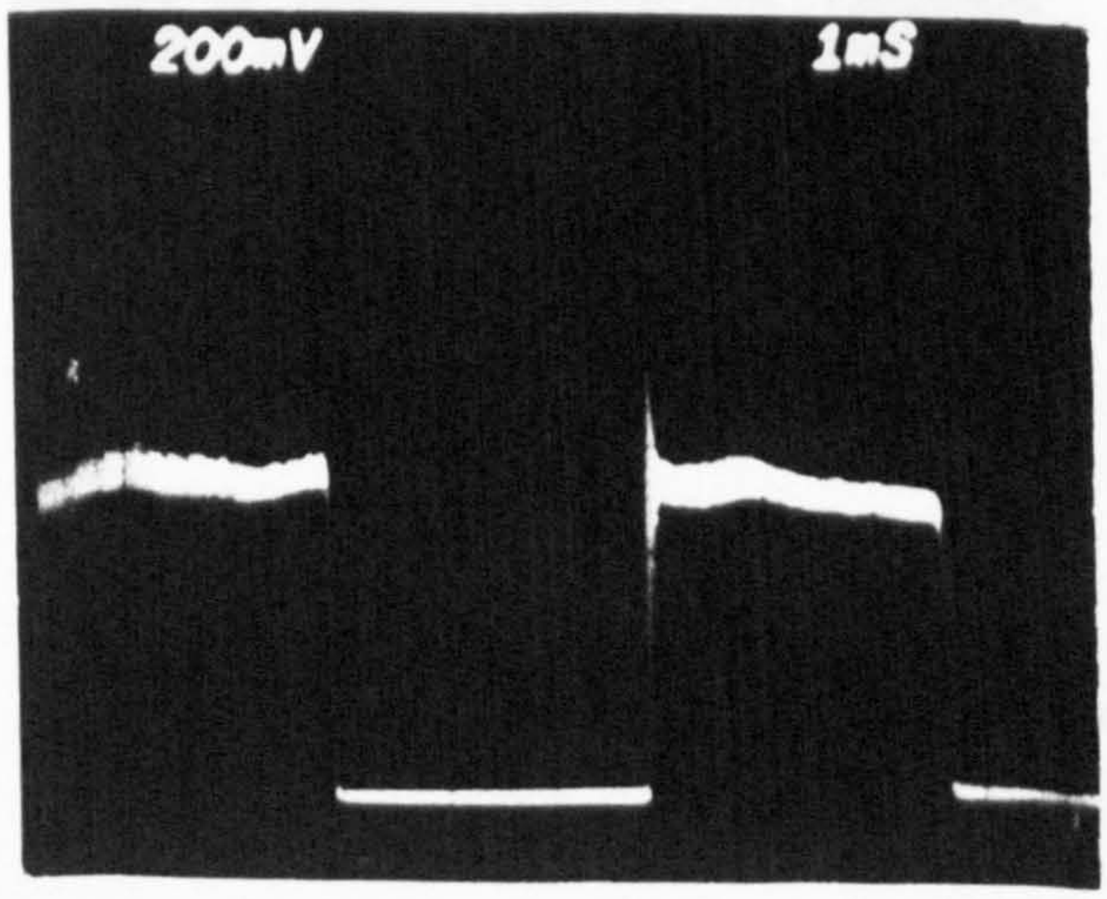

(e)

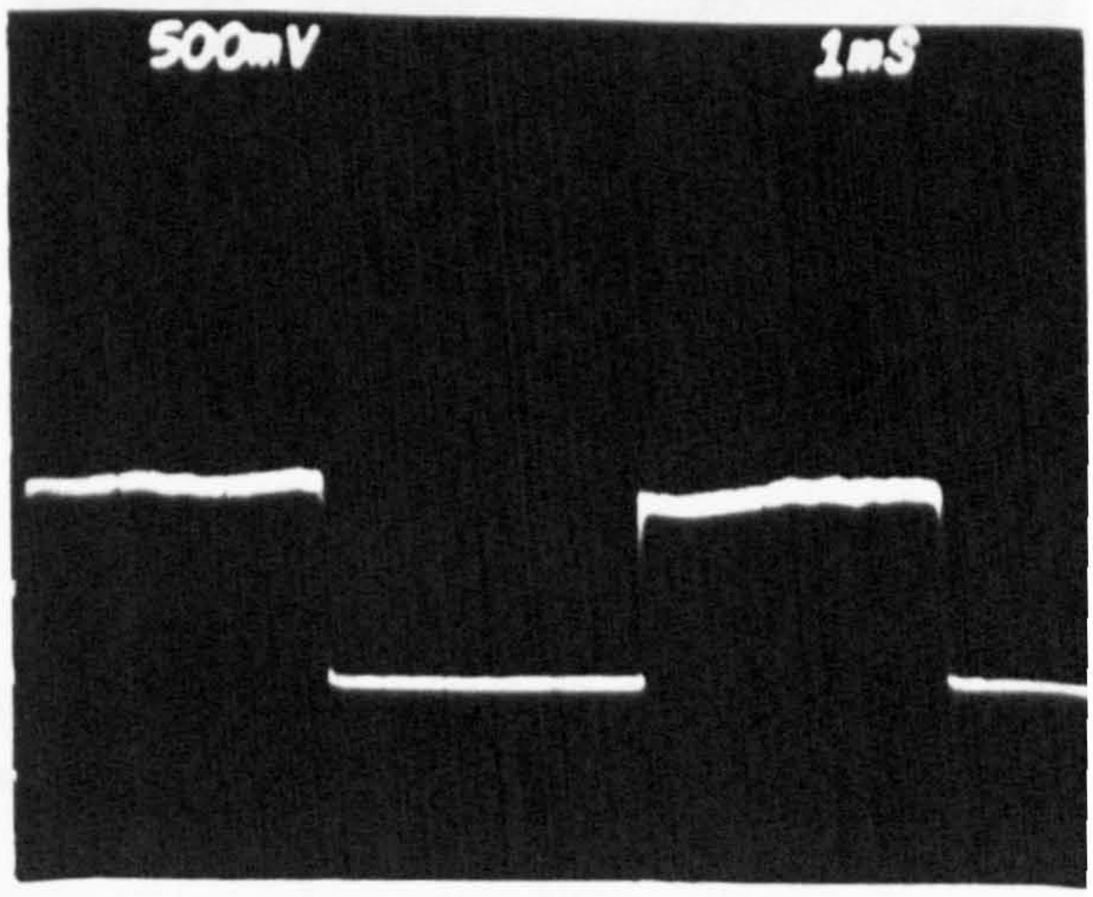

(f)

Figure 4.13: SBS amplifier output for increasing probe power operating below threshold for amplified spontaneous scattering, (time scale is 1 ms/div).

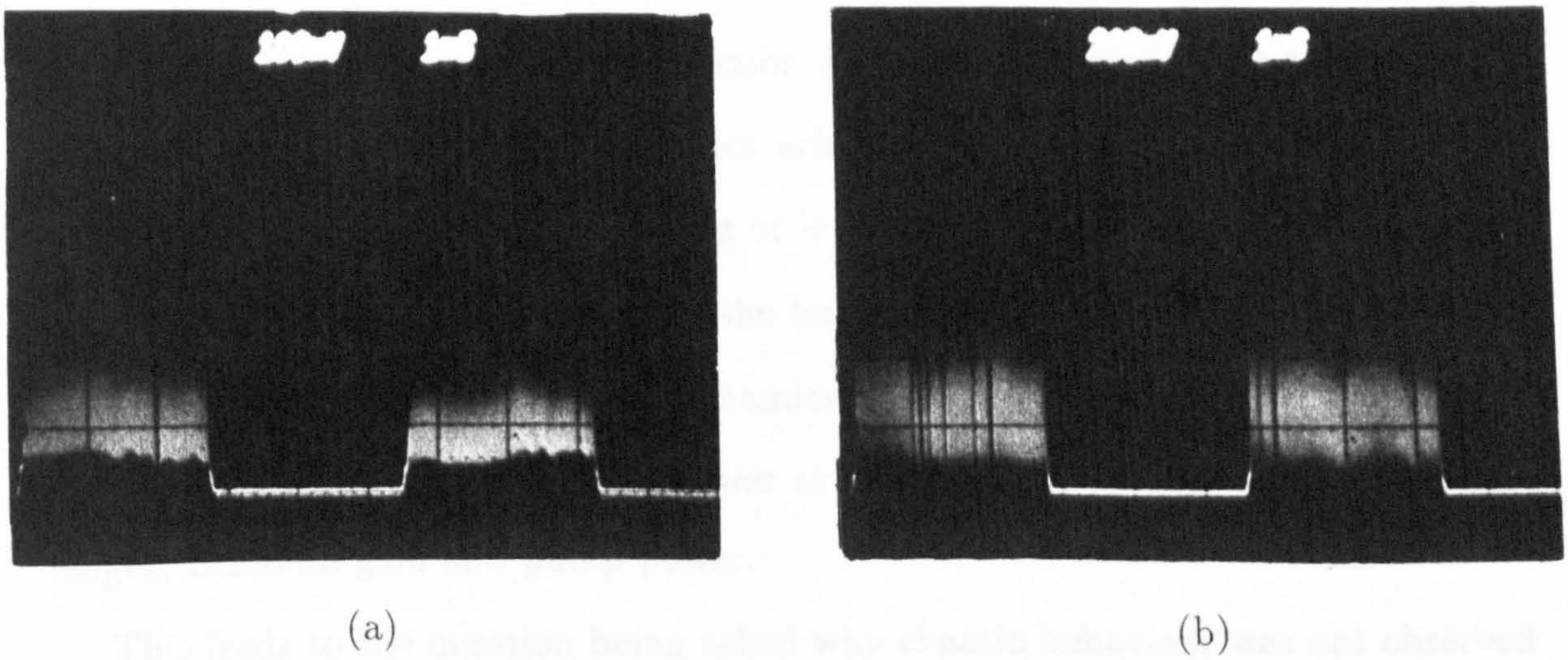

(a) (b)

(c) (d)

Figure 4.14: SBS amplifier output for increasing probe power, operating above threshold for amplified spontaneous scattering, (time scale is 1 ms/div).

Figure 4.14 (a) shows the signal for a launched power of $\sim$ 450 mW and is similar to that shown in figure 4.5 for the SBS generator. As the probe power was increased, figure 4.14 (b) to (d), the depth of modulation decreases and for a large probe signal of a few mW's, figure 4.14 (d), the SBS signal looks exactly like the probe and the depth of modulation is very small.

4.5.3 Comparison with Theoretical Results

The theoretical results presented in section 4.3.1 were obtained using a probe value of $\sim 10^{-12}$ to 10^{-14} W. The dynamics achieved do not depend on whether this signal is due to spontaneous scattering or is in fact a true probe signal, but as the probe was increased above this value the temporal behaviour began to change and for large probe values the chaotic dynamics disappeared and only dc operation is predicted theoretically. The probe power at which this occurs depends on the fibre length, Brillouin gain and pump power.

This leads to the question being asked why chaotic behaviour was not observed experimentally when using the amplifier with a pump power below threshold. When the probe power is very small the pump power must be very close to threshold to obtain an SBS signal which can be detected and the output is therefore a mixture of amplified probe and amplified spontaneous scattering. When a probe power was used so that the SBS signal due to the probe was much larger than that due to spontaneous scattering the theory predicts only a dc output. This was also found to be the case experimentally. So unfortunately the experiment cannot be conducted with the pump power required to produce a detectable signal from a probe signal of sufficiently low power to cause chaotic behaviour without also causing part of the SBS signal to contain amplified spontaneous scattering.

4.6 Conclusions

In the absence of feedback it has been found that SBS generated from the amplification of spontaneous scattering by a cw pump shows aperiodic behaviour with approximately 100% modulation depths. This response was found under all operating conditions investigated with neither oscillatory or dc operation being found. The bandwidth of the power spectra of the SBS was found to be $\sim$ 44 MHz (FWHM) and was found not to vary with the single-pass gain. The transmitted pump was also found to behave aperiodically - here the depth of modulation increases with pump power and gives a measure of the SBS conversion efficiency.

These results are believed to be the first experimental reports of such behaviour [HAR90]. Power spectra and phase portraits constructed from the SBS and transmitted pump signals are suggestive of chaotic dynamics but no precursor routes to chaos were found. Theoretical results show a quasi-periodic sequence to chaos on increasing pump power with periodic behaviour being predicted close to threshold. The theoretical model however takes no account of the spontaneous nature of probe signal and treats it as a single Stokes shifted frequency injected at the far end of the fibre. The full model should include terms to describe this as well as the XPM and SPM terms. Perhaps if this is done then the periodic behaviour predicted at low pump power will be masked by 'noisy' emission caused by the stochastic form of the probe.

Recent work by other workers [BOY90,GAE91], solving the standard coupled wave equations, includes a Langevin noise source term in the material equation. This describes the thermal fluctuations in the density of the medium that leads to spontaneous scattering. Unsurprisingly they found that the SBS signal is aperiodic - it would be expected that the amplified version of a noisy signal would also be noisy. They also found that the inclusion of nonlinear dispersive terms in their model does not change their results. So in the absence of feedback they concluded that the

noise term dominates, however, as will be shown in the next chapter, the addition of feedback changes the temporal behaviour drastically and this behaviour can only be accounted for by including nonlinear dispersion terms.

An SBS amplifier operating below threshold for amplification of spontaneous scattering to occur shows no chaotic behaviour and only amplifies the probe signal applied. Above threshold the SBS signal is a mixture of that due to the applied probe signal and that of spontaneous scattering. As the probe power is increased the probe contribution dominates and eventually the SBS signal has the same appearance as the probe. Theoretically this behaviour is also predicted when the probe signal exceeds a critical value determined by the pump power, Brillouin gain and fibre length. Experimentally the amplifier can only produce a detectable output which is a mixture of amplified spontaneous scattering and amplified probe when the probe signal is as small as that used to obtain the theoretical chaotic dynamics.

In the chapter 3 it was seen that SBS limits the power that can be transmitted by an optical fibre. This chapter shows a further problem to be overcome for communications in that, in the absence of feedback, the transmitted signal will also contain a modulated portion - the depth of modulation depending on the SBS conversion efficiency - however this can be solved in the following way. Instead of trying to send the signal directly down the fibre an SBS amplifier set-up should be used where the probe is used as the signal. If sufficiently large the probe will show no modulation independent of the pump power and in addition, instead of suffering attenuation the signal will be amplified.

Chapter 5

Temporal Behaviour of SBS with Feedback

5.1 Introduction

The inclusion of feedback does not significantly change the steady state behaviour, as was shown in chapter 3, the only effect being an increase in the effective Brillouin gain resulting in a drop in the threshold power and an increase in the SBS conversion efficiency. However, the results presented in this chapter will show that the addition of feedback dramatically alters the temporal behaviour of the process, even the small amount of feedback provided by the natural reflectivity of the fibre end faces being sufficient for this to occur. The effects of varying the pump power for a fixed reflectivity and varying the reflectivity for a constant pump power are now examined.

5.2 Natural Reflectivity

The reflectivity at normal incidence of the fibre end face should be given simply by the Fresnel reflection. However, as was explained in section 3.3.1, if the fibre cleave is not made perfectly normal and flat the reflectivity will be reduced. The reflectivity

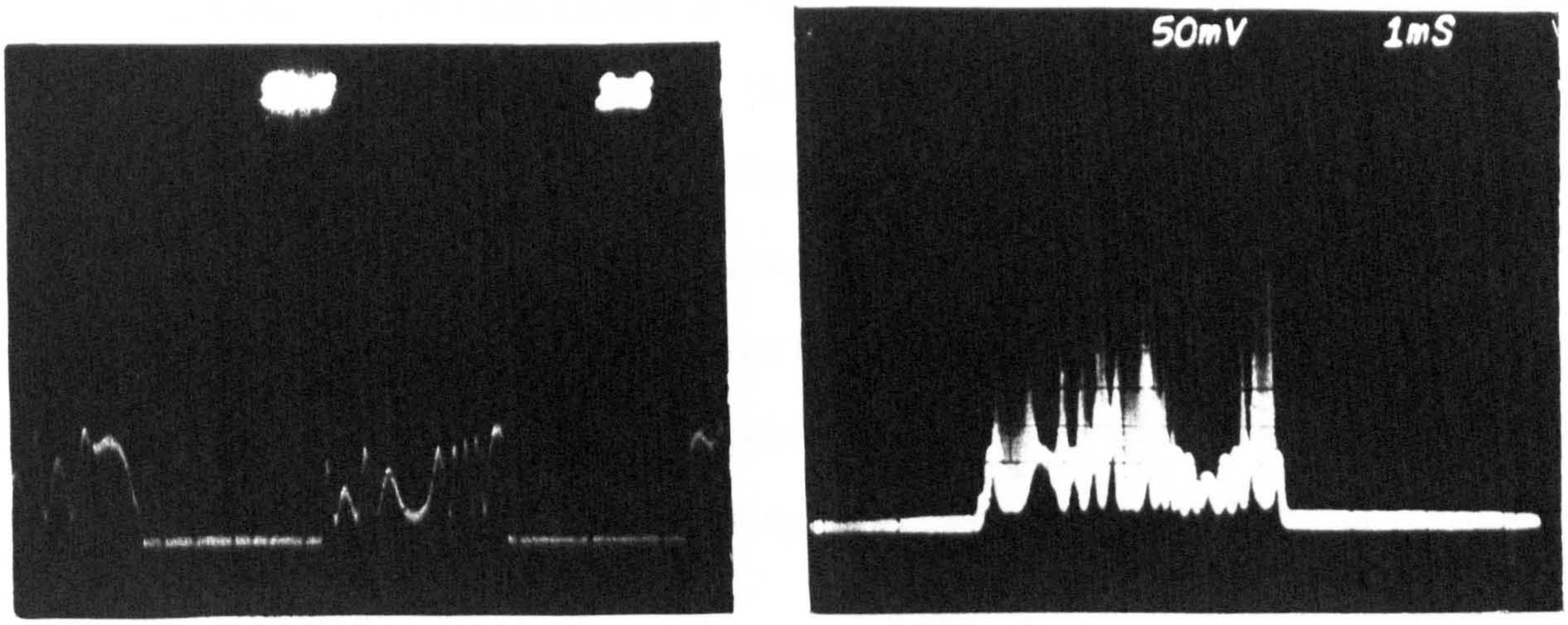

(a) (b)

Figure 5.1: Reflected signal (a) below and (b) close to threshold, (time scale is 1 ms/div).

can be measured using a short piece of fibre, for example 20 cm, index matched at the front end and measuring the transmitted and reflected power. For fibre LTI, where $n_{co} = 1.458$, the Fresnel reflection at normal incidence is 3.5% compared to the experimentally measured value of $3.3 \pm 0.5\%$ showing that careful cleaving of the fibre will give a reflectivity close to the Fresnel limit.

5.2.1 Temporal Behaviour

Again the same experimental setup as that shown in figure 3.2 was used, but this time no index matching was done and both ends of the fibre were cleaved carefully to give as large a reflectivity as possible. Below threshold the reflected signal is the combination of the reflections from the front and rear fibre interfaces and the signal shows slow (millisecond), deep modulations. This was caused by the interference pattern drifting through maxima and minima as the optical path length of the weak Fabry-Perot formed changes due to the temperature dependence of the refractive

index. The depth of modulation depends on the relative sizes and overlap of the two contributions - the two parts will not perfectly overlap if the front face is cleaved at an angle and the fibre loss causes the signal reflected from the rear to be attenuated. Figure 5.1 (a) shows an example of this together with (b) an example of the SBS signal for a pump power just above threshold both using a 40 m piece of LTI fibre. Any slight drift in the pump power around this region will either take the SBS below threshold or lead to a relatively large increase in the SBS signal, hence the slight instability in the pump power is passed on to the SBS which comes in bursts and gaps. The effect is also accentuated by the relatively poor stability of the laser at low operating powers.

Near to threshold the SBS signal again shows almost 100% modulation with the dc contribution caused by reflection of the pump from the fibre end, but this time the temporal behaviour is periodic with the oscillations having a period of $2n_{co}L/c$ - the fibre round-trip time - and the transmitted pump also shows these oscillations. Examples of the oscillations in the SBS and transmitted pump are given in figure 5.2. Figure 5.2 (a) shows the oscillations in the SBS for a fibre length of 23 m, $2n_{co}L/c \simeq 225$ ns, and figure 5.2 (b) shows an example of the oscillations in the transmitted pump this time for a fibre length of 100 m where the period is approximately 975 ns.

Figure 5.3 illustrates how the form of the chopped SBS signal changes as the pump power is increased from 0.25 W to 1.10 W for a 40 m length of LTI fibre. As the pump power is increased from threshold the SBS signal begins to show a small, slow modulation together with the addition of a small dc contribution not due to reflected pump. The modulation depth and the dc portion increase with pump power and the signal starts to show definite deep pulsations with short dc regions between. Further increasing the pump leads to the pulsations becoming shorter and their separation grows until the SBS signal is almost entirely dc with

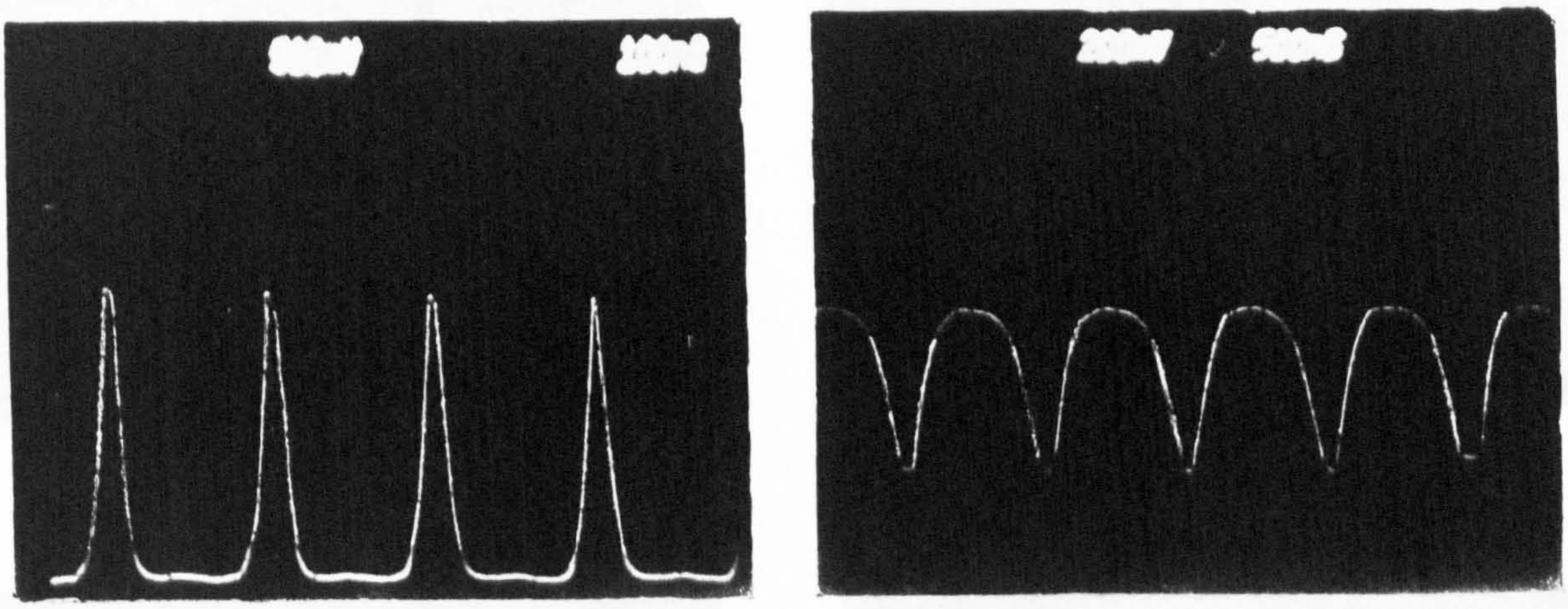

(a) (b)

Figure 5.2: Round-trip period oscillations in (a) SBS and (b) transmitted pump, (time scale is (a) 100 ns/div and (b) 500 ns/div).

only occasional spikes of oscillatory motion. The signal between the spikes still has a definite thickness which is not entirely due to amplifier noise and has an aperiodic appearance when viewed in an expanded form.

These features were also captured using the digitiser, see figure 5.4, but unfortunately the dc contribution was lost when the amplifier off-set was removed. The sampling rate was set to 320 ns to allow as larger time interval to be examined as possible, in this case ~ 5.25 ms, but this meant that the internal details of the modulations were lost. Close to threshold, figure 5.4 (a) the SBS signal shows an erratic modulation due to the small variations in the pump power leading to large changes in the SBS. As the power is increased, figure 5.4 (b) to (d), the depth of modulation increases until the signal eventually becomes almost dc, figure 5.4 (e). The separation of the spikes continues to increase until, in this case, at a pump power of 1.20 W the signal again starts to shows periodic oscillations, figure 5.4 (f).

The frequency composition of the SBS and the transmitted pump was deter-

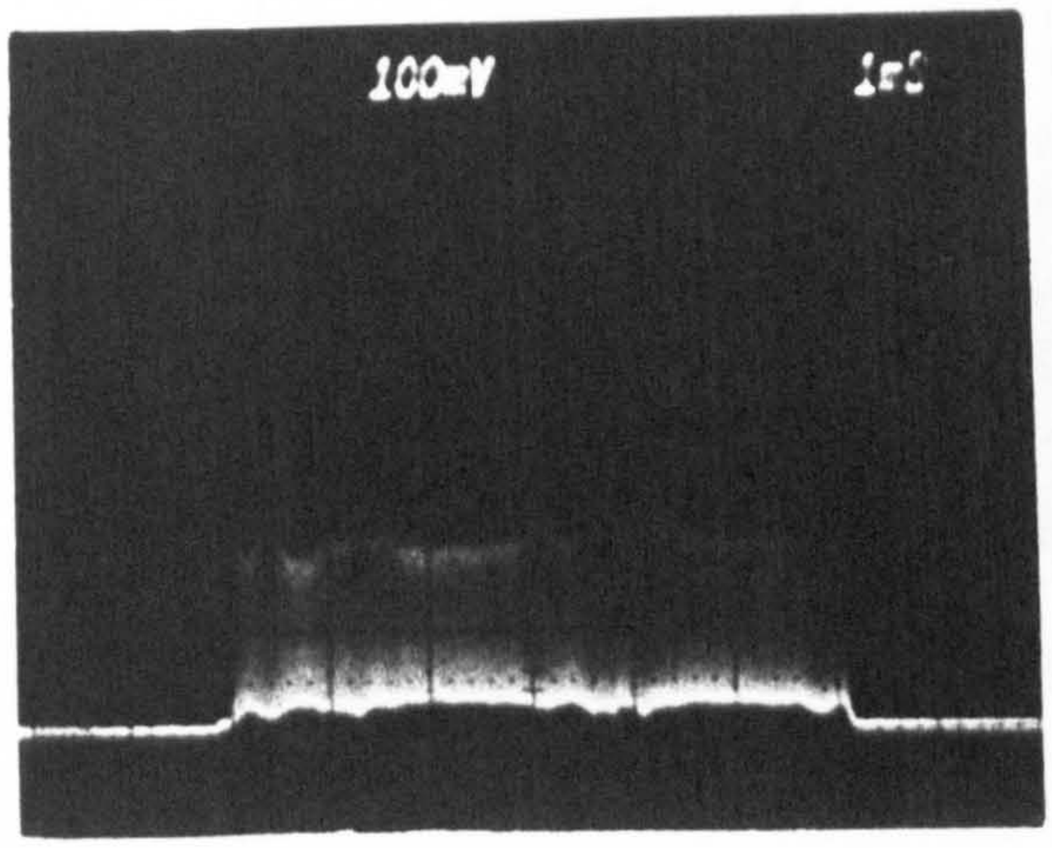

(a)

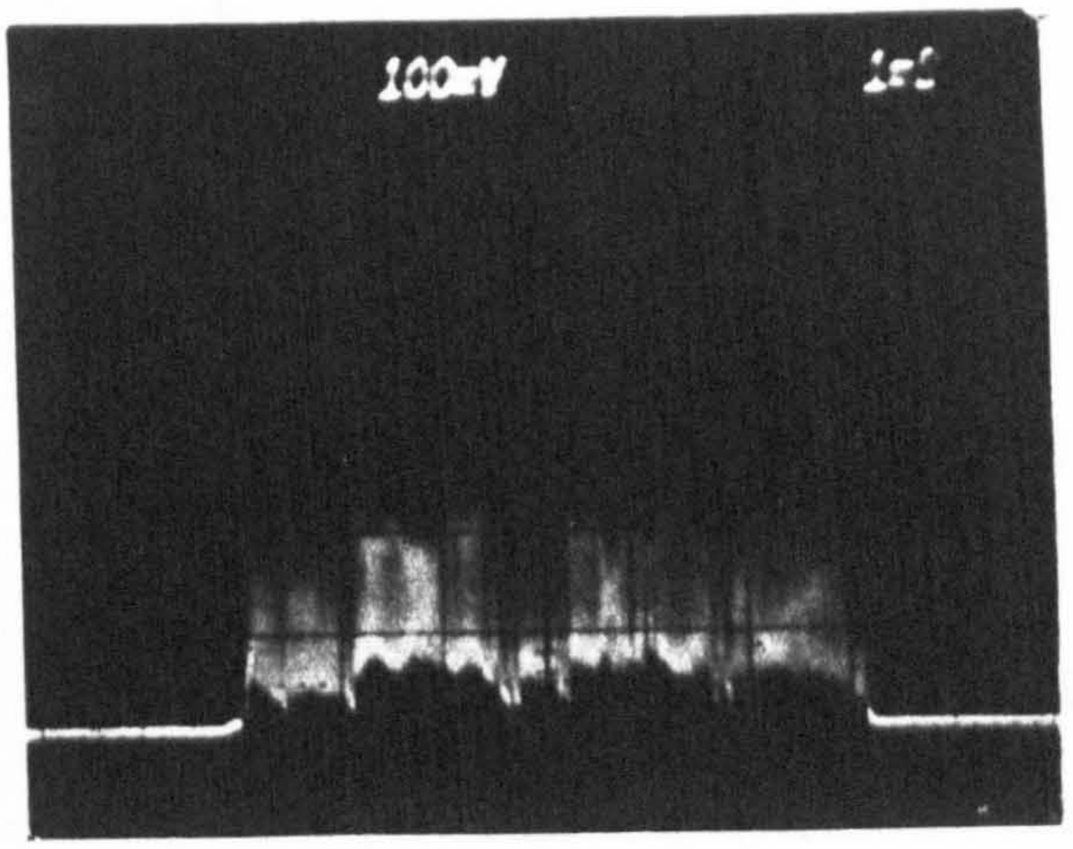

(b)

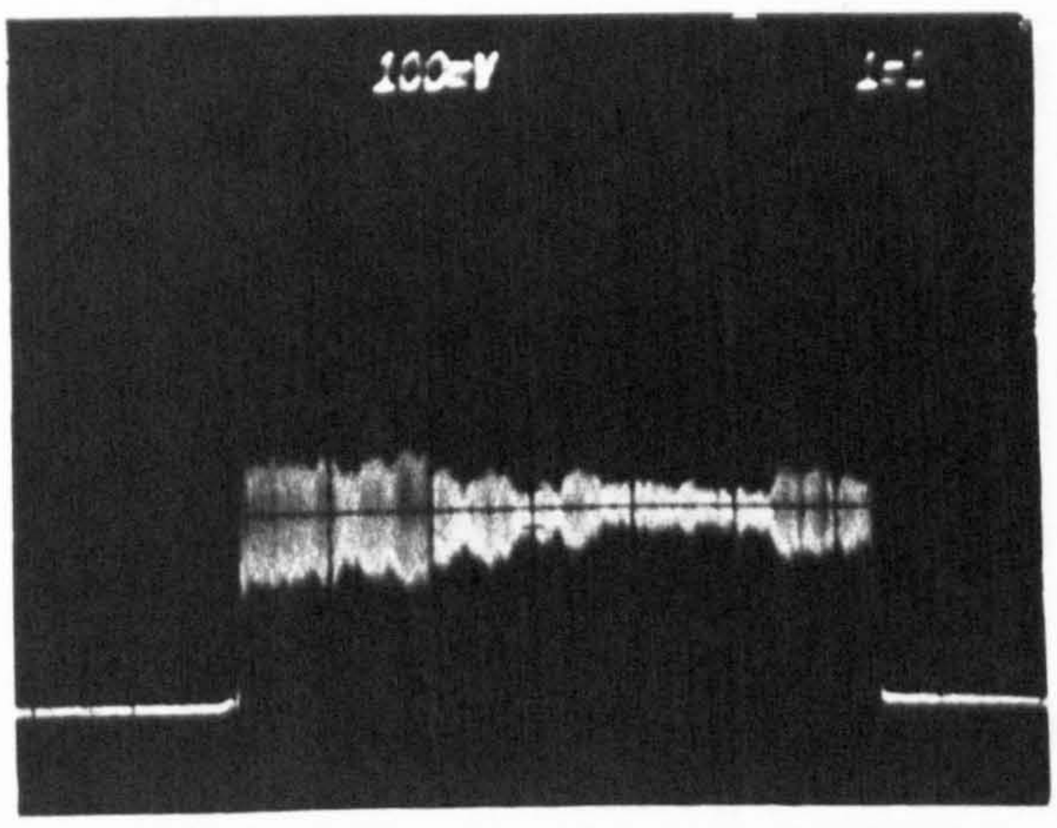

(c)

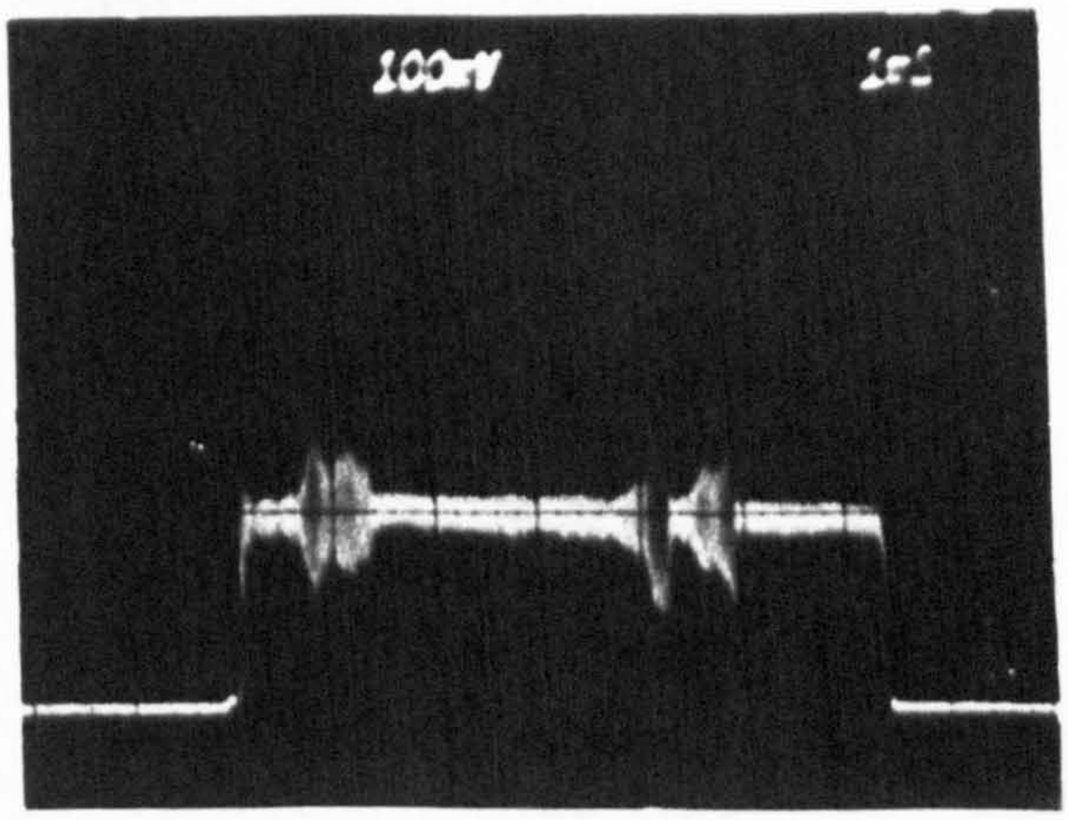

(d)

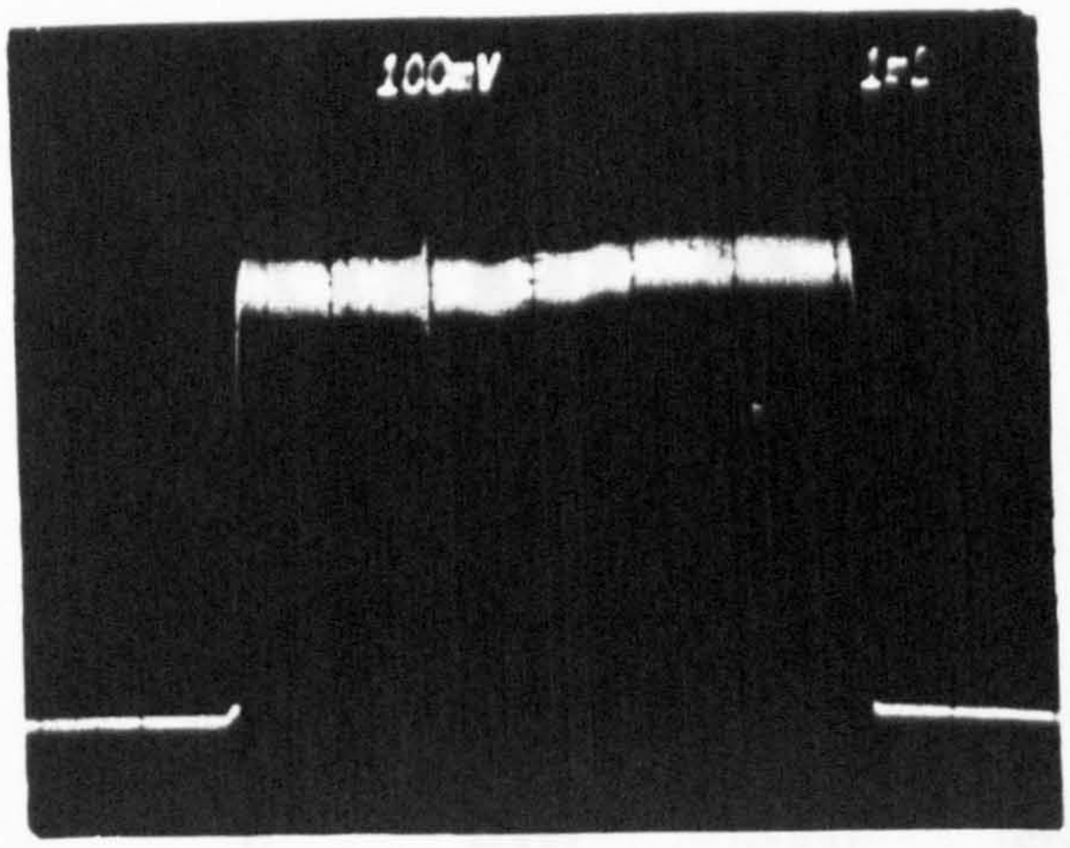

(e)

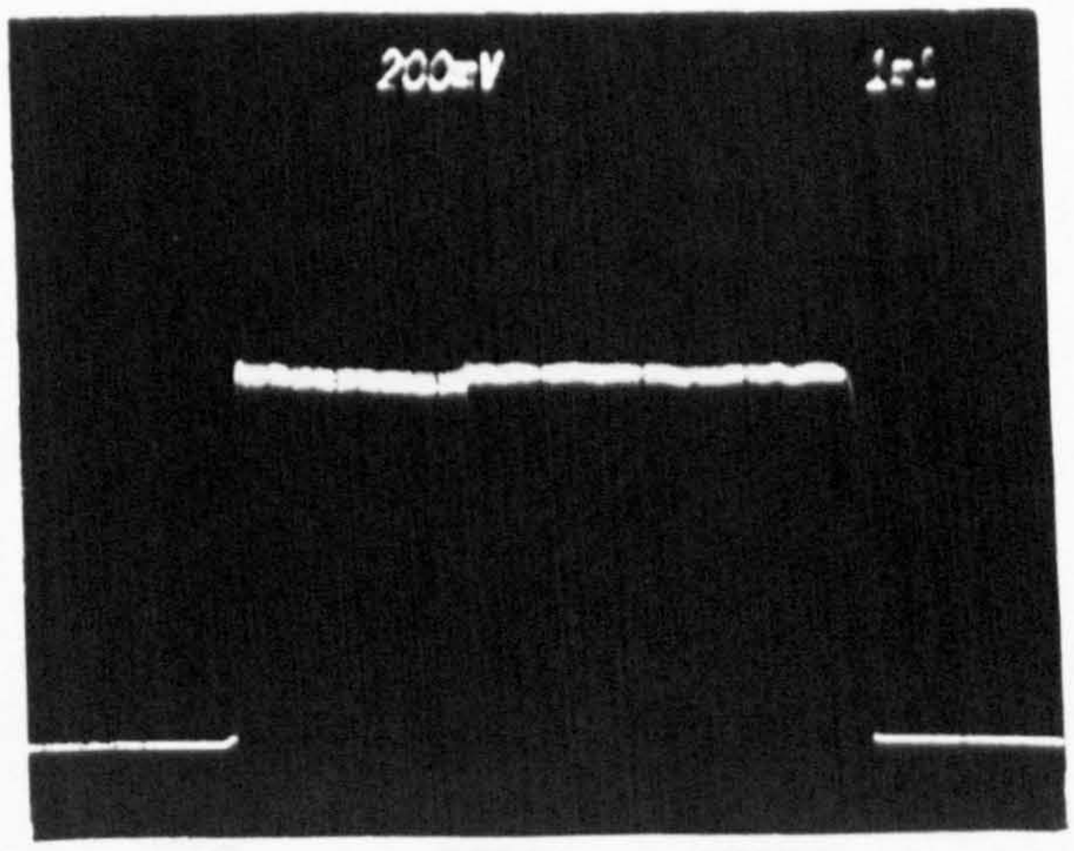

(f)

Figure 5.3: Variation of SBS with natural reflectivity on increasing pump power: (a) 0.25 W, (b) 0.40 W, (c) 0.45 W, (d) 0.66 W, (e) 0.88 W and (f) 1.10 W, (time scale is 1 ms/div).

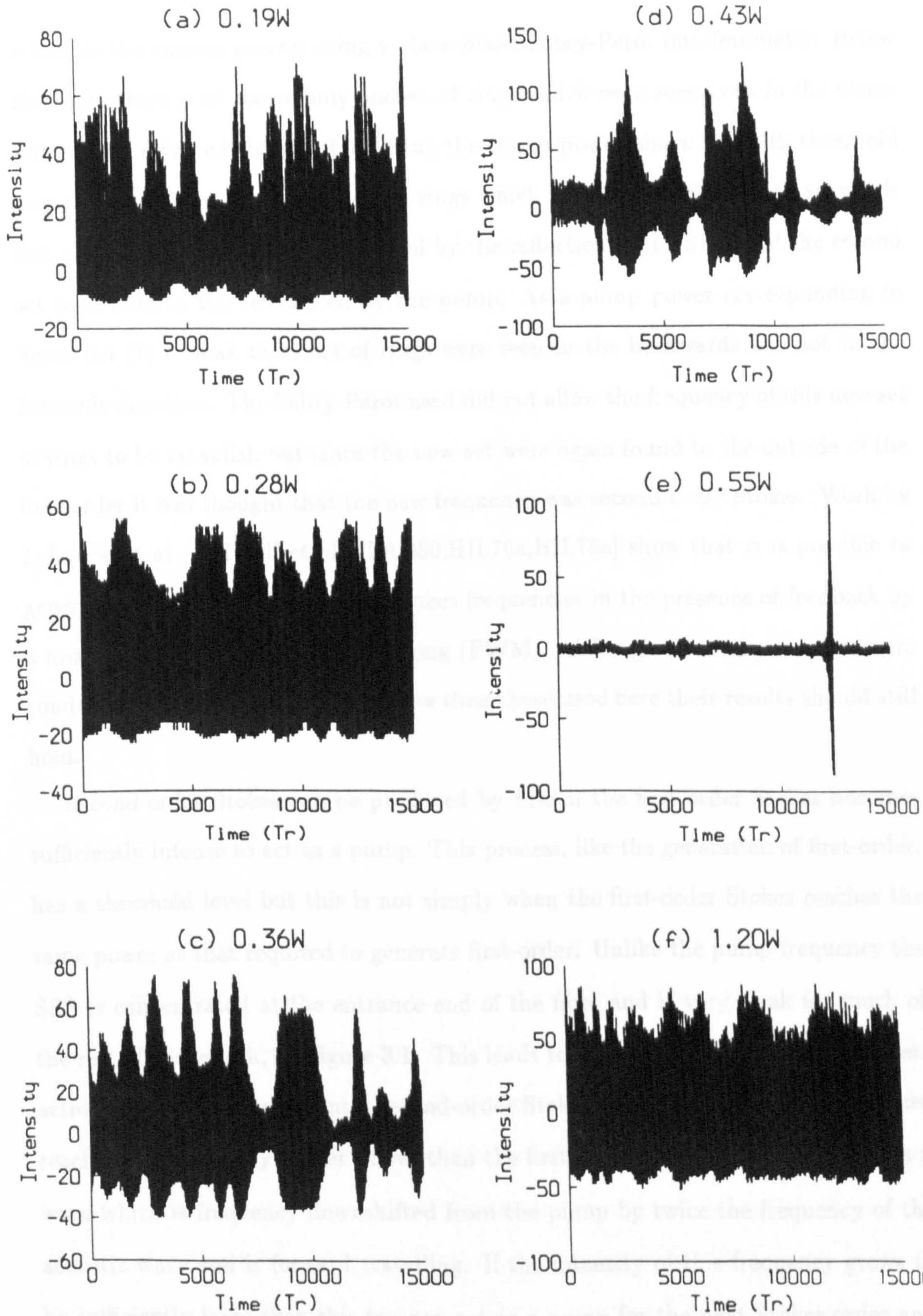

Figure 5.4: Modulations and pulsations in SBS caused by the addition of feedback

mined at the various powers using a plane-plane Fabry-Perot interferometer. Below threshold there is of course only one set of rings which were seen both in the transmitted and reflected signals. Increasing the pump power above the SBS threshold sees the generation of a second set of rings which were seen both in the backwards and also the forwards direction, caused by the reflection of the SBS, and the second set were outside the set caused by the pump. At a pump power corresponding to figure 5.4 (f) a weak third set of rings were seen in the backwards but not in the forwards direction. The Fabry-Perot used did not allow the frequency of this new set of rings to be establish but since the new set were again found to the outside of the first-order it was thought that the new frequency was second-order Stokes. Work by Labudde et al. and Hill et al. [LAB80,HIL76a,HIL78a] show that it is possible to generate multiple Stokes and anti-Stokes frequencies in the presence of feedback by a mixture of SBS and four-wave mixing (FWM). Although these experiments were conducted at much higher reflectivities than those used here their results should still hold.

Second-order Stokes can be produced by SBS if the first order Stokes becomes sufficiently intense to act as a pump. This process, like the generation of first-order, has a threshold level but this is not simply when the first-order Stokes reaches the same power as that required to generate first-order. Unlike the pump frequency the SBS is concentrated at the entrance end of the fibre and is very weak for much of the rest of the length, see figure 3.1. This leads to a reduction in the effective interaction length and consequently second-order Stokes requires that first-order Stokes reaches a significantly higher power than the first-order threshold. This produces a wave which is frequency downshifted from the pump by twice the frequency of the acoustic wave and is forward travelling. If the intensity of this frequency grows to be sufficiently large then this too can act as a pump for the next Stokes order and so on. This cascaded SBS will only produce waves whose frequencies are reduced by

odd multiples of the acoustic wave in the backward direction and by even multiples in the forward. Although these frequencies may be seen in the opposite directions through reflection it is unlikely that the reflected signals will become strong enough to act as pumps.

New frequencies can also be produced through FWM which unlike SBS has no threshold but can only occurs once first-order Stokes has been produced by SBS. First-order anti-Stokes ω_a and second-order Stokes ω_{2S} can both be generated by FWM of the pump ω_P and first-order Stokes ω_S reflected from the fibre input end thus

$$\omega_a = 2\omega_P - \omega_S \tag{5.1}$$

and

$$\omega_{2S} = 2\omega_S - \omega_P \tag{5.2}$$

with both frequencies travelling in the forward direction and being phase matched as shown in figure 5.5. The FWM process between beams that travel in pairs in opposite directions also exists but this is much weaker than the above situation. The two frequencies should also be produced in the backwards direction through FWM of the generated SBS and reflected pump although Labudde et al. show that only Stokes frequencies are intense enough to be detected and no anti-Stokes components were found in this direction. Again this is probably due to the spatial distribution of the Stokes signal reducing the gain for the production of the anti-Stokes frequency.

Therefore FWM allows the production of both Stokes and anti-Stokes in the forward direction but only for Stokes in the backwards direction. This being the case the new frequency which was detected must be second-order Stokes although both this frequency and first-order anti-Stokes should have been detected at the same pump power in the forward direction. These frequencies tend to be less intense and grow more slowly than second-order Stokes in the backwards direction and

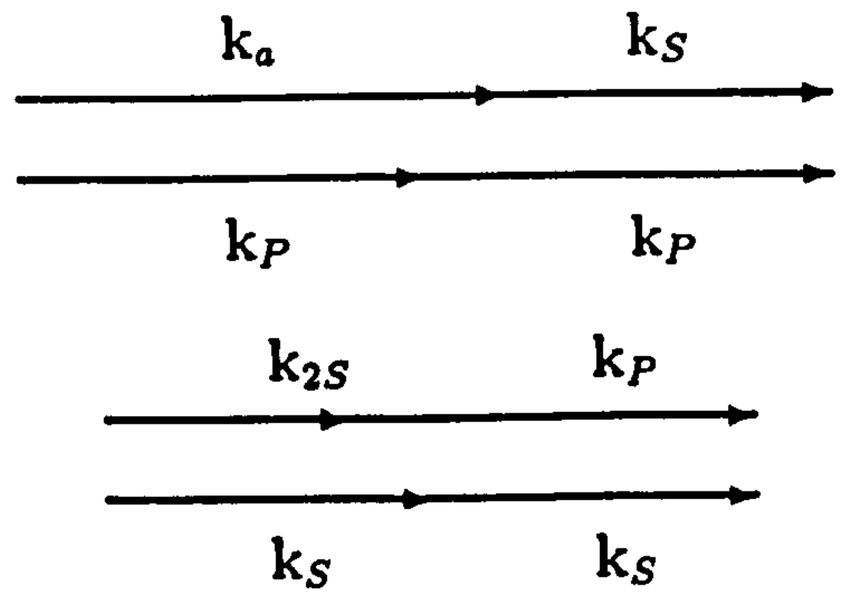

Figure 5.5: Phase matching conditions for four-wave mixing

so probably existed but the crude method of detection was unable to show their existence.

Since second-order Stokes produced by SBS with the first-order acting as pump would be forward travelling and the new frequency was seen in the backwards and not the forwards direction it is therefore thought that this must have been produced through FWM and is therefore second-order Stokes.

Increasing the pump power further sees a repeat of the first order behaviour with the modulations and pulsations again repeating. Although insufficient power was available to carry this through to the near dc state this would have been possible if a longer fibre had been used. When using this set-up to produce the probe signal for the amplifier experiments the pump power was chosen so that the SBS signal produced was in the stable region of operation and the SBS output was like that shown in figure 5.4 (e).

Having now established the macroscopic behaviour the sampling rate was reduced to 5 ns to allow the fine structure of the oscillations to be studied. Preliminary work using 100 m of the same fibre showed that a large number of dynamical features can be observed over a broad range of pump powers in both the SBS and the transmitted pump signals. Figure 5.6 shows examples of the time series and phase portraits of

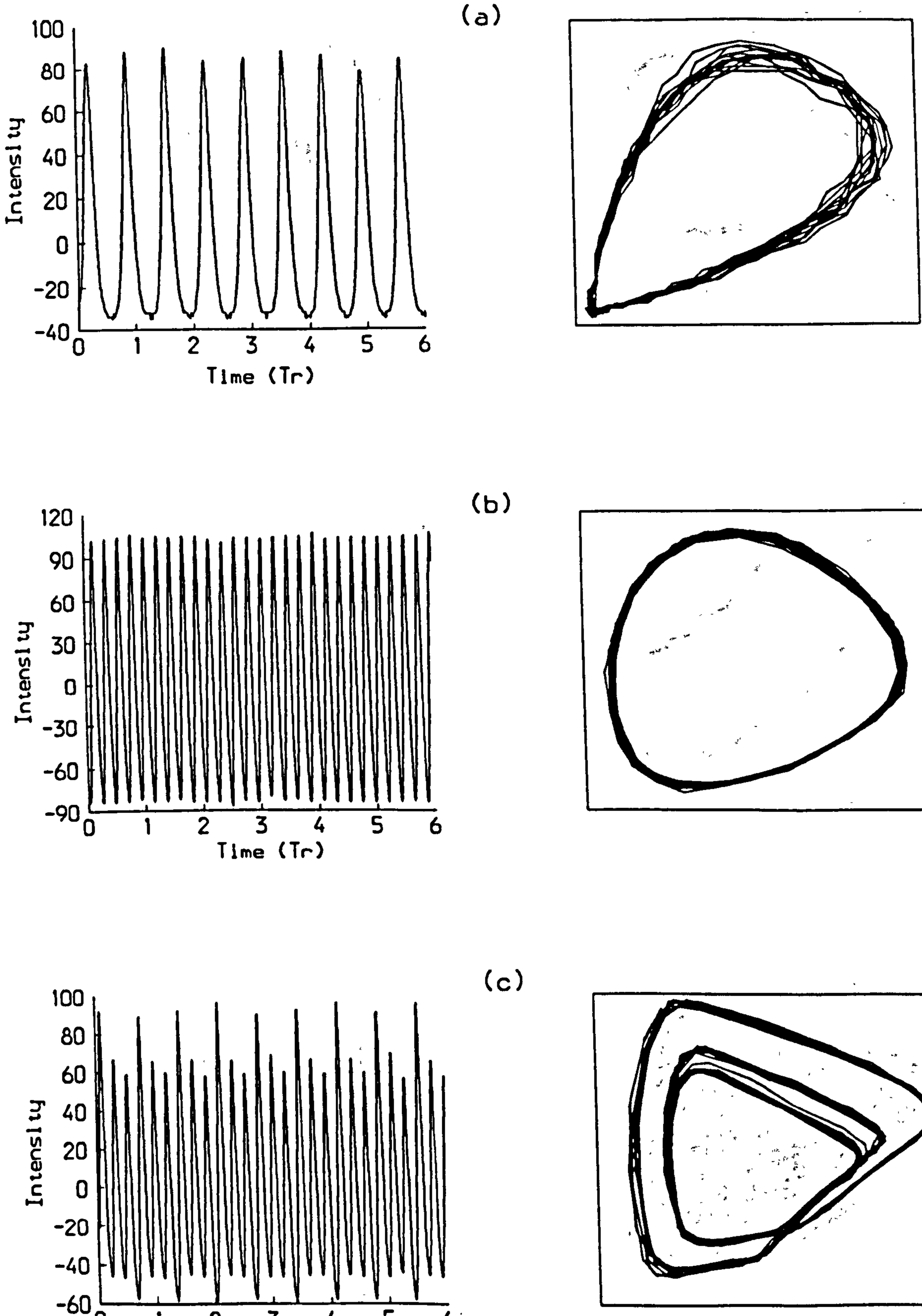

Figure 5.6: Examples of dynamical features, (a) low power limit cycle, (b) high power limit cycle and (c) period three.

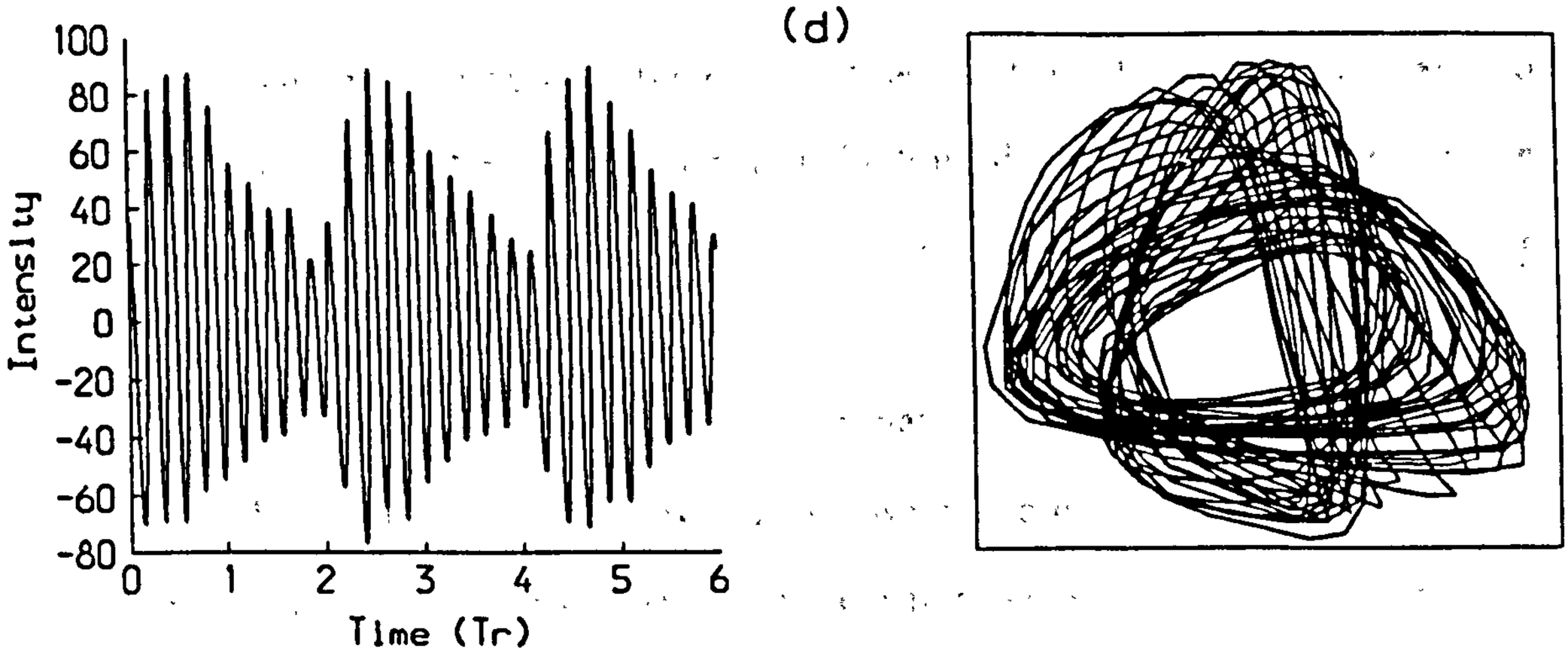

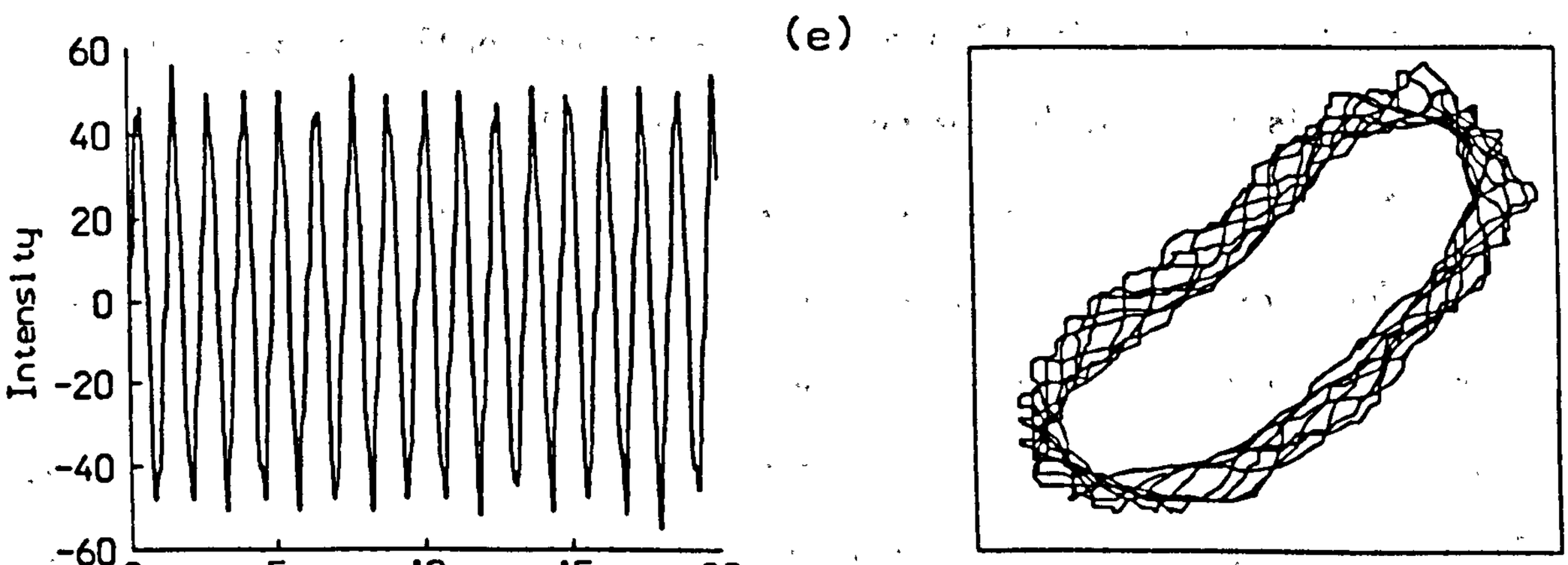

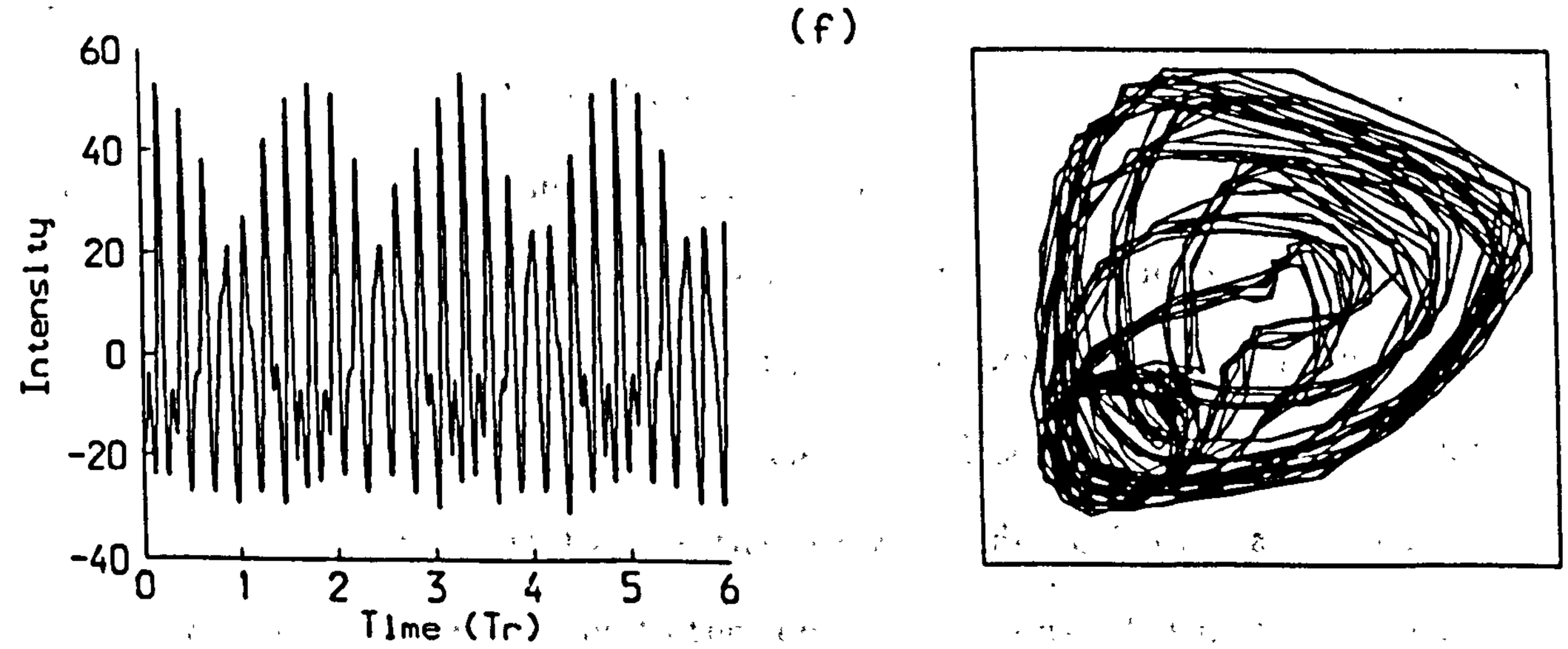

Figure 5.6: Examples of dynamical features, (d) homoclinic, (e) torus and (f) strange attractor.

some of the dynamical features detected. All these features tended to come and go as launched power and the optical length of the fibre drifted so that each recording tended to be different from the previous one and none of these features dominating at any specific power except perhaps the limit cycles. Figures 5.6 (a) and (b) both show limit cycle behaviour with type (a) dominating at low power and type (b) at high power. Period two and three oscillations were also observed and figure 5.6 (c) shows period three oscillations where the waveform repeats itself at a period which is three times the basic frequency. Figure 5.6 (d) shows a homoclinic orbit with a phase change occurring at intervals of $2T_r$, the oscillations having a basic frequency of $5/T_r$. The power spectrum of the waveform shown in figure 5.6 (e) again shows the presence of two frequencies, one at $1/2T_r$ and the weaker second frequency at $2/9T_r$ which combine to produce a torus in phase space. The waveform in figure 5.6 (f) results in the production of an attractor which is suggestive of weakly chaotic behaviour.

These early observations were not carried out in a systematic way but served to show the rich variety of dynamical features that can exist under certain operating conditions. The experiment was repeated but this time using a 40 m piece of LTI fibre. The shorter length should enable the experiment to be carried out in a more controlled manner as any drift in the launched power should cause a smaller variation in the SBS signal.

Figure 5.7 shows how the SBS signal changes as the pump power is increased. At powers near to threshold the SBS signal shows oscillations of period $2T_r$ which are not sinusoidal but instead have a spiked appearance and tend to show small, slow modulation, see figure 5.7 (a). A close study of the power spectrum shows that this is caused by the beating of two frequencies very close to $1/2T_r$. These oscillations produce a limit cycle attractor like that shown in figure 5.6 (a) and occur in the area of operation corresponding to the temporal response shown in figure 5.4 (a).

Increasing the power slightly causes the structure of the time series to change with

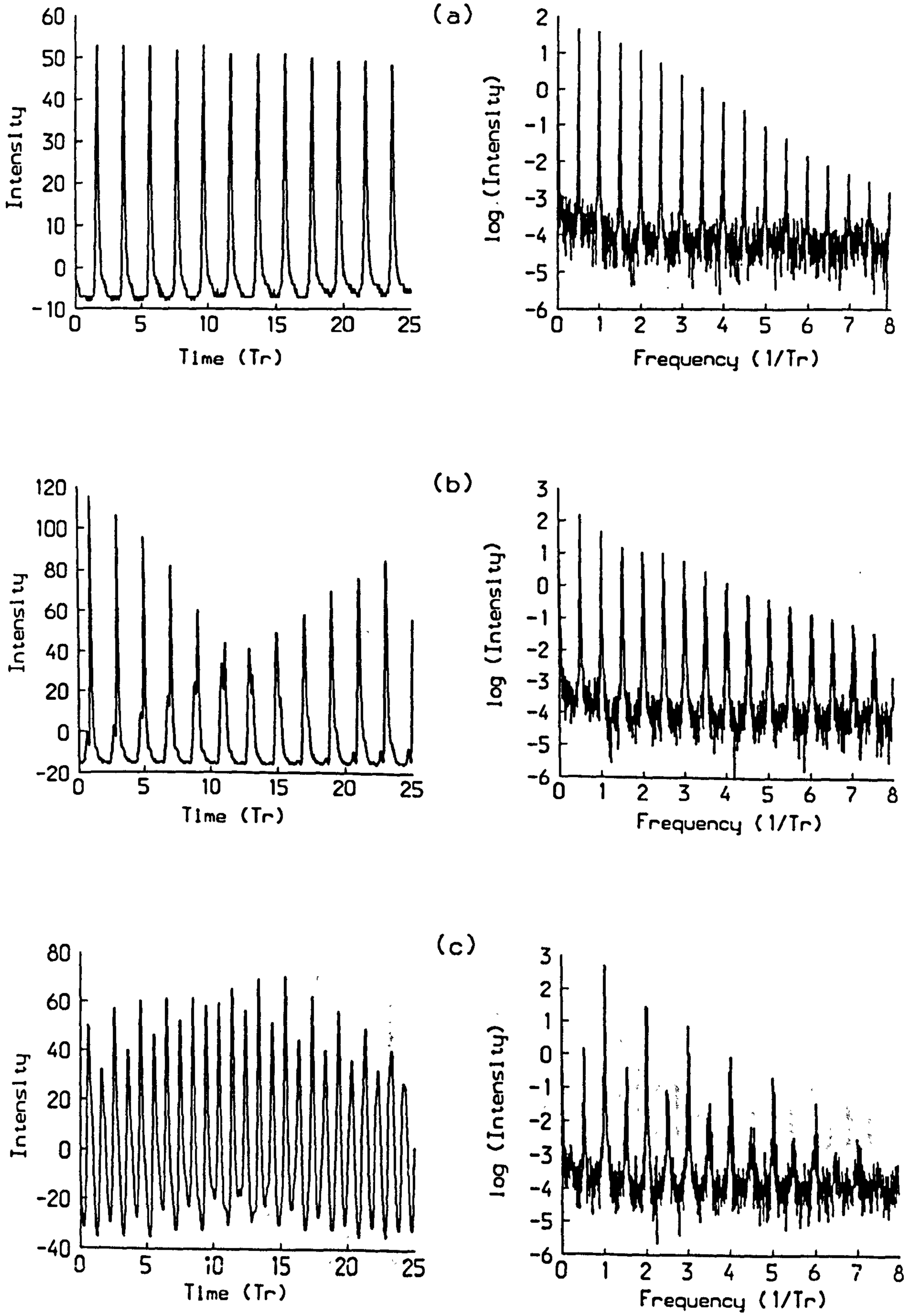

Figure 5.7: Change in SBS signal with increasing power (a) 0.19 W, (b) and (c) 0.26 W.

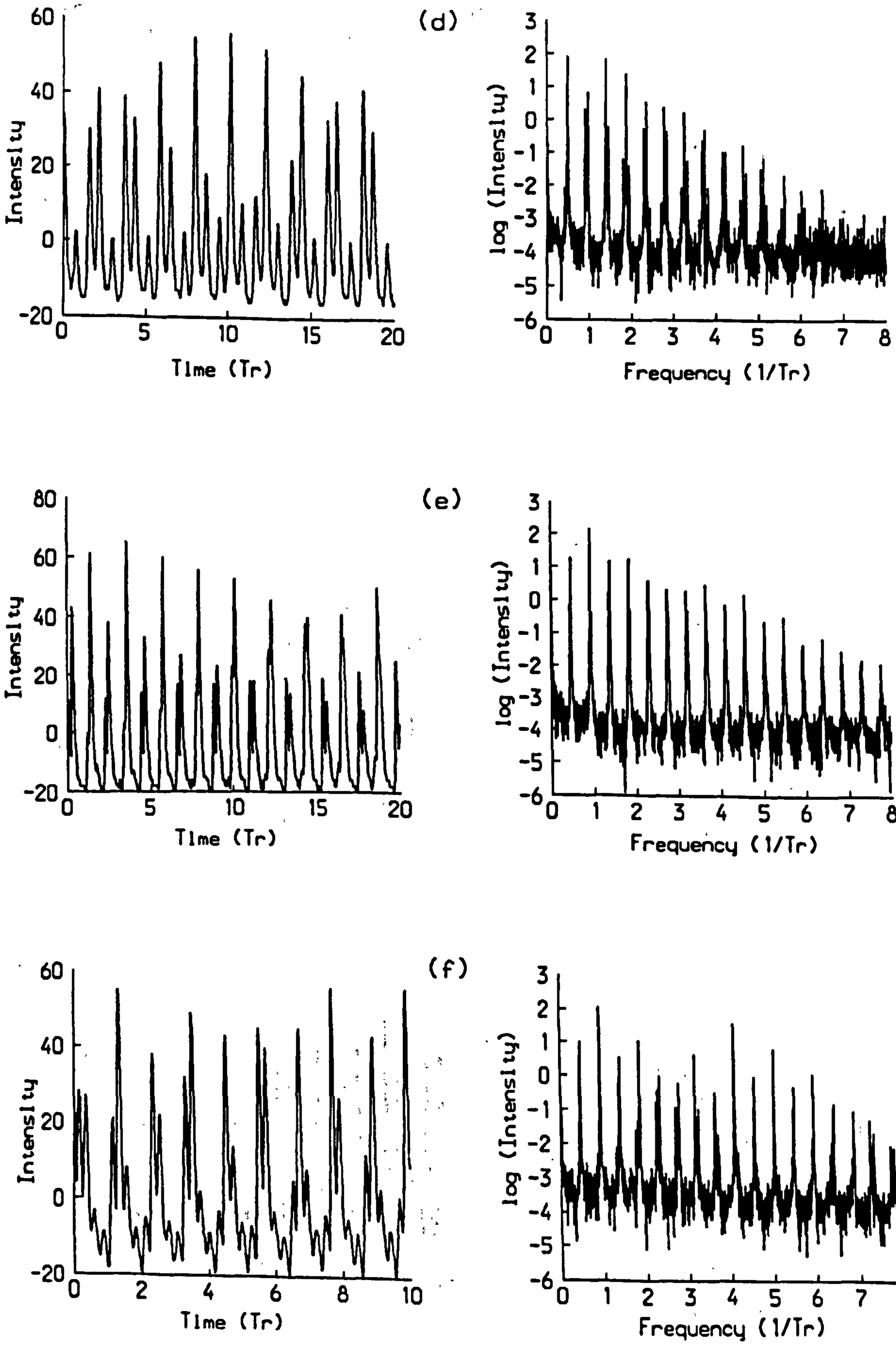

Figure 5.7: Change in SBS signal with increasing power (d) 0.28 W, (e) 0.30 W and (f) 0.39 W.

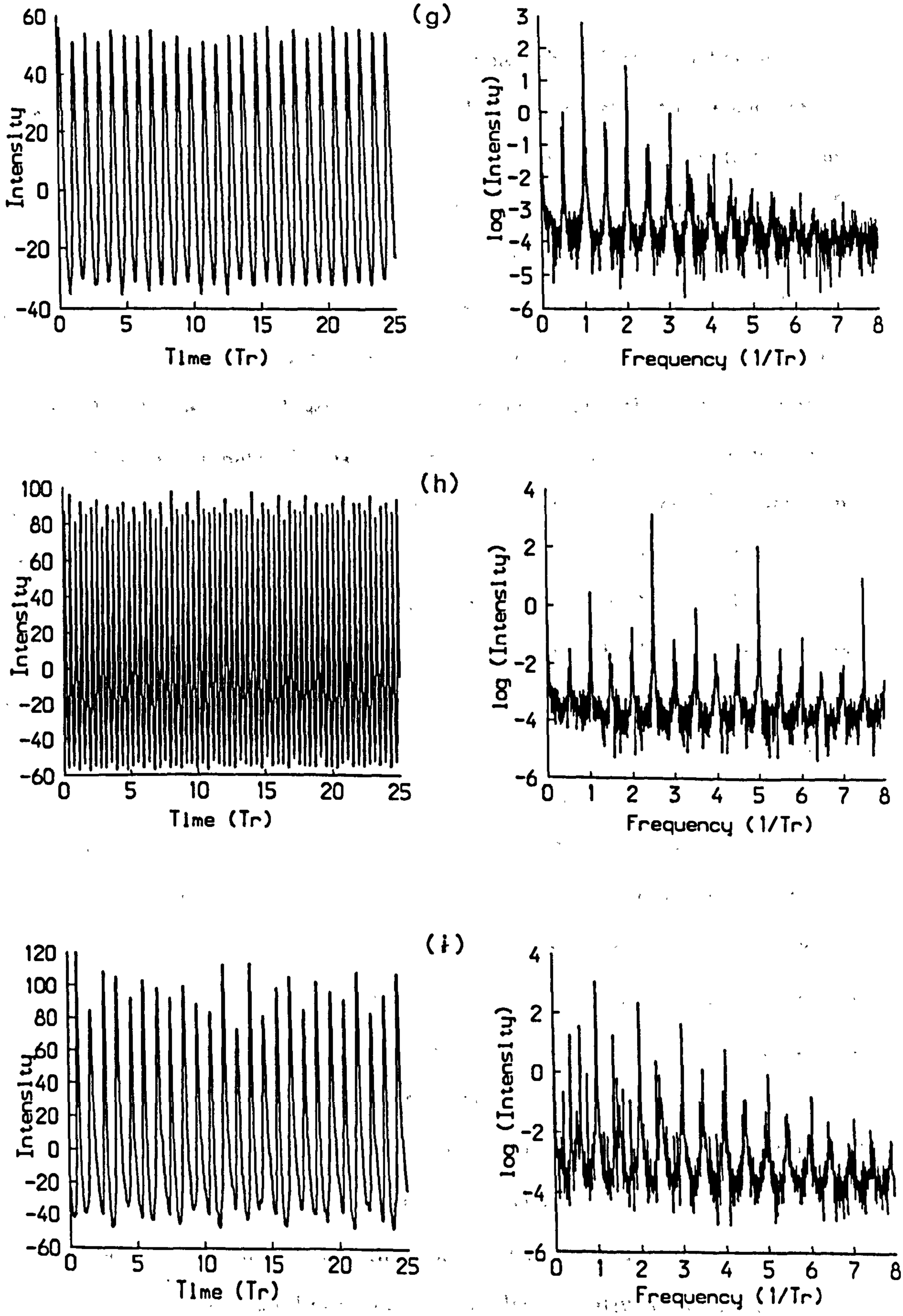

Figure 5.7: Change in SBS signal with increasing power (g) 0.37 W, (h) 0.48 W and (i) 1.20 W.

the appearance of a second set of $2T_r$ oscillations phase shifted from the first set by a varying amount of up to T_r. The two sets of oscillations compete with one another so that as the amplitude of one is increasing the other is decreasing leading to the time series being heavily modulated. Figure 5.7 (b) and (c) show the two extreme cases of this with (b) the two sets of oscillations very close together and (c) separated by T_r. The power spectra again both show the presence of two frequencies close to $1/T_r$. As the power was further increased the time series tended to become more complicated with a third and then a fourth set of oscillations occurring within the basic period of $2T_r$ which again compete with each other leading to a heavily modulated signal. Figures 5.7 (d) and (e) show examples of the time series for these two cases. In some cases the time series was found to contain as many as nine sets of oscillations within the cavity round-trip time and this is shown in figure 5.7 (f). Taking into account the slight changes in power which can occur due to the drifting of the launch conditions the number of sets of oscillations was seen to increase with pump power.

Sustained T_r oscillations with only a small depth of modulation were also detected, these were found to have a sinusoidal appearance and produce the second type of limit cycles like those shown in figure 5.6 (b). All these features were found in the power region where the SBS was found to be heavily modulated and show pulsations, as in figure 5.4 (b) to (d). At higher powers, corresponding to the region of short spikes like that shown in figure 5.4 (e), faster frequencies were occasionally observed, for example that shown in figure 5.7 (h), where the basic frequencies are integer multiples of the round-trip frequency $1/2T_r$.

The SBS still originates from the amplification of spontaneous scattering but the weak cavity formed by the fibre's natural reflectivity is enough to totally alter the temporal behaviour of the SBS and therefore the transmitted pump. At powers just above threshold the temporal behaviour of the SBS is relatively simple and consists of periodic pulses separated by the cavity round-trip time. However as the pump

power is increased the behaviour becomes much more complicated and the single pulses can break up so that there are many oscillations which compete against each other and grow and decay accordingly.

Although small, SPM will cause the pulses in the SBS to be frequency chirped so that the optical frequencies in the leading part of the pulse will be lowered and those in the trailing half raised. As the fibre is being used in its normal dispersion regime the SPM acting with GVD should lead to pulse broadening, but due to the short interaction length, the low peak powers involved and the size of the nonlinearity any broadening which does occur will be very small. However the frequency chirp may cause the Brillouin gain of the leading and trailing edges of the pulse to be reduced since these parts encounter frequency shifts which move them from the Stokes frequency. This may reduce pump saturation effects and allow other parts of the pulse, for example where the intensity is changing more slowly and hence the frequency shifts are smaller, to have greater gain and therefore grow. When more than one pulse exists the gain of each will depend on the intensity of the other pulses since the gain is affected by the amount of pump depletion.

Figure 5.7 (i) shows an example of the behaviour of the SBS signal at a pump power where second order Stokes is also produced. The power spectrum shows that the dominant frequency is $1/T_r$ but slower frequencies also exist which are not related to the cavity trip-time. At these power levels both the pump and the Stokes intensities are very large and the interactions between the reflected signals becomes significant leading to the time series being further complicated.

5.2.2 Comparison with Theory

Steady and relaxation oscillations with period $2T_r$ have also been found experimentally and theoretically in the presence of external feedback by Bar-Joseph et al. [BAR85]. However they found only $2T_r$ oscillations with none of the modulations

and pulsations which are described here. These oscillations were produced by varying reflectivity while keeping the pump power constant - this is investigated in the next section. Sustained oscillations were found only in a small reflectivity region with relaxation oscillations to a dc state at lower and higher reflectivities. Their theoretical model solves the standard SBS equations in a cavity, excluding nonlinear dispersion terms, neglecting the interaction between the backward pump and the forward SBS. This is much smaller than that between the forward pump and backward SBS when the cavity reflectivity is small, i.e. $R_1R_2 \ll 1$. However the additional features were found by solving equations 2.42 to 2.44 [JOH91] applying the boundary conditions $S_R(t,0) = \sqrt{R_1}S(t,0)$ and $S(t,L) = \sqrt{R_2}S_R(t,L)$, where S_R is the forward travelling SBS signal whose evolution is governed by

$$\frac{\partial S_R}{\partial \tau} + \frac{\partial S_R}{\partial \zeta} = -\frac{\beta S_R}{2} + iu(2|P|^2 + |S|^2)S_R. \tag{5.3}$$

R_1 and R_2 give the cavity reflectivity and the other parameters are as before. Neither of these models is able to describe the behaviour when second order Stokes is produced and to do so would mean including further terms to account for four-wave mixing and the cascading of SBS.

In the absence of nonlinear refraction, the solution of the above equations were found to give relaxation oscillations, which is in agreement with the with the work of Bar-Joseph. However the inclusion of the nonlinearity leads to the dynamical behaviour shown in figure 5.8. The physical values used to produce these results were chosen to correspond to typical values for silica fibres, i.e. Brillouin gain coefficient $g_B = 2.6 \times 10^{-11}$ mW^{-1}, loss coefficient $\alpha = 4.6 \times 10^{-3}$ m^{-1}, nonlinear refractive index coefficient $n_2 = 2 \times 10^{-22}$ m^{2}V^{-2} (based on the electronic contribution), SBS bandwidth $\Delta\nu_B = 143$ MHz and effective core area $A_{eff} = 20$ μm^2. The normalised parameters g and u shown for figures 5.8 (a)-(f) correspond to launched powers of 76, 102, 121, 143, 216 and 338 mW respectively into a 40 m long fibre

with reflectivities of 4% at either end.

Figure 5.8 (a) shows the theoretical SBS output at a pump intensity close to threshold. This shows an alternating two-wave structure leading to a deeply modulated signal, the basic oscillation frequency being $1/T_r$. Increasing the pump intensity sees the alternating wave mode disappear and this is replaced by sustained oscillatory behaviour with a periodic slow modulation, as shown in figure 5.8 (b). The period of the modulation decreases with pump intensity, figure 5.8 (c), until the modulation period approaches or is faster than the period of the basic $1/T_r$ oscillations. This leads to the temporal behaviour becoming faster and random as shown in figure 5.8 (d). Increasing the pump intensity further leads to an ending of the sustained oscillatory behaviour. This is replaced by a bursting mode of operation, see figure 5.8 (e), and eventually the bursting mode may be suppressed to give stable dc emission, figure 5.8 (f). Computational limits did not allow the monitoring of the busting mode of operation over a longer time. Therefore the change in burst length and separation with pump intensity could not be studied. Nevertheless these results show many of the same characteristics and trends as the experimental results presented in this section.

5.3 Addition of External Feedback

The reflectivity of the cavity was increased by butting a reflecting neutral density filter against the far end of the fibre. Using a filter of ND = 0.1, which has a transmittance of approximately 80%, the reflectivity was measured to be about six times greater than natural reflectivity, i.e. $\sim 20\%$. The total reflectivity of the cavity is still small, approximately 7.35×10^{-3}, so that interactions between reflected beams can still be neglected. Increasing the reflectivity leads to a reduction in the threshold power due to an increase the effective gain. Figure 5.9 shows how the SBS signal changes as the pump power is increased for a 25 m fibre, again LTI. Again the

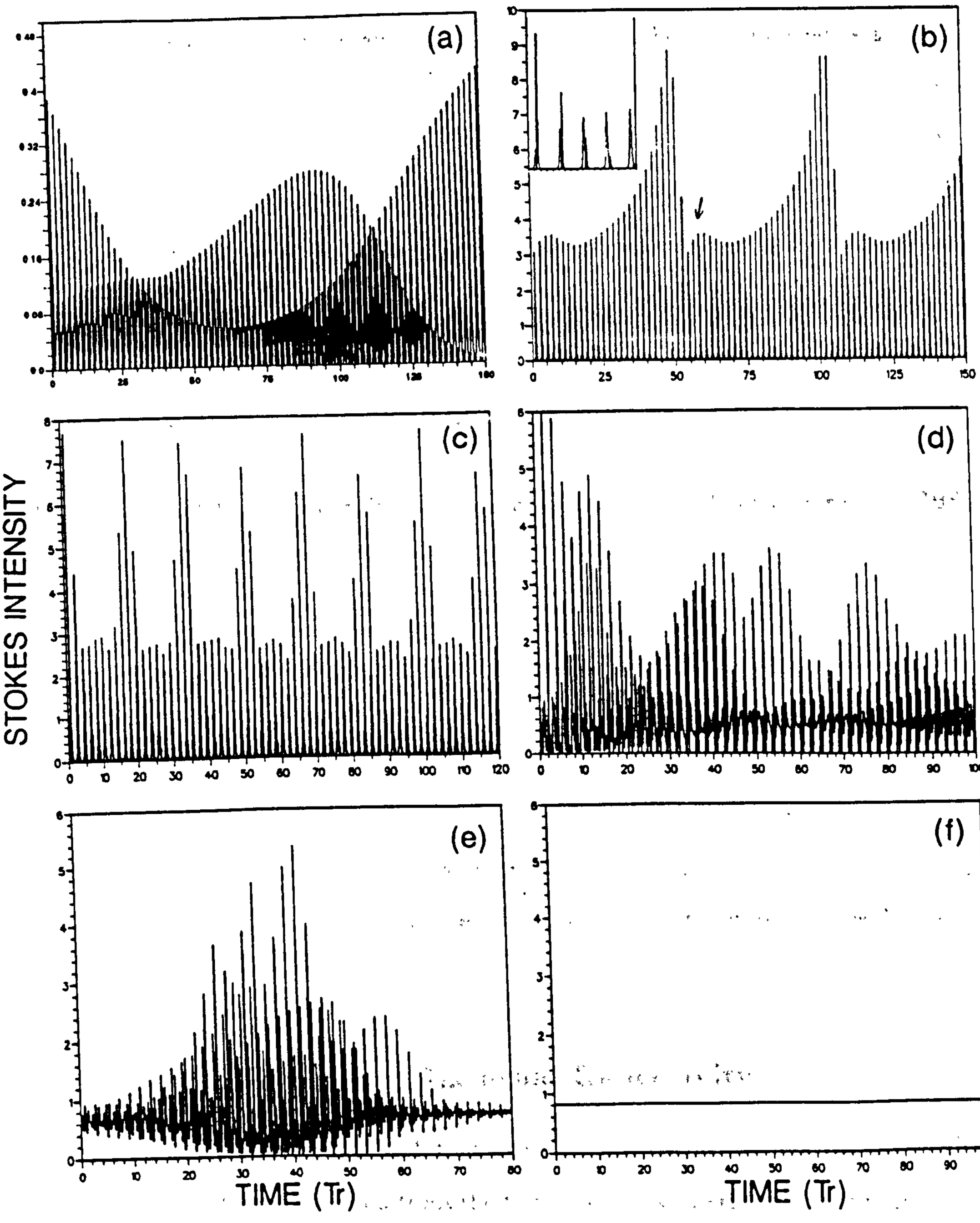

Figure 5.8: Theoretical time series of Stokes with natural reflectivity on increasing pump power (a) $g = 4.0, u = 0.12$, (b) $g = 5.4, u = 0.16$, (c) $g = 6.4, u = 0.19$, (d) $g = 7.5, u = 0.23$, (e) $g = 11.4, u = 0.34$ and (f) $g = 17.3, u = 0.53$; other parametrs are fixed at $\beta = 0.184$, $\beta_A = 90$ and $R_1 = R_2 = 4\%$. SBS intensity is in normalised units.

SBS goes through modulations and pulsations until it reaches the same near stable dc state as before, in this case at a pump power of 1.15 W compared to the threshold power of 0.21 W. Using a larger cavity reflectivity allowed the complete range of dynamical features to be seen over a smaller range of pump power. Theoretical results also predicted the same behaviour as that shown in figure 5.8 but at reduced powers.

5.4 Variation of Reflectivity

Having investigated the intensity dependency of the temporal behaviour of the SBS process the effect of varying the cavity reflectivity while keeping the pump constant is now examined. The far end of the fibre was index matched as before but the transmitted light was reflected by an external mirror and then relaunched into the fibre. By moving the microscope objective lens in and out and therefore changing the divergence of the emergent beam the reflectivity of the far end could be varied, see figure 5.10. The other end of the cavity was formed by the fibre's natural reflectivity. Using a 100% external mirror the maximum reflectivity was measured to be $\sim 60\%$, limited by coupling losses, allowing the reflectivity of the cavity to be varied between 1.05×10^{-6} and 2.1×10^{-2}.

5.4.1 Measurement of External Reflectivity

It was explained in section 5.2.1 that the reflected signal below threshold is the superposition of light reflected from the front and back interfaces of the fibre. This is modulated due to the optical length of the fibre changing caused by the temperature dependence of the refractive index. The average of the unmodulated and the modulated parts increases linearly as the reflectivity of the external mirror is increased. Comparison of the signal height with the mirror blocked and against the

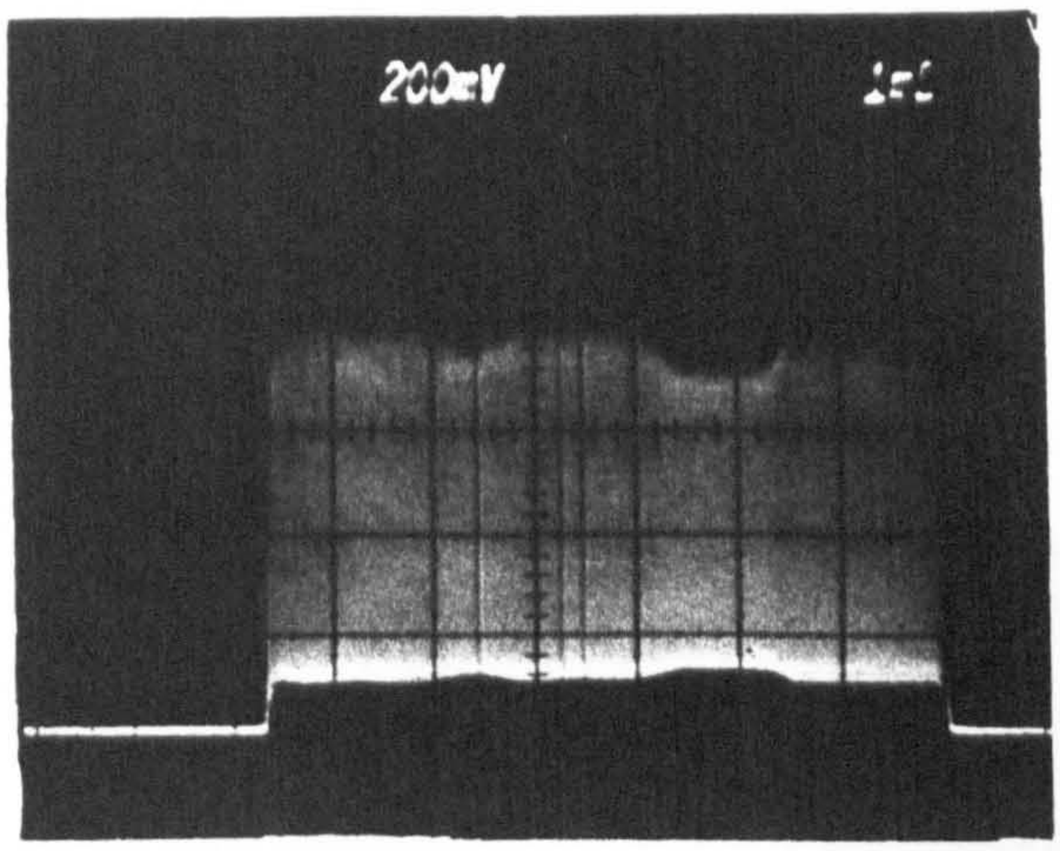

(a)

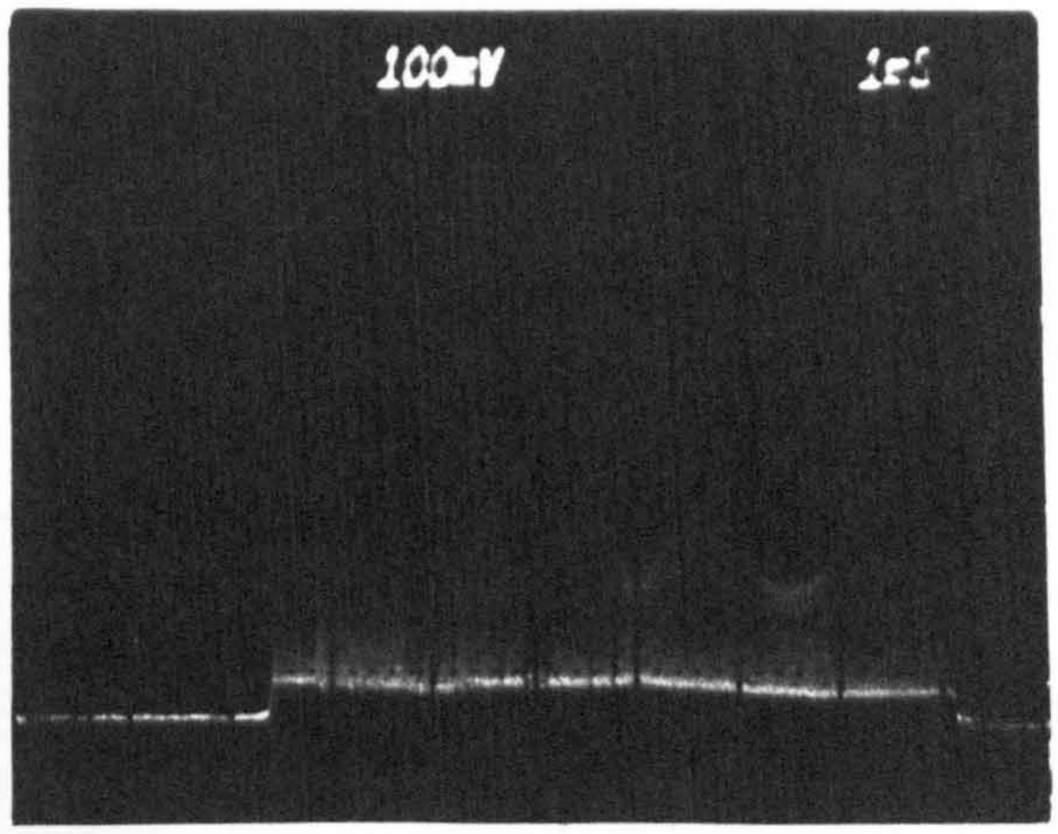

(b)

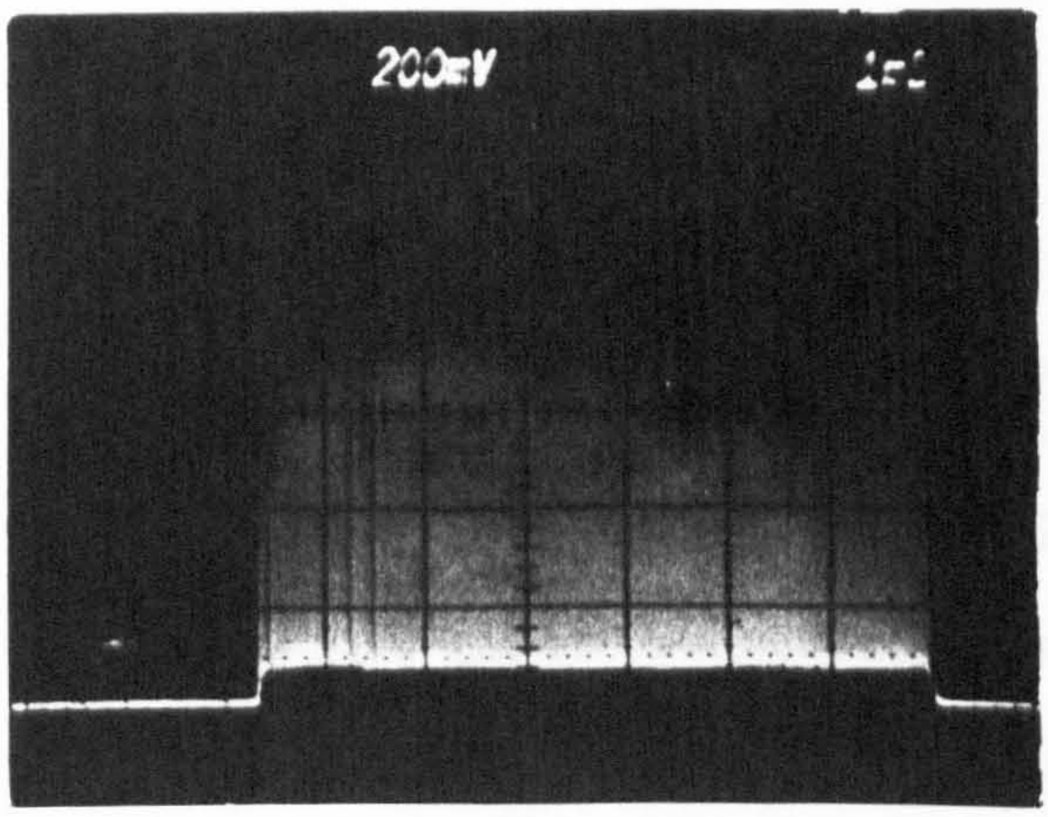

(c)

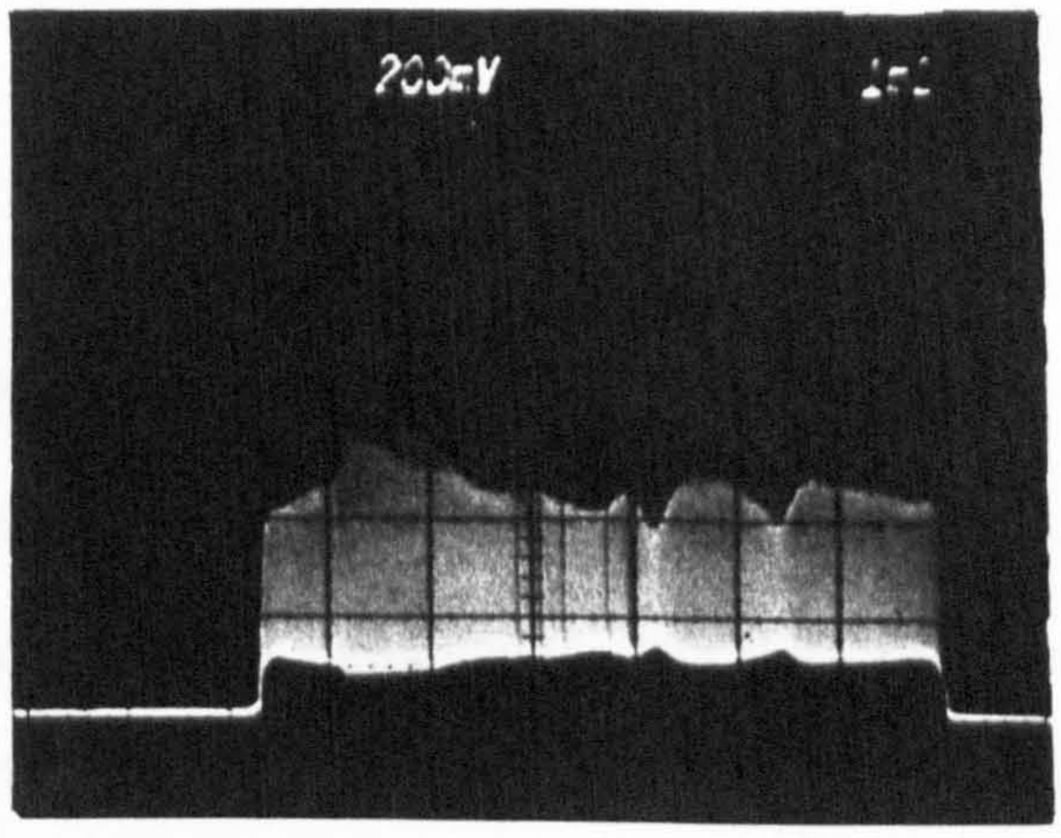

(d)

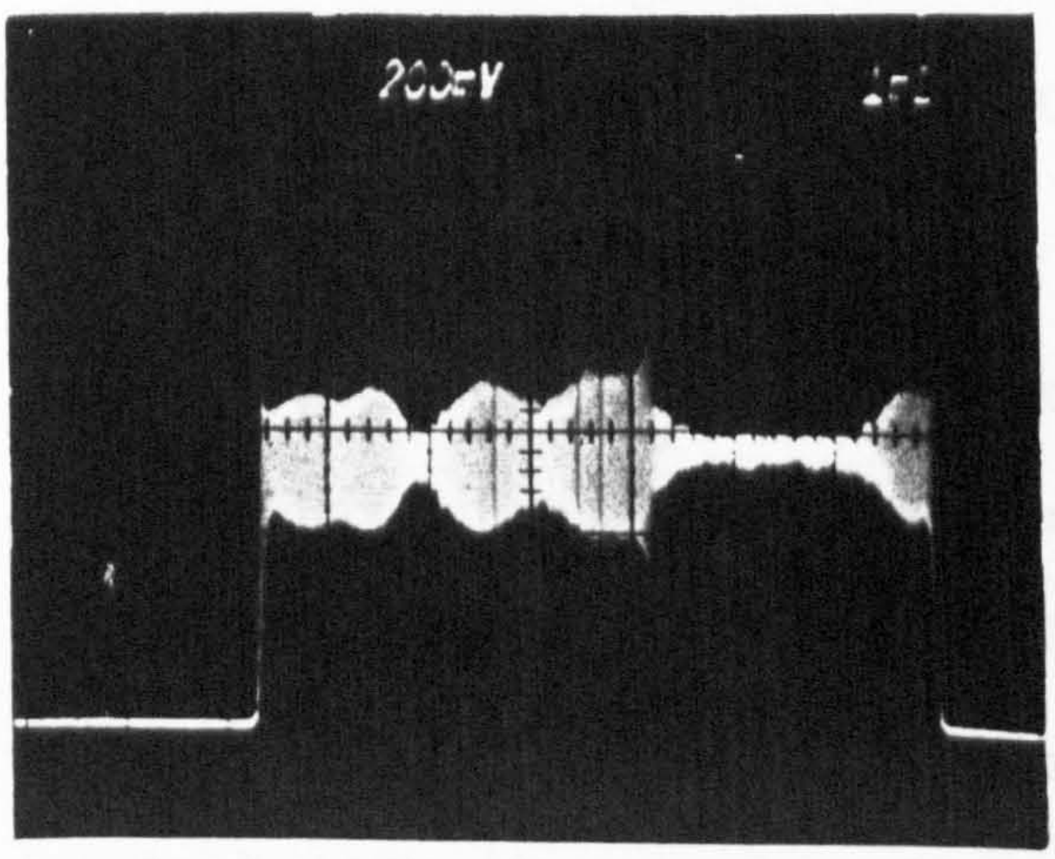

(e)

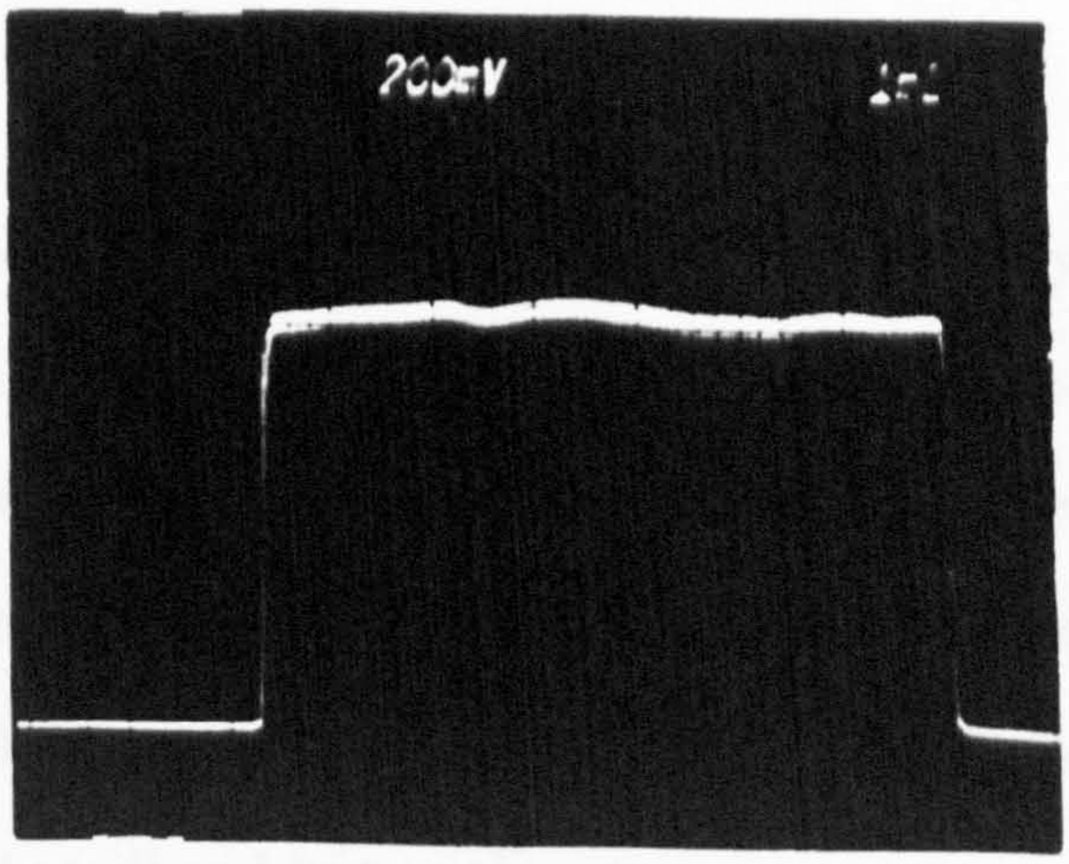

(f)

Figure 5.9: SBS signal with external feedback: (a) 0.35 W, (b) 0.43 W, (c) 0.55 W, (d) 0.66 W, (e) 0.91 and (f) 1.15 W, (time scale is 1 ms/div).

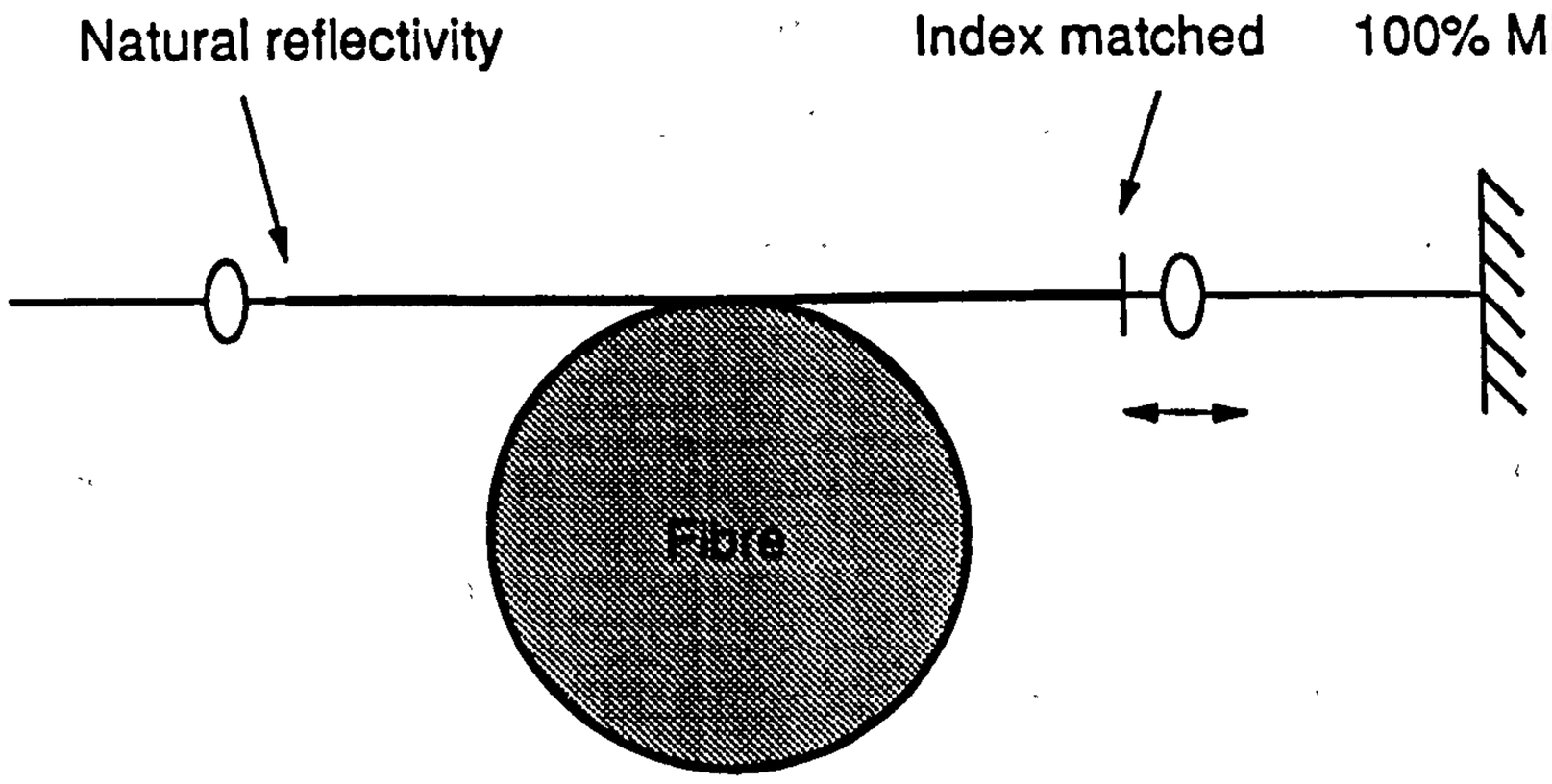

Figure 5.10: Variation of external reflectivity

fibre's natural reflectivity makes it possible to estimate the effective external reflectivity. This was cross checked by comparing the SBS signals when the reflectivity of the external mirror was calculated to be the same as natural reflectivity and these were found to exhibit similar temporal behaviour.

5.4.2 Temporal Behaviour

When the fibre was index matched at both ends the power spectra was entirely broadband with no discrete frequencies, like those spectra shown in chapter 4. Interestingly with the external mirror blocked and the rear end of the fibre index matched but no index matching at the front, the reflectivity was still sufficient for small discrete frequencies to be seen in the power spectrum. At powers just above threshold the power spectrum is entirely broadband but as the pump power was increased small peaks at the round-trip frequency and its harmonics were seen which grow in strength as the power was further increased. Figure 5.11 shows this effect

as the launched power was increased from (a) 100 mW, (b) 150 mW, (c) 220 mW to (d) 300 mW for a 50 m piece of HB 450 - polarisation maintaining fibre . The light was launched along one of the fibre's axes where the threshold power for this length and fibre was found to be $\sim$ 90 mW. The cavity effects are very small, even at high powers, and the SBS signal retains its aperiodic appearance. Although the total reflectivity is very small, only $\sim 1 \times 10^{-6}$, this is still sufficient for these weak cavity effects to be seen which is why the experiments in chapter 4 were carried out with the fibre index matched at both ends.

Using a 36.5 m piece of LTI fibre, a pump power was chosen so that there was still an SBS signal even with the path to the mirror blocked. The reflectivity was then gradually increased by moving the microscope objective towards the fibre and figure 5.12 shows how the chopped SBS signal and power spectrum changed as the reflectivity was varied while the pump was kept at a constant launched power of 400 mW.

Figure 5.12 (a) corresponds to a reflectivity at the far end of $< 0.25\%$ and the corresponding power spectrum shows only a few small discrete frequencies on a broadband background. It should be remembered that the spectrum analyser samples over a sweep time of 1.2 ms so all the fluctuations and different frequencies contained in the signal over this time will be captured. The reflectivity was increased to $\sim 0.5\%$, figure 5.12 (b), and the discrete frequencies in the power spectra grew in strength. With the reflectivity increased to $\sim 3.25\%$ the chopped signal starts to become modulated and the power spectra contains large discrete frequencies, figure 5.12 (c). A small increase to $\sim 3.75\%$, figure 5.12 (d) sees these modulations becoming larger while the discrete frequencies continue to grow. At a reflectivity of $\sim 5.75\%$ the SBS now comes in the form of definite pulsations, figure 5.12 (e), while at $\sim 20\%$, figure 5.12 (f), the signal is almost entirely dc with only occasional short bursts of periodic modulations and the power spectra has a large dc element.

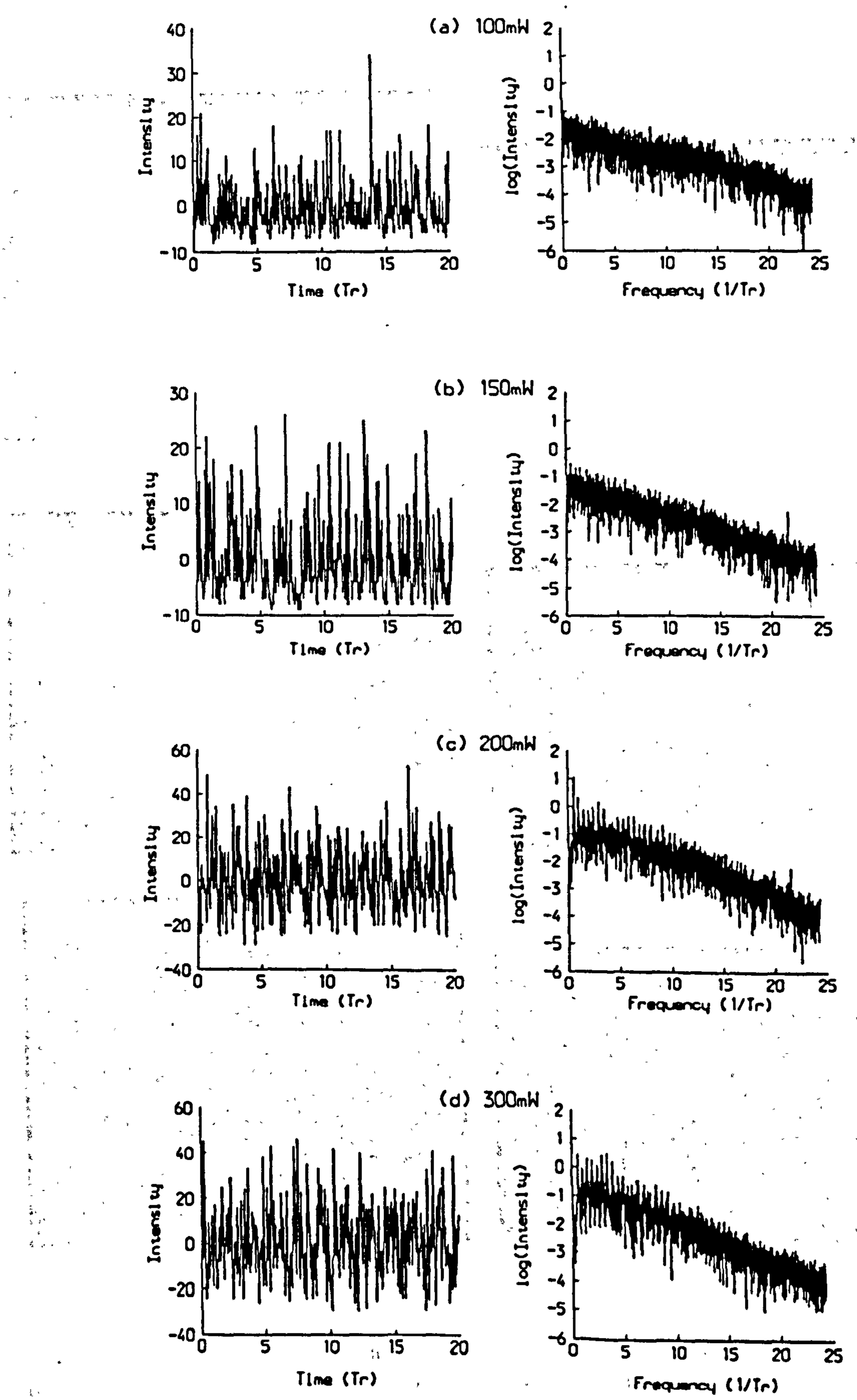

Figure 5.11: Effect of increasing pump power on SBS in a very poor cavity

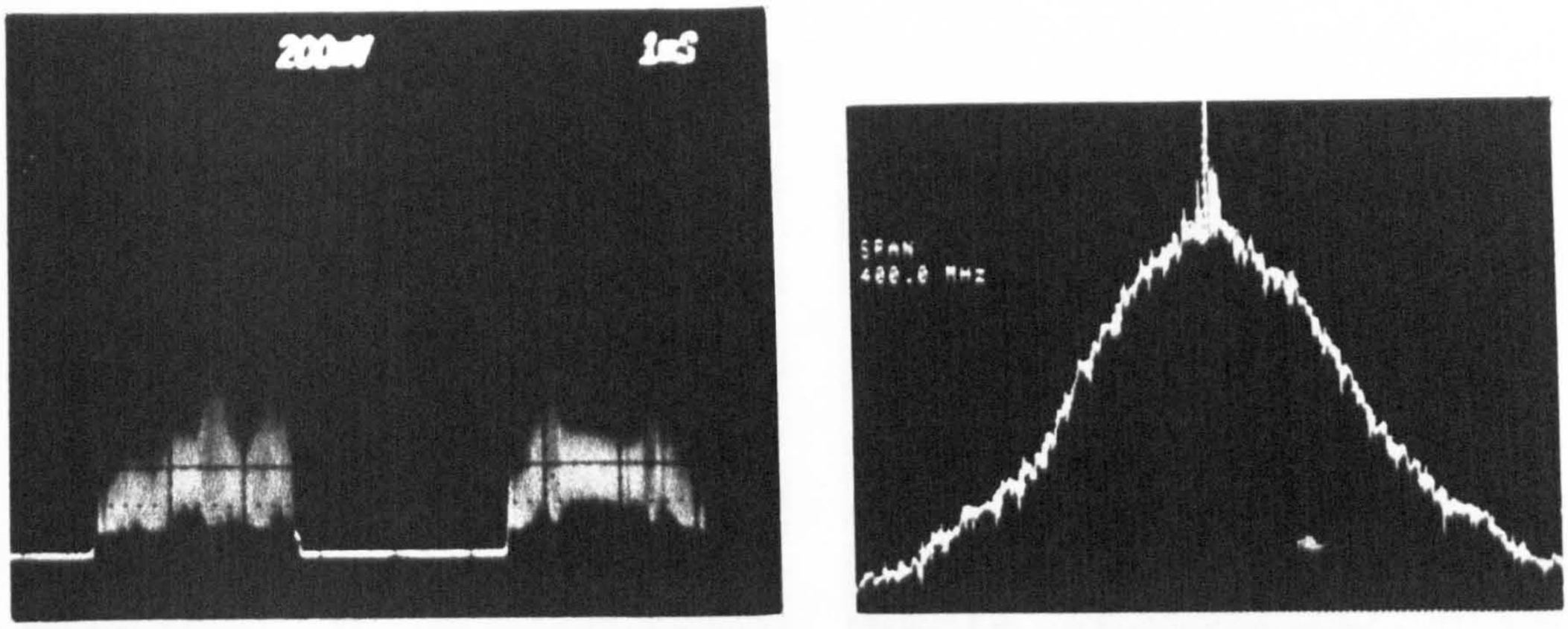

(a)

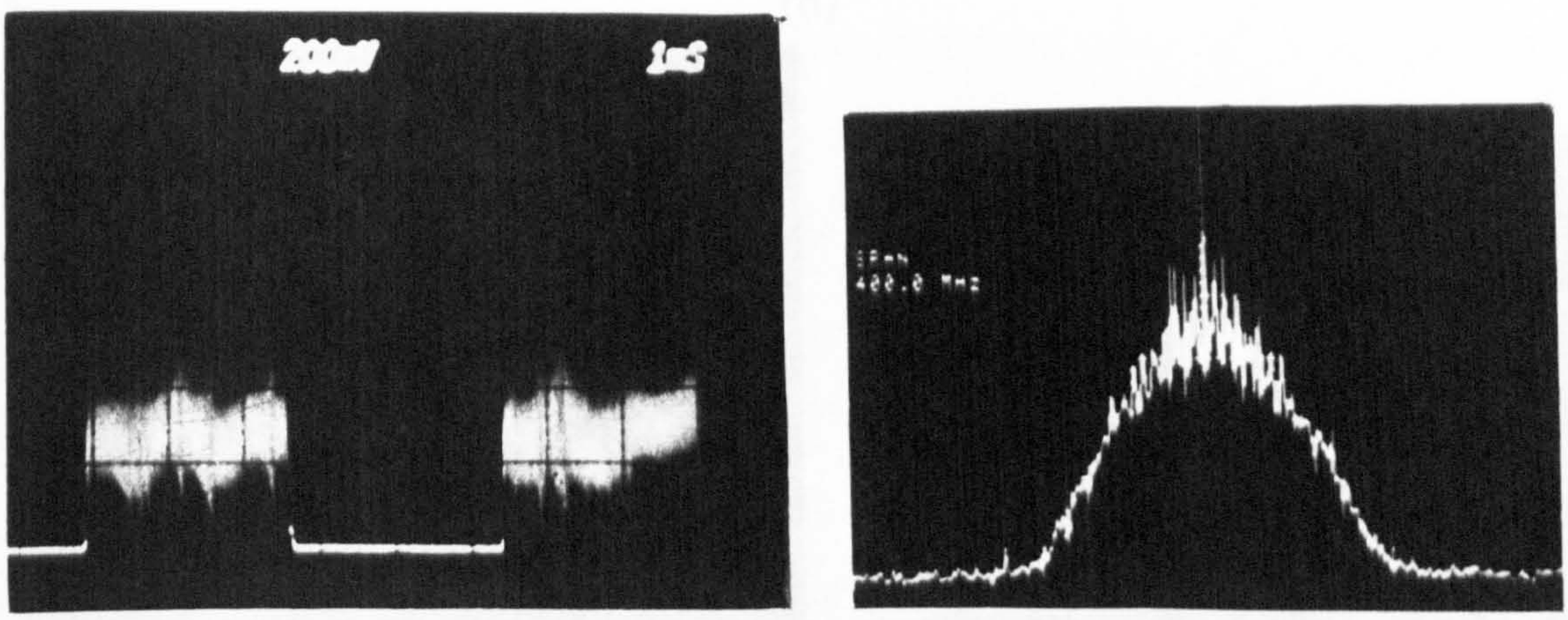

(b)

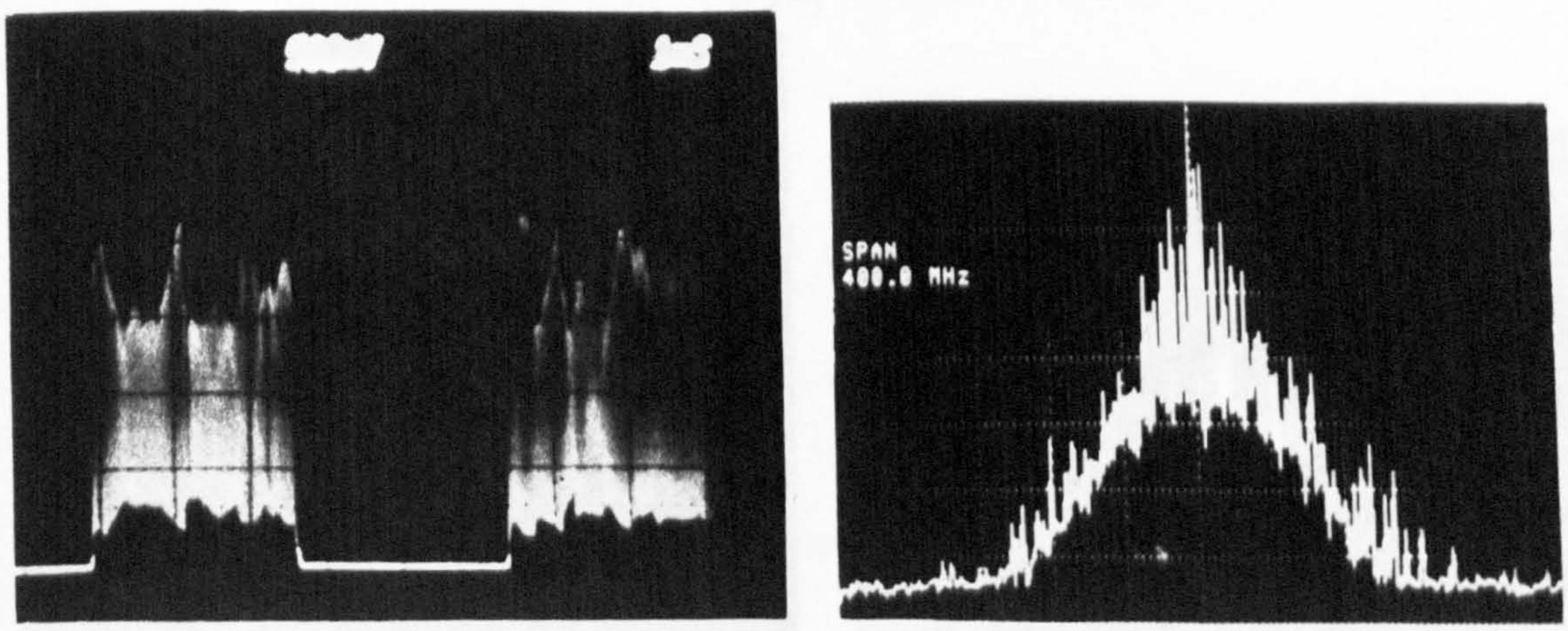

(c)

Figure 5.12: Effective of changing external reflectivity on SBS (a) $< 0.25\%$, (b) 0.5% and (c) 3.25%, (time scale is 1 ms/div and frequency span is 400 MHz, resolution bandwidth 30 kHz and sweep time 1.2 s).

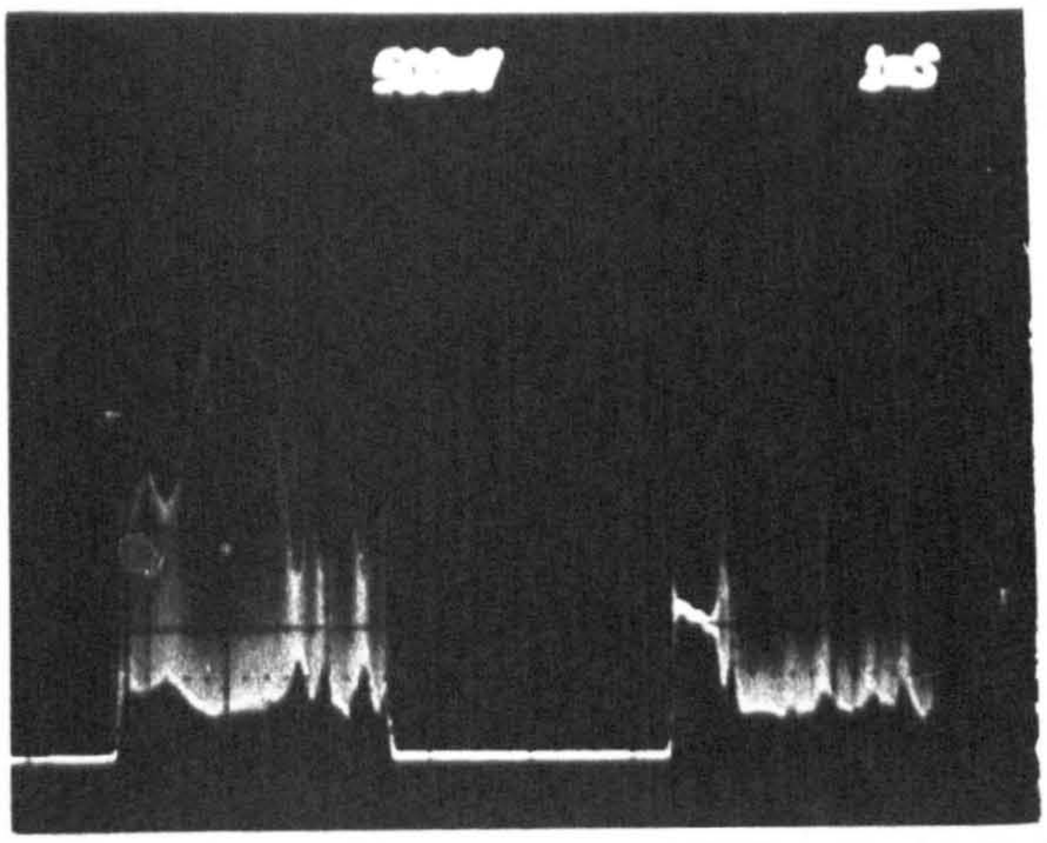

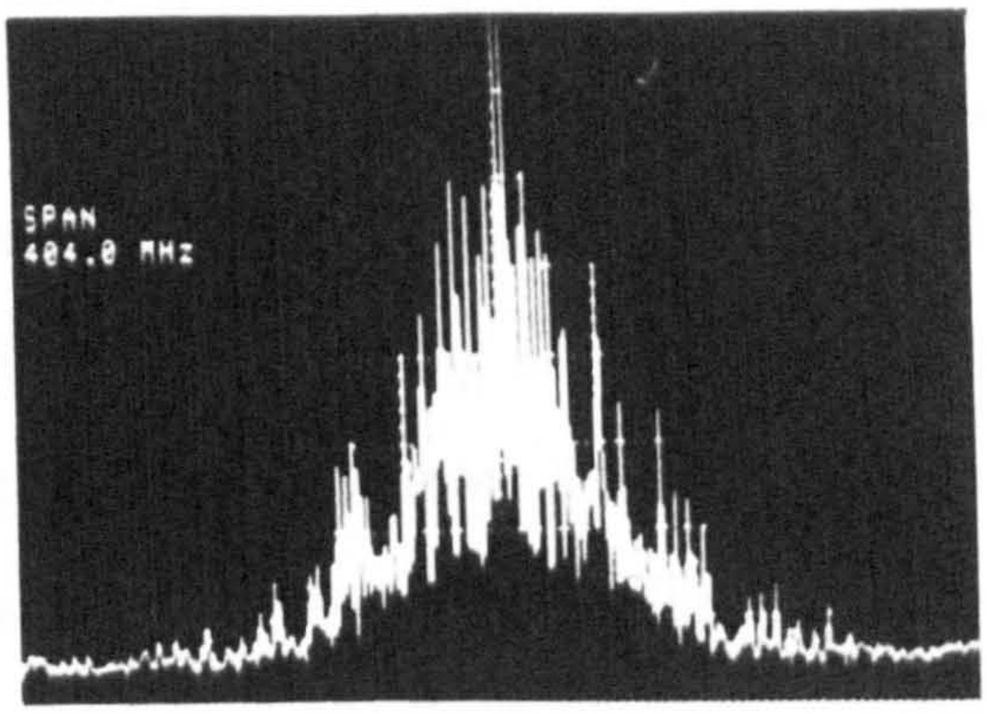

(d)

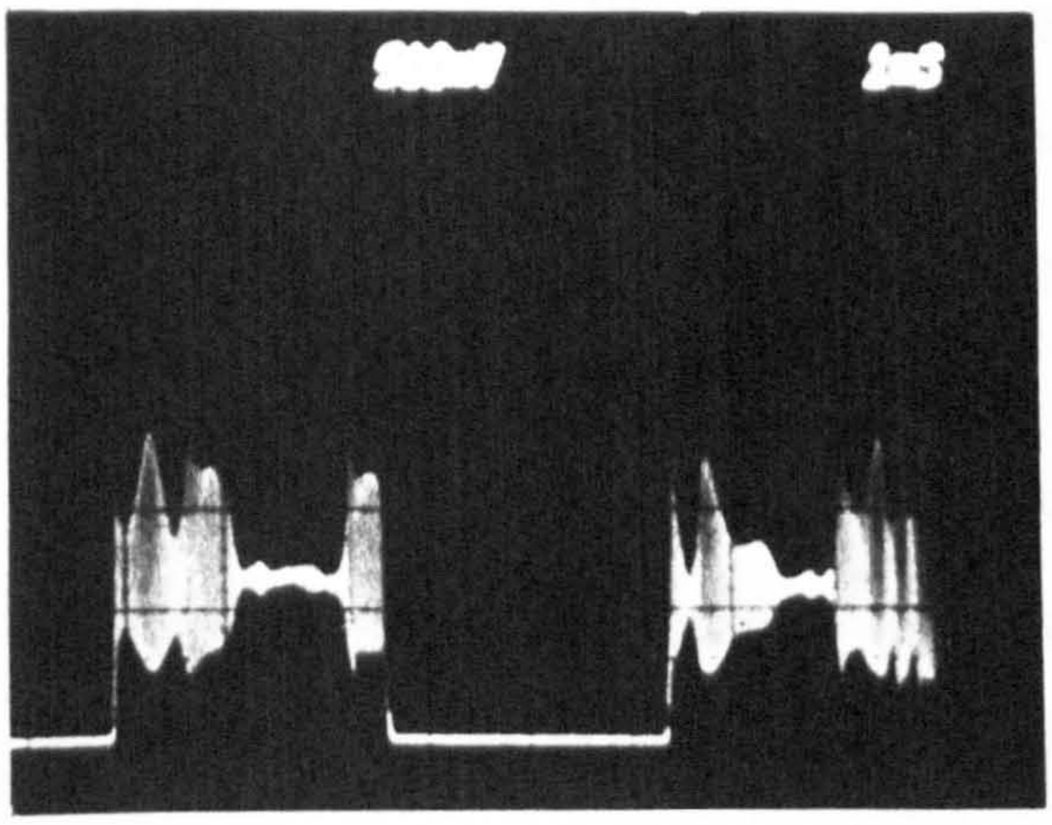

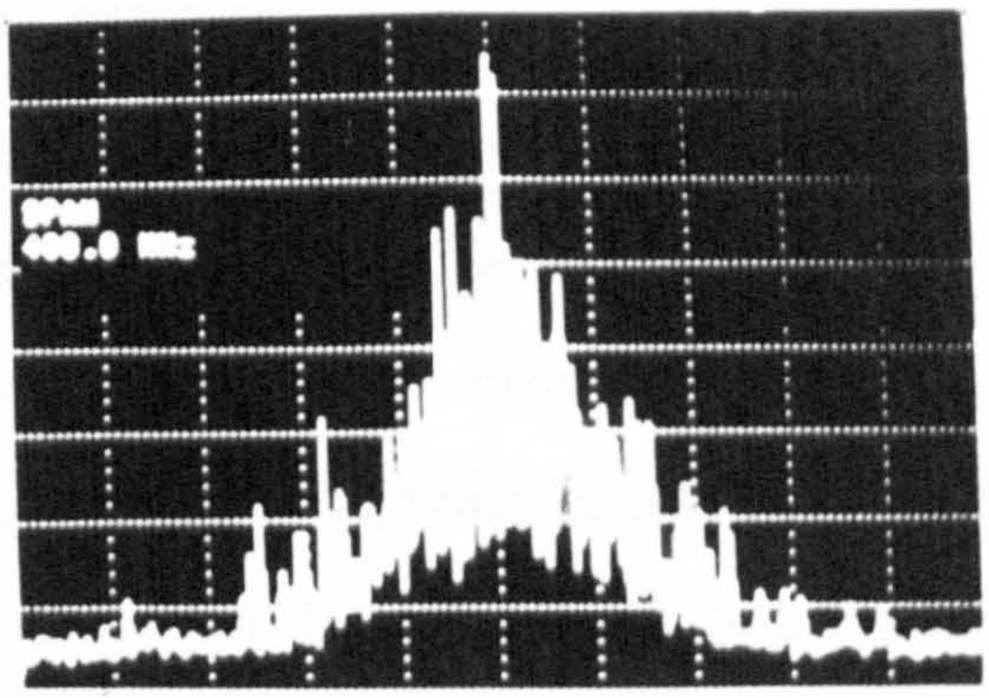

(e)

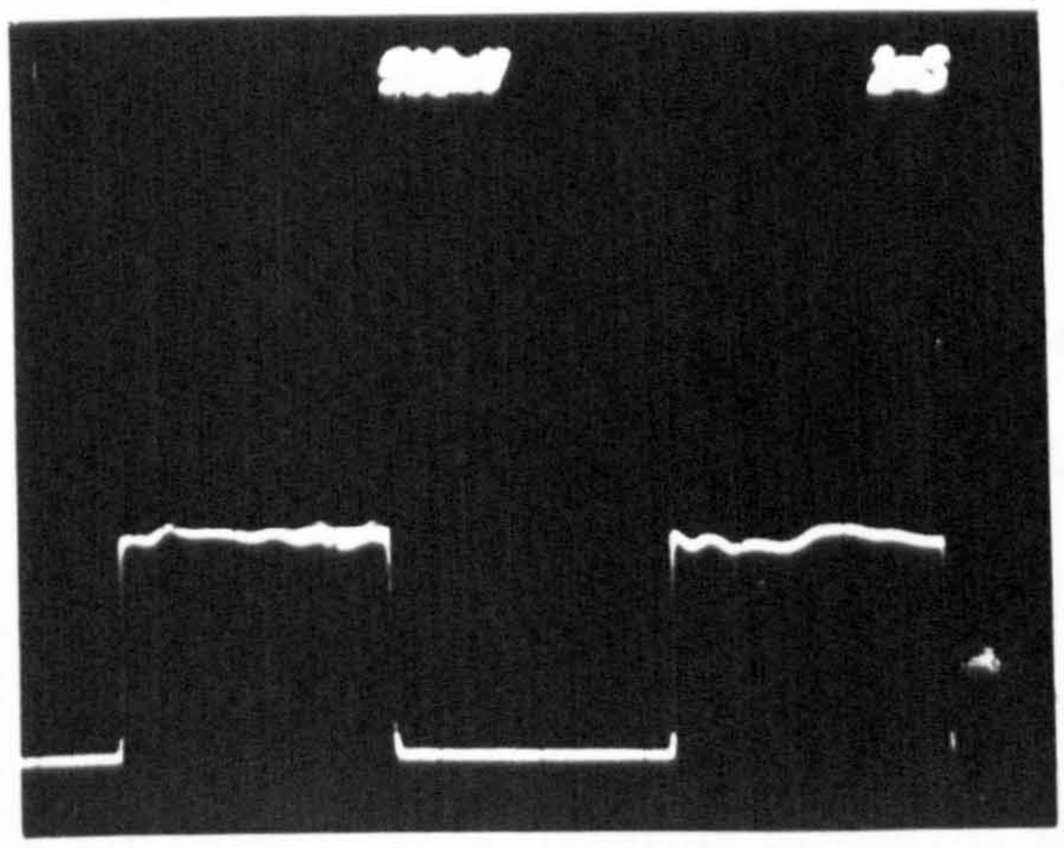

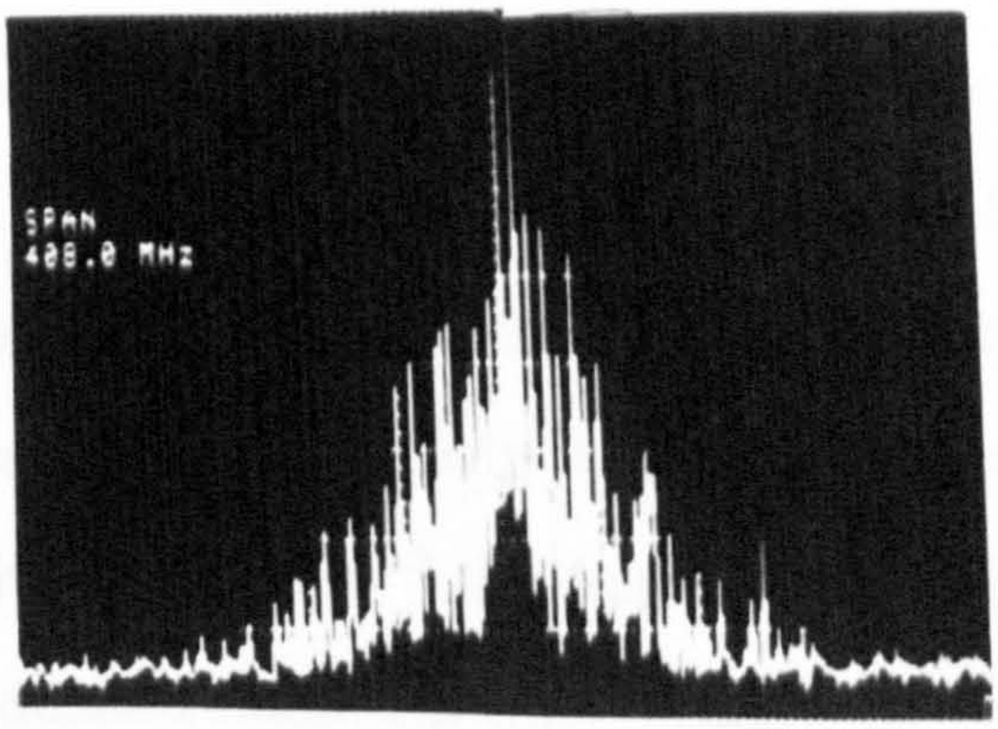

(f)

Figure 5.12: Effective of changing external reflectivity on SBS (d) 3.75%,(e) 5.75% and (f) 20% (time scale is 1 ms/div and frequency span is 400 MHz, resolution bandwidth 30 kHz and sweep time 1.2 s).

In chapter 3 it was found that increasing reflectivity has the same effect on the steady-state behaviour as increasing the Brillouin gain. In the first part of this chapter it was shown that increasing the gain by increasing the pump power turned sustained periodic signal to an almost dc signal. However in addition to increasing the gain raising the pump power also leads to a strengthen of both the SPM and XPM of the signals. An increase in the cavity reflectivity also results in stronger refractive effects as this increases the gain and therefore leads to a more intense SBS signal. So it would appear than increasing the reflectivity has the same effect as increasing the pump power but this also shows aperiodic oscillations turning into periodic ones. The SBS signals were again digitised using a 5 ns sampling rates to allow the temporal behaviour to be clearly examined.

Figure 5.13 (a) shows the time series and power spectrum with both ends of the fibre index matched and the external mirror blocked. The times series is clearly aperiodic and the power spectrum is broadband with no discrete frequencies. Removing the index matching at the front, causing an increase in reflectivity, results in the appearance of small peaks at the round-trip frequency and its harmonics in the power spectrum, figure 5.13 (b), the reflectivity of the cavity is $\sim 1 \times 10^{-6}$. As the cavity reflectivity is increased the discrete frequencies grow in strength as the SBS signal gradually becomes periodic in nature. Figure 5.13 (c) and (d) show the gradual transition to periodic behaviour. At a reflectivity of 1.14×10^{-3} the SBS shows modulated $2T_r$ oscillations and the power spectrum now shows large discrete frequencies with two main frequencies close to the round-trip frequency and only a small broadband shoulder. At a reflectivity of 1.66×10^{-3} the dominant frequencies are close to $1/T_r$ resulting in heavily modulated roundtrip-time oscillations.

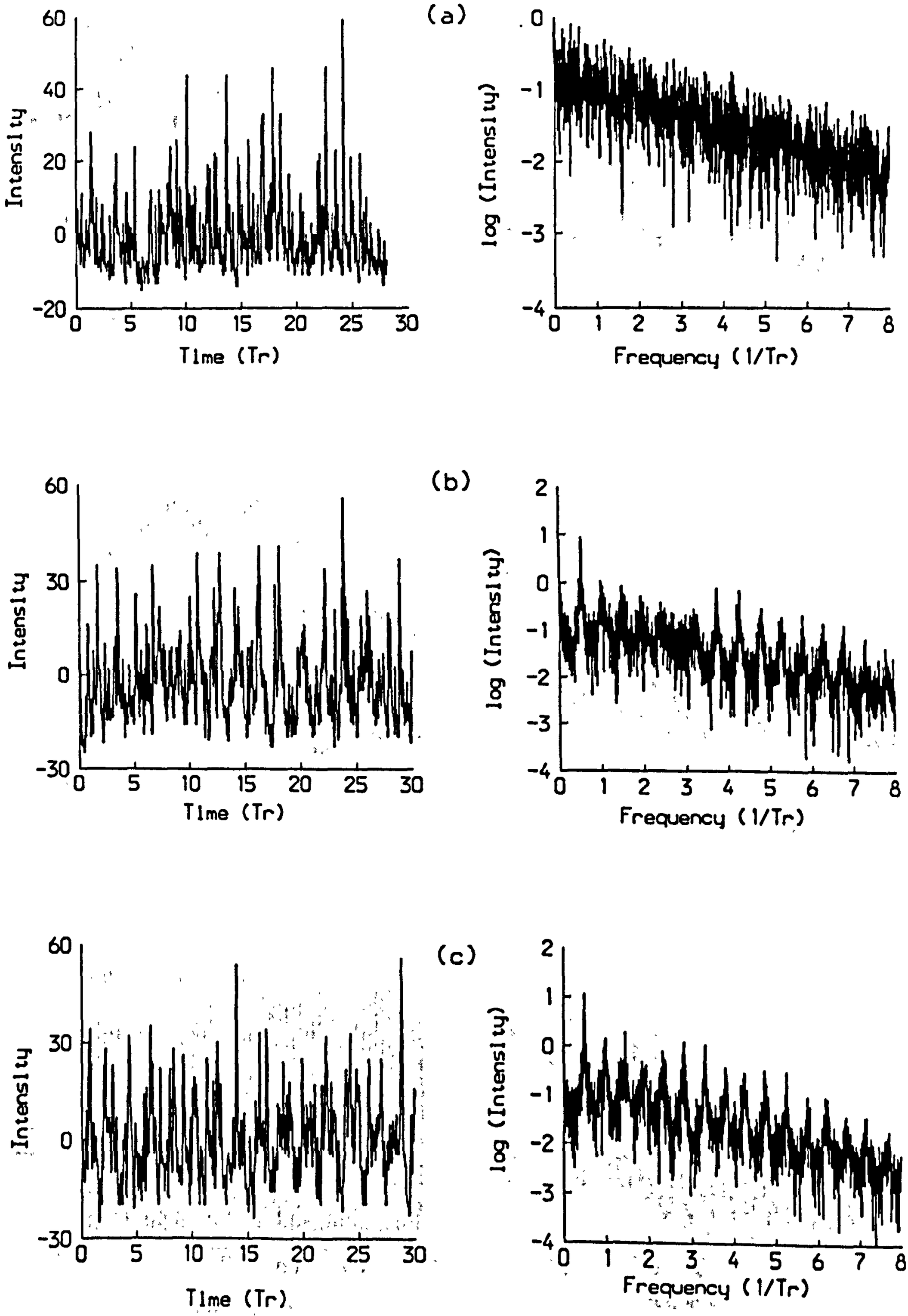

Figure 5.13: Change in SBS temporal behaviour with reflectivity (a) 9×10^{-10}, (b) 1×10^{-6} and (c) 1.75×10^{-4}.

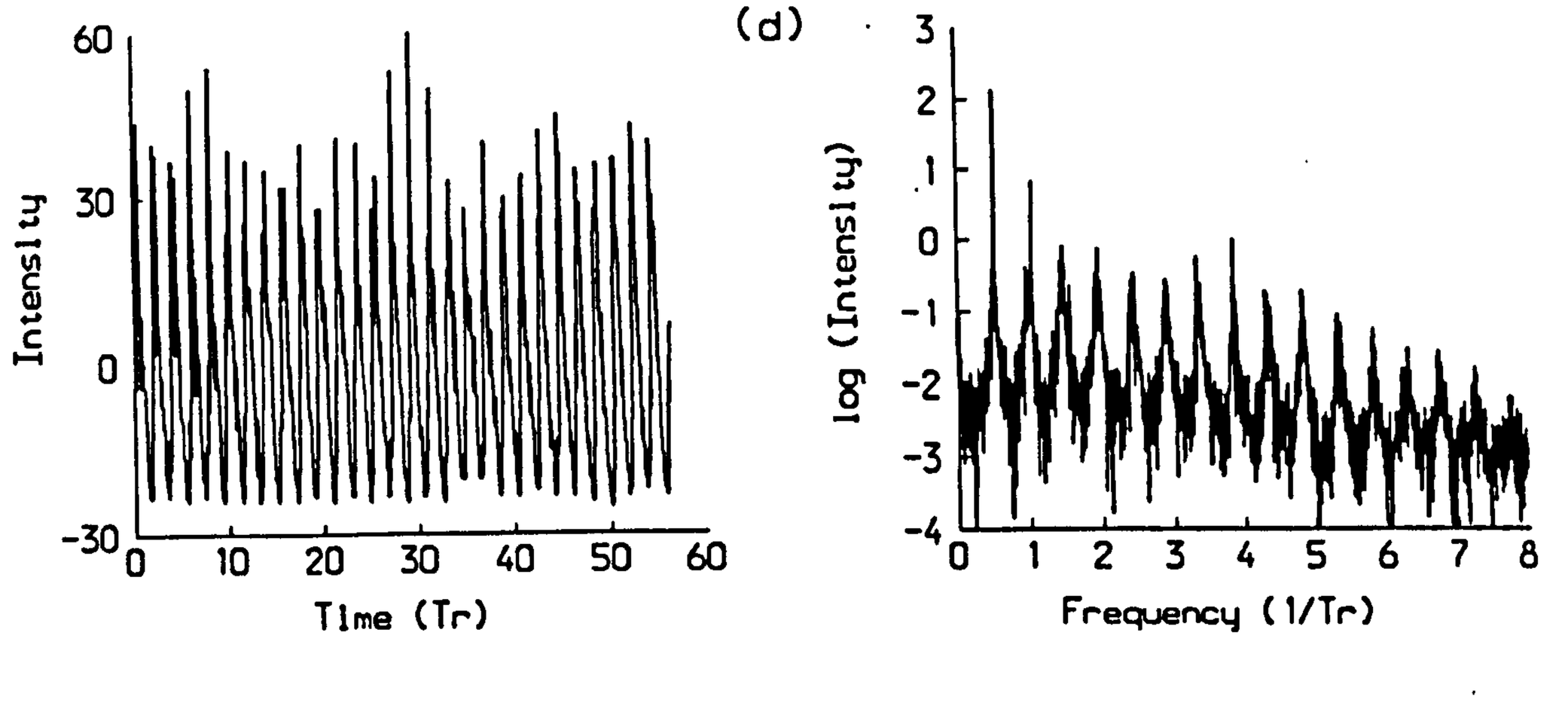

Figure 5.13: Change in SBS temporal behaviour with reflectivity (d) 5.25×10^{-4}, (e) 1.14×10^{-3} and (f) 1.66×10^{-3}.

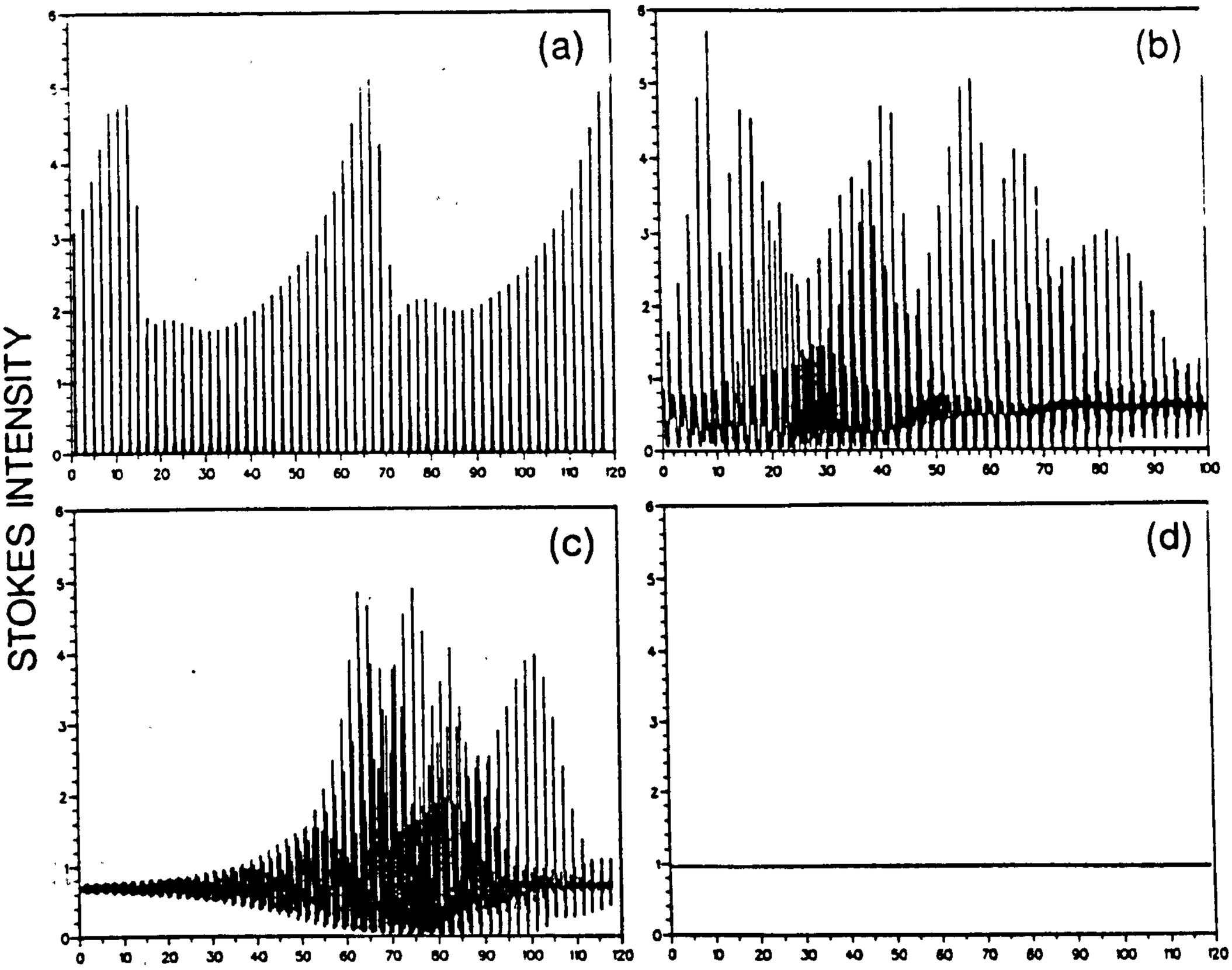

Figure 5.14: Theoretical change in dynamical behaviour on increasing cavity reflectivity (a) $R_1 = R_2 = 0.25\%$, (b) $R_1 = R_2 = 4\%$, (c) $R_1 = R_2 = 9\%$ and (d) $R_1 = R_2 = 36\%$. g and u are fixed at 8.7 and 0.26 repectively with the other normalised parameters the same as those used to produce figure 5.8. SBS intensity is in normalised units.

5.4.3 Comparison with Theory

Figure 5.14 shows a set of four temporal forms of the Stokes intensity for different reflectivities, 0.25%, 4%, 9% and 36% respectively, for a fibre length of 40 m and a pump power of 166 mW assuming the same physical values given in section 5.2.2. The output changes from sustained oscillation of basic frequency $1/2T_r$ with a slow modulation, to oscillations with a fast modulation, then to a bursting mode of operation and eventually to stable emission. Again this is the same sequence of events as show by both the theoretical and experimental results for increasing pump power and also for the cavity reflectivity experiment. However the theoretical results do not show the aperiodic behaviour at very low reflectivity and the results are achieved at different reflectivities. This is due to a higher value of pump power being used experimentally and therefore the theoretical values of the Brillouin gain and nonlinear refraction are smaller than those found in the experiment.

5.5 Conclusions

The addition of external feedback dramatically changes the temporal behaviour of the SBS and transmitted pump. Even the small amount of reflectivity caused by the Fresnel reflection of the cleaved end faces is sufficient to cause sustained and bursting oscillations.

At very low reflectivities and low pump powers the SBS power spectra are totally broadband. However increasing the gain and the phase modulation, by either increasing the pump power or the cavity reflectivity, sees the appearance of small peaks at the round-trip frequency which grow as these are further increased. At very low reflectivities the SBS was found to be aperiodic at all pump powers investigated, but at higher reflectivities, such as natural reflectivity, it was found to be periodic even very close to threshold. The area between these two cases was not investigated

thoroughly, but it was observed that as the reflectivity was increased from its very low value the power required to generate round-trip oscillations decreased.

If the cavity was formed by the fibre's natural Fresnel reflectivity as the pump power was increased the SBS went through modulations and pulsations to an almost dc state with only occasional short bursts of oscillations. If the pump power was further increased second order Stokes may be produced probably by four-wave mixing of the reflected SBS and pump. Investigation of the time series and power spectra show that the number of frequency components increases with pump power.

The same behaviour was found if the cavity reflectivity was varied instead of the pump. This also shows aperiodicity turning to periodicity at low reflectivity. The importance of the XPM and SPM terms in establishing this behaviour has also been shown - without them periodic or more usually dc operation is predicted. The dynamics have been found to be deterministic in origin and not due to, or unduly influenced by, the stochastic nature of the initial spontaneous Brillouin scattering with the very small nonlinear refraction terms causing this behaviour.

Chapter 6

Wavefront Dislocations in Optical Fibre Mode Patterns

6.1 Introduction

In recent years there has been considerable growth in the study of the spatial-temporal behaviour of physical and in particular nonlinear optical systems [ABR90]. In optical systems this usually means observing how the structure of a transverse pattern changes with time. The work presented in this chapter examines the structure of the transmitted mode patterns of optical fibres. The mode patterns could be changed in several ways, as is described later, sometimes resulting in the formation of singularities or dislocations in the optical wavefronts.

Optical wavefronts, surfaces of constant phase, can show singularities or dislocations analogous to those found in the lattice structure of crystals. The fundamental property of a dislocation is that if any closed loop enclosing the dislocation is traversed then there exists wavefronts which are passed through an odd number of times. Wavefront dislocations were first observed by Nye and Berry [NYE74] in experiments carried out using ultrasound in an attempt to understand radio echo patterns reflected from the bottom of the Antarctic ice sheet, although

they suspected that dislocations may often have been observed in phase sensitive experiments without their significance being appreciated. Wavefront dislocations have also been observed in the speckle patterns of scattered coherent light [BAR81a,BAR81b,BAR82,BAR83] and in the complicated mode patterns of multimode optical fibres [BAZ90].

In the case of a plane wave the wavefronts are a family of parallel planes perpendicular to the direction of propagation separated by a distance λ from one another and for a spherical wave they are a set of concentric spheres again a distance λ from one another. More generally for a real monochromatic field [ZEL85] $E_{real}(\mathbf{r}, z, t)$ and a slowly varying complex amplitude $E(\mathbf{r}, z)$ such that

$$E_{real}(\mathbf{r}, z, t) = \frac{1}{2}\left[E(\mathbf{r}, z)e^{-i\omega t+ikz} + E^*(\mathbf{r}, z)e^{i\omega t-ikz}\right] \tag{6.1}$$

the wavefront surface is defined by the equation

$$kz + \sin^{-1}\left[\frac{\text{Im } E(\mathbf{r}, z)}{|E(\mathbf{r}, z)|}\right] = \text{const.} \tag{6.2}$$

So if the intensity, $|E(\mathbf{r}, z)|^2 = [\text{Re}\{E(\mathbf{r}, z)\}]^2 + [\text{Im}\{E(\mathbf{r}, z)\}]^2$, is equal to zero then the argument of the inverse sine term in equation 6.2 is not defined and this should lead to peculiarities of the wavefront.

Figure 6.1 shows examples of two different types of dislocation, (a) an edge dislocation and (b) a screw dislocation. If the dislocation line is parallel to the wavefronts it is called an edge dislocation while if it is perpendicular it is called a screw dislocation and is the line along which successive wavefronts join up like a spiral staircase producing a helical surface which may be right- or left-handed with the singularity at the centre. Traversing any closed loop around the dislocation gives a phase shift of $2\pi n$, where n is an integer and is the strength of the dislocation, both the dislocations shown in figure 6.1 are first order or strength one. When this loop has been

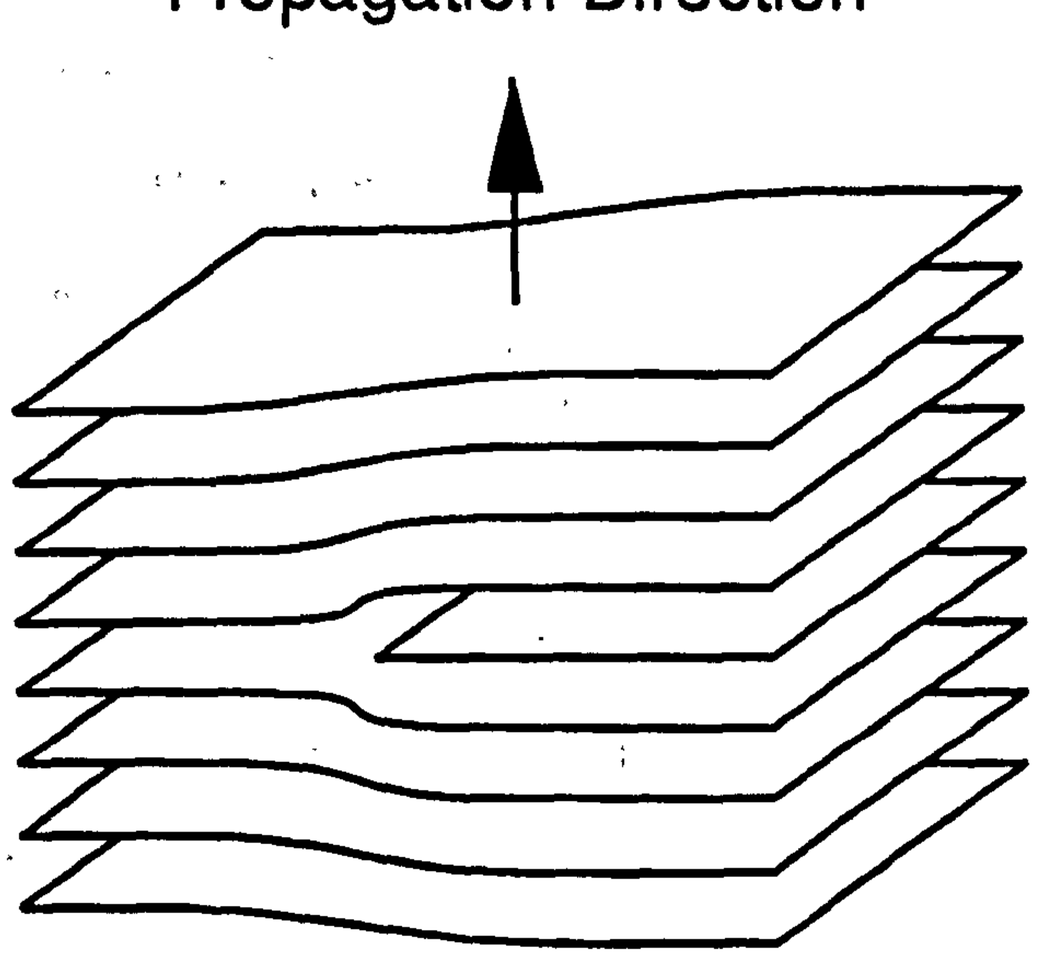

Figure 6.1: Single strength dislocations (a) edge and (b) screw.

shrunk to a point the phase at that point must have all values in the range $2\pi n$ which can only be satisfied when $|E(\mathbf{r}, z)| = 0$ and the phase is undefined, that is to say only when the real and imaginary part of the field are simultaneously equal to zero. At a given beam cross section $z = \text{const}$ the equation $\text{Re}\{E(x, y)\} = 0$ determines a system of lines in the plane $x - y$, while $\text{Im}\{E(x, y)\} = 0$ determines a second set with the intersection of these two sets of lines corresponding to points of zero intensity and hence dislocations in the wavefront. For first order dislocations it is sufficient for one pair of lines to intersect but higher order dislocations would require the intersection at one point of two or more pairs of lines, moreover second and higher order dislocations are unstable to small field distortions [ZEL85] and decay to a corresponding number of dislocations of unit strength while first order dislocations are stable to small perturbations of the field. For a small disturbance of the complex amplitude both system of lines will be slightly deformed and the points of intersection do not disappear but move to new locations. Second order dislocations have been produced by diffraction of light by specially synthesised holograms [BAZ90].

Consider a travelling wave which has been diffracted, scattered, diffracted or reflected so that it is formed by the interference of a large number of independent components. Dislocations are caused by destructive interference among the different contributions contained in the field. Usually in interference experiments dark fringes are produced because although the two interfering waves are out of phase their intensities are not completely matched - it is only on dislocation lines where the two waves have equal amplitude as well as being in anti-phase that the intensity vanishes. The interfering waves are formed in optical fibres by creating more than one fibre mode leading to coupling and mixing of the modes. Fibres which allow only a few modes as well as true multi-mode fibres were investigated.

6.2 Fibre Modes

The modes that a fibre can support, like any waveguide, can be found by solving the wave equation with the appropriate boundary conditions [SNY83, chpt 11-15]. The resulting solutions are Bessel functions with the number of modes allowed governed by the value of the normalised frequency parameter, V, which depends on the wavelength of the light used as well as the fibre diameter and composition,

$$V = \frac{2\pi a}{\lambda}\sqrt{n_{co}^2 - n_{cl}^2}, \tag{6.3}$$

where a is the core radius, λ the wavelength and n_{co} and n_{cl} are the refractive indices of the core and cladding respectively. As well as TE and TM modes, where the axial component of the electric or magnetic field is zero, hybrid modes exist where all six components of the electromagnetic field are nonzero. These modes, which result from skew ray propagation within the fibre, are designated HE_{lm} and EH_{lm} modes depending upon whether the components of the magnetic or electric field make the largest contribution to the transverse field [SNI61]. The exact expressions can be very complicated but fortunately in most step index fibres that are used the refractive index difference between the core and cladding is very small and it can be shown [GLO71] that the full set of modes can be approximated by a single set of linearly polarised (LP_{lm}) modes.

The condition for single-mode operation is $V < 2.405$ and the fundamental mode is referred to as LP_{01}. The number of modes supported can be found by calculating the value of V for that wavelength and then comparing this to the cut-off condition for each mode, see for example [ADA81, page 232], the larger the value of V the higher the number of modes that are allowed. In the case of a heavily multi-moded fibre the number of modes is given approximately by $N = \text{Int}\,(V^2/2)$ providing that $V \gg 1$.

Several different fibres were investigated ranging from single-mode fibres, where the mode pattern is almost a Gaussian, through fibres where only a few modes are supported and the output consists of several spots of irregular shape, to true multi-mode fibre where the transmitted mode is a complicated pattern containing several hundred elements. Examples of the mode patterns of these three cases are shown in figure 6.2. Only in the case of the single-mode fibre does the output consist of only one LP mode, in the other cases it is a mixture of all the modes which can be supported. Table 6.1 gives details of the number of modes each fibre will support at both 514.5 nm and 633 nm.

Fibre Type	Reference	No. of Modes (514.5 nm)	No. of Modes (633 nm)
Single Mode Argon Ion	SM 450	1	1
Single Mode HeNe	LTI	2	1
Single Mode Nd-YAG	SM 1060	6	4
Multi-mode	MM	~7450	~4900

Table 6.1: Number of modes supported

6.3 Experimental Observations of Dislocations

Wavefront dislocations are phase singularities and so interferometry must be used to find them, so a Mach-Zehnder interferometer was constructed for this purpose and the arrangement is shown in figure 6.1. The fibre to be examined made up one

(a)

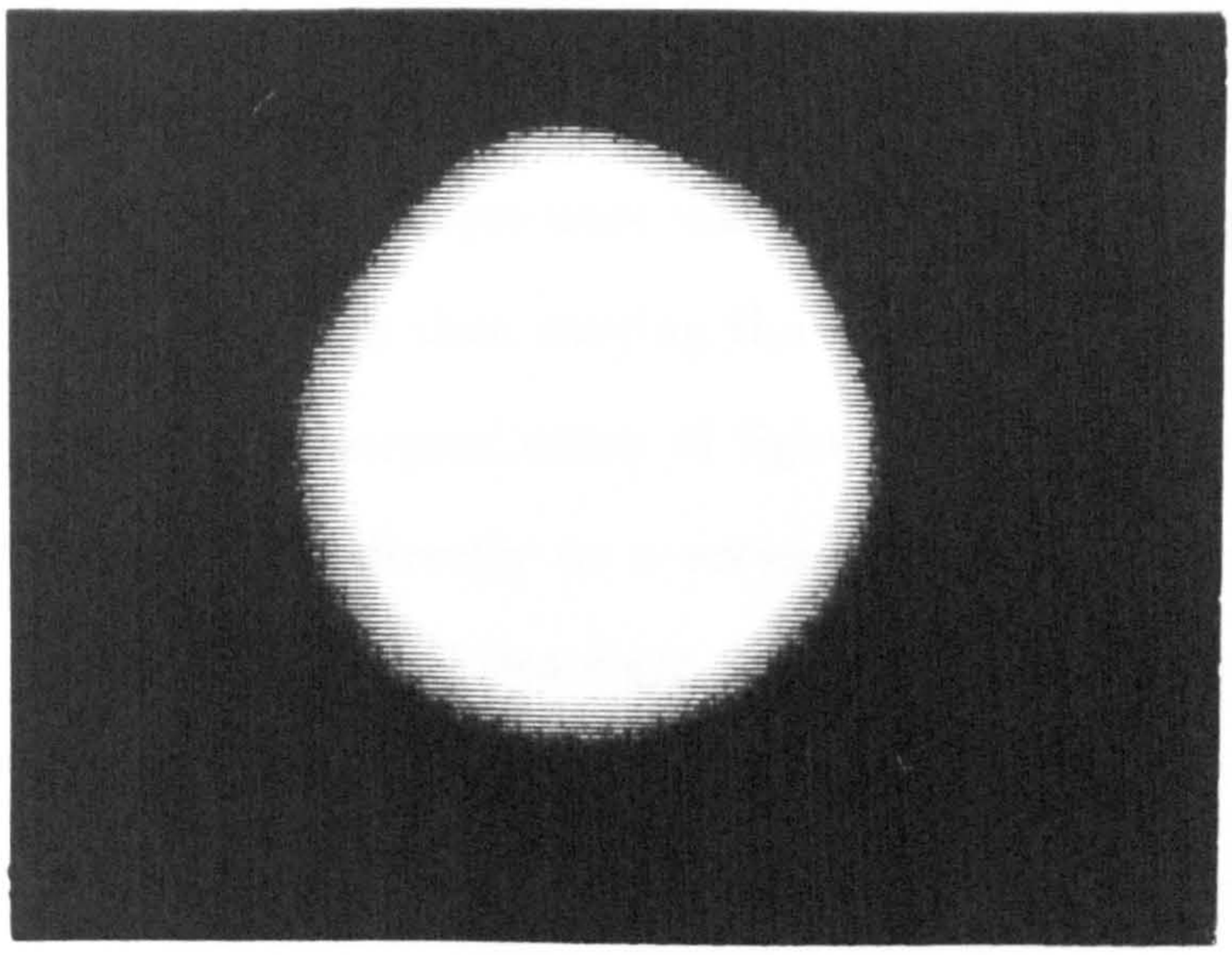

(b)

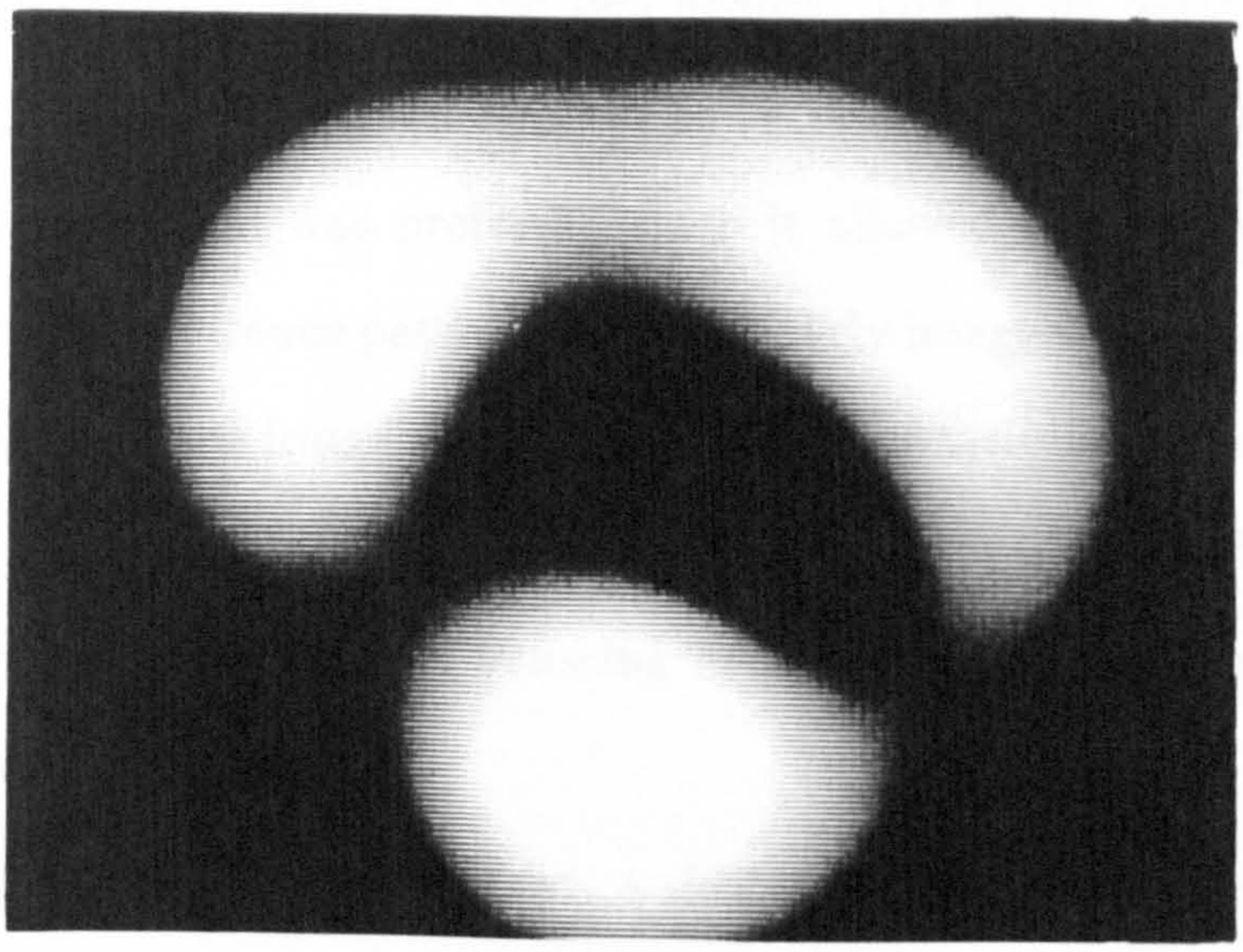

(c)

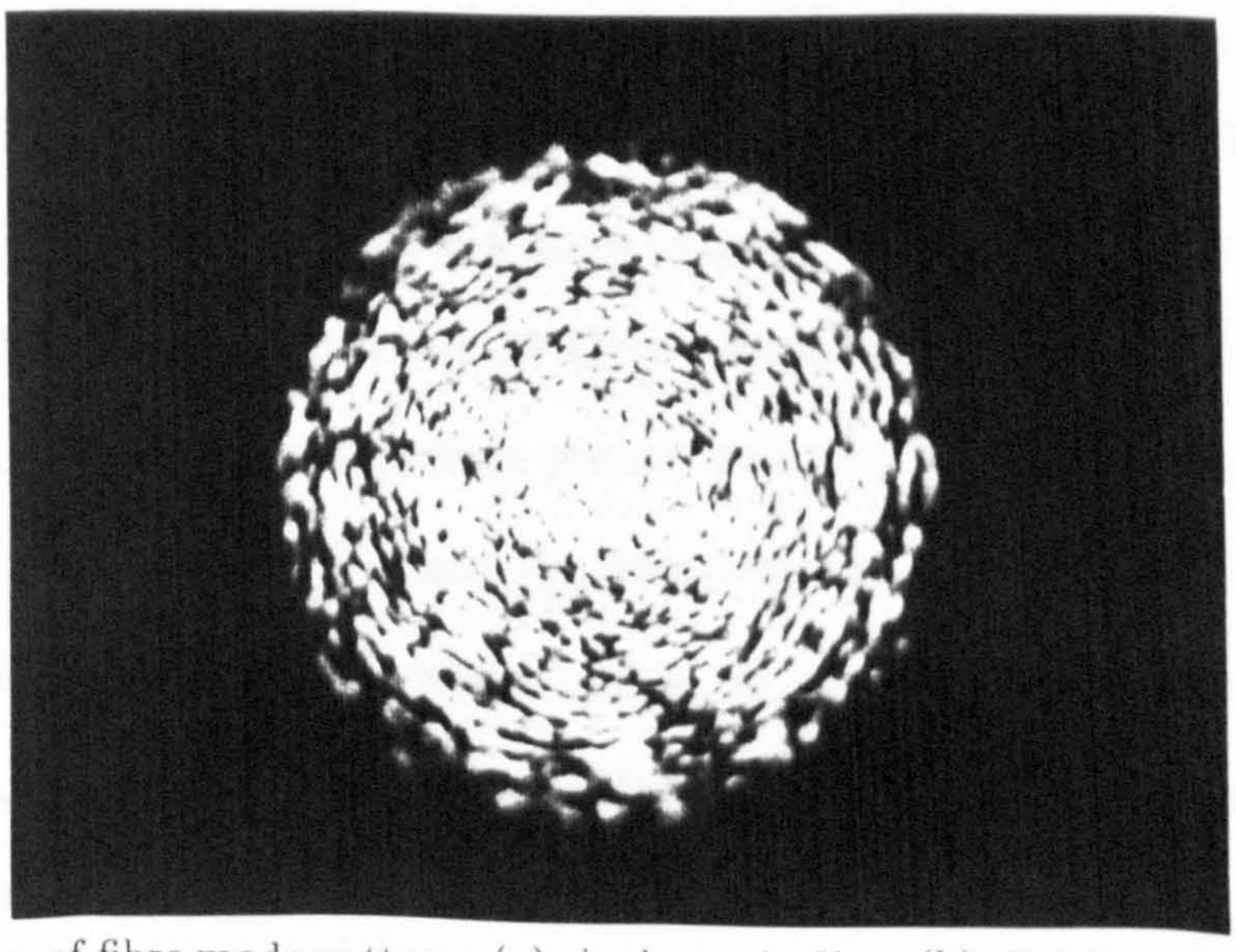

Figure 6.2: Examples of fibre mode patterns (a) single-mode fibre, (b) slightly multi-moded fibre and (c) multi-mode fibre.

arm of the interferometer and a short piece of an appropriate single-mode fibre was used in the other. This experimental arrangement allowed both circular and wedge fringes to be produced - circular fringes were made by allowing the light to diverge naturally from the two fibres and then moving the fibre ends or the beam splitter to suitably overlap the two emergent cones of light. The fringes were examined either using a CCD camera or directly on a screen placed at a suitable distance. Wedge fringes were created in one of two ways, either without the beam splitter by placing the two fibres in the same holder and so slightly displacing the two beams by using microscope objectives lenses and a beam splitter and introducing a small displacement of the optical paths of the two beams. The mode patterns were then focussed on the CCD camera placed a meter or two away to give a sufficiently large image. The second method was preferred since it allowed the mode patterns and their corresponding interference patterns to be properly imaged while also permitting controllable variation of the fringe separation. The fringe visibility is maximum when the two beams are of equal intensity, this was easily achieved either by varying the size of the reference beam through focussing or by changing the launch conditions to give a suitable launched power.

Two different laser sources were used, a simple Helium-Neon laser operating at 633 nm giving a maximum power of around 1 mW and an argon-ion laser giving about 4 W at 514.5 nm. The He-Ne laser has a short cavity length of $\sim$ 30 cm and has a linewidth small enough to produce fringes of good visibility. The Argon-ion laser has a multi-mode linewidth of about 10 GHz compared with 50 MHz when single-mode so the fringe visibility is therefore greatly reduced when operating multi-mode so the laser was used with an intracavity, temperature stabilised etalon to operate single longitudinal mode. Again when using the argon-ion laser it was necessary to use a Faraday isolator to stop any feedback to the laser from reflections from the fibre end faces, see section 3.2.1. The CCD camera is extremely sensitive and

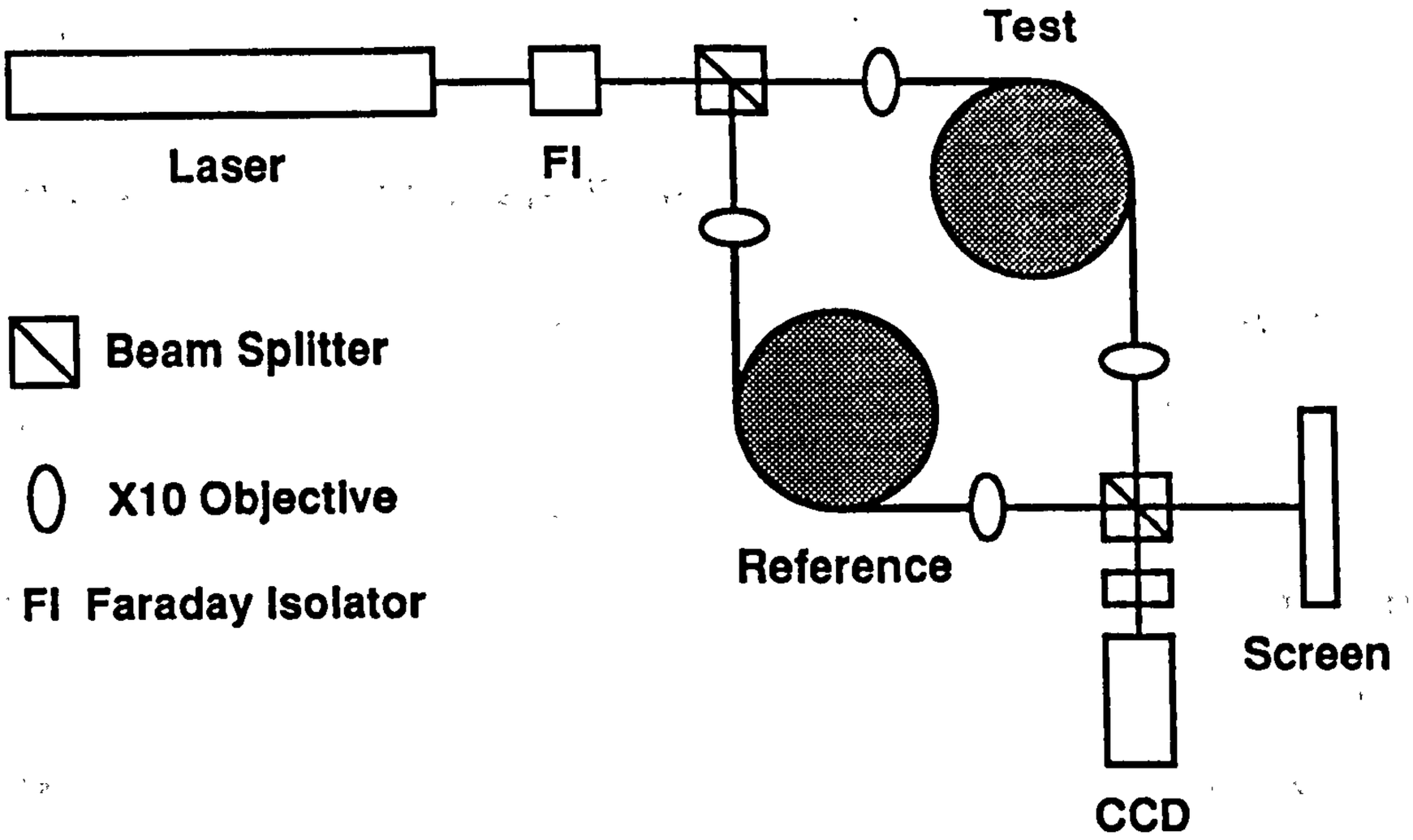

Figure 6.3: Mach-Zehnder interferometer used to study wavefront dislocations

allowed mode patterns of very low intensities to be seen.

6.3.1 Single-Mode Fibres

Single-mode fibres were used in both arms of the interferometer to produce fundamental modes from both fibres which gave either wedge or circular fringes depending on the experimental arrangement. The fringes were not stationary but drifted as the phase difference between the two beams varied because the optical paths lengths of the two arms changed with temperature as they were of unequal length. In the case of wedge fringes this makes the fringes move in one direction then stop and move back, circular fringes either expand outwards or collapse into the centre. The fringes can also be made to move by varying the launched power and this will be examined later. Examples of the observed fringes are shown in figure 6.4. No dislocations were observed when single-mode fibres were used in both arms of the interferometer. Any small circular fringe patterns which can be seen on these, and any of the following

figures, were caused by dirt on the neutral density filters used to protect the camera from saturation.

6.3.2 Slightly Over-Moded Fibres

Operating single-mode fibres at a longer wavelength than their cut-off wavelength makes it possible to generate mode patterns which are made up of only a few fibre modes. For example, fibre LTI operating at 514.5 nm will usually support two modes, LP_{01} and LP_{11}. LP_{01} is circular and LP_{11} produces two lobes but the mode pattern obtained is not a simple combination of the two but is usually two asymmetric spots. Figure 6.5 (a) shows an example of the mode pattern transmitted through a 2.0 m piece of LTI fibre using an argon ion laser at 514.5 nm. A 0.5 m piece of the same fibre was used in the other arm but this was made to behave as single-mode by either putting a few tight loops in the fibre or by using a mode scrambler.

The mode scrambler consists of two corrugated surfaces between which the fibre is placed, bringing these surfaces together causes small bends to be formed in the fibre. Perturbations in the fibre's straightness will cause light scattering and a redistribution of power among the guided modes of the fibre. Higher order modes also suffer greater attenuation than low order modes since power is coupled from the higher order guided modes to radiation modes. In these two ways the power from the higher order mode LP_{11} can be coupled to the lower order LP_{01} mode or to radiation modes.

Using the transmitted modes of these two fibres to produce wedge fringes results in the formation of fringes which contain a dislocation, see figure 6.5 (b). This shows two fringes coming together at the singularity with only one leaving to produce a 'Y'-shaped dislocation. The dislocation is of strength one, travelling a closed loop around the singularity results in a phase jump of 2π, and is found to occur in a dark region of the mode pattern. Figure 6.6 shows a similar dislocation in close-up, there

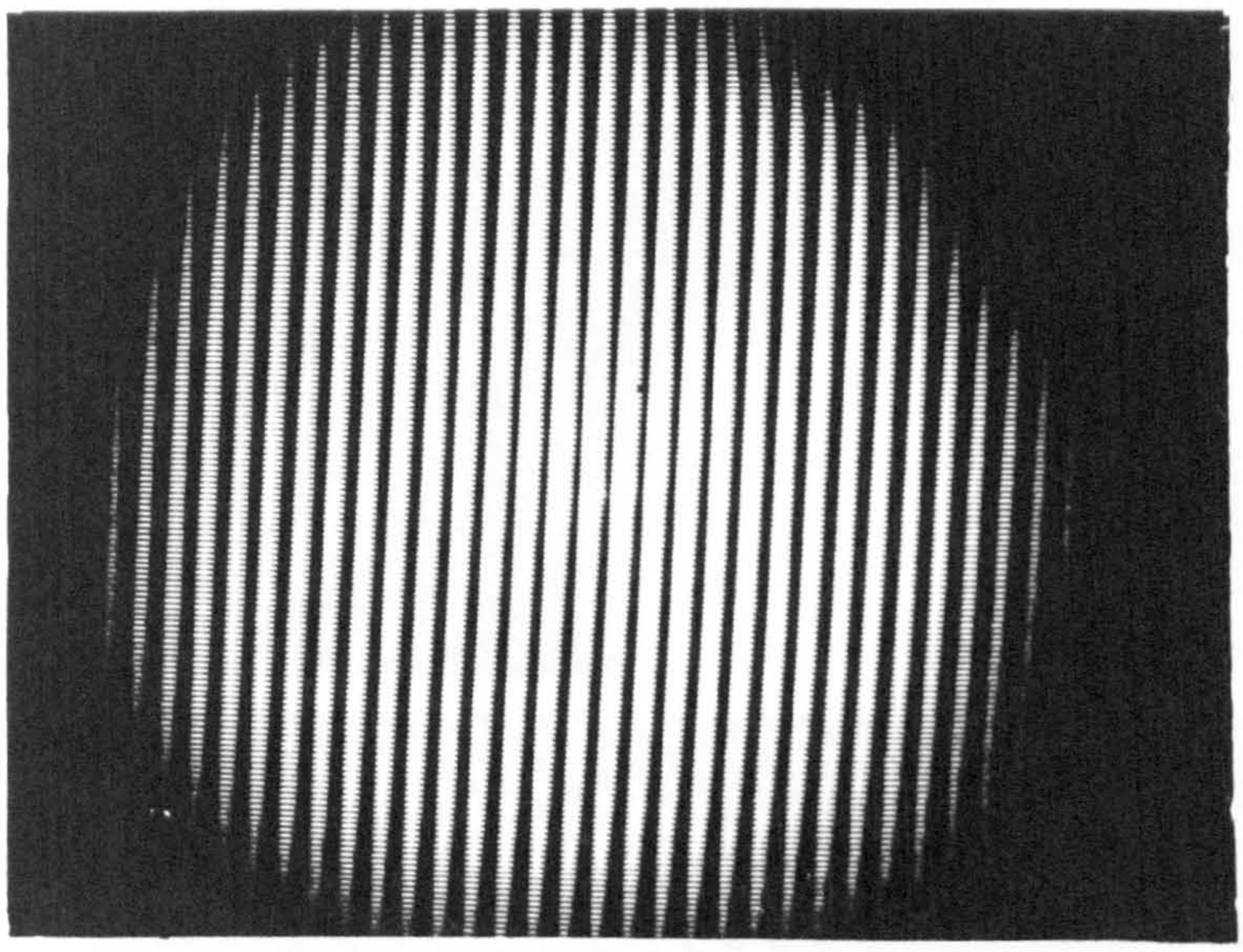

(a)

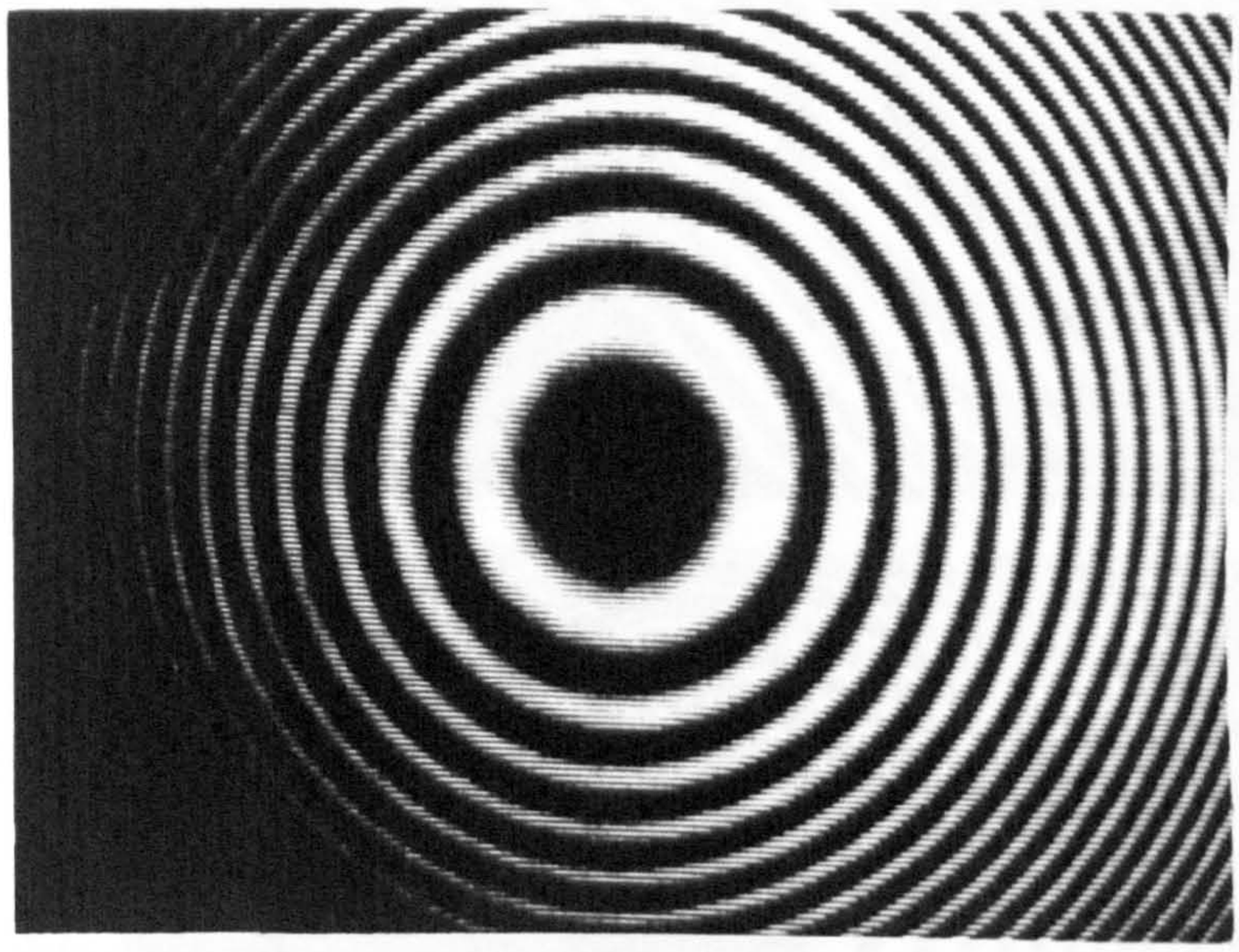

(b)

Figure 6.4: Fringes for single-mode fibre (a) wedge fringes and (b) circular fringes.

(a)

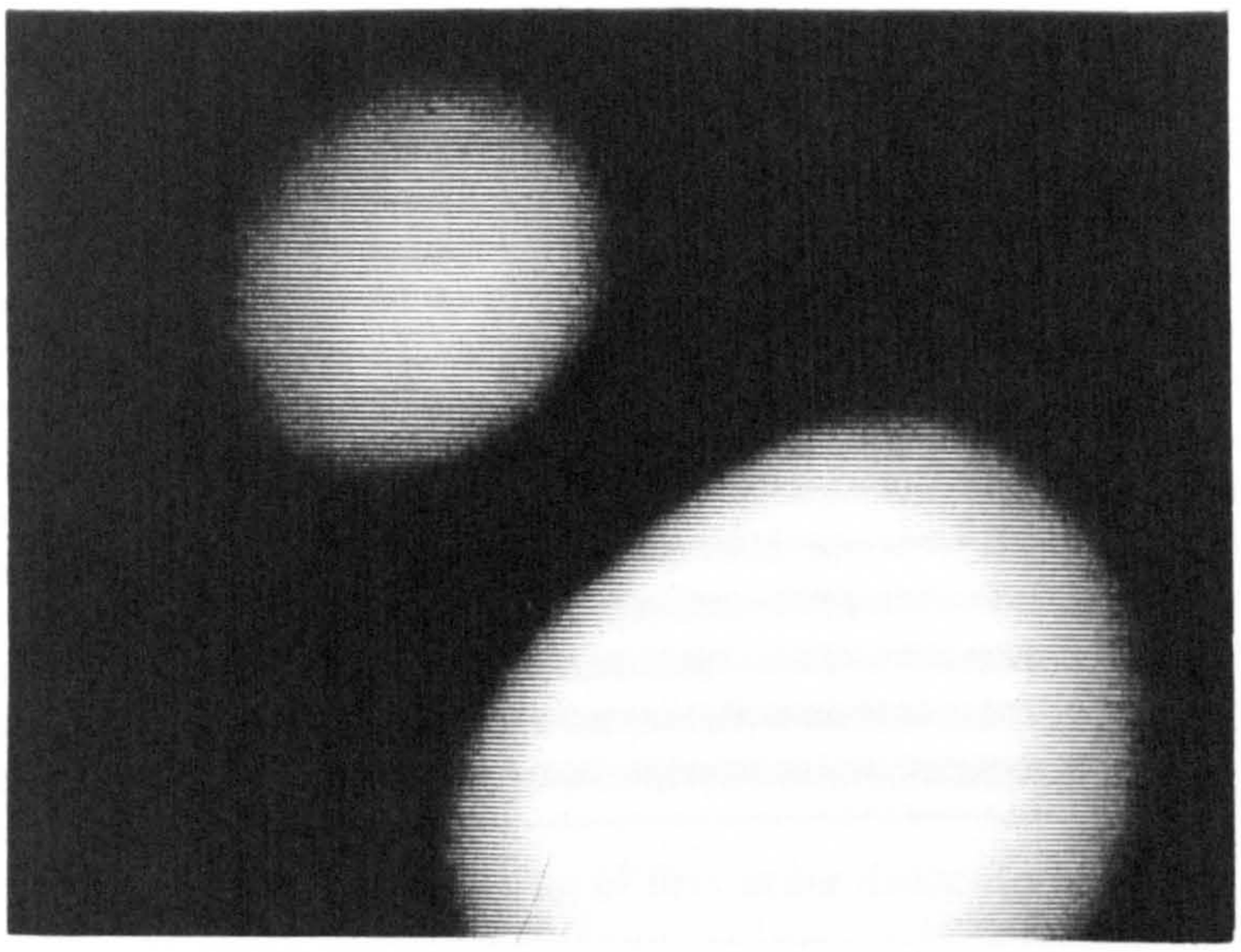

(b)

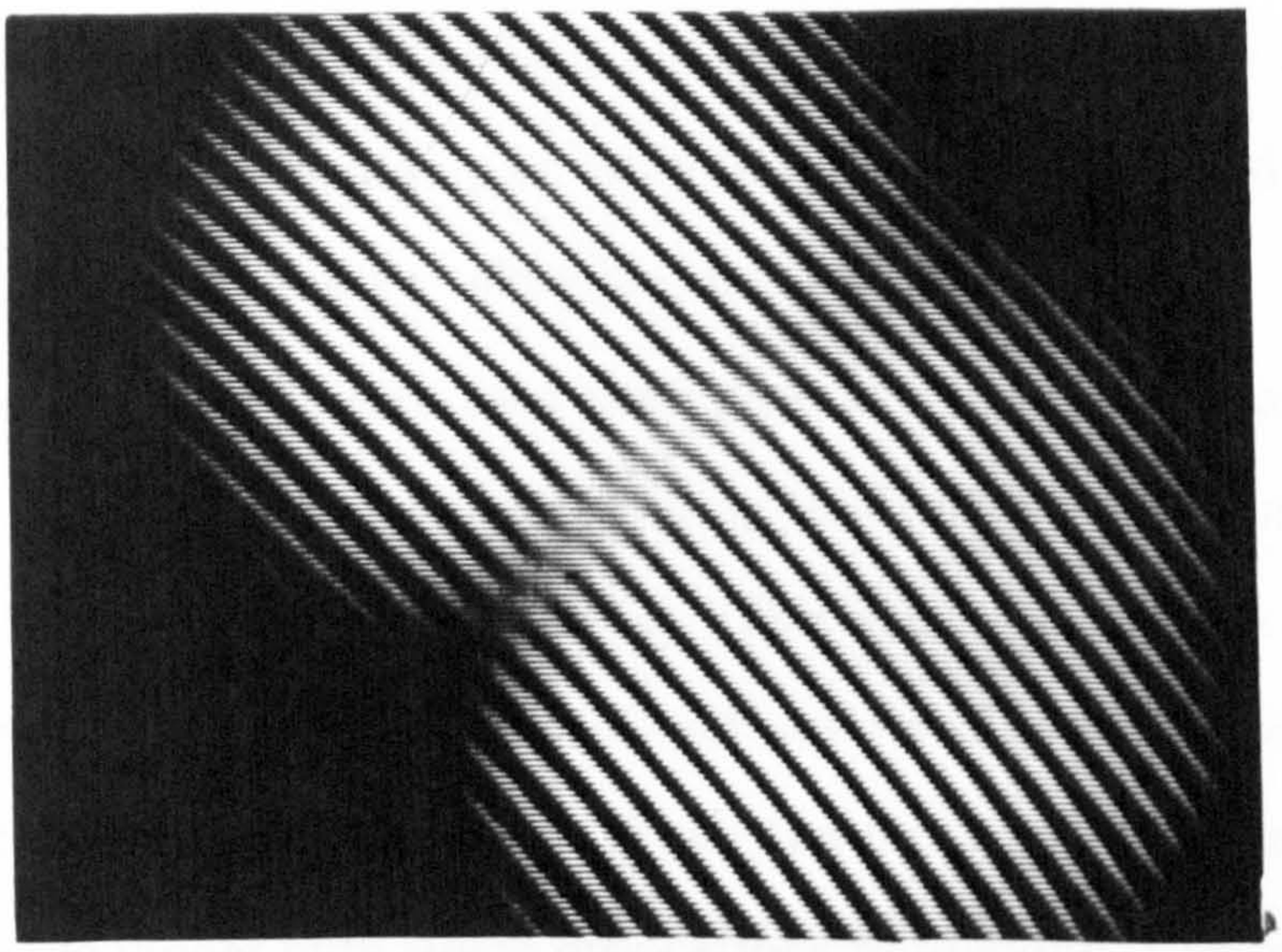

(c)

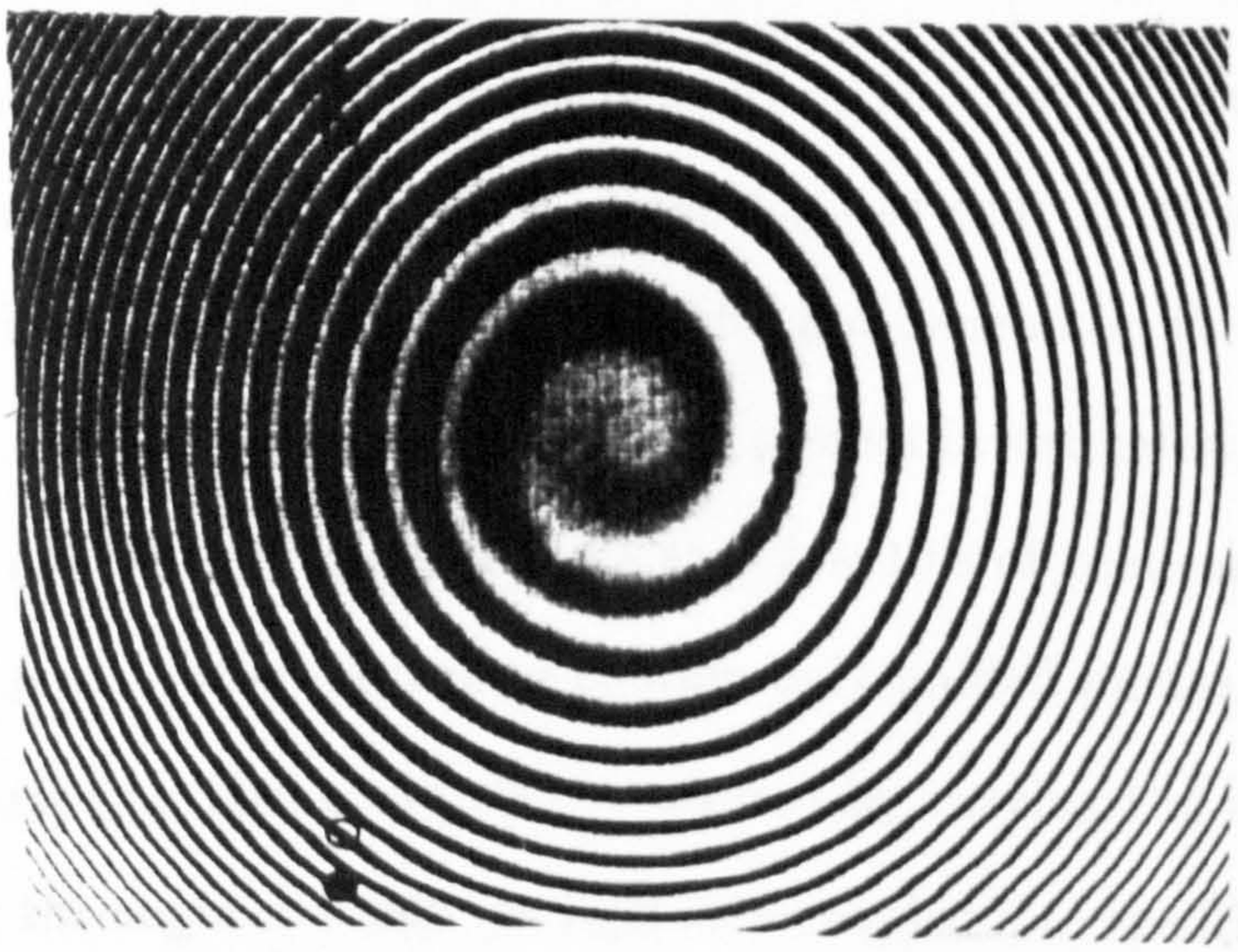

Figure 6.5: Observed patterns (a) mode pattern, (b) wedge fringes and (c) circular fringes

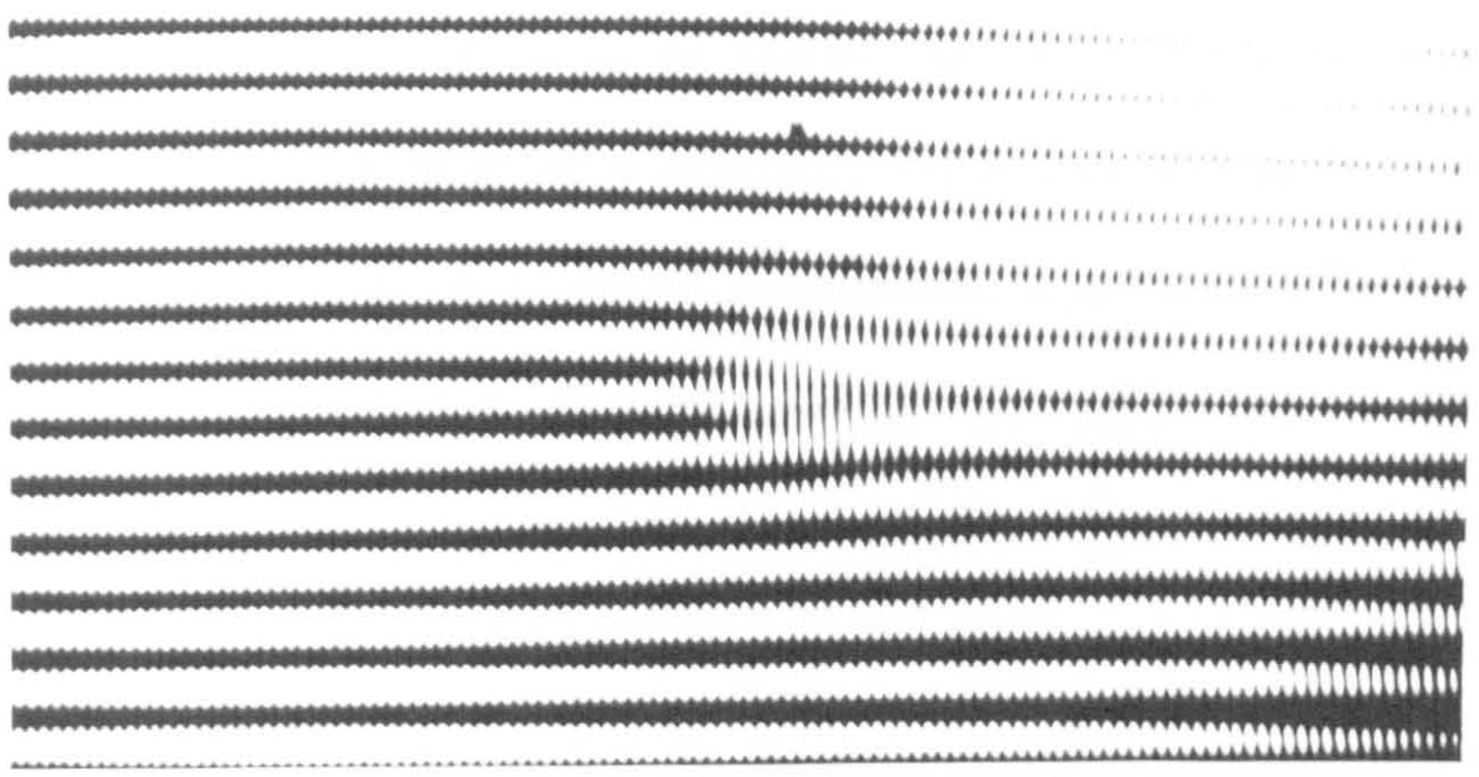

Figure 6.6: Close-up of first order dislocation

is one more fringe one the right-handside of the picture than on the left. The fact that the fringes seem to be made up of discrete vertical elements is due to the fact that the picture was taken from a television monitor.

If instead circular fringes were used then generally these show two of the rings joining together at the dislocation but centering the fringes on the singularity leads to the spiral pattern shown in figure 6.5 (c). This shows clearly the existence of a helical wavefront and therefore the dislocation is a screw dislocation with both right- and left-handed spirals being observed. When the mode pattern was a mixture of only two waveguide modes only single dislocations were found, they were not found to exist in matching pairs of right- and left-handed. Dislocations were always found in regions of low intensity, whether the intensity was exactly zero was impossible to determine. The formation of singularities did not depend on the pump power or the fibre length, they were found at all pump powers investigated, between ~2 W and less than 1 mW and in fibres as short as a few 10's of centimetres, as short as possible for the transmitted pattern to contain only guided modes.

The transmitted pattern could also be altered by varying the launch conditions and so changing the angle at which the light was coupled into the fibre. This reduces

the launch efficiency but allows the light to be coupled mainly into the higher order mode and so by carefully choosing the launch conditions the transmitted mode can be made to be almost entirely LP_{11}, as shown in figure 6.7 (a). Then, using the mode scrambler, light was gradually coupled from this mode to the lower order LP_{01} mode. As this was done a single dislocation appeared which moved as the mode pattern changed and then disappeared as the mode become almost entirely LP_{01}. The transition from LP_{11} to LP_{01} is shown in figure 6.7 with the dislocation appearing at the top right-handside in figure 6.7 (b), moving towards the centre of the picture and then outwards until it disappears and the transmitted mode is LP_{01}, figure 6.7 (f).

This establishes the requirement of mode mixing for dislocations to occur - dislocations were not found when the mode was entirely LP_{01} or LP_{11}. The dislocations moves as the proportion of each mode and hence the transmitted pattern changes. This is the simplest case of mode mixing, the modes being the two lowest order ones, and only single first order dislocations were observed.

The electric field of the LP_{11} mode is antisymmetrical with the field equal to zero on a line between the two lobes and the phase switches sign across this line. However this mode on its own does not show any dislocations since the field is zero along a line and not at a point singularity, i.e. traversing a closed loop around a point on this line leads to a phase shift equal to zero and hence the phase is well defined at any point.

These experimental results show that wavefront dislocations were only found when at least two modes were present, but is it possible to explain these observations by the superposition of the two wavefronts, i.e. can two or more spherical wavefronts be combined to create a helical wavefront? In cylindrical coordinates the equation of a helical surface is $\theta - z =$ constant but it is not obvious how this can be decomposed into spherical waves. A brief attempt to analyse this problem was made and this

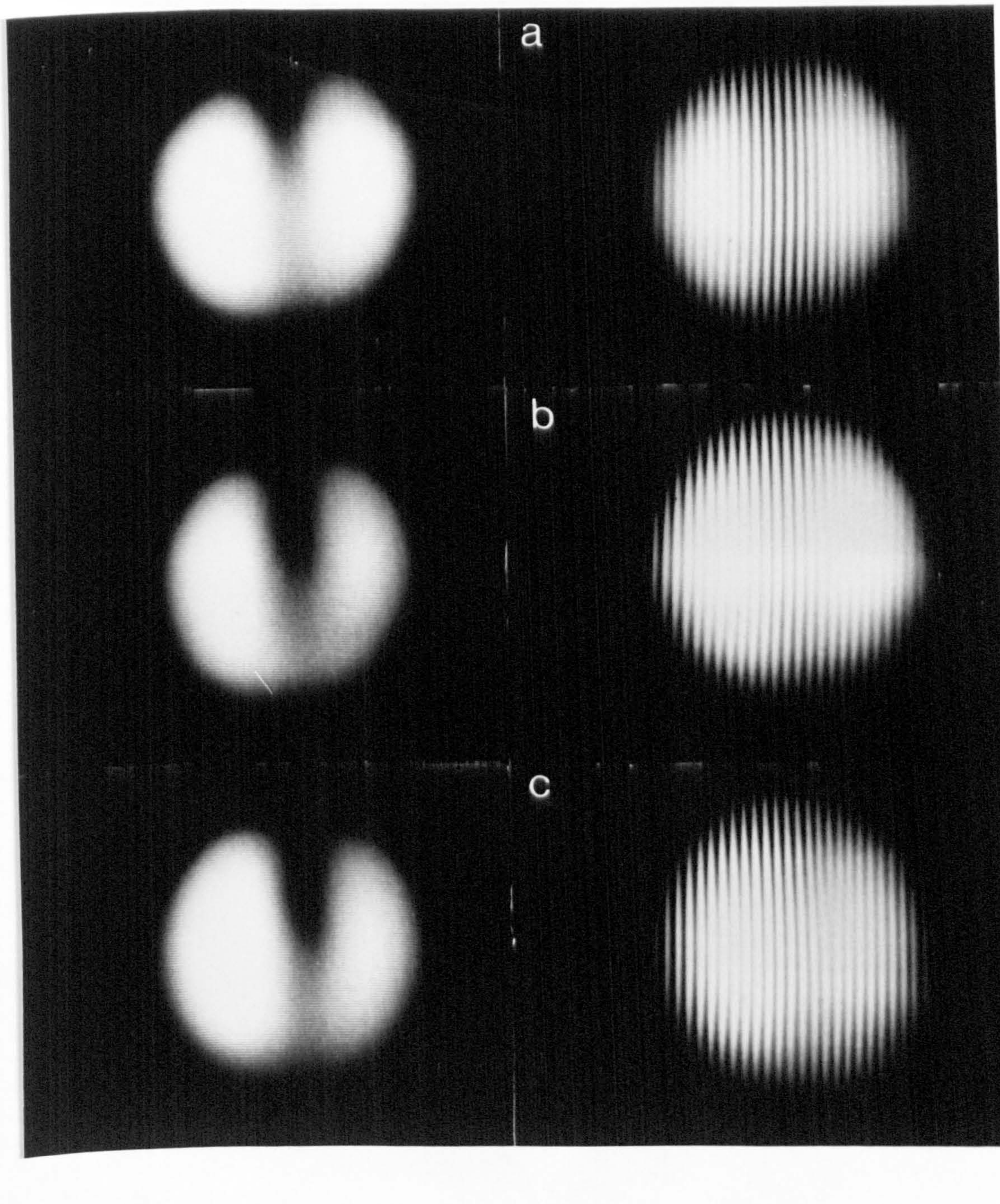

Figure 6.7: Dislocation caused by mixing of LP_{11} and LP_{01} modes

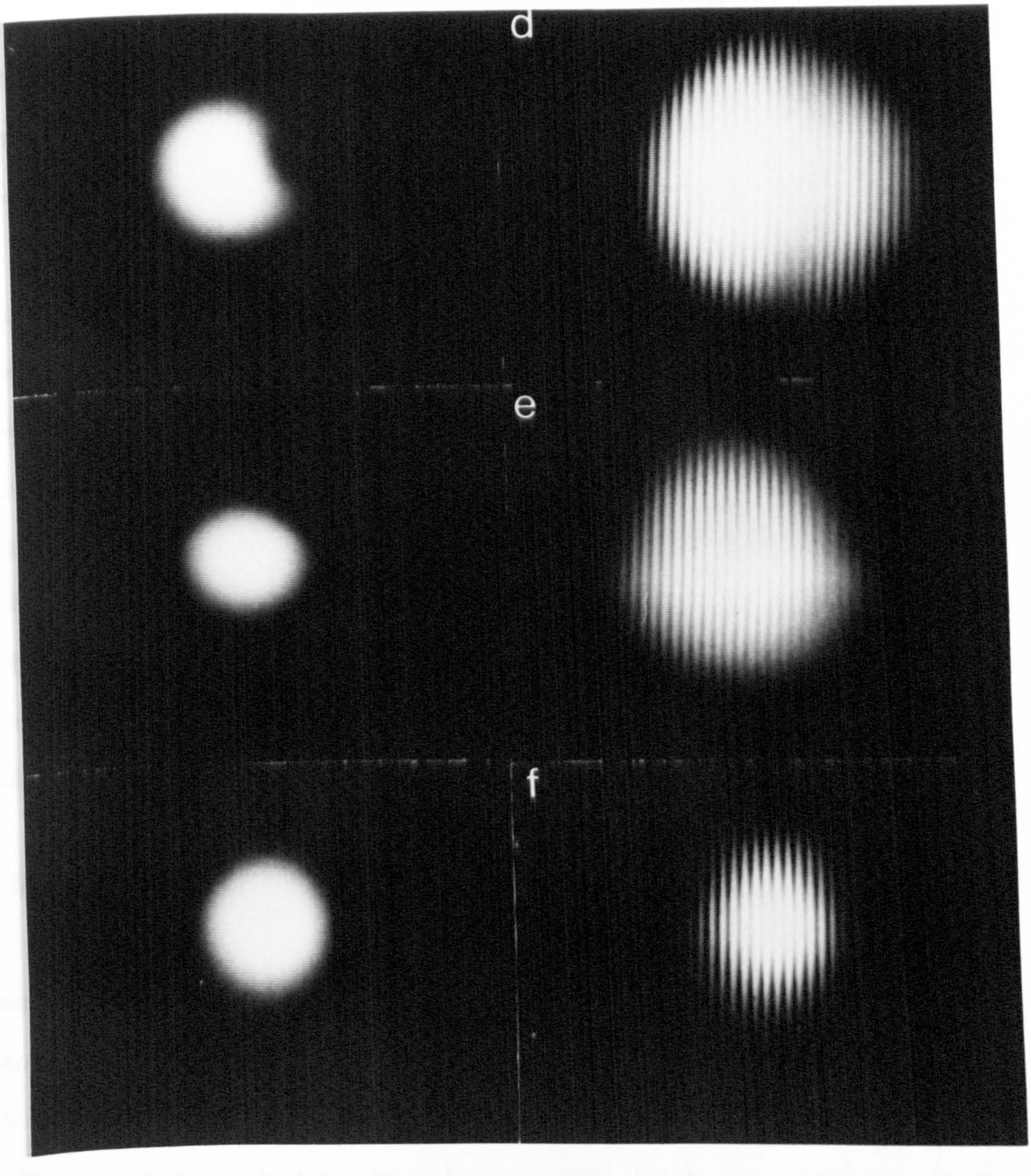

Figure 6.7: Dislocation caused by mixing of LP_{11} and LP_{01} modes

is described below, although the model used is a very simplified version of the real case.

Consider the LP_{11} mode to be created in the far field by the interference of two point sources of equal amplitude separated by $2a$, where a is approximately the fibre core radius, and out of phase by π radians. Then like a Young's double slit experiment this will produce fringes in the far field where the central region along the line $x = 0$, see figure 6.8, is dark due to the phase difference of the two sources. Figure 6.9 shows the fringe pattern produced along the line $y = 0$ by these two sources assuming that the distance OC is $10^4 a$. There are of course many other orders of fringes but we consider only the two central maxima since the cone of light emitted from the fibre only allows these. If the field distribution along the y-axis is considered then the combination of these two fields will give an intensity pattern similar to the LP_{11} mode.

If a third point source is added at C, to simulate the LP_{01} mode, again of equal intensity and out of phase from A by some value $\Delta\phi_C$ then the summation of these fields at the point P represents the field E_P at that point. Hence

$$E_P = E_o \left[\exp(i(kr_A - \omega t)) + \exp(i(kr_B - \omega t + \pi)) + \ exp(i(kr_C - \omega t + \Delta\phi_C))\right] \tag{6.4}$$

where the modes are assumed to have the same propagation constant k, frequency ω and amplitude E_o and r_A, r_B and r_C are the distances from the points A, B and C to P. This allows the intensity at P to be calculated.

Figure 6.10 shows the intensities along $y = 0$ for $\Delta\phi_C = 0$ and $\Delta\phi_C = \pi/5$, the intensities along $x = 0$ being constant. This shows that varying the phase of the source at C from the other two leads to the intensity pattern becoming asymmetrical, like those found experimentally when two modes were present (see figure 6.5 (a)).

The interferometer experiments can be mimicked by adding a fourth source at D

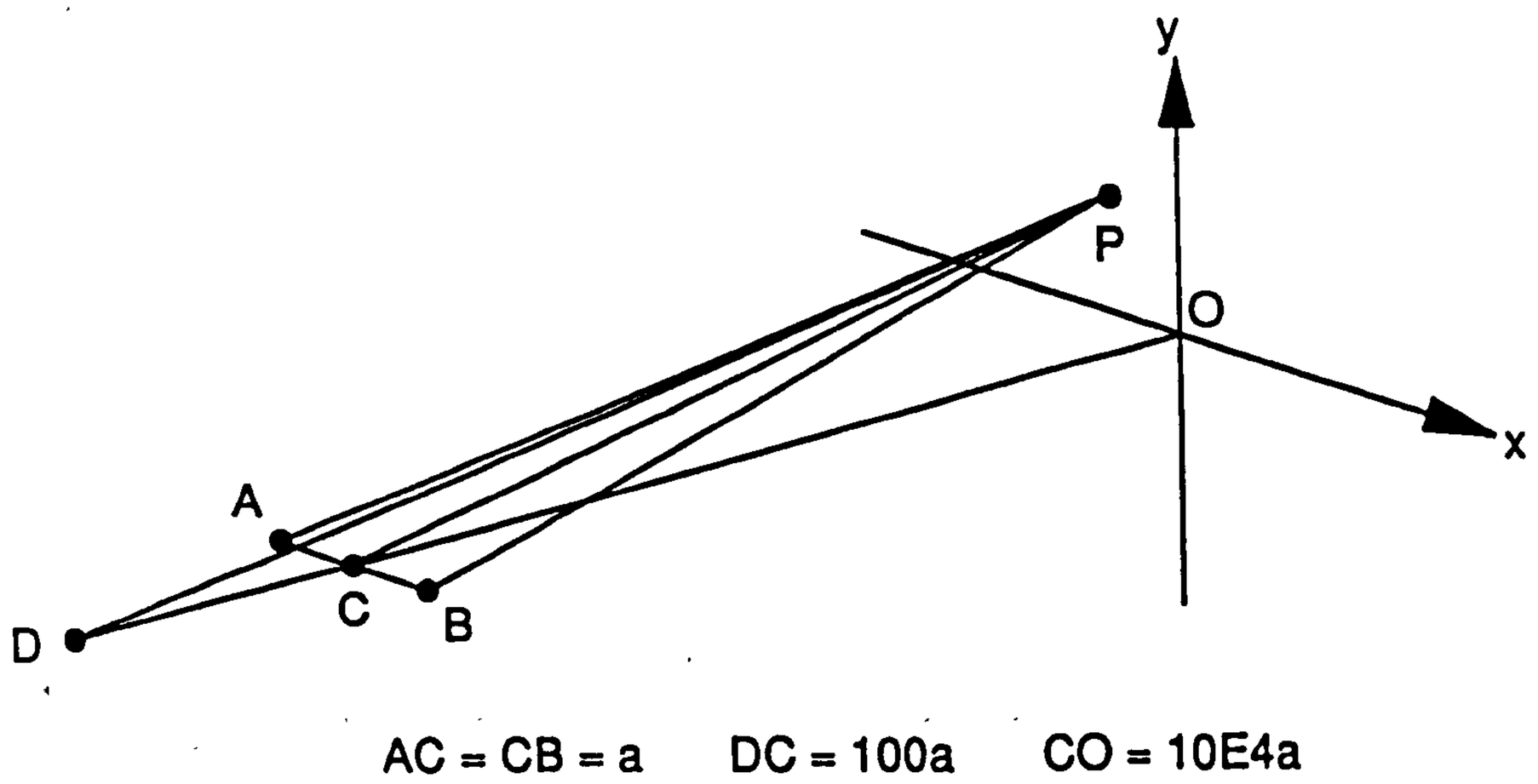

Figure 6.8: Geometry of point sources to recreate mode pattern

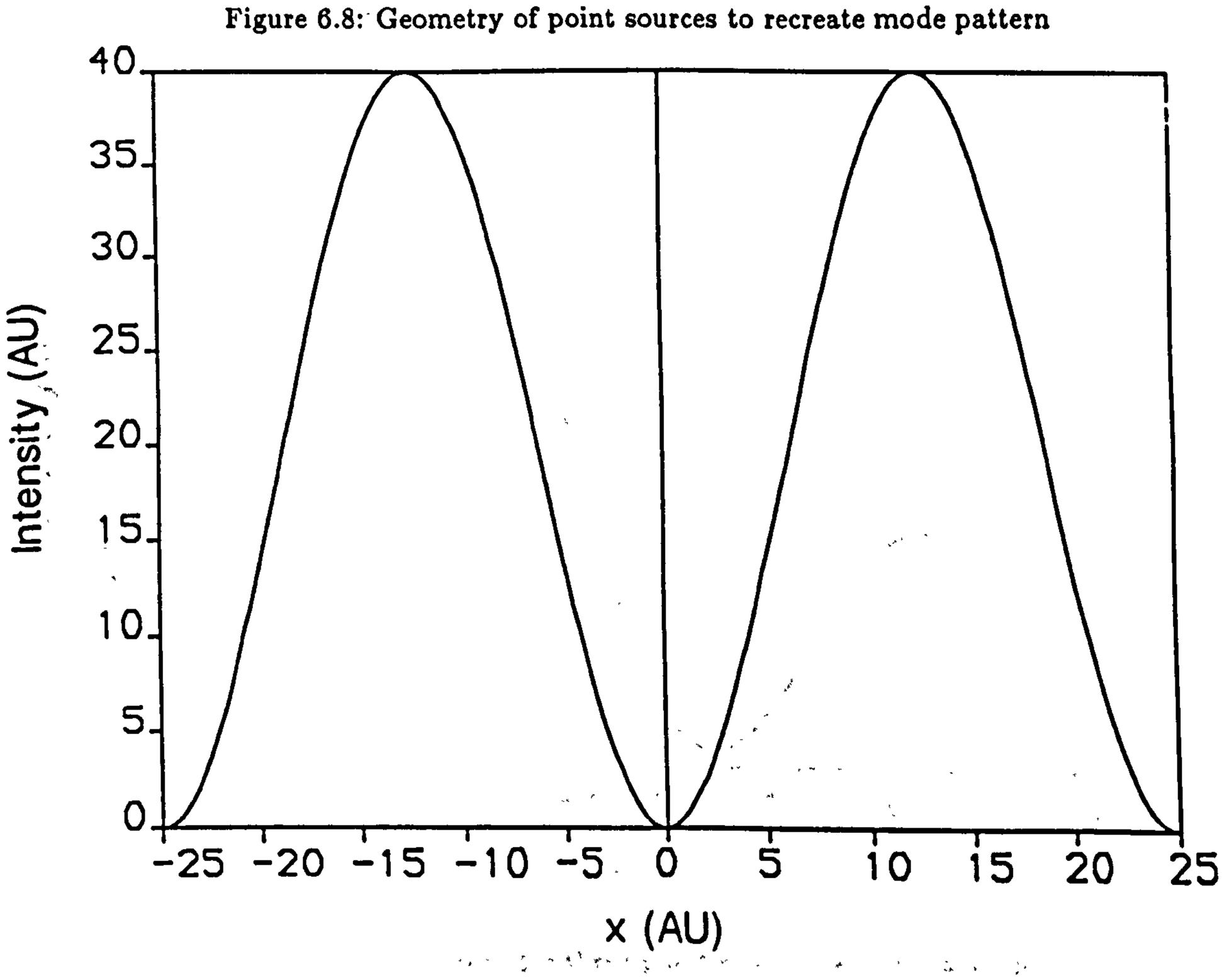

Figure 6.9: Interference pattern for two point source in antiphase

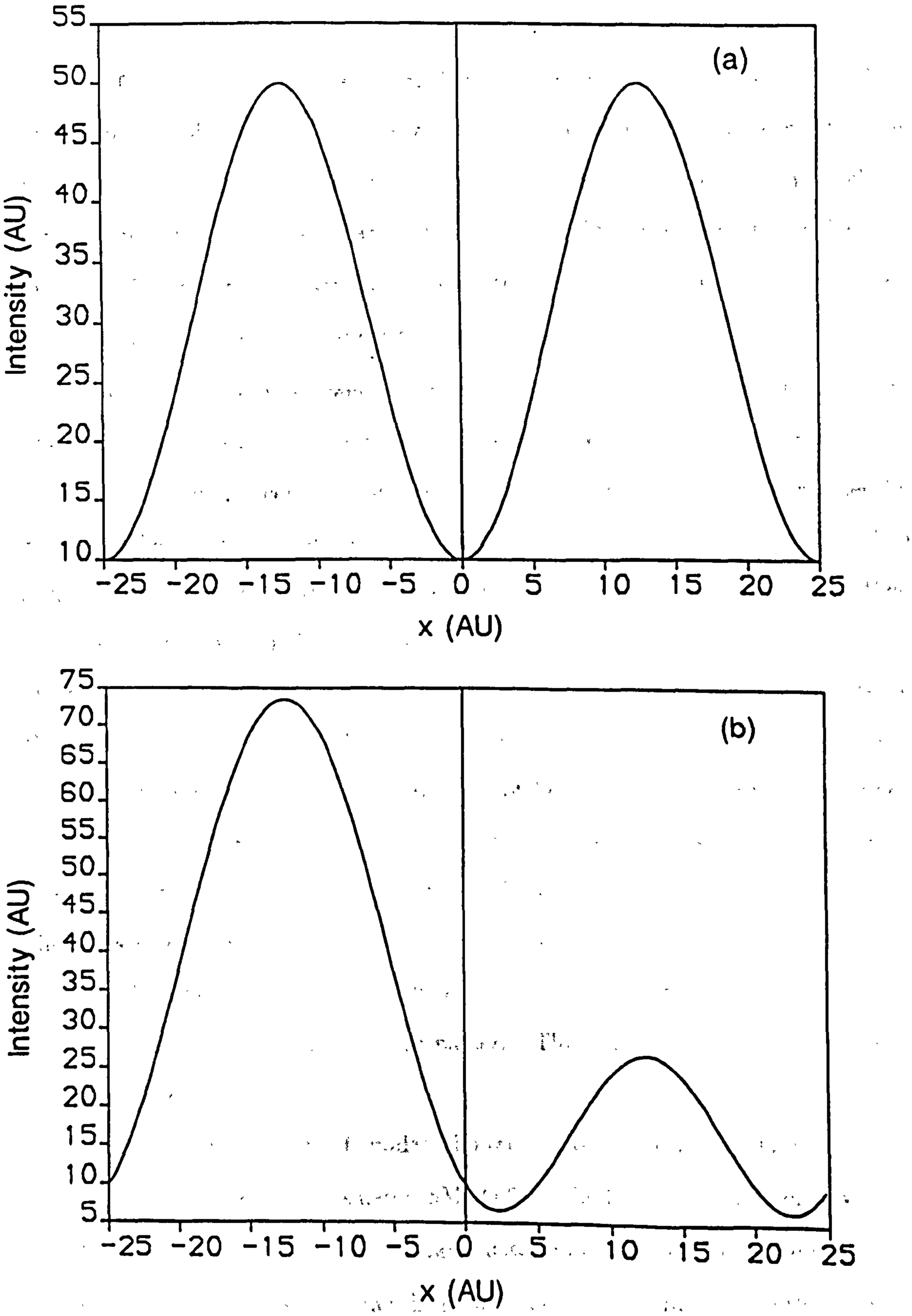

Figure 6.10: Interference pattern for three point source, (a) $\Delta\phi_C = 0$ and (b) $\Delta\phi_C = \pi/5$

displaced from C, by in this case 10^2a. Again this may be out of phase with A but for the purpose of this analysis $\Delta\phi_D$ was taken to equal zero. This means that the intensity pattern in the far field should now contain higher frequency fringes whose period is determined by the separation of C and D. This was found to be the case and figure 6.11 and 6.12 shows the fringe pattern produced along the x- and y-axes again for $\Delta\phi_C = 0$ and $\pi/5$ respectively.

Let us now consider the intensity patterns that a helical wavefront would produce when sectioned along $x = 0$ and $y = 0$. From figure 6.5 (c) it can seen that if a point at a maxima, a certain distance from the centre of the helix, is rotated by π radians then this will then be at a minima, i.e. the fringe maxima and minima either side of a line through the centre of the helix are displaced from each other. The maxima and minima in the fringe patterns shown in figures 6.11 and 6.12 occur at approximately the same distances either side of the origin, apart from those at the centre of figure 6.12 (a). No extra maxima or minima were seen to be created and these therefore represent circular and not helical fringe patterns. This model therefore does not seem to show that a helical wavefront can be constructed from a linear combination of spherical wavefronts. A fuller model would take into account the transverse amplitude variations in the four fields as well as varying the relative field amplitudes and $\Delta\phi_D$ but it should be possible to create a three dimension representation of the intensity fringe pattern. This fuller examination may yield a helical wavefront.

The maximum number of modes allowed is now increased to four by using a fibre of slightly larger core diameter, SM 1060, at the Helium-Neon laser wavelength of 633 nm. Again the shape of the transmitted mode pattern could be changed by using the mode scrambler, varying the launch conditions or by twisting the fibre. The maximum number of dislocations observed was three although this could be reduced to two or one by the above methods but at least one dislocation was always seen and

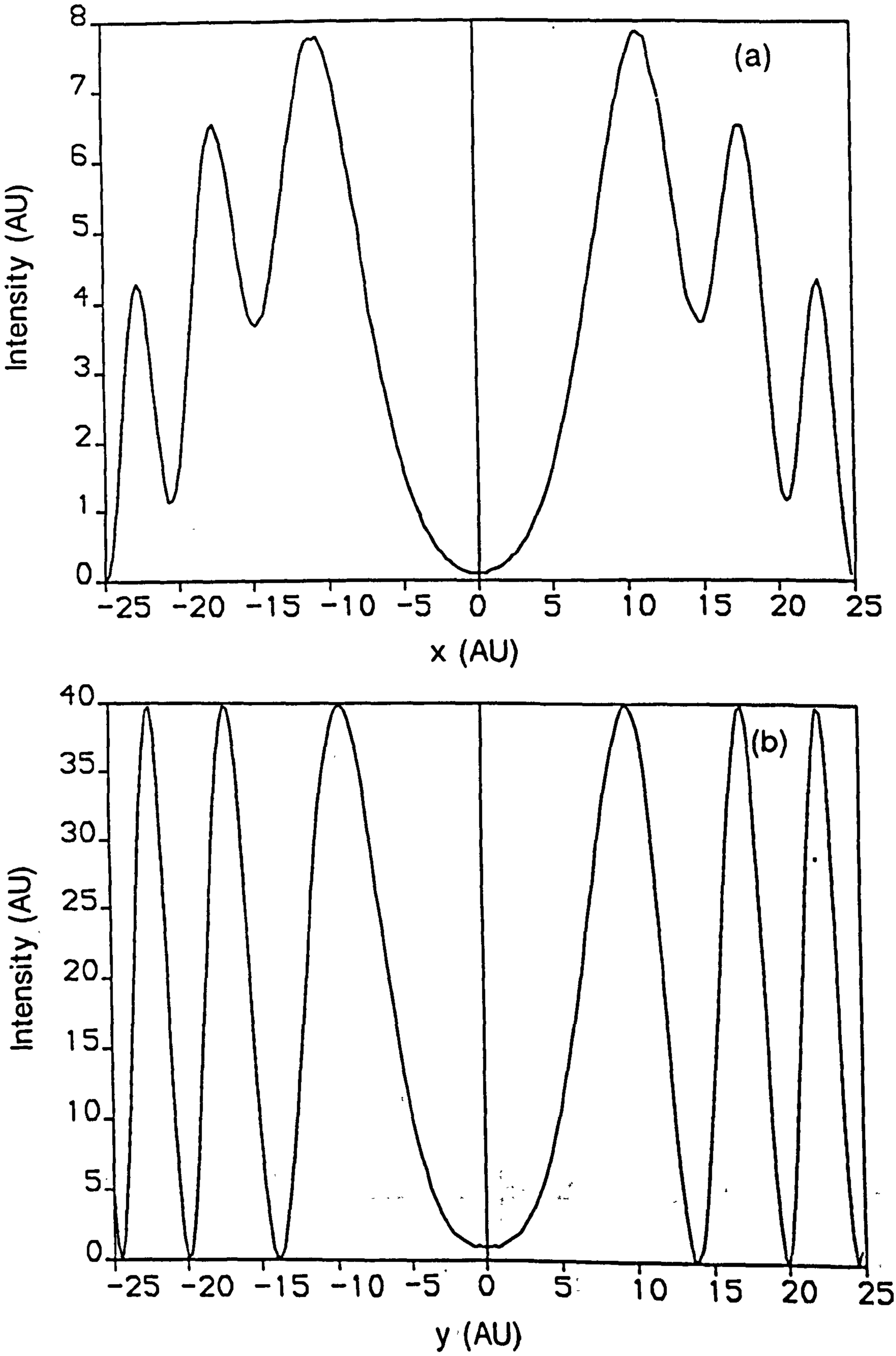

Figure 6.11: Interference pattern for four point sources with $\Delta\phi_C = 0$, (a) along x-axis, (b) along y-axis.

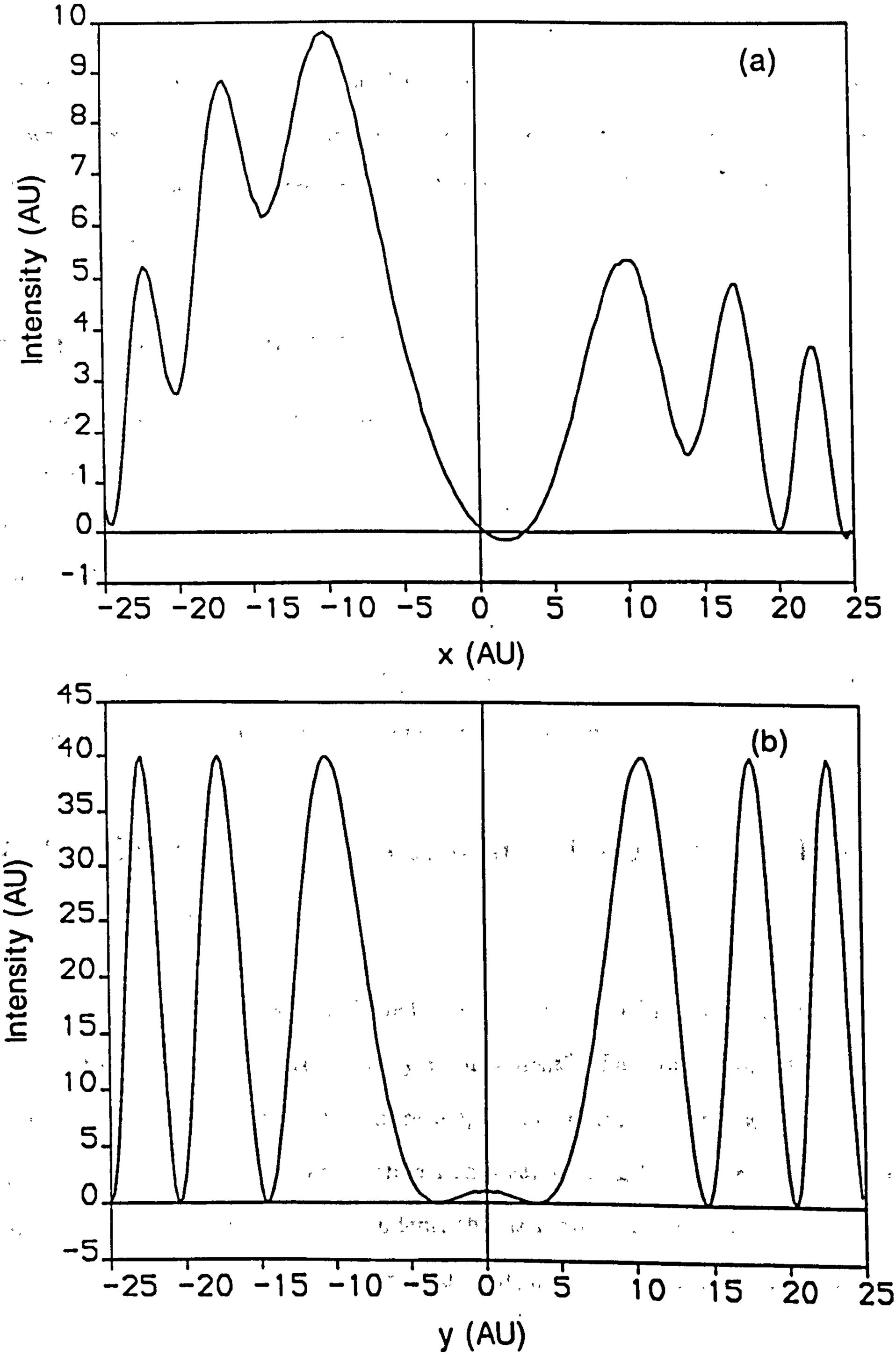

Figure 6.12: Interference pattern for four point sources with $\Delta\phi_C = \pi/5$, (a) along x-axis, (b) along y-axis.

the transmitted mode pattern could not be made to be entirely LP_{01}. Figure 6.13 shows an example of the transmitted mode pattern and the wedge fringes observed when three dislocations were present. Again all the dislocations observed were of unit strength.

6.3.3 Multi-Mode Fibres

The experiments so far have shown that increasing the number of allowed modes increases the number of dislocations observed. Therefore if the number of modes is increased significantly by using multi-mode fibre then the number of dislocations should also increase drastically. Figure 6.14 shows a small part of the central region of the fringe pattern, like that shown in figure 6.2 (c), using multi-mode fibre (MM) at 633 nm. Even this small part of the transmitted pattern contains many singularities which occurs in both senses but again only in first order.

6.4 Estimation of Intensity-Dependent Refractive Index

The previous section has established the requirement of mode mixing for a dislocation to occur but is this the only requirement? The formation of dislocations was found to be independent of fibre length and pump power suggesting that the process involved is linear rather than nonlinear mixing but the refractive index in silica fibres is still intensity-dependent, this is mainly due to temperature changes caused by absorption of the transmitted light, and the following section describes a method of estimating this.

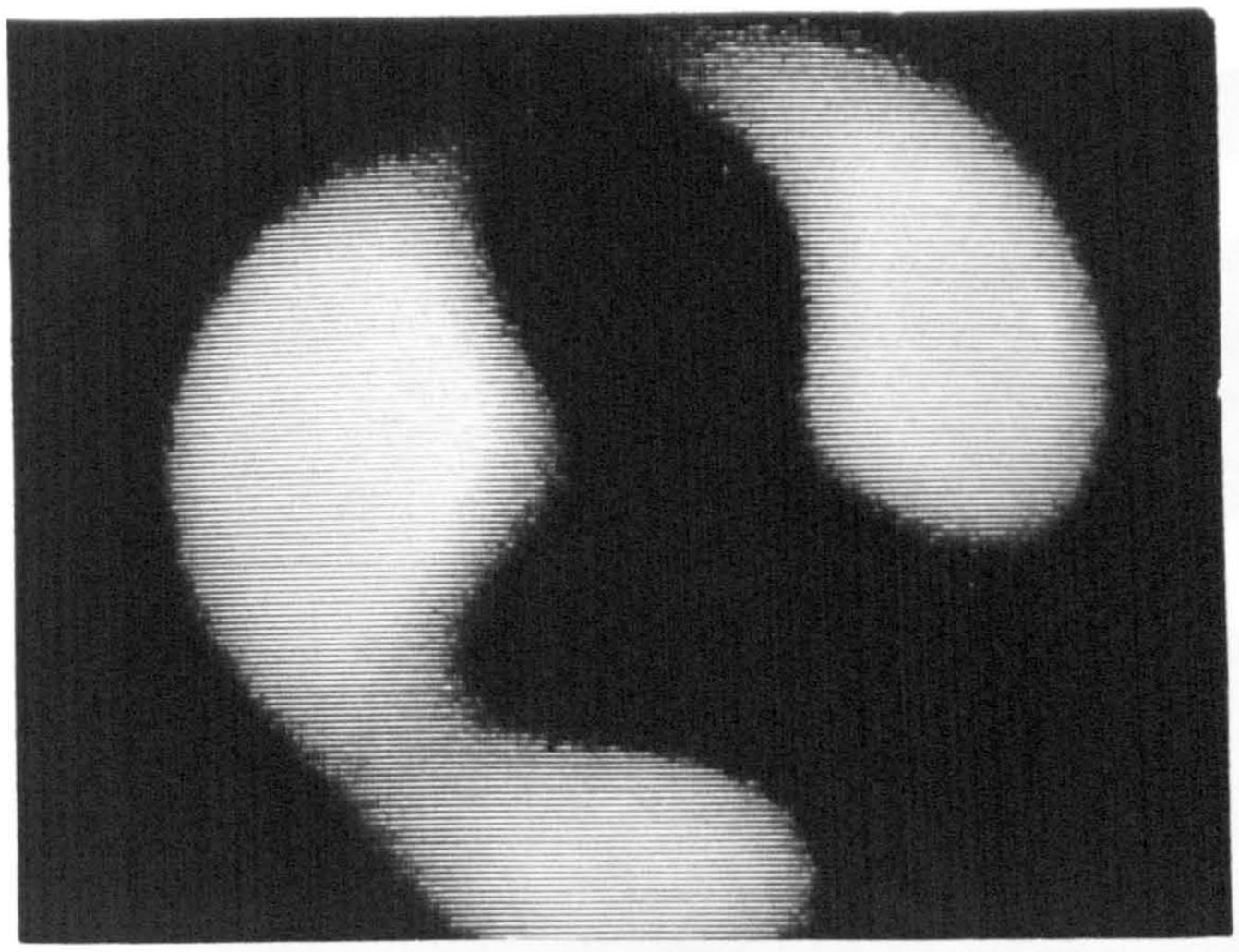

(a)

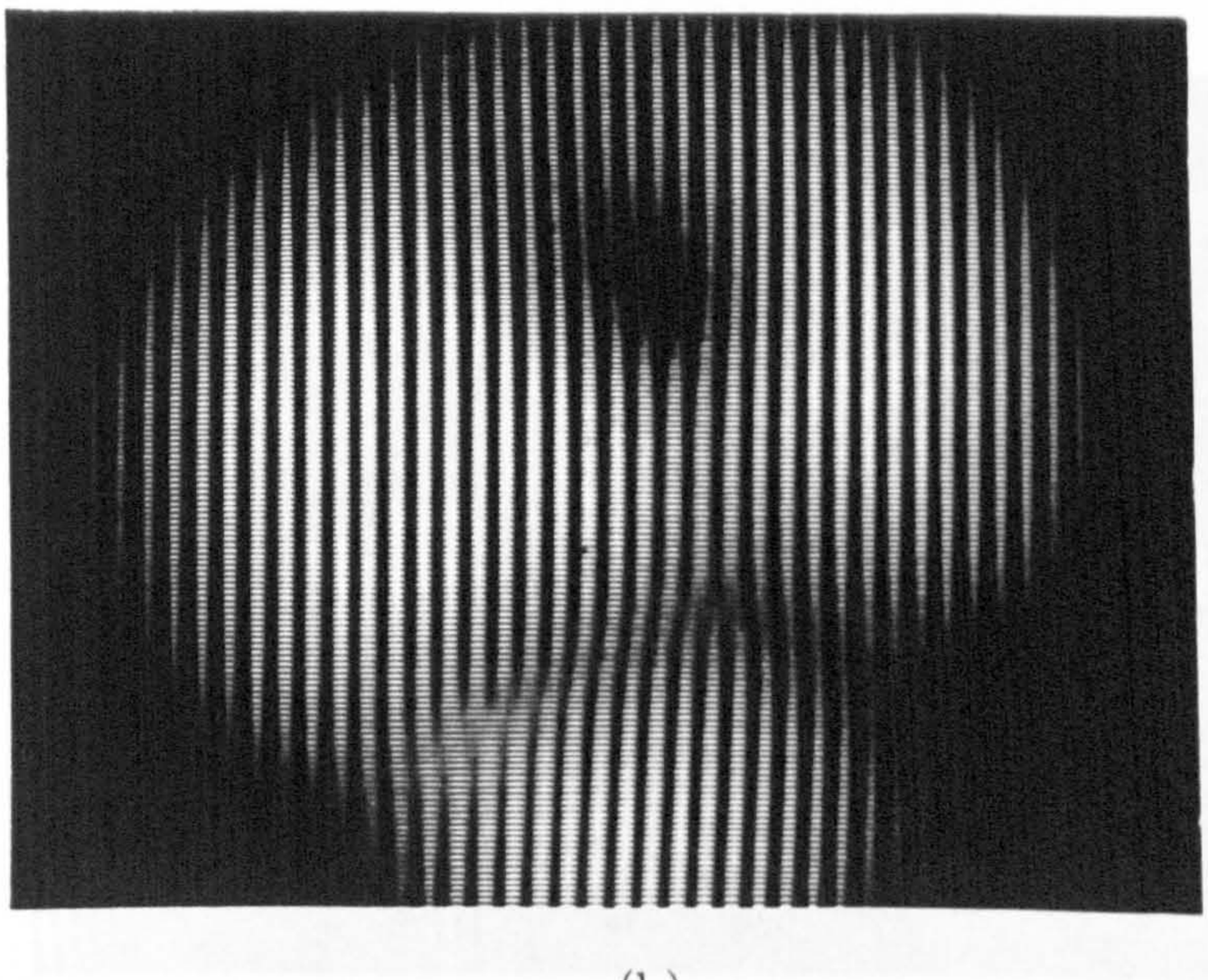

(b)

Figure 6.8: (a) Mode pattern and (b) fringes for four-mode fibre

6.4.1 Introduction

Optical fibre Mach-Zehnder interferometers, like the one used here, have also been used to measure external temperature and pressure changes [HOC79,HUG80,LAG81]. Changing the external pressure or temperature differences between the two arms of the interferometer causes the phase difference to change resulting in a displacement of the fringe pattern. A knowledge of the fibre parameters allows the change in pressure or temperature to be calculated. If however the temperature of one of the arms is changed internally through absorption of the transmitted light then this too will lead to a movement of the fringe pattern.

The phase change $\frac{\Delta\phi}{\phi}$ due to a temperature change ΔT is made up of three contributions - the change in fibre length due to thermal expansion or contraction, the temperature induced change in refractive index and also the change in refractive index due to strain. This can be written as [LAG81]

$$\frac{\Delta\phi}{\phi} = \frac{\Delta l}{l} + \frac{\Delta n}{n} = \epsilon_z + \frac{1}{n}\left(\frac{\partial n}{\partial T}\right)_\rho \Delta T + \left(\frac{\delta n}{n}\right)_T \tag{6.5}$$

where ϵ_z is the axial strain in the core due to the length change and ρ is the core density. The last term in equation 6.5 is the strain term and can be expressed in terms of the strains and the elastooptic coefficients. For silica the largest of these contributions, by about two orders of magnitude, is the term due to the temperature dependence of the refractive index and $\frac{dn}{dT}$ is typically 1×10^{-5} °C^{-1} [HOC79] although this varies with both temperature and wavelength. So equation 6.5 can be rewritten as

$$\frac{1}{L}\frac{\Delta\phi}{\Delta T} = \frac{2\pi}{\lambda}\left(\frac{dn}{dT}\right). \tag{6.6}$$

At a wavelength of $\lambda = 514.5$ nm this gives $\frac{1}{L}\frac{\Delta\phi}{\Delta T} = 122$ radians/°C-m or put another way, a fringe displacement of 19.4 fringes per °C per meter of fibre.

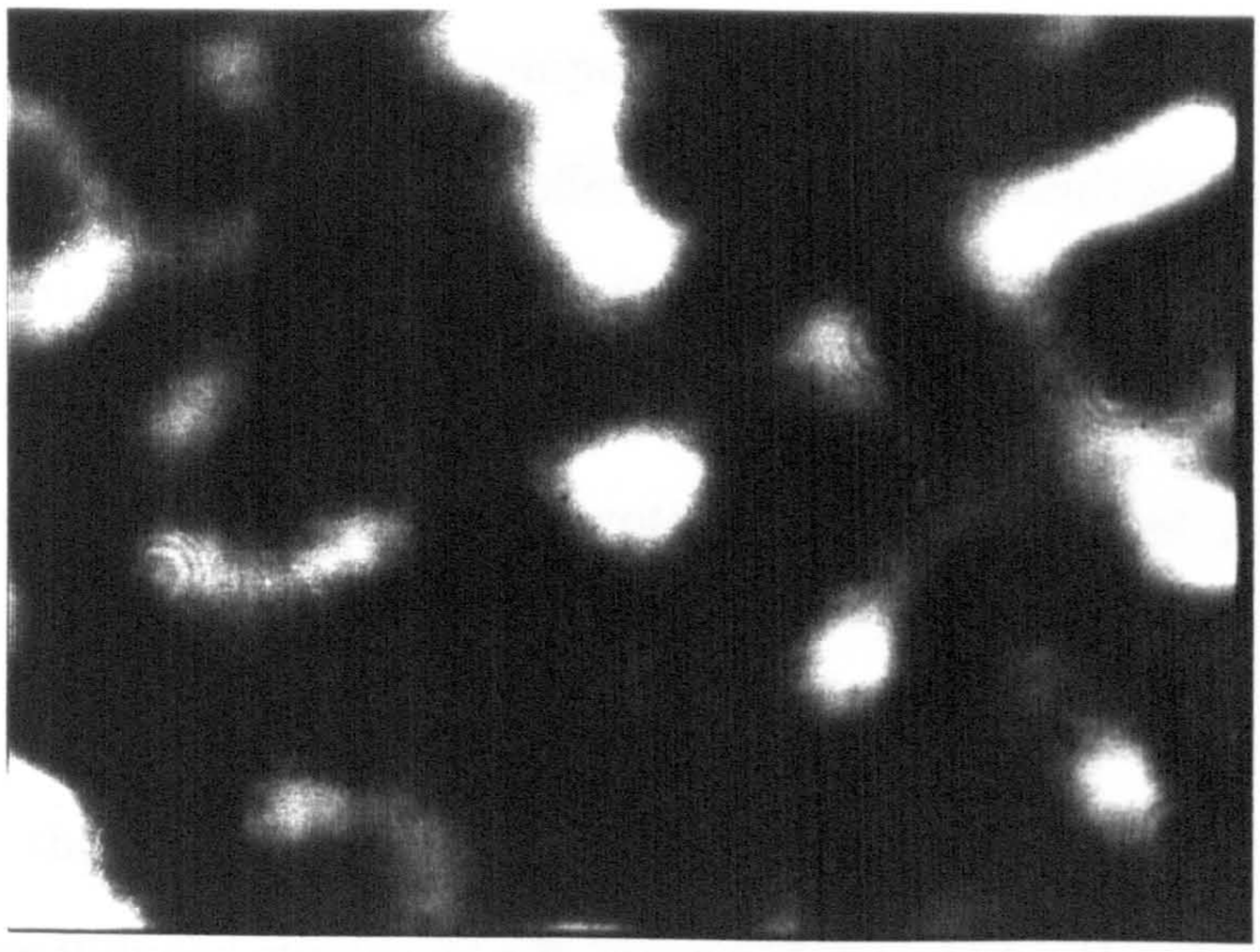

(a)

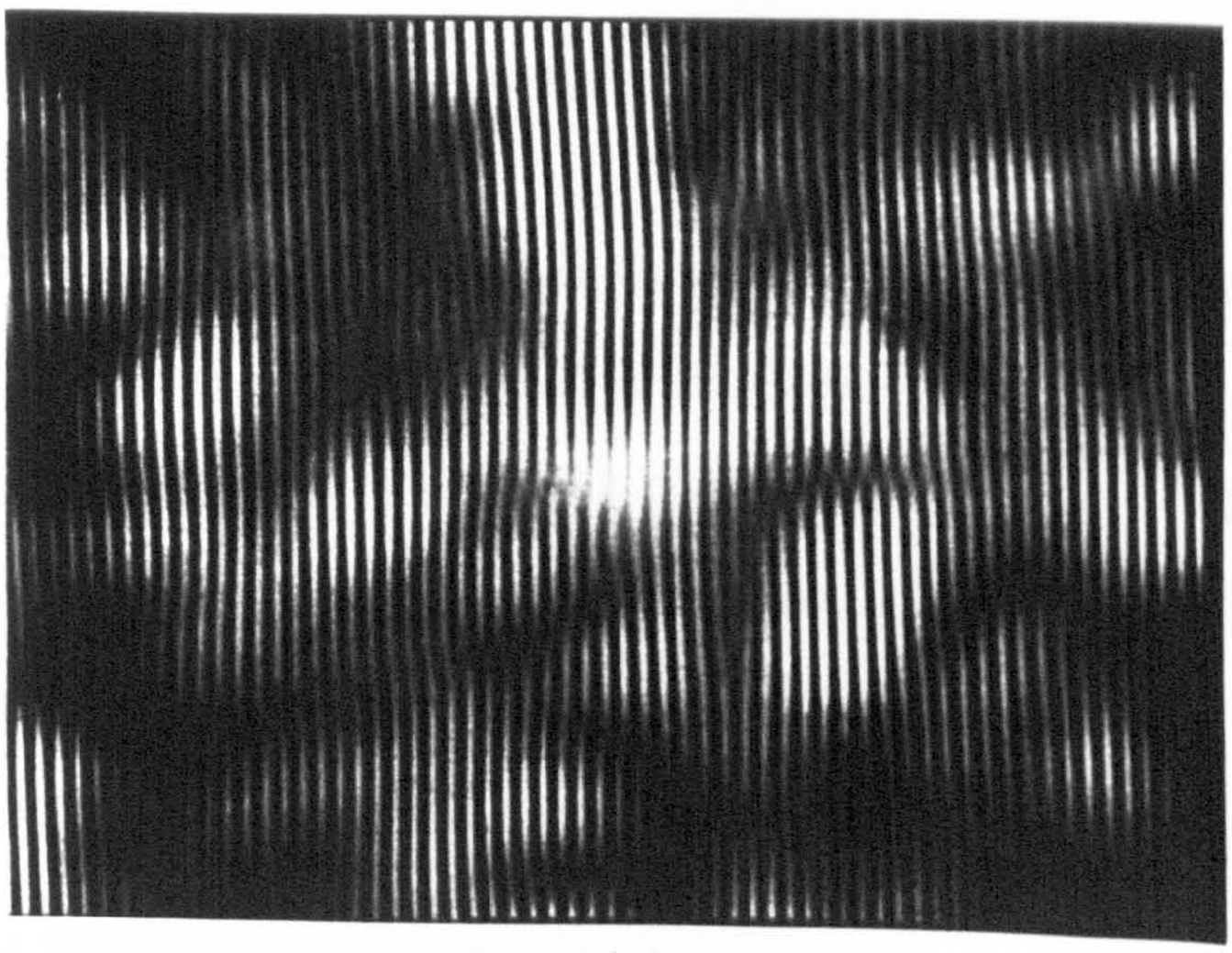

(b)

Figure 6.9: (a) Part of the multi-mode fibre mode pattern and (b) associated fringes

6.4.1 Introduction

Optical fibre Mach-Zehnder interferometers, like the one used here, have also been used to measure external temperature and pressure changes [HOC79,HUG80,LAG81]. Changing the external pressure or temperature differences between the two arms of the interferometer causes the phase difference to change resulting in a displacement of the fringe pattern. A knowledge of the fibre parameters allows the change in pressure or temperature to be calculated. If however the temperature of one of the arms is changed internally through absorption of the transmitted light then this too will lead to a movement of the fringe pattern.

The phase change $\frac{\Delta\phi}{\phi}$ due to a temperature change ΔT is made up of three contributions - the change in fibre length due to thermal expansion or contraction, the temperature induced change in refractive index and also the change in refractive index due to strain. This can be written as [LAG81]

$$\frac{\Delta\phi}{\phi} = \frac{\Delta l}{l} + \frac{\Delta n}{n} = \epsilon_z + \frac{1}{n}\left(\frac{\partial n}{\partial T}\right)_\rho \Delta T + \left(\frac{\delta n}{n}\right)_T \tag{6.5}$$

where ϵ_z is the axial strain in the core due to the length change and ρ is the core density. The last term in equation 6.5 is the strain term and can be expressed in terms of the strains and the elastooptic coefficients. For silica the largest of these contributions, by about two orders of magnitude, is the term due to the temperature dependence of the refractive index and $\frac{dn}{dT}$ is typically 1×10^{-5} °C^{-1} [HOC79] although this varies with both temperature and wavelength. So equation 6.5 can be rewritten as

$$\frac{1}{L}\frac{\Delta\phi}{\Delta T} = \frac{2\pi}{\lambda}\left(\frac{dn}{dT}\right). \tag{6.6}$$

At a wavelength of $\lambda = 514.5$ nm this gives $\frac{1}{L}\frac{\Delta\phi}{\Delta T} = 122$ radians/°C-m or put another way, a fringe displacement of 19.4 fringes per °C per meter of fibre.

6.4.2 Measurement of Phase Change

An interferometer was constructed with a 1 m piece of single-mode fibre in the reference arm and a 5.7 m piece in the sensor arm arranged to produce circular fringes. The light to the sensor arm was blocked but allowed through the reference arm and this was allowed sufficient time to reach a steady temperature. The sensor arm was then unblocked to create the circular fringes which moved outwards as the temperature was increasing and then slowed to a random movement caused by fluctuations in the environment. A small area photodiode was placed in the interference pattern and connected to a chart recorder where the fringe movement was captured as a series of maxima and minima as successive fringes crossed the detector, figure 6.15 shows an example of such a recording. The temperature rises most quickly when light is first introduced into the fibre and then approaches its equilibrium value at a decreasing rate. This is shown clearly in figure 6.15 as the period of the oscillations increases with time, the amplitude of the oscillations also increases with time but this is merely due to attenuation of the amplitude of the high frequency oscillations caused by the slow response of the chart recorder. Care was taken to achieve the best possible launch efficiency so that as much as possible as the light was confined to the core of the fibre and so light should only be absorbed in the effective core area. A knowledge of the launched power, fibre absorption and other thermal coefficients should allow the heat equation to be solved giving the temperature rise and hence the phase change. If the only contribution to the phase change is $\frac{dn}{dT}$ then for small temperature changes the fringe displacement should be proportional to the launched power.

For short fibre lengths the launched power is approximately equal to the transmitted power and figure 6.16 shows that the fringe displacement is in fact proportional to the transmitted power. The fact that the phase change takes place over several seconds means that the nonlinearity is slow which is also suggestive of a thermal

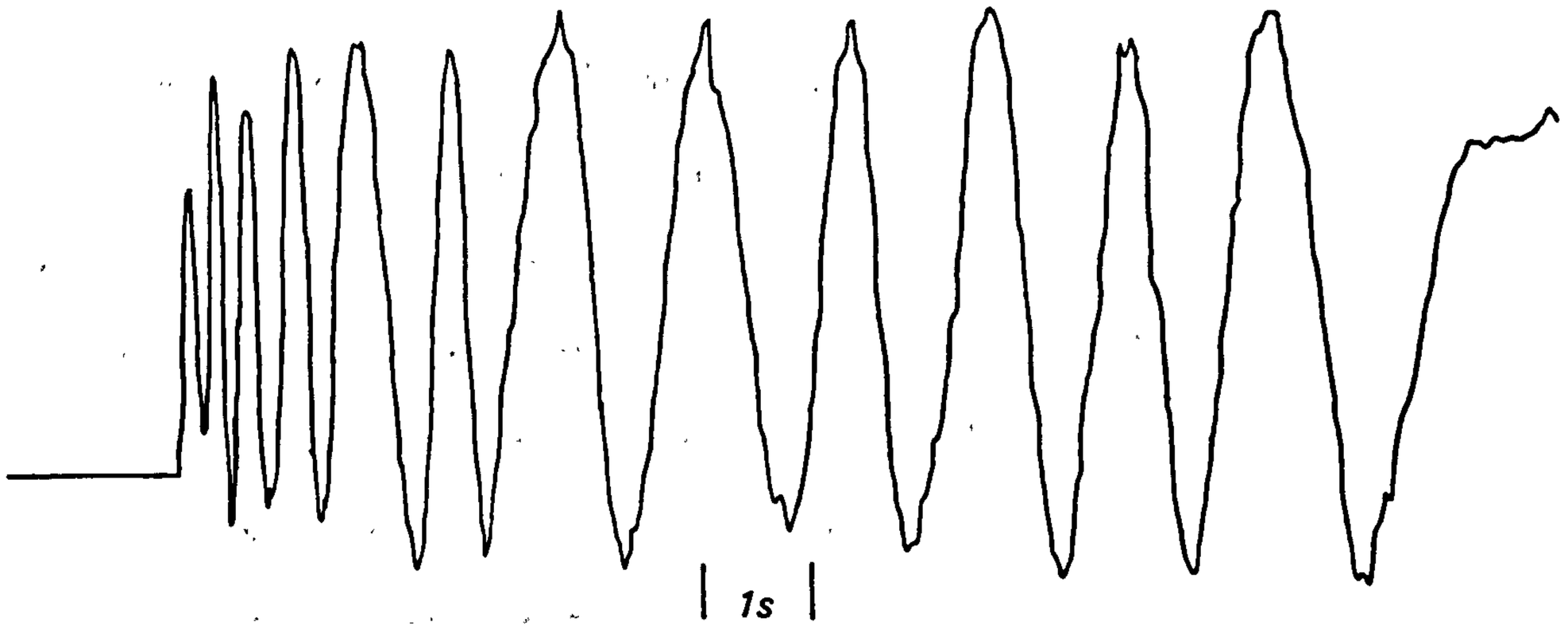

Figure 6.10: Example of chart recorder output for a transmitted power of 240 mW

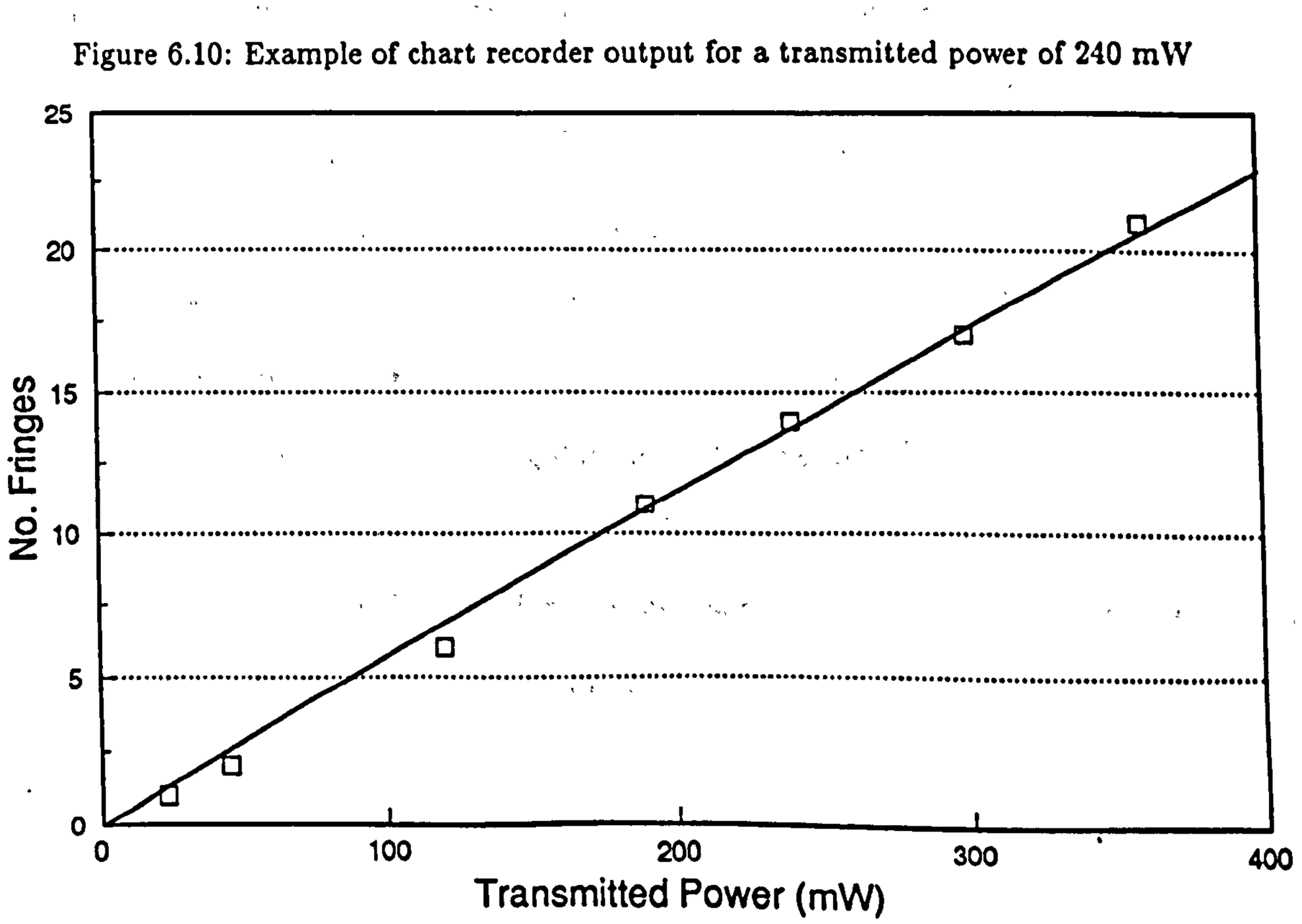

Figure 6.11: Fringe displacement against transmitted power

effect. In conclusion it would appear that the dominant nonlinearity here is due to the temperature induced change in refractive index.

To obtain the size of the nonlinearity, $\frac{dn}{dT}$, from these results requires the solution of the heat equation with the appropriate boundary conditions for the different materials that make up the fibre. It can be assumed that light is absorbed only in the effective area of the fibre and that the core and cladding have thermal properties which are not significantly different from that of bulk silica. Unfortunately information about the thermal properties of the buffer coating, in this case uv-cured urethane acrylate, could not be found, even from the manufacturers, and so the calculation was not carried out.

6.5 Conclusions

It has been shown in this chapter that phase singularities or dislocations can exist in the wavefronts of the optical patterns transmitted by optical fibres. The dislocations were found to be screw dislocations and always of first order. Dislocations were not found when transmitted mode pattern contain only one fibre mode and the necessity for the mixing of fibre modes was shown. This allows interference between the contributions from the different modes creating zeros in the intensity of the transmitted pattern causing singularities. Increasing the number of fibre modes leads to a larger number of dislocations being observed. Due to the fact that the creation of dislocations did not depend on laser power or fibre length it was thought that the mode-mixing process was linear.

Chapter 7

Conclusions

This thesis has studied both the steady-state and temporal behaviour of SBS in germania doped single-mode silica optical fibres. Systems examined included an SBS generator, where the SBS was produced by amplification of spontaneous scattering, both without and with optical feedback and also an SBS amplifier, where the amplification is of a probe signal at the Stokes frequency shift from the pump produced elsewhere.

Calculating a 'probe' value from the threshold conditions allows the characteristics of the SBS and transmitted pump power for the SBS generator to be produced using the solutions to the coupled wave equations. These show that both the pump and SBS are at their most intense in the first part of the fibre and then decay rapidly. SBS can severely attenuate the transmitted pump and the maximum power that can be transmitted by a fibre is determined by the effective interaction length and the Brillouin gain. The theoretical achieved steady-state behaviour is consistent with the experimental data showing that the parameters used, which were also used to produce the theoretical temporal behaviour, were correct. Also the fact that the steady-state behaviour found here is consistent with that found by others, see for example [AGR89a], shows that the experimental arrangements used provide suitable test-beds to examine the temporal response.

Adding a cavity around the Brillouin medium has the same effect as increasing the Brillouin gain leading to an increase in the SBS conversion efficiency and a decrease in threshold power. Apart from this, the steady-state behaviour with and without cavity was found to be identical, i.e. the shapes of the curves are the same in both cases but they are displaced from one another. The reflectivities used here were low, only about 3.5% at each end, so that at the pump powers and fibre lengths used, a maximum of 500 mW using a 100 m fibre, only first order Stokes was produced. Increasing the reflectivity, pump power or fibre length sufficiently would see the generation of multiple orders of Stokes and anti-Stokes components through four-wave mixing [HIL76a].

The SBS amplifier was operated in the saturated regime, where the pump is heavily depleted, and the output power was found to vary almost linearly with the both the pump and applied probe power. The gains achieved were modest, typically only 100 to 200, but the conversion of pump to SBS was large, for example 75% of a 0.5 W pump being converted to SBS using a 4 mW probe and a 100 m piece of LTI fibre in the amplifier.

The temporal behaviour of SBS generated from spontaneous scattering without feedback using a cw pump was found to be aperiodic with modulation depths of approximately 100%. This was found to be the case under all the operating conditions investigated, from threshold to a maximum pump power of about 4 W using a variety of different lengths of standard single-mode fibre between 25 m and 300 m and also a 50 m piece of polarisation maintaining fibre. Neither oscillatory or dc operation was observed. The bandwidth of the power spectra of the SBS was found to be ~44 MHz (FWHM) and did not vary with the single-pass gain. The transmitted pump also behaves aperiodically, the depth of modulation increases with pump power and gives a measure of the conversion efficiency. Power spectra and phase portraits produced from the SBS and transmitted pump signals are suggestive of

chaotic dynamics but no precursor routes to chaos were found. Since this behaviour does not depend on feedback, this is an example of open flow, and the bandwidth of the chaotic SBS was found to be independent of the SBS gain it is thought that this type of behaviour should occur for any fibre length at any power above threshold.

These observations were the first to find the temporal behaviour of the SBS to be aperiodic under conditions of no external reflectivity and where only first-order Stokes was generated. These results not only provided the impetus for further experimental research but also for the theoretical analysis, by Lu and Harrison, which was carried out in tandem to these experiments.

Work to determine whether this behaviour is stochastic or deterministic is continuing, but similar behaviour, which is deterministic, has been predicted theoretically [LU91a]. This was achieved by solving the standard coupled wave equations but including terms to account for self- and cross-phase modulation of the light waves. These terms were traditionally neglected since the nonlinear dispersion in silica fibres, and hence the SPM and XPM, was thought to be too small to effect the behaviour but this work proves otherwise. Further investigations into the influence of stochastic processes (noise) on deterministic behaviour may help to show that the SBS dynamics without feedback are truly chaotic. The role of nonlinear dispersion alone in promoting the dynamics may be clarified by considering this in the absence of SBS, i.e. by operating at powers below the SBS threshold. With optical feedback such systems are analogous to those considered by Ikeda [NAK83].

An SBS amplifier operating at pump powers below the threshold for amplification of spontaneous emission shows no chaotic behaviour and only amplifies the applied probe. Above threshold the SBS signal is a mixture of that due to the probe and that to spontaneous emission. As the probe power is increased this term dominates and eventually the SBS signal has the same appearance as the probe.

The purpose of these experiments was to attempt to examine the response of

the SBS signal when the behaviour of the probe signal was known. Unfortunately the spontaneous scattering term cannot be removed, unless the system is cooled to absolute zero, and hence the true probe was always the combination of the applied probe plus spontaneous scattering. Theory predicts only dc behaviour above a certain probe value, determined by the pump power, fibre length etc. Unfortunately the amplifier can only produce a detectable output which is a mixture of amplified spontaneous scattering and amplified probe when the probe is below this value.

SBS not only limits the power that can be transmitted by an optical fibre but in the absence of feedback also causes the transmitted signal to contain a modulated portion. If however instead of sending the signal directly down the fibre an SBS amplifier was used, then if sufficiently large the signal will show no modulation independent of the pump power and will be amplified instead of being attenuated.

The addition of feedback dramatically changes the temporal behaviour of both the SBS and the transmitted pump. The small reflectivities of the cleaved fibre end faces, $\sim 3.5\%$, is sufficient to produce sustained and bursting oscillations again in both the SBS and transmitted pump signals. Reflections of this size are often found in practical systems caused by connectors and splices as well as bare cleaved fibre ends, meaning that the behaviour described below may dominate when SBS occurs in such systems.

At very low reflectivities and pump powers the SBS power spectra are entirely broadband and the time series aperiodic. Increasing the gain and phase modulation, by either increasing the pump power or cavity reflectivity, leads to small peaks appearing in the power spectra at the cavity round-trip frequency. These grow as the power or reflectivity is increased.

At higher reflectivities, such as natural, the SBS was periodic even close to threshold. As the pump power was increased the SBS went through modulations and pulsations to an almost dc state with only occasional short bursts of oscilla-

tions. The detailed structure of the time series show groups of round-trip period oscillations competing against each other. This leads to some decaying while others grow resulting in a highly modulated signal. At low powers there is only one set of oscillations but the number increases with power and as many as nine sets were observed. If the pump power was increased sufficiently then second-order Stokes SBS was produced by four-wave mixing of the SBS reflected from the fibre end and the pump. With the onset of second-order Stokes the temporal behaviour again becomes periodic and the depth of modulation increases with pump power. Insufficient pump powers was available to generate higher-order Stokes frequencies but it is thought that this would have been possible using a fibre longer than the 40 m used here.

If instead the cavity reflectivity was varied with the pump power fixed then similar results were achieved. Operating the pump above threshold for SBS without feedback shows aperiodic behaviour becoming periodic as the cavity reflectivity was raised. The temporal behaviour then followed the same route to an almost dc state as was found on increasing pump power. It is thought that increasing the reflectivity will also lead to the generation of higher order Stokes frequencies if the pump power is high enough. These were not found here as the pump power was only 400 mW using a 36.5 m piece of LTI fibre with reflectivities of 3.5% at one end and a maximum of 20% used at the other.

Theoretically similar results were achieved showing the importance of the XPM and SPM terms in establishing this behaviour. Without these terms only sustained or relaxation oscillations of round-trip period are predicted.

Brillouin lasers have been produced, both using Fabry-Perot [HIL76a] and optical-fibre ring resonator [HIL76b] setups, but little has been said of their temporal behaviour. The work presented in this thesis has shown that the SBS process, under most operating conditions, does not give a dc output and perhaps these system de-

serve further investigation. The Fabry-Perot Brillouin laser, which has been shown to generate multiple Stokes and anti-Stokes frequencies, is similar to the low reflectivity resonators studied here and therefore it is thought likely that the output of such a laser will only be dc in certain limited operating conditions. In contrast to this the Brillouin ring laser has the Stokes frequency circulating in one direction and the pump in the other. Therefore since the two frequencies are not travelling in the same direction no new frequencies should be produced by four-wave mixing and unless the Stokes component becomes intense enough to act as a pump for second-order Stokes only these two frequencies will occur. The work above showed a region of stable SBS at high pump powers or reflectivity before the onset of second-order Stokes. The ring-laser configuration should not allow the production of second-order Stokes so perhaps such a system will be stable above certain pump powers and cavity reflectivity.

SBS in multimode fibres has been identified as a means of phase conjugation [ROH91] but here also temporal instabilities were found in the conjugate signal. If stable operating conditions could be found then this system may be developed into a fast, real-time, low-power phase conjugation system therefore extending the work carried out here in single-mode fibres to multi-mode fibres may prove valuable.

Although the work presented here is specific to stimulated Brillouin scattering other stimulated scattering processes such as stimulated Raman or stimulated thermal Rayleigh scattering may yield similar results. These processes are governed by equations similar to those of SBS, in the case of stimulated Raman scattering the analysis is simplified through adiabatic elimination of the material equation due to the large gain bandwidth. Theoretical work, again by Lu and Harrison [LU91b], has shown chaotic dynamics to prevail, in the absence of feedback, almost from the onset of SRS with no evidence of precursor dynamical scenarios. Again the rich dynamical behaviour is a consequence of the interplay between the nonlinear refraction and the

gain.

In conclusion this thesis provides the first experimental evidence that the temporal response of SBS in optical fibres is very seldom dc. In the majority of operating conditions, varying both pump power and cavity reflectivity, the SBS is either aperiodic, perhaps chaotic, or periodic, with periods relating to the cavity round-trip time, and deeply modulated.

The final area of research was examining the existence of phase singularities in the wavefronts of optical fibres was investigated. These occur at points in the mode pattern where the electric field is exactly equal to zero and the phase is undefined. The dislocations were found to be screw dislocations and always of first order. When the transmitted mode pattern was entirely one mode no singularities were found. They were only observed when the pattern was a mixture of at least two different modes showing the need for mode mixing. This allows interference between contributions from different modes to create the required zeros in intensity. Increasing the numbers of fibre modes leads to a larger number of dislocations. The creation of dislocations was found not to depend on the fibre length or pump power and so the mixing process was thought to be linear.

Appendix A

Fibre Parameters - Manufacturer's Data

Fibre type - SM 450

Single-mode argon ion fibre - Manufactured by York V.S.O.P.

Serial No. YD357-01A

Optics		Geometry	
Cut-off Wavelength	460nm	Core diameter	3.1μm
Attenuation	20dB/km at 488nm	Cladding diameter	125μm
Numerical Aperture	0.11	Coating diameter	244μm
Optimum Launch Spot-size	3.4μm		

Composition

Core	silica 5 wt% germania
Inner Cladding	phosphorus/fluorine-doped silica
Coating	Single coat uv acrylate
	Type - DeSoto 131

Fibre type - HB 450

Hi-Bi argon ion fibre - Manufactured by York V.S.O.P.

Serial No. YD567-00

Optics		Geometry	
Cut-off Wavelength	430nm	Core diameter	2.2μm
Attenuation	20dB/km at 488nm	Cladding diameter	125μm
Beat length	1.4mm at 633nm	Coating diameter	244μm
Linearly extrapolated to	1.1mm at 488nm*		
Numerical Aperture	0.11		
Optimum Launch Spot-size	3.6 μm		

Composition	
Core	silica 5 wt% germania
Inner Cladding	phosphorus/fluorine-doped silica
Coating	Single coat uv acrylate

Type - DeSoto 131

* This value was obtained by linear extrapolation but since the beat length is a function of the two propagation constants, which vary with wavelength, this type of extrapolation may not hold for this particular fibre.

Fibre type - LTI

Single-mode HeNe fibre - Manufactured by Lightwave Technology

Optical fibre F1506C, ID No. T2180CABCA-2

Optics

Cut-off Wavelength	617nm
Attenuation	25dB/km at 514nm
Numerical Aperture	0.11
Core refractive index	1.457 to 1.458
Cladding refractive index	1.453

Geometry

Core diameter	4.8μm
Cladding diameter	125μm
Coating diameter	250μm

Composition

Core	Silica/5% germania
Cladding	Pure fused silica
Coating	uv acrylate

References

[ABR90] N. B. Abraham and W. J. Firth, "Overview of transverse effects in nonlinear-optical systems", J. Opt. Soc. Am. B7(6), 951-962, (1990).

[ADA81] M. J. Adams,"An Introduction to Optical Waveguides", Wiley, New York, (1981).

[AGR89a] G. P. Agrawal, "Nonlinear Fiber Optics", Academic Press, San Diego (1989).

[AGR89b] G. P. Agrawal, P. L. Baldeck and R. R. Alfano, "Modulation instability induced by cross-phase modulation in optical fibers", Phys. Rev. A 39(7), 3406-3414, (1989)

[AND76] N. F. Andreev, V. I. Bespalov, A. M. Kiselev, A. M. Kubarev and G. A. Pasmanik, "Formation of pulses in stimulated scattering of light in extended media. Modulation of the intensities of transmitted and backscattered radiations", Sov. J. Quantum Electron. 6(10), 1223-1225, (1976).

[AOK87] Y. Aoka, K. Tajima, I. Mito,"Observation of stimulated Brillouin scattering in single-mode fibres with single-frequency laser-diode pumping", Opt. Quantum Electron. 19(2), 141-143, (1987).

[AOK88] Y. Aoki and K. Tajima,"Stimulated Brillouin scattering in a long single-mode fibre excited with a multimode pump laser", J. Opt. Soc. Am. B5(2), 358-363, (1988).

[BAR81a] N. B. Baranova, B. Ya. Zel'dovich, A. V. Mamaev, N. F. Pilipetskil and V. V. Shkukov, "Dislocations of the wavefront of a speckle-inhomogeneous field (theory and experiment)", JETP Lett. 33(4), 195-199, (1981).

[BAR81b] N. B. Baranova and B. Ya. Zel'dovich, "Dislocations of the wave-front surface and zeros of the amplitude", Sov. Phys. JETP 53(5), 925-929, (1981).

[BAR82] N. B. Baranova, B. Ya. Zel'dovich, A. V. Mamaev, N. F. Pilipetskii and V. V. Shkunov, "Dislocation density on wavefront of a speckle-structure light field", Sov. Phys. JETP 56(5), 983-988, (1982).

[BAR83] N. B. Baranova, A. V. Mamaev, N. F. Pilipetsky, V. V. Shkunov and B. Ya. Zel'dovich, "Wave-front dislocations: topological limitations for adaptive systems with phase conjugation", J. Opt. Soc. Am. 73(5), 525-528, (1983).

[BAR85] I. Bar-Joseph, A. A. Friesem, E. Lichtman and R. G. Waarts, "Steady and relaxation oscillations of stimulated Brillouin scattering in single-mode optical fibers", J. Opt. Soc. A. B2(10), 1606-1611, (1985).

[BAR86] I. Bar-Joseph, A. Dienes, A. A. Friesem, E. Lichtman, R. G. Waarts and H. H. Yaffe, "Spontaneous Mode Locking of Single and Multi-mode Pumped SBS Fiber Lasers", Opt. Commun. 59(4), 296-298, (1986).

[BAZ90] V. Yu. Bazhenov, M. V. Vasnetsov and M. S. Soskin, "Laser beams with screw dislocations in their wavefronts", JEPT Lett. 52(8), 429-431, (1990).

[BER81] M. V. Berry, "Singularities in Waves and Rays", in "Physics of Defects", eds. R. Balian et al., North-Holland, (1981).

[BLA88] R. Blaha, E. W. Laedke, A. M. Rubenchik and K. H. Spatschek, "Stability of the Steady-State-Stimulated Brillouin Scattering", Europhys. Lett. 7(3), 237-242, (1988).

[BLO85] K. J. Blow, N. Doran and B. P. Nelson, "All-fiber pulse compression at 1.32 μm", Opt. Lett. **10**(8), 393-395, (1985).

[BOY90] R. W. Boyd, K. Rzazewski and P. Narum, "Noise initiation of stimulated Brillouin scattering", Phys. Rev. A**42**(9), 5514-5521, (1990).

[CHI64] R. Y. Chaio, C. H. Townes and B. P. Stiocheff, "Stimulated Brillouin scattering and Coherent Generation of Intense Hypersonic Waves", Phys. Rev. Lett. **12**(21), 592-595, (1964).

[COT82] D. Cotter,"Observation of Stimulated Brillouin Scattering in Low Loss Silica Fibre at 1.3μm", Electron. Lett. **18**(12), 495-496, (1982).

[COT83] D. Cotter, "Stimulated Brillouin Scattering in Monomode Optical Fiber", J. Opt. Commun. **4**(1), 10-19, (1983).

[COT87] D. Cotter, "Fibre nonlinearities in optical communications", Opt. and Quantum Electron. **19**(1), 1-17, (1987).

[CRC85] "CRC Handbook of Chemistry and Physics", ed. R. C. Weast, CRC Press, Loca Ratan, Florida, (1985).

[DIA89] E. M. Dianov, A. Ya Karasik, A. V. Lutchnikov and A. N. Pilipetskii, "Saturation effects at backward-stimulated scattering in the single-mode regime of interaction", Opt. Quantum Electron. **21**(5), 381-395, (1989).

[DUF18] G. Duffing, "Erzwungene Schwingungen bei Verlanderlich Eigenfrequenz", Vieweg, Braunschweig, (1918).

[ECK85] J.-P. Eckmann and D. Ruelle, "Ergodic theory of chaos and strange attractors", Rev. Mod. Phys. **57**(3), 617-656, (1985).

[ENN69] R. H. Enns and I. P. Batra, "Saturated and Depletion in Stimulated Light Scattering", Phys. Lett. **28A**(8), 591-592, (1969).

[FOR87] R. L. Fork, C. H. B. Cruz, P. C. Becker and C. V. Shank, "Compression of Optical Pulses to 6 Femtoseconds by using Cubic Phase Compression", Opt. Lett. **12**(7), 483-485, (1987).

[GAE89] A. L. Gaeta, M. D. Skeldon and R. W. Boyd, "Observation of instabilities of laser beams counterpropagating through a Brillouin medium", J. Opt. Soc. Am. **B6**(9), 1709-1713, (1989).

[GAE91] A. L. Gaeta and R. W. Boyd, "Stochastic dynamics of stimulated Brillouin scattering in an optical fibre", Phys. Rev. **A44**(5), 3205-3209, (1991).

[GLE88] J. Gleick "Chaos", Cardinal, London, (1988).

[GLO71] D. Gloge, "Weakly Guiding Fibers", Appl. Opt. **10**(10), 2252-2258, (1971).

[HAR90] R. G. Harrison, J. S. Uppal, A. Johnstone and J. V. Moloney, "Evidence of Chaotic Stimulated Brillouin Scattering an Optical Fibers", Phys. Rev. Lett. **65**(2), 167-170, (1990).

[HEI79] D. Heiman, D. S. Hamilton and R. W. Hellwarth, "Brillouin scattering measurements on optical glasses", Phys. Rev. **B19**(12), 6583-6592, (1979).

[HIL76a] K. O. Hill, D. C. Johnson and B. S. Kawasaki, "cw generation of multiple Stokes and anti-Stokes Brillouin-shifted frequencies", Appl. Phys. Lett.

29(3), 185-187, (1976).

[HIL76b] K. O. Hill, B. S. Kawasaki and D. C. Johnson, "cw Brillouin laser", Appl. Phys. Lett. **28**(10), 608-609, (1976).

[HIL78a] K. O. Hill, D. C. Johnson, B. S. Kawasaki and R. I. MacDonald, "cw three-wave mixing in single-mode optical fibers", J. Appl. Phys. **49**(10), 5098-5106, (1978).

[HIL78b] K. O. Hill, Y. Fujii, D. C. Johnson and B. S. Kawasaki, "Photosensitivity in optical fiber waveguides: Applications to reflection filter fabrication.", Appl. Phys. Lett. **32**(10), 647-649, (1978).

[HOC79] G. B. Hocker, "fiber-optic sensing of pressure and temperature", Appl. Opt. **18**(9), 1445-1448, (1979).

[HOR89] T. Horiguchi, M. Tateda, N. Shibata and Y. Azuma, "Brillouin gain variation due to the polarization-state change of the pump or Stokes fields in standard single-mode fibers", Opt. Lett. **14**(6), 329-331, (1989).

[HUG80] R. Hughes and R. Priest, "Thermally induced optical phase effects in fiber optic sensors", Appl. Opt. **19**(9), 1477-1483, (1980).

[IPP72] E. P. Ippen and R. H. Stolen, "Stimulated Brillouin scattering in optical fibers". Appl. Phys. Lett. **21**(11), 539-540, (1972).

[IPP75] E. P. Ippen, "Nonlinear effects in Optical Fibers", in "Laser Applications to Optics and Spectroscopy", eds. S. F. Jacobs, M. Sargent III, J. F. Scott and M. O. Scully, Addison-Wesley, 213-244, (1975).

[JOH71] R. V. Johnson and J. H. Margurger, "Relaxation Oscillations in Stimulated Raman and Brillouin Scattering", Phys. Rev. A4(3), 1175-1182, (1971).

[JOH91] A. Johnstone, Weiping Lu, J. S. Uppal and R. G. Harrison, "Sustained and bursting oscillations in stimulated Brillouin scattering with external feedback feedback in optical fibre", Opt. Commun. **81**(3,4), 222-224, (1991).

[KAD88] R. Kadiwar, P. Bayvel and I. P. Giles, "Stimulated Brillouin scattering in polarisation maintaining all-fiber ring resonators.", in "Fiber Optic and Laser Sensors VI", SPIE **985**, 339-343, (1988).

[KAI72] W. Kaiser and M. Maier, "Stimulated Rayleigh, Brillouin and Raman spectroscopy" in "Laser Handbook" **2**, ed. F. T. Arecchi and E. O. Schulz-Dubois, North Holland, Amsterdam, 1078-1150, (1972).

[KRO65] N. M. Kroll, "Excitation of Hypersonic Vibrations by Means of Photoelastic Coupling of High-Intensity Light Waves to Elastic Waves ", J. Appl. Phys. **36**(1), 34-43, (1965).

[KUZ88] E. A. Kuzin, M. P. Petrov and A. A. Fotiadi, "Fiber-optic stimulated-Brillouin-scattering amplifier", Sov. Phys. Tech. **33**(2), 206-209, (1988).

[LAB80] P. Labudde, P. Anliker and H. P. Weber, "Transmission of Narrow Band High Power Laser Radiation through Optical Fibers", Opt. Commun. **32**(3), 385-390, (1980).

[LAG81] N. Lagakos, J. A. Bucaro and J. Jarzynski, "Temperature-induced optical phase shifts in fibers", Appl. Opt. **20**(13), 2305-2308, (1981).

[LIC87a] E. Lichtman, A. A. Friesem, R. G. Waarts and H. H. Yaffe, "Stimulated Brillouin scattering excited by two pump waves in single-mode fibres", J. Opt. Soc. Am. B**4**(9), 1397-1403, (1987).

[LIC87b] E. Lichtman and A. A. Friesem, "Stimulated Brillouin scattering excited by a multimode laser in single-mode optical fibers", Opt. Commun. 64(6), 544-548, (1987).

[LIC89] E. Lichtman, R. G. Waarts and A. A. Friesem, "Stimulated Brillouin Scattering Excited by a Modulated Pump Wave in Single-Mode Fibers", J. Lightwave Tech. **7**(1), 171-174, (1989).

[LOR63] E. N. Lorentz, "Deterministic non-periodic flow", J. Atmos. Sci. **20**, 130-141, (1963).

[LU91a] Weiping Lu, "Dynamics of Nonlinear Optical Systems", PhD Thesis, Heriot-Watt University, (1991).

[LU91b] Weiping Lu and R. G. Harrison, "Nonlinear Dynamics and Chaotic Features in Stimulated Scattering Phenomena", Europhysics Lett. **16**(7), 655-660, (1991).

[MAR78] D. Marcuse, "Gaussian approximation of the fundamental modes of graded-index fiber", J. Opt. Soc. Am. **68**(1), 103-109, (1978).

[MAR86] D. Marcuse, "Coupling Efficiency of Front Surface and Multilayer Mirrors as Fiber-End Reflectors", J. Lightwave Technol. LT-4(4), 377-381, (1986).

[MIZ91] V. Mizrahi, S. LaRochelle and G. I. Stegeman, "Physics of photosenstive-grating formation in optical fibers", Phys. Rev. **A43**(1), 433-438, (1991).

[MOL80] L. F. Mollenauer, R. H. Stolen and J. P. Gordon, "Experimental Observations of Picosecond Pulse Narrowing and Solitons in Optical Fibers", Phys. Rev. Lett. **45**(13), 1095-1098, (1980).

[MON87] C. Montes and J. Coste, "Optical turbulence in multiple stimulated Brillouin backscattering", Laser and Particle Beams 5(2), 405-411, (1987).

[NAK81] H. Nakatsuka, D. Grischkowsky and A. C. Balant, "Nonlinear Picosecond Pulse Propagation Through Optical Fibers With Positive Group Velocity Dispersion", Phys. Rev. Lett. 47(13), 910-913, (1981).

[NAK83] H. Nakatsuka, S. Asaka, H. Itoh, K. Ikeda and M. Matsuoka, "Observations of Bifurcation to Chaos in an All-Optical Bistable System", Phys. Rev. Lett. 50(2), 109-111, (1983).

[NAR88] P. Narum, A. L. Gaeta, M. D. Skeldon and R. W. Boyd, "Instabilities of laser beams counterpropagating through a Brillouin-active medium", J. Opt. Soc. Am. B5(3), 623-628, (1988).

[NEL85] B.P. Nelson, B. J. Ainslie, J. Ainslie and R. Wyatt, "Design and Manufacture of Fibres with Specific Dispersion Properties", Electron. Lett. 21(7), 274-276, (1985).

[NIK83] B. Nikolaus and D. Grischkowsky, "90-fs tunable optical pulses obtained by two-stage pulse compression", Appl. Phys. Lett. 43(3), 228-230, (1983).

[NYE74] J. F. Nye and M. V. Berry, "Dislocations in wave trains", Proc. R. Soc. Lond. A **336**, 165-190, (1974).

[PAC80] N. H. Packard, J. P. Crutchfield, J. D. Farmer and R. S. Shaw, "Geometry from a Time Series", Phys. Rev. Lett. 45(9), 712-716, (1980).

[PEL75] J. Pelous and R. Vacher, "Thermal Brillouin scattering measurements of the attenuation of longitudinal hypersounds in fused quartz from 77 to 300K", Solid State Commun. 16(3), 279-283, (1975).

[POH70] D. Pohl and W. Kaiser, "Time-Resolved Investigations of Stimulated Brillouin Scattering in Transparent and Absorbing Media: Determination of Phonon Lifetimes", Phys. Rev. B1(1), 31-43, (1970).

[POL27] B. van der Pol, "On Relaxation-oscillations", Phil. Mag. **2**(7), 978-992, (1927).

[POY88] L. J. Poyntz-Wright, M. E. Fermann and P. St. J. Russell, "Nonlinear transmission and color-center dynamics in germanosilicate fibers at 420 -540 nm", Opt. Lett. **13**(11), 1023-1025, (1988).

[RAN84] C. J. Randall and J. R. Albritton, "Chaotic Nonlinear Stimulated Brillouin Scattering", Phys. Rev. Lett. **52**(21), 1887-1890, (1984).

[RED88] I. R. Redmond, M. R. Taghizadeh, "Continuously Variable Laser Beam Attenuator", European patent no. 88109667.1, U.S. patent no. 200 872, filed June (1988).

[ROH91] W. B. Roh, P. T. Ryan and K. A. Wink, "Phase Conjugation via Stimulated Brillouin Scattering in Multimode Optical Fiber", submitted to Opt. Lett.

[ROW79] N. L. Rowell, P. J. Thomas, H. M. van Driel and G. I. Stegeman, "Brillouin spectrum of single-mode optical fibres", Appl. Phys. Lett. **34**(2), 139-141, (1979).

[SHA81] R. Shaw, "Strange attractors, chaotic behavior, and information flow.", Z. Naturf. **36a**, 80-112, (1981).

[SHE84] Y. R. Shen, "The Principles of Nonlinear Optics", Wiley, New York (1984).

[SHE88] R. M. Shelby, M. D. Levenson and S. H. Perlmutter, "Bistability and other effects in a nonlinear fiber-optic ring resonator", J. Opt. Soc. Am. B 5(2), 347-357, (1988)

[SMI72] R. G. Smith, "Optical Power Capacity of Low Loss Optical Fibers as Determined by Stimulated Raman and Brillouin Scattering", Appl. Opt. 11(11), 2489-2494, (1972).

[SNI61] E. Snitzer, "Cylindrical Dielectric Waveguide Modes", J. Opt. Soc. Am. 51(5), 491-498, (1961).

[SNY83] A. W. Snyder and J. D. Love, "Optical Waveguide Theory", Chapman and Hall, London, (1983).

[STO78] R. H. Stolen and Chinlon Lin, "Self-phase-modulation in silica optical fibers", Phys. Rev. A **17**(4), 1448-1453, (1978)

[STO79] R. H. Stolen, "Polarization effects in Raman and Brillouin lasers", IEEE J. Quantum. Electron. **QE15**(10), 1157-1160, (1979).

[SUD89] S. Sudo, H. Itoh, K. Okamoto and K. Kubodera,"Generation of 5 THz optical pulses by modulation instability in optical fibers", Appl. Phys. Lett. **54**(11), 993-994, (1989).

[TAI86] K. Tai, A Hasegawa and A. Tomita, "Observation of Modulation Instability in Optical Fibers", Phys. Rev. Lett. **56**(2), 135-138, (1986).

[TAN66] C. L. Tang, "Saturation and Spectral Characteristics of the Stokes Emission in the Stimulated Brillouin Process", J. Appl. Phys. **37**(8), 2945-2955, (1966).

[THO79] P. J. Thomas, N. L. Rowell, H. M. van Driel and G. I. Stegeman, "Normal acoustic modes and Brillouin scattering in single-mode optical fibers",

Phys. Rev. B19(10), 4986-4998, (1979).

[THO86] J. M. T. Thompson and H. B. Stewart, "Nonlinear Dynamics and Chaos", Wiley, Chichester, (1986).

[TKA89] R. W. Tkach and A. R. Chraplyvy, "Fibre Brillouin Amplifiers", Opt. Quantum Electron. **21**(S), S105-S112, (1989).

[TRE69] E. B. Treacy, "Optical Pulse Compression With Diffraction Gratings", IEEE J. Quantum. Electron. QE-**5**(9), 454-458, (1969).

[UED80] Y. Ueda, "Steady motions exhibited by Duffing's equation : a picture book of regular and chaotic motions.", in "New Approaches to Nonlinear Problems in Dynamics", ed. P. J. Holmes, SIAM, Philadelphia, 311-322, (1980).

[UES81] N. Uesugi, M. Ikeda and Y. Sasaki, "Maximum Single Frequency Input Power in a Long Optical Fibre determined by Stimulated Brillouin Scattering", Electron. Lett. **17**(11), 379-380, (1981).

[UPP91] J. S. Uppal, Weiping Lu, A. Johnstone and R. G. Harrison, "Generic Chaotic Behavior of Stimulated Brillouin Scattering", in "Nonlinear Dynamics in Optical Systems" **7**, eds. N. B. Abraham, E. Garmire and P. Mandel, OSA, 558-561, (1991).

[VAL86] G. C. Valley, "A Review of Stimulated Brillouin Scattering Excited with a Broad-Band Pump Laser", IEEE J. Quantum. Electron. QE**22**(5), 704-712, (1986).

[WIN86] H. G. Winful, "Nonlinear Optical Phenomena in Single-mode Fibres", in "Optical-Fiber Transmission", ed. E. E. Basch, Sams, Indianapolis, 179-240, (1986).

[WRI77] F. J. Wright, "Wavefield Singularities", PhD Thesis, H. H. Wills Physics Laboratory, Bristol University, UK (1977).

[WRI79] F. J. Wright, "Wavefront Dislocations and Their Analysis Using Catastrophe Theory", in "Structural Stability in Physics", eds. W. Guttinger and H. Eikmeier, Springer-Verlag, Berlin, 141-156, (1979).

[YAR85] A. Yariv, "Optical Electronics", Holt, Reinhart and Winston, New York, (1985).

[ZEL85] B. Ya. Zel'dovich, N. F. Pilipetsky and V. V. Shkunov, "Principles of Phase Conjugation", Springer-Verlag, Berlin, (1985).